Nonlinear and Multi-Wave Effects in Fast-Scale Laser-Plasma Interactions

by

Ryan Roger Lindberg

BS (University of Illinois, Urbana-Champaign) May, 1999
MA (University of California, Berkeley) December, 2003

A dissertation submitted in partial satisfaction of the
requirements for the degree of
Doctor of Philosophy

in

Physics

in the

GRADUATE DIVISION
of the
UNIVERSITY OF CALIFORNIA, BERKELEY

Committee in charge:
Jonathan S. Wurtele, Chair
Stuart D. Bale
Eliot Quataert

Spring 2007

The dissertation of Ryan Roger Lindberg is approved:

Chair Date

Date

Date

University of California, Berkeley

Spring 2007

Nonlinear and Multi-Wave Effects in Fast-Scale Laser-Plasma Interactions

Ryan Roger Lindberg

Abstract

Nonlinear and Multi-Wave Effects in Fast-Scale Laser-Plasma Interactions

by

Ryan Roger Lindberg
Doctor of Philosophy in Physics

University of California, Berkeley

Jonathan S. Wurtele, Chair

A new model of kinetic effects in Langmuir wave dynamics is developed. A nonlinear distribution function is constructed that accounts for particle separatrix crossing and self-consistent electrostatic evolution, assuming that the Langmuir wave changes slowly with respect to the particle bounce frequency in the wave. Using simple physical arguments, the distribution function is shown to be nearly invariant in the canonical action, such that slow evolution results in an overall translation of the distribution in action. Requirements of self-consistency with the electrostatic potential yield the key properties of the nonlinear distribution function, including a frequency shift of the wave and the incoherent energy associated with developing the final, phase-mixed state. These Bernstein-Greene-Kruskal (BGK) type waves naturally arise in weakly driven, thermal plasmas, and extend earlier work on nonlinear plasma waves by Morales and O'Neil and by Dewar. The bulk properties of these BGK-type waves are used to develop a fluid model describing nonlinear, kinetic Langmuir waves in a driven plasma that is shown to agree closely with electrostatic particle simulations over a wide range of temperatures ($0.1 \leq k\lambda_D \leq 0.4$). This model is then applied to the fundamental problem of including kinetic effects in Raman backscatter.

To obtain the coupled mode equations relevant to Raman backscatter in a plasma, we average the Vlasov-Maxwell system over the fine spatio-temporal scales of the laser phase. The resulting set of envelope equations coupling the two counter-propagating lasers with

the plasma wave is then analyzed in two limits: that of an initial, linear Langmuir wave, and that of the time-asymptotic state in which the particles become phase-mixed in the wave. In the former limit, the standard natural frequency and Landau damping is obtained, while the latter case leads to a vanishing damping and a nonlinear frequency shift of the wave, in agreement with recent numerical results. Energy conservation is employed to provide a smooth transition from one regime to the next, using the fact that the energy dissipated by Landau damping must be equal to the increase in kinetic energy of the plasma electrons. These results build on the ideas of nonlinear Landau damping studied by O'Neil, while in the small amplitude limit our work reproduces that of Dewar on instability saturation through trapping.

The resulting extended three-wave model is compared with kinetic simulations for a wide range of system parameters, relevant to both inertial confinement fusion and Raman laser amplification in a plasma. Particle trapping and the resulting decrease in Landau damping gives rise to an increase in the Langmuir wave amplitude above linear theory expectations, as has been observed in recent experiments and Vlasov simulations. The extended three-wave model captures the essential physics of this "kinetic enhancement" that may lead to undesirably large levels of Raman scatter in the context of inertial confinement fusion. The Raman amplifier, in which Raman scattering is used to transfer energy from a long pump laser to a short seed pulse, can be adversely affected by the nonlinear frequency shifts arising from the trapped particles, with a resulting decrease in efficiency. The extended three-wave model is proposed as a simulation tool for efficiently evaluating this temperature scaling for present and future experiments.

Jonathan S. Wurtele
Dissertation Committee Chair

To my parents, Roger and Sharon, and my sister Steph and brother Mark.

Contents

List of Figures

List of Tables

Acknowledgments

There are many people without whom I would not have finished or even started graduate school. So much so, I will have a hard time thanking everyone and thanking them properly. But I will try.

First, I'd like to thank my thesis advisor, Prof. Jonathan Wurtele. Jonathan introduced me to a whole new branch of physics and helped me discover what research really is. He instilled in me the necessity of reducing mathematical arguments into basic, physical terms, while giving me the freedom to go wherever the problems might take me. Jonathan freely gave of his time and energy to help me, whether that was getting up early for my talk at Princeton or coming in on the weekends to help me finish the thesis, and for that, I am grateful. I'd also like to thank my thesis committee for reading this thesis and for their kind and generous feedback. Prof. Stuart Bale was good enough to step on to my committee on such short notice and share his excitement and his insight with me. Prof. Eliot Quataert both gave me encouraging and helpful feedback and taught me everything I know about astrophysical gas dynamics.

I can hardly imagine making it through without the help and guidance of my fellow graduate student office-mates: Andy Charman and Vladimir Gorgadze. Andy helped spawn some of the central ideas behind the BGK-type waves, and he was always available to help guide me past subsequent difficulties (both perceived by me and not) with his physical intuition and attention to rigor. Outside the office Andy encouraged me get a little culture, with films and fine food and insightful conversation, along with a series of fine Friday afternoon lunches out in the sun. Vladimir insisted that there was no integral not

worth trying to calculate, and that every equation deserved due process to find its analytic solution. After the calculations were done, Vladimir could always be counted on to find a place to kick back: I still smile when I think of the AAC Workshop in Stony Brook and the Victory Day celebration, and his hospitality in Moscow will never be forgotten. I'd also like to thank some of the scientists from Lawrence Berkeley Lab, specifically Bill Fawley for showing an early interest in my studies, and to Carl Schroeder and Brad Shadwick for great lunches with physics and sun and drink and for sharing their insight into physics and their additional perspective on the field.

I'd like to thank both Prof. Nat Fisch and Prof. Szymon Suckewer for inviting me to Princeton, for sharing their time and showing me around the lab, and for providing such warm hospitality. Additionally, I appreciate the help and discussions from Nikolai Yampolsky, Shuanglei Li, and Jun Ren that made my stay both productive and pleasant.

I acknowledge the help and input of the scientists at Livermore, specifically Dick Berger who was kind enough to introduce me to the lab and its people, to lend some space and discuss physics, and to generally insure that my stay at Livermore was pleasant. Additionally, I acknowledge the help of Dave Strozzi; the long conversations on plasma waves, Raman scatter, and fusion energy in general helped focus some of my investigations. Finally, I would like to thank the Department of Energy and the High Energy Physics Division for funding the bulk of my graduate career, and acknowledge additional funding from Lawrence Livermore National Laboratory and its Intra-University Transaction program.

Now I come to some of the more personal acknowledgments. First in my mind and heart is my family. As I get older I realize how blessed I am. My parents have always been encouraging without being pushy, forgiving without being lax. My dad showed me curiosity and wonder, gave me lessons and a laugh. My mom showed me what it means to listen and to give, to persevere and to sing. Throughout my many years of schooling both have been a comfort, a refuge, an inspiration. Most good things I have I owe to them. Next, I'd like to thank my big sister, Stephanie. Balancing job and raising a family is tough for anyone, and Stephie does it with skill, love, and grace that I find amazing. And

she'll still find time for a triathalon. Her lovely daughters Audrey and Lindsey are a joy; her husband Jason has been a pleasure, and I value those late conversations on science, surgeries, chess, climbing, or kickboxing. Finally, I want to thank my little brother Mark, who really isn't so little anymore. I thank him for mixing his exuberance for life with his faith in himself and his path; for knowing what is worth fighting for and for taking the path less traveled. He has shown me much in how one can live, and live happy.

The rest of my family has also provided support and motivation to help me make it through. I especially want to thank Uncle Ron and Auntie Eileen, for offering up their warmth and their hospitality: with the beautiful sunsets, the delicious food, and the fun conversation, their home served as a relaxing refuge. I also want to thank Brent, who has grown up before my eyes from a little boy to a young man (even though Team Stinky can't buy a game of pool they do make a mean ride). Then there are Grandpa and Grandma, Uncle Mark and Aunt Cheri, Auntie Roberta, and the cousins, ... you all have been wonderful.

I want to express my gratitude to those who made graduate school the fun time that it was. Here, I thank my fellow physicist friends not already mentioned; while we might have chatted now and again about Hamiltonians or Wigner functions or black hole thermodynamics, or spent a few too many hours slogging through problem sets, those pale in comparison with the friendship... I'd like to thank Peter Shepard for those nights of chess, Brown Shugga, the hand-me-downs, and the Barry. For inviting me out to the mountains to escape it all and for brightening my summer days by helping me recognize the veritable kaleidoscopic flux before me. Finally, I thank Peter for helping me through a difficult time with a steady diet of The Graduate, The Albatross, and good conversation... I thank Mike Grobis for being one of my first graduate school friends and for helping me navigate the early years of class and meet new people. For the groggy mornings at 64 Kelvin, for basketball, and the Gladiator monikers. For "game tempo" and the related Matlab softball simulator, ping pong, and the house dance; there were many great memories and I hope there will be many more... I'd like to give thanks to Kevin Moore, my thesis-writing

partner in crime, a fellow figure of the living room, typing away as we alternate between coffee and beer. I thank him for recognizing the greatness of Las Palmas and CrocoDuck and Makin' it Right. For Team DMSK and the indie rock and the Daily Show; for being so indignant, for the biking to work and the kicking it at home, we had many good days at 5741... I acknowledge Mike Boylan-Kolchin, fellow aficionado of the collisionless Boltzmann equation and co-president of the Budlight Fan Club. For the mornings of tennis, the evenings at Blake's, and for the entire days of March Madness. For introducing me to the joys of "O Fantasy" and the ability to recognize movies (*Kickboxer* has kickbox*ing*), while also ready to argue the philosophical and moral implications in Vigilante- vs. Bandit-style justice. For being a great roommate as we troll for a terrible movie or some Cheaters... Additionally, I thank a few others who made everything more fun: Jared Mehl, Matt Langner, John Sample, Nadir Jevanjee, Mike Wahl, and the ψ^* team; it's been a great run.

Then of course there are a few non-physicists deserving thanks. To Rich and Farah Meraz, you were terrific roommates and wonderful people to spend time with. Rich, I thank you for our romps from the White Horse to those comfy couches, chatting about biology and the difficulties we all face. To Farah with her travel, introducing me to Lexi and just hanging out. We all had a great home... I thank the lovely Liz Mazur. For the hot-tubs and the hikes, the dinners at fancy homes in the hills and the Sizzler, for just being there with style and grace. Especially down this last sprint, Liz has been there for me in ways I would not have imagined; with care and support and love and cookies.

I'd like to thank the boys from college, Ben Ertlé and Nathan Rau, who continue to be great friends even after we have each gone our separate ways. Without Ben I would have probably never started down this road, while Nathan helped me keep some perspective as I travelled it. I thank them for opening up their new families to me, and for always being there. For the boys from back home, Dave NC, John McBride, Edwin Lee, and Bimal Vyas, I thank you all.

As my roommate and fellow Spring 2007 physics PhD Kevin Moore pointed out,

in some ways this thesis marks the completion of "25$^{\text{th}}$ grade" for me. There is a long list of teachers who have helped me survive this run even before graduate school, and subsequently encouraged me to turn it into a bit of a marathon. First, I want to thank my college thesis advisor at University of Illinois Urbana-Champaign, Prof. Aida El-Khadra; I think I was her first undergraduate advisee, and while she treated me like a graduate student, she did so with extreme patience. I also want to thank many of the faculty of the now-defunct Department of Theoretical and Applied Mechanics: Prof. Scott White, who gave me my first taste of research with his work in advanced materials; Prof. Don Carlson who was almost like the department grandfather; and Prof. Petros Sofronis, who I credit with helping begin my move from Mechanical Engineering to Mechanics, which eventually brought me to physics.

I want to thank those teachers who influenced me early on, such that I clearly remember those long school days of youth, and remember them fondly: Mr. Warfield and Mr. Johnson who almost had me convinced that Literature was *the* subject worth studying; Mr. Petersen who made chemistry fun and interesting and whose great teaching was sadly cut short [I will always remember Mole Man]; Mrs. Branding who somehow dealt with our class during three years of our early adolescence and at the same time managed to teach us some math; and Mrs. Cimaroli who nurtured my natural love of learning back when I was strong-headed and generally maladjusted.

Finally, a partial list of some things that helped make graduate school possible: Big Lebowski, Budlight, Cole Coffee, college program at San Quentin, Journey, International Soccer Club, Law & Order, Samuel Smith's, sunny days on the porch, ...

List of Symbols and Notation

Symbol	Name	Definition
a_0	Complex, dimensionless "pump" laser	$\frac{e}{m_e c^2}A$ with fast phase $e^{-i(\omega_0 t + k_0 z)}$
a_1	Complex, dimensionless "seed" laser	$\frac{e}{m_e c^2}A$ with fast phase $e^{-i(\omega_1 - k_1 z)}$
$\omega_2,\ k_2$	Beat frequency, wavevector	$\omega_2 = \omega_0 - \omega_1,\ k_2 = k_0 + k_1$
τ	Scaled time	$\omega_p t$
ζ	Scaled longitudinal coordinate	$k_2 z$
u	Scaled longitudinal velocity	$k_2 z/\omega_p$
σ	Scaled thermal spread	$k\lambda_D \equiv k v_{\rm th}/\omega_p$
ω_L	Linear frequency of BGK-type wave	Solution to (0.1a)
ω_r	Real part of the linear frequency	$\Re(\omega)$ solving (0.1b)
ν_ℓ	Landau damping rate	$-\Im(\omega)$ solving (0.1b)
$f(u,\zeta;\tau)$	Scaled electron distribution function	
$\dfrac{\delta n}{n_0}$	Dimensionless density perturbation	$\displaystyle\int du\ f(u,\zeta;\tau) - 1$
$\phi(\zeta)$	Dimensionless electrostatic potential	$\phi(\zeta) = \frac{e k_2^2}{m_e \omega_p^2}\Phi(\zeta)$
θ	Langmuir wave phase	$\theta \equiv \zeta + \omega_L \tau + \psi$
ϕ_n	Langmuir harmonic amplitudes	$\displaystyle\phi(\zeta) = \sum_{n=1}^{\infty} \phi_n \cos(n\theta)$
$\delta\omega$	Nonlinear Langmuir frequency shift	$\frac{d}{d\tau}\psi$
$g_1,\ \mathcal{G}$	Complex Langmuir wave envelope	$g_1 \approx -\phi_1 e^{-i\psi},\ \mathcal{G} \equiv -i g_1 e^{i(\omega_2 - \omega_L)\tau}$
(p,θ)	Electron momentum and phase	$\theta \equiv \zeta + \omega_L\tau + \psi,\quad p \equiv u + \omega_L$
(J,Ψ)	Canonical action, angle coordinates	$\displaystyle J = \oint d\theta\ p(\theta, H; \tau)$
$\mathcal{E}$	Dimensionless electric field	$\mathcal{E} = \frac{m_e \omega_p^2}{e k} E_z$

$$1 + \frac{1}{\sigma^2}\left[1 + \frac{\omega_L/\sigma}{\sqrt{2\pi}}\ \mathscr{P}\int_{-\infty}^{\infty} dx\ \frac{e^{-x^2/2}}{x - \omega_L/\sigma}\right] = 0 \tag{0.1a}$$

$$\frac{1}{\sigma\sqrt{2\pi}}\frac{\partial}{\partial\omega}\left[\mathscr{P}\int dx\ \frac{e^{-x^2/2}}{x - \omega/\sigma} + i\pi e^{-\omega^2/2\sigma^2}\right] = 1. \tag{0.1b}$$

Chapter 1

Overview

Ever since Tonks and Langmuir [1] described and gave indisputable evidence for longitudinal, electrostatic oscillations in a plasma, Langmuir waves have played an important role in plasma physics. So much so that even though plasmas support a host of waves, Langmuir waves are often referred to as plasma waves or plasma oscillations, and their characteristic frequency $\omega_p \equiv \left(\frac{4\pi e n_0}{m_e}\right)^{1/2}$ is *the* plasma frequency (m_e is the electron mass, e the magnitude of its charge, and n_0 the ambient electron density).

In 1949, Pines and Bohm [2] clearly demonstrated that Langmuir waves are essentially a collective phenomenon, describable in terms of collective coordinates for scale-lengths greater than the Debye length $\lambda_D \equiv v_{\rm th}/\omega_p$, where, for a plasma with temperature T_e the thermal speed $v_{\rm th} \equiv \sqrt{T_e/m_e}$. This collective behavior is one of the defining features of plasma. About the same time, Landau [3] showed that linear Langmuir waves have an imaginary part to their oscillation frequency, so that electrostatic waves in a plasma decay through the process of Landau damping. About ten years later, Jackson [4] provided and Dawson [5] improved upon a physical mechanism for this collisionless damping in terms of the resonant wave particle interaction: particles moving slightly slower than the phase velocity of the wave v_p are accelerated and take energy from the wave, while those particles whose velocities are slightly faster than v_p transfer energy to the wave. In the

case of a Langmuir wave with $v_p \gtrsim v_{\rm th}$ in a Maxwellian plasma, for example, there is an excess of particles whose velocity is slower than v_p, resulting in a net increase of the particle kinetic energy and commensurate damping of the electrostatic wave. Nonlinear modifications to the distribution function were shown by O'Neil [6] to arrest the process of Landau damping for sufficiently large amplitude waves: if electrons perform many trapped oscillations before Landau damping significantly changes the wave amplitude, then the trapped particles effectively phase-mix in the wave and flatten the distribution in velocity, resulting in a stationary final distribution of nonzero electrostatic amplitude.

Although it was not explicitly noted at the time, the phase-mixed final state described by O'Neil has much in common with the nonlinear, stationary solutions first described by Bernstein, Greene, and Kruskal (BGK) [7]. Formally, BGK waves are static solutions of the one-dimensional Vlasov-Poisson system for which the distribution is a function of the conserved particle energy $H = \frac{1}{2}m_e v^2 - e\Phi(z)$. As shown in Ref. [7], any sufficiently smooth electrostatic potential can be self-consistently realized with an appropriate distribution function $f(H)$ which includes both trapped and untrapped particles. While these distributions may at first appear to describe a very specialized class of solutions, they arise in a wide range of nonlinear phenomena, including the nonlinear stages of Landau damping [6, 8] and other instabilities [9, 10], and furthermore have been used to develop certain theories of shock waves [11] and double layers (see, e.g., [12] and references therein). BGK-type waves have been excited and controlled in non-neutral plasmas [13, 14], have been associated with the nonlinear evolution of stimulated Raman and Brillouin scattering in laser-plasma experiments [15, 16], and have been directly observed in auroral and other space plasmas [17, 18].

While BGK waves are of fundamental interest to a wide range of plasma physics, our focus will center on a certain class of BGK-type waves that naturally arise as long-lived, nonlinear Langmuir waves in plasmas that are driven on or near resonance. These waves have a particular importance for laser-plasma interactions, as they dynamically appear in the later, nonlinear stages of the Raman scattering instability.

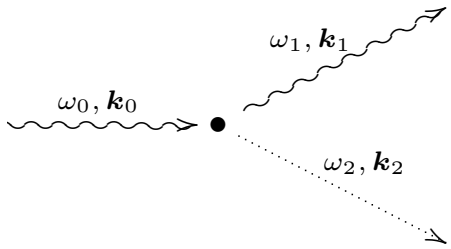

Figure 1.1: Feynman diagrammatic picture of Raman scatter in a plasma. Conservation of energy and momentum dictates that $\omega_0 = \omega_1 + \omega_2$ and $\boldsymbol{k}_0 = \boldsymbol{k}_1 + \boldsymbol{k}_2$, corresponding to the classical resonance conditions.

In quantum mechanical language, Raman scattering can be simply described as the resonant decay of an incident photon into a frequency down-shifted daughter photon and a Langmuir oscillation (or plasmon) [19, 20, 21]. A Feynman diagram representation of the Raman interaction is given in Fig. 1.1, where the frequency and wavevectors satisfy the resonance conditions

$$\omega_0 = \omega_1 + \omega_2 \,, \qquad\qquad \boldsymbol{k}_0 = \boldsymbol{k}_1 + \boldsymbol{k}_2, \tag{1.1}$$

with the subscript 0 indicating the incident photon, 1 the scattered photon, and 2 the Langmuir wave, so that ω_2 is approximately the plasma frequency ω_p.

The Raman interaction can give rise to an instability in which significant levels of incident laser light is scattered. If, for example, the propagating laser encounters a density fluctuation in the plasma, a transverse current given by the product of the density perturbation and the quiver velocity of the electrons is produced. This current then generates a scattered electromagnetic wave satisfying the resonance conditions (1.1), which in turn beats with the incident laser, amplifying the initial density perturbation. The resulting feedback can lead to significant energy being reflected from this "plasma grating." The characteristic growth rate of the linear Raman instability is

$$\gamma_{\mathrm{R}} \equiv \sqrt{\boldsymbol{a}_0^2\, \omega_0\, \omega_p/2} \,, \tag{1.2}$$

where $\boldsymbol{a}_0 \equiv \frac{e}{mc_e^2}\boldsymbol{A}_0$ is the root mean square dimensionless vector potential of the incident, "pump" laser. Note that instability occurs only if the growth rate γ_{R} is sufficiently large to

overcome the damping of the plasma and scattered waves, or, alternatively, the gradients in the plasma over which the resonance condition (1.1) approximately holds (see, e.g., Ref. [22, Ch. 7] and references cited therein).

The theoretical and numerical studies in this thesis are motivated, in part, by the importance of Langmuir wave dynamics to Raman scattering in plasma. From the perspective of inertial confinement fusion, Raman backscatter is a deleterious instability that can significantly decrease the laser energy on target, and furthermore produce hot electrons which make it more difficult to compress the deuterium-tritium capsule. For this reason, it is necessary to understand how Raman scattering scales with laser parameters, such as intensity, wavelength, and phase coherence, and with plasma parameters, such as density and temperature. Additionally, nonlinear processes must be identified and understood. These processes can both increase Raman scattering through decreased Landau damping [6, 8], or nonlinearly saturate the instability via particle trapping and the associated nonlinear frequency shifts [23, 24, 25], the trapped particle instability [26], or possibly through Langmuir wave-breaking [27, 28].

Premature saturation of the Raman instability can lead to undesirably low efficiencies for schemes that use Raman backscatter as a means to exchange energy from a long, low intensity laser to a short, high intensity laser pulse [29, 30]. For this application, the Raman interaction is initiated by a short, seeding laser, with the ultimate goal being significant transfer of the pump energy into the seed. In this case, the Raman interaction should ideally be "turned off" until the pump reaches the seed pulse, after which time premature saturation of Raman scattering may lead to decreased amplification efficiency and degraded amplified pulse characteristics.

These two schemes view the Raman instability from different perspectives, with fusion applications looking to limit Raman scattering to some tolerable, low level, while the Raman amplifier requires maximal Raman coupling when the counter-propagating lasers overlap. Nevertheless, both applications require an understanding of the nonlinear kinetic effects to properly assess appropriate parameter regimes, and to develop the reduced

numerical tools useful for theoretical analysis.

1.1 Findings of this thesis

In this thesis, we develop a new analysis of nonlinear distribution functions associated with slowly-driven waves. These waves have particular relevance to plasma physics in general and Raman scattering in particular as they naturally arise in plasmas that are driven on or near the Langmuir resonance. By trapping particles self-consistently in the electrostatic potential, they give rise to long-lived, BGK-type solutions that are not damped by (collisionless) Landau damping. We then use the bulk properties of this dynamic distribution to develop a simplified kinetic model of Raman backscatter, hereafter referred to as an extended three-wave model. We compare our model predictions to results from Vlasov simulations, and investigate the nonlinear growth and saturation of Raman scattering in contexts relevant to both the inertial confinement fusion community and the scenario of plasma-based Raman amplification.

We begin in Chapter 2 by introducing the nonlinear distribution function associated with slowly-evolving Langmuir waves in a warm plasma. The critical theoretical development is an action-angle description of particle motion including separatrix crossing in the slowly-evolving wave. By dividing the fast angular dependence from the slow evolution of the action, we find that these waves are described by an electron distribution function that is invariant in the action difference for the untrapped particles, while invariant in the action for the trapped particles. Self-consistency with the Poisson equation yields the slowly-evolving mean action of the distribution, from which an amplitude dependent frequency shift of the Langmuir wave is obtained that compares well with simulations.

In Chapter 3 the Vlasov-Maxwell system for Raman backscatter is reduced to a set of three coupled-mode equations including thermal and kinetic effects. We derive this extended three-wave model by averaging the Vlasov-Maxwell system over the short spatio-temporal scales associated with the laser phase, assuming that the transverse gradients

are small. We thereby obtain a set of coupled envelope equations describing the resonant interaction between three modes given by the two counter-propagating lasers and the Langmuir wave. The Langmuir wave envelope equation contains terms involving second-order velocity moments of the distribution function. In two limits the system can be closed: in the linear limit these additional terms gives rise to the complex frequency associated with a Landau-damped "quasi-mode," while in the time asymptotic limit the distribution approaches that of the BGK-type wave of Ch. 2, with its associated zero damping and nonlinear frequency shift. To interpolate between these two limits, we develop a simple theory based on energy conservation and resonant particle phase-mixing in the Langmuir wave, through which a smooth transition can be numerically interpolated. This results in a model that includes the linear and nonlinear physics in a unified and consistent, albeit somewhat heuristic, manner.

In Chapter 4 we compare the extended three-wave model to fully kinetic codes (both Vlasov and particle-based) in a variety of different regimes. We illustrate some basic features of the driven Langmuir waves which can grow to levels above those predicted by linear calculations assuming a constant value of Landau damping. Because particles phase-mix in these driven waves (associated with the flattening of the distribution in velocity-space), Landau damping vanishes and the waves will continue to grow. We show that in this case the Langmuir wave growth is saturated by the nonlinear frequency shift, which detunes the plasma response from the resonant drive. Finally, we apply our extended three-wave model to the transient amplification of a short laser seed pulse in plasma. Further applications of the theory would be to develop an efficient multi-dimensional code to model Raman backscatter.

In parallel to the analysis in chapters 2-4, we present a few new aspects of one dimensional plasma fluid models in Ch. 5. We first obtain a Hamiltonian warm fluid model that is both canonical yet given in terms of the physical, Eulerian velocity and electric fields. This is unusual, since continuum models in Eulerian coordinates generally have noncanonical Hamiltonian formulations. We use this model to show, in a simple and straightforward

manner, that the cold, nonrelativistic Langmuir wave has a natural frequency ω_p that is independent of its amplitude. We close by showing a simple, geometric explanation of why this is true.

We conclude in Ch. 6 with some possible extensions and applications of this thesis to future research.

Appendix A contains some clarifications of previous work regarding separatrix crossing in slowly-varying Hamiltonian systems. Specifically, we consider the evolution of a distribution of particles initially of the same canonical action and spread uniformly in the canonical angle as they cross a slowly-evolving separatrix, a situation relevant to the particle trapping described in Ch. 2. We show that upon crossing, the action of nearly all the particles changes by some small amount, while the distribution in angle becomes bunched due to the slowing of some particles as they near the hyperbolic fixed points. This bunching in angle only vanishes logarithmically with the slowness parameter, so that its effect is important to the results of Ch. 2 for physically realistic parameters.

Chapter 2

Nonlinear Langmuir waves in a slowly driven plasma

2.1 Introduction

Much of the progress in understanding Langmuir waves has been from the linear viewpoint, obtained by assuming that the perturbation of the plasma from its (Maxwellian) equilibrium is assumed to be "sufficiently small," such that second order terms in the perturbation may be neglected. Under these conditions, one can derive the normal modes of the distribution function (the singular Case-Van Kampen modes [31, 32]) or, alternatively, the Landau damped "quasi-modes" of the electric field [3, 4]. A basic result of these linear analyses is that smooth, electrostatic perturbations tend to zero through the process of Landau damping.

That such damping is not universal was first pointed out by Bernstein, Greene, and Kruskal (BGK) [7], who included the particles trapped in the electrostatic wave to formulate nonlinear distribution functions that give rise to stationary electrostatic disturbances. Explicit constructions of sinusoidal, small-amplitude BGK waves were later derived by Holloway and Dorning [33], in which they showed that arbitrarily small amplitude waves

can exist without being Landau damped. BGK distributions are functions $f_e(H)$ of the conserved particle energy $H = \frac{1}{2}m_e v^2 - e\Phi(z)$ (where m_e is the electron mass, e is the magnitude of its charge, z is the longitudinal position, and v is the longitudinal velocity), whose charge density generates the self-consistent electrostatic potential $\Phi(z)$ via Poisson's equation. Thus, BGK distributions are static solutions to the one-dimensional Vlasov-Poisson system

$$\frac{d}{dt}f_e(v,z;t) = \frac{\partial f_e}{\partial t} + v\frac{\partial f_e}{\partial z} + \frac{e}{m_e}\frac{\partial \Phi}{\partial z}\frac{\partial f_e}{\partial v} = 0 \tag{2.1a}$$

$$\frac{\partial^2}{\partial z^2}\Phi(z) = 4\pi e\int dv\ f_e(v,z;t) - 4\pi e n_i(z), \tag{2.1b}$$

where f_e is the electron distribution function at time t, normalized such that its marginalization in velocity is the electron density

$$\int_{-\infty}^{\infty} dv\ f_e(v,z;t) = n_e(z,t),$$

and we consider the ions to have a time-independent density $n_i(z)$, implying that the time-scales of interest are sufficiently fast such that ion motion can be neglected.

In this chapter, we extend previous work on nonlinear plasma waves. First, we introduce and characterize nonlinear Langmuir wave solutions to the Vlasov-Poisson system (2.1) that are naturally occurring BGK-like waves. These waves (and the distribution functions that generate them) have particular relevance to laser-plasma physics, in that they dynamically arise as kinetic, nonlinear Langmuir waves in systems that are weakly-driven on or near resonance. To obtain these solutions, we use the canonical action-angle coordinates, finding that the plasma is well described by a simplified distribution function that is invariant in the canonical action difference for the plasma bulk. In this way, we obtain near-equilibrium solutions that approximate the fully time-dependent distribution function when the resonant forcing is small. While these notions may be reminiscent of adiabatic theory, we do not invoke adiabatic invariance. Our calculation is more in the spirit of an averaged theory, in that the dynamical dependence on the canonical angle is

ignored on the grounds of rapid effective phase-mixing in the Langmuir wave, while the particle action evolves self-consistently.

Because these nonlinear, kinetic Langmuir waves arise naturally in slowly-driven systems, their bulk properties can be used to illuminate basic plasma processes and obtain reduced descriptions of complex phenomena. For example, the nonlinear frequency shift of the thermal Langmuir resonance is an important quantity in any reduced model of Raman scattering in plasma [34, 35, 36, 37], and our results extend those of Morales and O'Neil [24] and Dewar [25] to colder plasmas and larger electrostatic potentials $\Phi(z)$. We will discuss such an implementation in a Langmuir envelope code in the following chapter.

We introduce the nonlinear distribution in Sec. 2.2. We begin with the single particle equations-of-motion for a weakly-driven system dominated by the slowly-evolving electrostatic potential, and proceed to introduce the relevant action-angle coordinates. Assuming that these coordinates naturally divide the evolution into fast (canonical angle) and slow (canonical action) components, we argue that slow evolution and phase-space area conservation result in an electron distribution function that remains invariant in the action difference for the bulk, for which we mean that any change in the action is reflected throughout the untrapped distribution, while the trapped distribution remains invariant in the canonical action, i.e., the particle action is effectively conserved. Note that because the untrapped distribution is only found to be invariant in the action difference, the mean canonical action may increase as the wave is slowly excited. We will discuss this important departure from previous work in Sec. 2.2.3. Following this, we use Coulomb's law and the demands of self-consistency in Sec. 2.2.4 to derive the functional relationship between the mean action and the amplitude of the potential. Under our present assumptions, this fully specifies the distribution, from which we then extract the natural frequency of the BGK-type wave. To compare this theory with previous results, we present the small-amplitude limits of the mean action and frequency shift in Sec. 2.3, for which the dynamics can be approximated by that of a pendulum. Finally, we compare the frequency of these nonlinear Langmuir waves to those obtained from self-consistent particle simulations in Sec. 2.4 for

thermal plasmas with $0.1 \leq k\lambda_D \leq 0.4$, where $\lambda_D \equiv v_{\rm th}/\omega_p$ is the Debye length.

2.2 The nonlinear electron distribution function relevant for a weakly-driven plasma

In this section we present the single particle equations relevant to a weakly-driven plasma wave in the action-angle formalism. This results in a natural separation of time-scales, from which a simplified, approximate form of the distribution can be determined.

2.2.1 Single-particle equations of motion

In what follows we ignore transverse variation, assuming that the dominant dynamics are along the longitudinal axis z. We also neglect the motion of the background ions, and furthermore assume that the longitudinal force on the electrons can be divided into two components: the first is given in terms of an external driving potential $V(z,t)\sin(\omega t + kz)$, which could arise, for example, from a ponderomotive force resulting from the beating of two lasers. We assume that this external forcing can be expressed as an amplitude $V(z,t)$ modulating a carrier oscillation at frequency ω and wavenumber k. The second force derives from the self-consistent electrostatic potential $\Phi(z,t)$ of the plasma electrons. Thus, Newton's equation of motion for the longitudinal electron coordinate $z(t)$ is given by

$$\frac{d^2}{dt^2}z(t) = \frac{\omega_p^2}{k^2}\frac{\partial}{\partial z}\Big[\phi(z,t) - \mathcal{V}(z,t)\sin(\omega t + kz)\Big], \tag{2.2}$$

where we have scaled the potential by the kinetic energy associated with the nominal phase velocity of the wave, introducing the dimensionless potentials

$$\phi(z,t) \equiv \frac{ek^2}{m_e\omega_p^2}\Phi(z,t), \qquad\qquad \mathcal{V}(z,t) \equiv \frac{k^2}{m_e\omega_p^2}V(z,t), \tag{2.3}$$

and the cold, linear plasma frequency corresponding to the equilibrium density $n_0 = n_i$ is

$$\omega_p \equiv \left(\frac{4\pi e^2 n_0}{m_e}\right)^{1/2}, \quad \text{where} \quad n_0 \equiv \lim_{t\to-\infty}\int dv\ f_e(v,z;t).$$

In the equation of motion (2.2) we have assumed the dynamics to be nonrelativistic, requiring that the potentials remain sufficiently small such that $|e\Phi|\,,\ |V| \ll m_e c^2$, where c is the speed of light *in vacuo*; note that the electrostatic potential will satisfy this relation for all time if the nominal phase velocity is much less than the speed of light, $(\omega/k)^2 \ll c^2$.

To further simplify (2.2), we assume that the normalized amplitude of the external driving potential $\mathcal{V}(z,t)$ has a slow spatio-temporal variation with respect to its carrier phase, so that

$$\left|\frac{\partial}{\partial z}\ln\mathcal{V}(z,t)\right| \ll k\ , \qquad\qquad \left|\frac{\partial}{\partial t}\ln\mathcal{V}(z,t)\right| \ll \omega. \tag{2.4}$$

The nearly-periodic, weak external drive then sets a natural spatial length-scale for the slowly-evolving, self-consistent electrostatic potential $\phi(z,t)$. In order to facilitate subsequent discussion regarding the separation of time-scales and our resulting choice of coordinates, we expand ϕ as a Fourier series of dimensionless eikonal amplitudes:

$$\phi(z,t) = \sum_{n=1}^{\infty}\phi_n(z,t)\cos\{n[(\omega t + kz) + \psi(z,t)]\}. \tag{2.5}$$

Because $\phi(z,t)$ is excited by the slowly-varying potential $\mathcal{V}(z,t)$, the eikonal conditions (2.4) imply that the harmonic amplitudes $\phi_n(z,t)$ and the phase shift $\psi(z,t)$ are similarly slowly-varying. In the limit of small forcing, we now express (2.2) as a Hamiltonian system appropriate for action-angle variables. We introduce the dimensionless time $\tau \equiv \omega_p t$, the scaled (linear) frequency $\omega_L \equiv \omega/\omega_p$, and the dimensionless coordinates given by the phase in the electrostatic wave θ and its corresponding canonical momentum p:

$$\theta \equiv \omega t + kz + \psi\ , \qquad\qquad p \equiv \dot{\theta} - \dot{\psi} \equiv \dot{\theta} - \delta\omega = k\dot{z} + \omega_L, \tag{2.6}$$

where $\psi = \psi(\tau)$ is the single-particle analog of the phase-shift introduced above, chosen for any single-wavelength "bucket" of interest. The over-dot in (2.6) denotes the normalized time derivative $\frac{d}{d\tau} \equiv \frac{1}{\omega_p}\frac{d}{dt}$ so that the frequency shift $\delta\omega \equiv \dot{\psi}$. To further simplify our discussion, we assume that the potential is well described by the electrostatic field, namely, that $\mathcal{V} \ll \max|\phi| \equiv \phi_{\max}$. Thus, we consider the case in which the single-particle dynamics

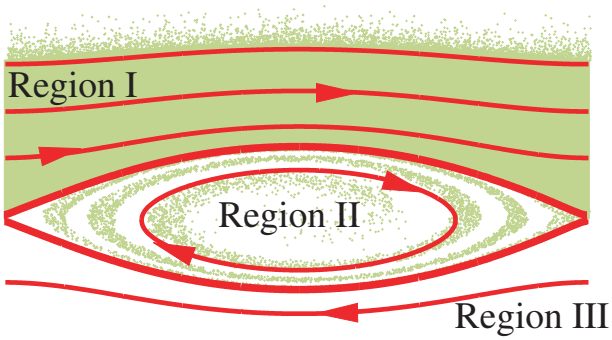

Figure 2.1: Phase space schematic for a Langmuir wave overlaid on the results of a self-consistent particle simulation. Region I (above the separatrices) consists of the plasma bulk making up the wave; region II contains the trapped particles between the separatrices; region III contains those particles moving too fast to be trapped in the wave.

is dominated by the self-consistent field, with the external drive serving as an energy source through which the amplitude of ϕ is changed. Note that this assumption is consistent with the constraint that the eikonal amplitudes ϕ_n and frequency shift $\delta\omega$ have slow spatio-temporal variation, and leads to the following approximate equations of motion

$$\dot{\theta} = p + \delta\omega(\tau) \,, \qquad\qquad \dot{p} = \frac{\partial}{\partial\theta}\phi(\theta,\tau). \tag{2.7}$$

The system (2.7) can be obtained from the Hamiltonian

$$\mathcal{H}(p,\theta;\tau) = \frac{1}{2}\left[p + \delta\omega(\tau)\right]^2 - \phi(\theta;\tau). \tag{2.8}$$

Here, we summarize a few general features regarding the Hamiltonian (2.8) that will be important to our subsequent discussions. The frozen orbits of $\mathcal{H}$ are defined as the level sets $\mathcal{H}(p,\theta;\tau) = H$ at a fixed time τ, for which the parameters ϕ_n and $\delta\omega$ are constant and the motion is periodic. A representative phase portrait of the frozen orbits is shown in Fig. 2.1, superposed on a phase-space snapshot taken from a self-consistent particle simulation. Generically, we see that phase space is divided into three distinct regions, separated by the trajectories joining the hyperbolic fixed points at $\theta = \pm\pi$, $p = -\delta\omega$, for which $H = \phi_{\max}$. These separatrices partition the "rotational" motion of regions I and III, for which $H > \phi_{\max}$, from the "libration" about the stable fixed point at

$\theta = 0$ in region II, where $H < \phi_{\max}$. Associated with these frozen orbits, there exists a canonical transformation to action-angle coordinates $(p, \theta; \tau) \to (J, \Psi; \tau)$, with the action proportional to the phase-space area of the frozen orbit:

$$\begin{aligned} J(H;\tau) &\equiv \frac{1}{2\pi} \oint d\theta \; p(\theta, H; \tau) \\ &= \frac{1}{2\pi} \oint d\theta \; \Big\{ \sqrt{2[H + \phi(H;\tau)]} - \delta\omega(\tau) \Big\}. \end{aligned} \tag{2.9}$$

The utility of the action-angle coordinates in this setting lies in their division of the motion into two distinct time-scales: the natural frequency of the canonical angle $\dot{\Psi} \sim 1$ gives the time over which the particles complete oscillations in the wave, while the slow time-scale set by the external drive yields the time over which the action may significantly evolve, $\dot{J} \sim \mathcal{V}$. Furthermore, since J is related to the phase-space area, incompressible Hamiltonian flow significantly restricts its evolution. We use these facts in the next section to obtain a simplified, approximate description of the nonlinear electron distribution function.

2.2.2 Phase-mixing and the integral invariant of Poincaré-Cartan

The central assumption for our distribution function action *ansatz* is that the Langmuir wave amplitude and frequency are slowly-evolving, meaning that the parameters $\phi_n(\tau)$ and $\delta\omega(\tau)$ of the Hamiltonian do not vary appreciably over one period of the motion. For nearly all electrons, i.e., all except the exponentially few in a narrow range about the separatrix, the condition of "slowness" can be written as

$$\frac{1}{\sqrt{\phi_1}} \left| \frac{d}{d\tau} \ln \phi_1 \right| \sim \frac{1}{\sqrt{\phi_1}} \left| \frac{d}{d\tau} \ln \delta\omega \right| \sim \epsilon, \qquad \epsilon \ll 1. \tag{2.10}$$

As previously noted, while these conditions are reminiscent of adiabatic evolution, we do not explicitly invoke adiabaticity; rather, we use the slowness condition (2.10) to justify our assumption that the distribution function remains essentially uniform in the canonical angle Ψ throughout its evolution. We will see that this knowledge coupled with the integral invariant of Poincaré-Cartan indicates that the distribution function of the bulk is essentially invariant in action difference $J - \bar{J}(\tau)$, while the trapped distribution is nearly

invariant in the particle action. Here, $\bar{J}(\tau)$ is the slowly-varying mean to be determined from the constraints of self-consistency. We refer to this particularly invariant-in-action distribution as the action *ansatz*.

Prior to explaining our approximate distribution function, we review the Poincaré-Cartan integral invariant in the context of a one degree of freedom non-autonomous system. Suppose that two simple, closed curves γ_1 and γ_2 encircle the same tube of trajectories generated by $\mathcal{H}$ in the extended 2+1 dimensional phase space of (p, θ, τ). In this case, the integral of the 1-form $p\,d\theta - \mathcal{H}\,dt$ along the two curves is identical (see, e.g., [38]). If we consider both γ_1 and γ_2 to consist of simultaneous phase-space points, namely, that each lies in a plane of constant t, we have

$$\oint_{\gamma_1} d\theta\, p = \oint_{\gamma_2} d\theta\, p, \tag{2.11}$$

which is a form of Liouville's theorem, where the final curve $\gamma_2 = \gamma_1(\tau)$ is the image under the flow of the initial curve γ_1. These integrals should not be confused with the action J: while J is evaluated along the frozen orbit of a given point in phase space, the curves $\gamma_{1,2}$ in (2.11) are determined by a family of trajectories evolving under the flow of $\mathcal{H}$. Nevertheless, under slow evolution given by (2.10), we will argue that the curves γ can be associated, to within $O(\epsilon)$, with the appropriate pairs of frozen orbits, in which case (2.11) indicates that the relative change in J among the particles is small.

The untrapped distribution function

We begin our discussion with those electrons that begin and remain far from the separatrices. Specifically, we consider an initial curve γ_1 defined by the locus of points initially at two values of velocity as shown in Fig. 2.2(a). As also indicated in Fig. 2.2(b), since in an initially Maxwellian plasma $v \propto J$, the boundary of this curve is given by the two values of the action, denoted here as J_1^+ and J_1^-. As the wave is excited, the phase points evolve in time to the curve γ_2 on the right-hand side of Fig. 2.2. Since the flow is Hamiltonian, (2.11) dictates that the phase-space area (in either the θ-p or J-Ψ plane)

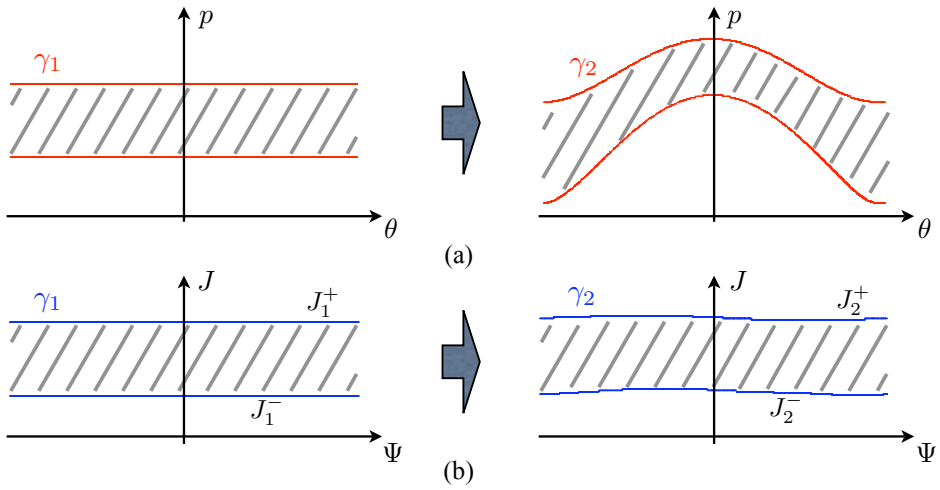

Figure 2.2: Dynamics of a tube of untrapped trajectories slowly driven on resonance. The particles remain essentially uniform in Ψ and can be identified [within $O(\epsilon)$] with a frozen orbit along the upper and lower portions of γ. Since the area enclosed by γ_1 equals that enclosed by γ_2, the difference in J between the boundaries is invariant, although its centroid, or mean $\bar{J}$ may change. Choosing a family of γ_1 indicates that the untrapped distribution is essentially invariant in the difference $J - \bar{J}(\tau)$.

bound by γ_1 equals that bound by γ_2, so that the shaded areas in Fig. 2.2(a) are equal, as are those in Fig. 2.2(b). While this is true in general (the system is Hamiltonian), stronger but approximate conclusions can be drawn when the parameters vary slowly in time. Evidence of this is indicated by Fig. 2.2, where we see that while the shaded region in the θ-p plane undergoes significant deformation, the same area remains approximately rectangular in J-Ψ plane. We explain and use this result to determine a simplified form for the distribution function.

Far from the separatrices, it is clear that the slowness conditions (2.10) imply that the electrons make many oscillations before the parameters of the wave significantly change, so that a set of these particles that is initially uniform in canonical angle remains so under evolution by (2.8). This in turn implies that the particles do not "bunch" in the angle Ψ, so that any change in the shape of γ_1 in the J-Ψ plane must result from changes in J. However, we know that the action changes $\sim O(\epsilon)$ over an orbit, so that the curve of phase trajectories γ_2 can be identified, to $O(\epsilon)$, as the conjunction of two frozen orbits with

definite actions J_2^+ and J_2^- as indicated in Fig. 2.2(b). Note this is only approximately true, as evidenced by the slight $O(\epsilon)$ undulations in J, so that γ_2 is only approximately rectangular in the J-Ψ plane. Nevertheless, under slow evolution the Poincaré-Cartan invariant results in the following relationship [accurate to $O(\epsilon)$] :

$$J_1^+ - J_1^- = J_2^+ - J_2^-. \tag{2.12}$$

Thus, we have shown that the relative difference in the area is invariant under slow, Hamiltonian flow far from the separatrices. By considering a foliation of nested flux tubes $\gamma_{1,2}$, we see that slow evolution leads to an untrapped distribution that is invariant in the action deviation $J - \bar{J}$, with only a slow temporal change in the mean $\bar{J}(\tau)$. This is in a sense a generalization of adiabatic motion for which J itself is taken to be conserved so that, from (2.9), any shift in area would be due to a changing phase velocity (and commensurate frequency shift $\delta\omega$).

The trapped distribution function

As particles approach the separatrix where $H \to \phi_{\max}$ and the nonlinear period logarithmically diverges, the previous arguments based on the curve γ remaining essentially uniform in Ψ with only small deviations in J cannot be used. In this case, we invoke the dynamics obtained via the theory of separatrix crossing in slowly-evolving systems, reviewed in Appendix A (for original references see, e.g., [46, 47, 40, 41]). One central result of these works (and as shown in the Appendix), is that upon crossing the separatrix, the canonical action of any trajectory[1] changes by a fixed amount determined by the change in orbit topology (in our case, this increases the action by a factor of two as the orbit transitions from "rotational" to "librational" motion) and a Ψ-dependent deviation whose magnitude is $O(\epsilon)$. Furthermore, if we consider a set of initial conditions that is uniform in canonical angle and with the same action, the deviation in J averaged over

[1]This is true excluding the exponentially few $\left[\text{i.e., } O\left(e^{-1/\epsilon}/\epsilon\right)\right]$ particles that pass very close to the hyperbolic fixed point. Since these particles can spend an arbitrarily long time tracing the stable manifold, they lead to long, diffuse phase-space tendrils.

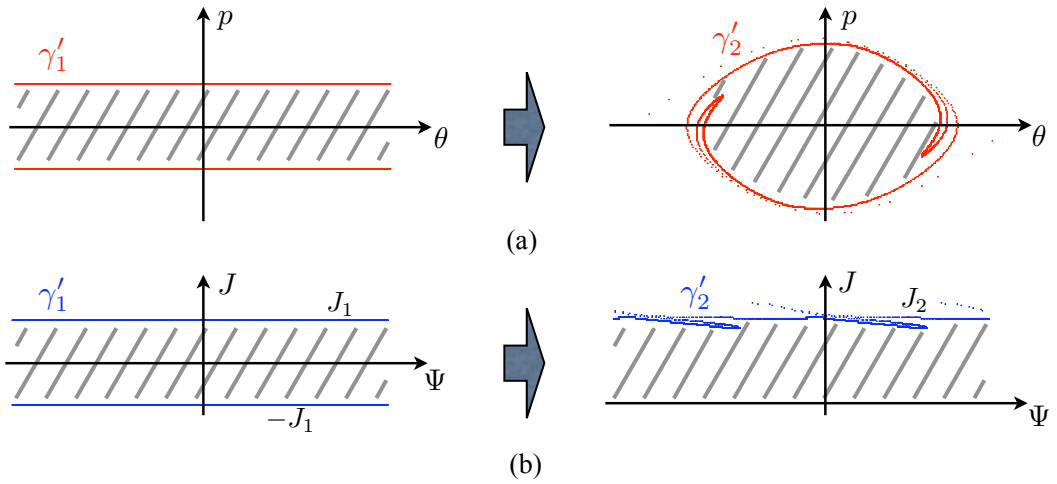

Figure 2.3: Dynamics of a tube of trajectories that become trapped in the wave. The initially symmetric flux tube γ_1' in (a) evolves to γ_2' that can be identified [to $O(\epsilon)$] with the single trapped orbit whose action is $J_2 = 2J_1$, as shown in (b). Further evolution conserves the area enclosed, and therefore the trapped action. Furthermore, while there is some bunching in Ψ (note the striations), a family of γ_1' chosen over a width in J of $O(\epsilon)$ will displace this bunching over the entire range in Ψ (see Fig. 2.4), thereby indicating that the trapped distribution remains uniform in canonical angle and invariant in the canonical action.

these trajectories after crossing vanishes. Thus, to this set of initial conditions one can ascribe [to $O(\epsilon)$] the trapped orbit whose action is twice the initial value.

Returning to the discussion of the trapped particle distribution, we consider an initial flux tube γ_1' whose boundaries are chosen to be symmetric about the phase velocity, i.e., given by the strips of particles initially uniform in canonical angle whose actions are J_1 and $-J_1$ as shown in Fig. 2.3. The Poincaré-Cartan invariant associated with γ_1' is the area between the two segments, and therefore proportional to $2J_1$. Furthermore, from the discussion in the previous paragraph, we can associate the curve γ_2' in the trapped region with the frozen orbit whose action is $2J_1$. Thus, the distribution is transported up to the separatrix in such a way as to conserve the action difference, while after the particles are trapped and essentially following the frozen, trapped orbit, the Poincaré-Cartan invariant (2.11) implies that their canonical action is conserved.

Thus, we have seen that the conclusions regarding action evolution after crossing

into the trapped region are much the same as that for the bulk, the primary difference being that after the separatrix is crossed the curve γ_2' nearly closes, and the action of the trapped distribution is conserved. What we have not shown, however, is how the trapped distribution depends upon the canonical angle. In a naïve picture, the infinitesimal strip of particles in region I with the same action J and spread over $0 \leq \Psi < 2\pi$ would be mapped across the separatrix to the strip from $0 \leq \Psi < \pi$ that then rotates in region II. As shown in [41], this picture is essentially true in the limit $\epsilon \to 0$, although as discussed in the Appendix A, this approximation is corrected by terms $\sim 1/\ln(1/\epsilon)$, which vanish too slowly with ϵ for the parameters considered here[2].

If the angle Ψ were rigidly mapped across the separatrix, than the initial rectangle in the Ψ-J plane from Fig. 2.3(a) would be mapped across the separatrix to the rectangle in (b), only along one-half of the curve γ_2' the value of the distribution would be that transported from the bulk (region I), while the other half would inherit its value from region III. Since there typically are many more particles in the plasma bulk, this in turn implies that along the trapped orbit the distribution would not be uniform in Ψ. In actuality, there are striations in the rectangle as seen in Fig. 2.3 and the distinct values of f are not cleanly divided one-half from the next, but the basic conclusion still holds: along the frozen orbit associated with γ_2' the distribution roughly has two disparate values, one given by what was once the bulk (region I) and the other derived from the passing particles (region III).

To show that the distribution remains, in some approximate sense, uniform in angle, we consider a family of curves whose initial action is in a small neighborhood of J_1 (i.e., initially within $O(\epsilon)$ to the upper boundary of γ_1'). Each curve crosses the separatrix in succession, displaced from the next by a relative phase in the canonical angle up to 2π. Since $\dot{\Psi}$ is of order one, while $\dot{J} \sim \epsilon$, the set of curves initially lying in the plasma bulk results in a "barber-pole" type structure in the Ψ-J plane, with the width in Ψ at fixed

[2]Refs. [39, 40] claim that this "bunching" in Ψ persists in $\epsilon \to 0$ limit; even if this is true, our subsequent arguments will still hold.

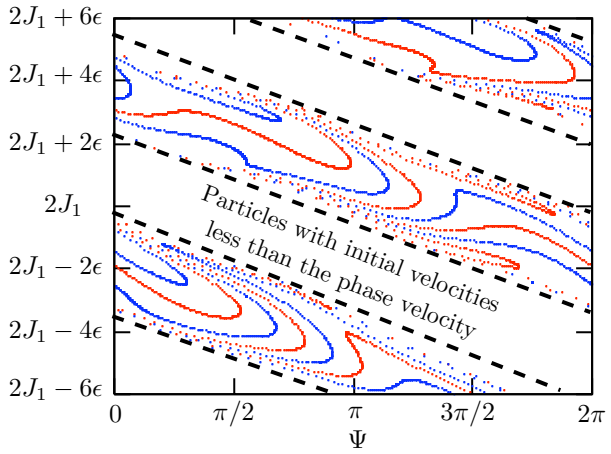

Figure 2.4: The crossing strips associated with the trapped particles originating in the plasma bulk, modeled as a pendulum. Successive red and blue lines were initially spaced about J_1 by an amount ϵ, and each set was initially uniformly distributed in canonical angle. As a result of the crossing, these lines become quite convoluted, but nevertheless occupy a strip whose width in Ψ is approximately π, bounded by lines whose slope is $O(\epsilon)$. The white regions would be occupied by initially passing particles. We see that averaged over scales in J larger than $\sim 4\epsilon$, the distribution is approximately uniform in Ψ.

J of the filled stripes approximately π, while their slope is $O(\epsilon)$. We show an example of this phenomenon in Fig. 2.4, taken from the slowly-evolving pendulum. Fig. 2.4 shows significant undulations and deformations of the lines of initially fixed action; nevertheless, the distribution essentially fills the "crossing ribbon" of width π with a slope $\sim \epsilon$. Furthermore, we see that course-graining the distribution in action over a region whose size $\sim O(\epsilon)$ would average these stripes away, resulting in an approximate distribution that is nearly uniform in canonical angle. Thus, we see that $f(J, \Psi; \tau)$ in the trapped region is, to $O(\epsilon)$, uniform in Ψ as well as being invariant in the canonical action.

From the previous arguments, we have seen that the slowly-evolving distribution function is nearly uniform in canonical angle and parametrized in time by the slowly-evolving mean $\bar{J}(\tau)$. It can therefore be approximately written in the following simple form:

$$\frac{1}{n_0} f_e(J, \Psi; \tau) \equiv f(J, \Psi; \tau) \to \frac{1}{2\pi} f(J; \tau) = \frac{1}{2\pi} f\big(J; \bar{J}(\tau)\big) \,. \tag{2.13}$$

Note that we have scaled $f(J)$ such that its phase space average over one spatial "bucket"

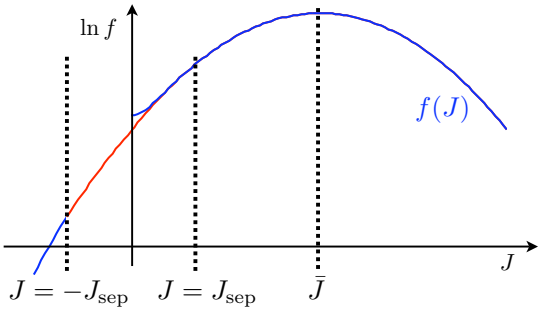

Figure 2.5: Theoretical invariant-in-action distribution, plotted on a log scale and with the action halved in the trapped region so that J is continuous. For this scaling, the blue line $f(J)$ is Maxwellian (along the red), except in the trapping region. In this case, $f = 0$ for $-J_{\rm sep} \leq J \leq 0$, while those particles initially in this portion of the distribution have been added to that for which $0 \leq J \leq J_{\rm sep}$; these additional particles give rise to the slight deviation from the Gaussian, which is most apparent near $J = 0$.

$2\pi/k$ (i.e., over the canonical angle) is approximately[3] unity

$$\int dJ d\Psi \, \tfrac{1}{2\pi} f\big(J; \bar{J}(\tau)\big) = \int dJ \, f\big(J; \bar{J}(\tau)\big) \approx 1. \tag{2.14}$$

In this way, we see that our action *ansatz* approximately holds: the electron distribution function remains essentially invariant in the action difference $J - \bar{J}(\tau)$ for the untrapped particles, and invariant in J itself for the trapped particles. The definition of J (2.9) implies that to lowest order the slowly-excited Langmuir wave gives rise to an overall translation of the distribution in the Ψ-J plane given by the offset $\bar{J}$ which, as we shall see, depends on the potential amplitude. This is to be contrasted with the work of Dewar [25] and Bénisti and Gremillet [42], in which the distribution is taken to be constant in action J, i.e., $\bar{J} \equiv 0$, so that any shift in the phase-space area centroid is compensated by a change in the phase velocity via $\delta\omega$. We explore this important difference further in the next subsection. Finally, since the action J is discontinuous at the separatrices, in subsequent plots we scale the trapped action by a factor of one-half, in which case the distribution averaged over the angle Ψ looks like the schematic plotted in Fig. 2.5.

[3]This average is exactly unity if the external drive is independent of z; slow spatial dependence results in small deviations (which give rise to long-range electrostatic fields).

2.2.3 Action non-conservation in a slowly-evolving system

Previous studies have taken the distribution to be invariant in the action J, largely motivated by earlier work on particle motion in an external, sinusoidal potential. While adiabatic motion far from the separatrix has a rather long history[4], to our knowledge Best [44] was the first to note that the adiabatic invariant was nearly conserved even when crossing the separatrix. The evidence in [44] is purely numerical, but sufficiently compelling to inspire the initial work of Dewar [25]. Subsequently, Timofeev [45] developed the theoretical tools to prove that for the pendulum the action is, to lowest order, conserved at a separatrix crossing. The numerous and independent extensions of Ref. [45] published in 1986 [46, 47, 48] served as the theoretical basis for the invariant-in-action theory presented by Bénisti and Gremillet [42]. While we use this neo-adiabatic theory in Appendix A to derive a few important relations relevant to our previous discussions, we note that the general adiabatic invariance need not, in general, apply to particles moving self-consistently in a plasma wave.

Consider, for the moment, the Lagrangian (co-moving) electron displacement in a cold plasma. In this case, it is well known [49] (and explicitly shown in Sec. 5.2.1) that, below wave-breaking, the restoring force due to the electrostatic field is linearly proportional to the displacement of the particle. Thus, each electron moves in a simple harmonic oscillator potential, with the particle action proportional to the particle energy. In this case, increasing the amplitude (energy) of the electrostatic field requires a commensurate change in the particle action, since the frequency is constant.

From the viewpoint of the particle phase in a slowly-evolving (Eulerian) field, we show in Sec. 5.2.3 that in the cold electrostatic potential there exists an orbit (the cold orbit) for which the frequency is independent of the particle energy. The frequency of nearby orbits is similarly nearly constant, in which case the standard adiabatic theorems do not

[4]The most famous incident being at the 1911 Solvay Conference, when Einstein used action invariance to answer Lorentz's question of what happens in a slowly-varying pendulum initially in some quantum state. Apparently, action invariance in the classical pendulum was first noted by Rayleigh in 1902 [43].

apply. Furthermore, for the orbit with constant frequency we have

$$1 = \omega(H) = \frac{d\Psi}{d\tau} = \frac{\partial \mathcal{H}}{\partial J}, \tag{2.15}$$

so that the full Hamiltonian for the weakly-driven particle phase can be written as

$$\mathcal{H}(J, \Psi; \tau) = J + \mathcal{V}\, \mathcal{H}_1(J, \Psi; \tau), \tag{2.16}$$

with $\mathcal{V} \ll 1$, implying that the coupling to the (bounded) perturbation $\mathcal{H}_1$ is small. For such a weak drive, (2.16) indicates that in order to significantly change the particle energy (and hence, the energy of the Langmuir wave), one must proportionally change the particle action. Note that this action non-conservation is associated with particles in the bulk of the plasma, rather than the result of any complications due to violation of the slowness conditions when crossing the separatrix. Thus, the non-conservation of J is related to the resonance between the drive and the Langmuir wave. Furthermore, as shown in the previous section, any change in action must be reflected, in part, amongst all the untrapped particles due to the incompressible Hamiltonian flow, and therefore the existence of even one such orbit is sufficient to shift the distribution in action.

To illustrate the distributions satisfying our action *ansatz*, we have performed a number of single-wavelength particle simulations, described in greater detail in Sec. 2.4, that solve the periodic Vlasov-Poisson system. We include representative results in Fig. 2.6, obtained with a drive potential $\mathcal{V} = 0.01$ and initial Maxwellian distribution whose width $k\lambda_D \equiv \sigma = 0.3$. In Fig. 2.6(a), we see the characteristic flattening of $f(v)$ near the phase velocity that is associated with particle trapping. For the same values of ϕ_1, Fig. 2.6(b) demonstrates that the distribution in J (integrated over Ψ) remains nearly Gaussian in the canonical action. Note that to obtain this plot we have divided J by two in the resonance region to make the action continuous at the upper separatrix. Furthermore, except for the slight oscillations near the resonance region, $f(J)$ has a constant variance σ^2 and a slightly increasing mean[5] from its inital value ω_L.

[5] Although difficult to see here, $\Delta\bar{J}$ is plotted for comparison in Fig. 2.8.

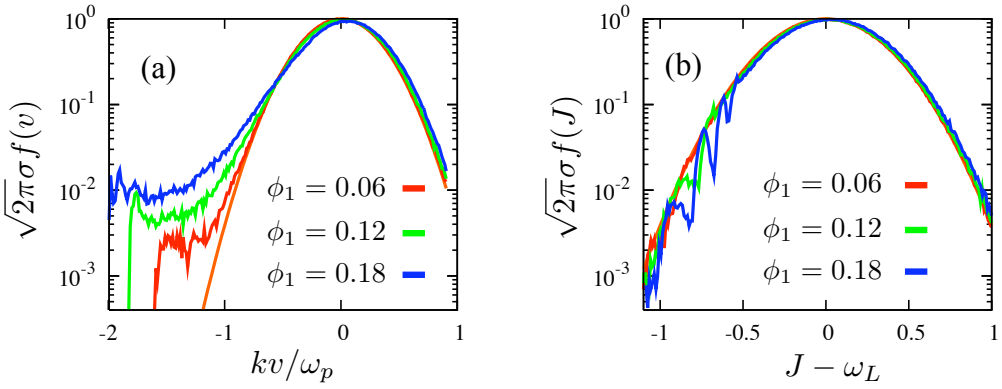

Figure 2.6: Wavelength averaged distribution functions for three values of the electrostatic potential ϕ_1 using $k\lambda_D = 0.3$. In velocity-space, (a) shows the flattening of $f(v)$ near the phase velocity $kv_p/\omega_p \approx 1.16$ that is characteristic of particle trapping. At the same time, (b) demonstrates that the distribution remains nearly invariant in the relative area, with a small change in the mean $\bar{J}$ from ω_L as the wave is excited, and slight oscillations of $f(J)$ in the resonance region.

2.2.4 Parameterizing the nonlinear distribution function

In the previous section we showed that the distribution function satisfies the action *ansatz*, remaining essentially invariant in difference $J - \bar{J}(\tau)$ for the untrapped particles, while invariant in J for the trapped particles. Now we turn to parameterizing this distribution by imposing the constraints of self-consistency, namely, that the assumed distribution function must also act as a source for the appropriate electric field via Maxwell's equations. To facilitate this discussion, we introduce another "area" related to the action J in the following manner:

$$\mathcal{I}(H;\tau) = \frac{1}{2\pi}\oint d\theta\,\sqrt{2[H+\phi]} = J(H;\tau) + \delta\omega \qquad H \geq \phi_{\rm m}, \tag{2.17a}$$

$$\mathcal{I}(H;\tau) = \frac{1}{4\pi}\oint d\theta\,\sqrt{2[H+\phi]} = \frac{1}{2}J(H;\tau) \qquad H < \phi_{\rm m}. \tag{2.17b}$$

Since $\mathcal{I}$ is proportional to the canonical action J, the untrapped distribution is invariant in the difference $\mathcal{I} - \bar{\mathcal{I}}$, while the trapped distribution is invariant in $\mathcal{I}$. Furthermore, the definitions (2.17) suggest a natural method of using the Poisson equation to determine the mean $\bar{\mathcal{I}}(\tau)$ consistent with a given potential amplitude, thereby parameterizing f. From this description, we use the Ampère-Maxwell Law to calculate the frequency shift $\delta\omega$ of

the wave and compare $\delta\omega$ with previous results.

Self-consistency and the Poisson equation

First, our nonlinear distribution function must give rise to a charge separation commensurate with the electrostatic potential $\phi(z,t)$. This is summarized by the Poisson equation (2.1b), which, using the dimensionless potential (2.3) and distribution function (2.13), is

$$\frac{\partial^2\phi}{\partial\zeta^2} = \int du\, \frac{1}{2\pi} f\big[\mathcal{I}(u,\zeta;\phi);\bar{\mathcal{I}}(\tau)\big] - 1. \tag{2.18}$$

Here, $\zeta \equiv kz$ is the scaled longitudinal coordinate, while $u \equiv vk/\omega_p$ is its scaled velocity. The Poisson equation (2.18) is an implicit relationship for the average area $\bar{\mathcal{I}}$ in terms of the full potential ϕ; in order to solve this numerically, we use the dimensionless Fourier-eikonal expansion (2.5). Multiplying (2.18) by $\cos\theta$ and integrating over a wavelength, we obtain:

$$0 = \left[1 + \frac{2}{\phi_1}\left\langle \cos\theta \right\rangle_{\mathcal{PS}}\right] \phi_1 \equiv \varepsilon\big(\bar{\mathcal{I}};\phi\big)\,\phi_1, \tag{2.19}$$

where we have introduced the "nonlinear dielectric function" $\varepsilon\big(\bar{\mathcal{I}};\phi\big)$ and the phase space average

$$\langle \mathcal{X} \rangle_{\mathcal{PS}} \equiv \int_{-\infty}^{\infty} du \int_{-\pi}^{\pi} d\zeta\, \frac{1}{2\pi} f\big[\mathcal{I}(u,\zeta;\phi),\bar{\mathcal{I}}(\tau)\big]\, \mathcal{X}(u,\zeta).$$

Furthermore, the higher harmonics of the potential are given similarly by

$$\phi_n = -\frac{2}{n^2}\left\langle \cos(n\theta) \right\rangle_{\mathcal{PS}}. \tag{2.20}$$

We solve the system (2.19)-(2.20) iteratively as a function of ϕ_1. Our procedure can be summarized with the following (presumably convergent) series:

$$\bar{\mathcal{I}}^{j+1} = \bar{\mathcal{I}}^{j} - \frac{\varepsilon\big(\bar{\mathcal{I}}^j;\phi^j\big)}{\frac{\partial}{\partial\bar{\mathcal{I}}^j}\varepsilon\big(\bar{\mathcal{I}}^j;\phi^j\big)} \tag{2.21a}$$

$$\phi_n^{j+1} = -\frac{2}{n^2}\left\langle \cos(n\theta) \right\rangle_{\mathcal{PS}}. \tag{2.21b}$$

To solve (2.21), we choose a level of ϕ_1 near zero and calculate the mean area $\bar{\mathcal{I}}^1$ and harmonics ϕ_n^1, assuming initial values $\bar{\mathcal{I}}^0 = \omega_L$ and $\phi_n^0 = 0$ [the expression for ω_L is

subsequently given by (2.53)]. We then iterate (2.21) until $\varepsilon(\bar{\mathcal{I}}, \phi) \approx 0$, for which we have $\bar{\mathcal{I}}(\phi_1)$ and the potential $\phi(\zeta)$. We then use these as initial values for the next iteration at a larger value of ϕ_1, thereby mapping out the entire function $\bar{\mathcal{I}}(\phi_1)$.

The Ampère-Maxwell law and resulting frequency shift

To complete the characterization of the action distribution function, we calculate an expression for the frequency shift as a function of the potential amplitude ϕ_1 and the mean $\bar{\mathcal{I}}$. To determine $\delta\omega$, we use the fact that the plasma tends to set up a return current to erase any long-range electric fields. To make this more explicit, we consider the 1-D Coulomb gauge condition: $\boldsymbol{\nabla}\cdot\boldsymbol{A} = \frac{\partial}{\partial z}\big(\hat{\boldsymbol{z}}\cdot\boldsymbol{A}\big) = 0$, implying that the functionally-transverse vector potential can be taken to be geometrically transverse as well, i.e., $\boldsymbol{A}\cdot\hat{\boldsymbol{z}} = 0$. In this case, the longitudinal component of the Ampère-Maxwell equation is given by

$$\frac{\partial^2}{\partial\tau\partial\zeta}\phi(\zeta,\tau) = \int du\, \frac{1}{2\pi} f\big[\mathcal{I}(u,\zeta;\phi), \bar{\mathcal{I}}(\tau)\big]\, u. \tag{2.22}$$

Integrating (2.22) over one period in ζ, we have

$$\frac{\partial^2}{\partial\tau\partial\zeta}\phi(\zeta,\tau) = \int du\, \frac{1}{2\pi} f\big[\mathcal{I}(u,\zeta;\phi), \bar{\mathcal{I}}(\tau)\big]\, u. \tag{2.23}$$

Since we assume the potential $\phi(\zeta,\tau)$ to be slowly-varying, the expression (2.23) approximately vanishes. Note that this would be exactly true in the limit of a time-independent, nonlinear mode (similar to the BGK family), and expresses the fact that the plasma electrons carry no net momentum [50]. Using $u \propto (p - \omega_L) \equiv \big(\frac{d}{d\tau}\theta - \delta\omega - \omega_L\big)$, we have

$$\delta\omega(\tau) = \Big\langle \tfrac{d}{d\tau}\theta \Big\rangle_{\mathcal{PS}} - \omega_L. \tag{2.24}$$

We note, as shown in Ref. [51], that the scale length of the transverse variation must be much greater than the collisionless skin depth c/ω_p for the one-dimensional approximation associated with (2.22) to hold.

2.3 The pendulum Hamiltonian relevant for small values of the potential

To make direct comparisons with previously published results, we compute the linear and small amplitude limits of the mean area $\bar{\mathcal{I}}$ and frequency shift $\delta\omega$. In this limit, for which the electrostatic energy is much greater than the thermal energy, $\phi_1 \ll \sigma^2$, we can assume that the potential consists of a single harmonic, so that $\phi_n = 0$ for $n \geq 2$. This implies that the Hamiltonian (2.8) becomes that of a classical physical pendulum, so that

$$\mathcal{H}(p,\theta;\tau) \to \tfrac{1}{2}[p+\delta\omega(\tau)]^2 + \phi_1(\tau)\big[1-\cos\theta\big]. \tag{2.25}$$

In this case, we can obtain analytical results suitable for comparison to those previously published.

2.3.1 Dynamics of the classical physical pendulum

In this subsection, we review the well-known dynamics of the pendulum Hamiltonian (2.25) relevant for calculating the frequency shift in the small amplitude limit. The canonical action of the pendulum is well-known (see, e.g., [52, Sec. 1.3]), from which we obtain the following expressions:

$$|\kappa| \geq 1: \qquad \mathcal{I}(\kappa) = \mathcal{I}_s \kappa\, \mathscr{E}(1/\kappa) \tag{2.26a}$$

$$|\kappa| < 1: \qquad \mathcal{I}(\kappa) = \mathcal{I}_s\big[\,\mathscr{E}(\kappa) + \big(\kappa^2-1\big)\,\mathscr{K}(\kappa)\big], \tag{2.26b}$$

where we have defined the scaled energy κ and the separatrix action $\mathcal{I}_s$ as

$$\kappa^2 \equiv \frac{H(\tau)}{2\phi_1(\tau)}, \qquad\qquad \mathcal{I}_s \equiv \frac{4}{\pi}\sqrt{\phi_1(\tau)}\,. \tag{2.27}$$

Here, the complete elliptic integrals of the first and second kind, $\mathscr{K}(\kappa)$ and $\mathscr{E}(\kappa)$, are respectively defined in the usual way:

$$\mathscr{K}(\kappa) \equiv \int_0^{\pi/2} d\alpha\, \frac{1}{\sqrt{1-\kappa^2\sin^2\alpha}}, \qquad \mathscr{E}(\kappa) \equiv \int_0^{\pi/2} d\alpha\, \sqrt{1-\kappa^2\sin^2\alpha}\,. \tag{2.28}$$

The nonlinear period is calculated using the Hamiltonian relations

$$\mathcal{T}(\kappa) = \frac{2\pi}{\Omega(\kappa)} = 2\pi \frac{\partial J}{\partial \mathcal{H}} = 2\pi \frac{\partial J}{\partial \kappa} \frac{\partial \kappa}{\partial \mathcal{H}} \,. \tag{2.29}$$

Using the definitions (2.26) and the linear relationship between $\mathcal{I}$ and J, we have

$$|\kappa| \geq 1: \quad \mathcal{T}(\kappa) = \frac{2\,\mathscr{K}(1/\kappa)}{\kappa\sqrt{\phi_1}} \,; \qquad\qquad |\kappa| < 1: \quad \mathcal{T}(\kappa) = \frac{4\,\mathscr{K}(\kappa)}{\sqrt{\phi_1}}. \tag{2.30}$$

In subsequent analysis, we find that more straightforward calculations can be obtained using the scaled energy κ and time τ as variables. Thus, we conclude this section by relating the coordinates (κ, τ) to (p, θ). Using the definitions (2.6) and (2.27), we have

$$p + \delta\omega(\tau) = \frac{d\theta}{d\tau} = 2\kappa\sqrt{\phi_1}\sqrt{1 - (1/\kappa^2)\sin^2(\theta/2)} \,. \tag{2.31}$$

Rewriting this expression, we have

$$|\kappa| \geq 1: \qquad \frac{d(\theta/2)}{\sqrt{1 - (1/\kappa^2)\sin^2(\theta/2)}} = \kappa\sqrt{\phi_1}\, d\tau, \tag{2.32a}$$

$$|\kappa| < 1: \qquad \frac{d\alpha}{\sqrt{1 - \kappa^2 \sin^2\alpha}} = \sqrt{\phi_1}\, d\tau, \tag{2.32b}$$

with $\sin(\theta/2) \equiv \kappa \sin\alpha$. We take the indefinite integral of (2.32), obtaining

$$|\kappa| \geq 1: \ \cos(\theta/2) = \mathrm{cn}\Big(1/\kappa, \kappa\sqrt{\phi_1}\tau\Big) \,, \tag{2.33a}$$

$$|\kappa| < 1: \ \cos(\theta/2) = \mathrm{dn}\Big(\kappa, \sqrt{\phi_1}\tau\Big) \,, \tag{2.33b}$$

where we have set the origin of time to zero without loss of generality, and the functions $\mathrm{cn}(\kappa, x)$ and $\mathrm{dn}(\kappa, x)$ are the Jacobi elliptic functions defined via the inverse of incomplete elliptic integral of the first kind in the usual manner:

$$x(\kappa, y) \equiv \int_0^y dz\, \frac{1}{\sqrt{1 - \kappa^2 \sin^2 z}} \;\Rightarrow\; \cos y \equiv \mathrm{cn}(\kappa, x) \equiv \frac{1}{\kappa}\sqrt{\kappa^2 - 1 + \mathrm{dn}^2(\kappa, x)} \,.$$

Finally, differentiating (2.33) and using (2.31) yields

$$|\kappa| \geq 1: \ p = 2\kappa\sqrt{\phi_1}\ \mathrm{dn}\Big(1/\kappa, \kappa\sqrt{\phi_1}\tau\Big) - \delta\omega(\tau) \tag{2.34a}$$

$$|\kappa| < 1: \ p = 2\kappa\sqrt{\phi_1}\ \mathrm{cn}\Big(\kappa, \sqrt{\phi_1}\tau\Big) - \delta\omega(\tau). \tag{2.34b}$$

Phase space averages

Here, we write compact expressions for phase space averages in the pendulum approximation using the distribution function action *ansatz*, namely that f remains uniform in canonical angle Ψ and invariant in the difference $\mathcal{I} = \bar{\mathcal{I}}$ for the bulk. To begin, we note that for fixed parameters ϕ_1, $\delta\omega$, there exists a canonical transformation on phase space $(p, \theta) \leftrightarrow (H, \tau)$ for which the independent evolution parameter can be taken to be the coordinate θ. Since the transformation is canonical, the Jacobian is unity and we have the following relation between the integration measures:

$$dp\, d\theta = dH\, d\tau = \frac{dH}{d\kappa} d\kappa\, d\tau = 4\phi_1 \kappa\, d\kappa\, d\tau. \tag{2.35}$$

Thus, phase space averages can be written as

$$\left\langle \mathcal{X} \right\rangle_{\mathcal{PS}} \equiv \int_{-\infty}^{\infty} dp \int_{-\pi}^{\pi} d\theta\; f(p, \theta; \tau) \mathcal{X}(p, \theta) \rightarrow \int_{-\infty}^{\infty} d\kappa\; 4\phi_1 \kappa \int_{0}^{\mathcal{T}} d\tau\; f(\kappa; \tau) \mathcal{X}(\kappa, \tau). \tag{2.36}$$

Assuming that the average action does not change significantly during one period of oscillation, i.e., that the slowly-evolving conditions (2.10) are met, we can take the nearly constant distribution $f(\kappa; \tau)$ outside the integral over τ. Hence, in what follows we will suppress the dependence of f on the time τ. Using the definitions (2.26), the invariant distribution function divides into four natural pieces: one of untrapped particles in region I, another below both separatrices in region III, and two associated with the trapped particles of region two, depending on whether they entered from region I (+) or region II (−); these are respectively encapsulated in the following definitions

$$f_{\mathrm{I}}(\kappa) \equiv \frac{\mathcal{I}_s\, \mathscr{K}(1/\kappa)}{\sigma\sqrt{2\pi}} \exp\left[-\tfrac{1}{2\sigma^2} \left\{ \mathcal{I}_s \kappa\, \mathscr{E}(1/\kappa) - \bar{\mathcal{I}} \right\}^2 \right] \tag{2.37a}$$

$$f_{\mathrm{III}}(\kappa) \equiv \frac{\mathcal{I}_s\, \mathscr{K}(1/\kappa)}{\sigma\sqrt{2\pi}} \exp\left[-\tfrac{1}{2\sigma^2} \left\{ \mathcal{I}_s \kappa\, \mathscr{E}(1/\kappa) + \bar{\mathcal{I}} \right\}^2 \right] \tag{2.37b}$$

$$f_{\mathrm{II}}^{\pm}(\kappa) \equiv \frac{\mathcal{I}_s \kappa\, \mathscr{K}(\kappa)}{\sigma\sqrt{2\pi}} \exp\left[-\tfrac{1}{2\sigma^2} \left\{ \mathcal{I}_{\mathrm{s}} \left[\mathscr{E}(\kappa) + (\kappa^2 - 1)\, \mathscr{K}(\kappa) \right] \pm \bar{\mathcal{I}} \right\}^2 \right]. \tag{2.37c}$$

From (2.37), we see that the distribution is essentially Gaussian in the variable $\mathcal{I}$ with a slowly-varying average $\bar{\mathcal{I}}$ and fixed variance σ^2. Furthermore, the definitions (2.37) were

chosen to facilitate the calculation of the phase space average $\langle\cdot\rangle_{\mathcal{PS}}$; our conventions imply that

$$\int_1^\infty d\kappa\ \big[f_{\rm I}(\kappa)+f_{\rm III}(\kappa)\big]+\int_0^1 d\kappa\ \big[f_{\rm II}^-(\kappa)+f_{\rm II}^+(\kappa)\big]=1. \tag{2.38}$$

Using the definitions (2.37) in (2.36), the average of an observable $\mathcal{X}(p,\theta)$ over phase space is written as

$$\begin{aligned}\big\langle\mathcal{X}(p,\theta)\big\rangle_{\mathcal{PS}}=&\int_1^\infty d\kappa\ f_{\rm I}(\kappa)\int_0^{\mathcal{T}}d\tau\ \frac{\mathcal{X}(\kappa,\tau)}{\mathcal{T}(\kappa)}+\int_1^\infty d\kappa\ f_{\rm III}(\kappa)\int_0^{\mathcal{T}}d\tau\ \frac{\mathcal{X}(-\kappa,\tau)}{\mathcal{T}(\kappa)}\\&+\int_0^1 d\kappa\ f_{\rm II}^-(\kappa)\int_0^{\mathcal{T}}d\tau\ \frac{\mathcal{X}(\kappa,\tau)}{\mathcal{T}(\kappa)}+\int_0^1 d\kappa\ f_{\rm II}^+(\kappa)\int_0^{\mathcal{T}}d\tau\ \frac{\mathcal{X}(-\kappa,\tau)}{\mathcal{T}(\kappa)}.\end{aligned} \tag{2.39}$$

2.3.2 BGK-type self-consistency

Now we turn to imposing the constraints of self-consistency in the small-amplitude, pendulum limit. To determine the nonlinear dielectric function (2.19), we calculate the phase space average $\langle\cos\theta(\kappa,\tau)\rangle_{\mathcal{PS}}$. Using the trigonometric identity $\cos\theta=2\cos^2(\theta/2)-1$, the pendulum identity (2.33), and the phase space averaging (2.39), we have

$$\begin{aligned}\big\langle\cos\theta(\kappa,\tau)\big\rangle_{\mathcal{PS}}=&\int_1^\infty d\kappa\ \big[f_{\rm I}(\kappa)+f_{\rm II}(\kappa)\big]\int_0^{\mathcal{T}}d\tau\ \frac{2\,{\rm cn}^2\big(1/\kappa,\kappa\sqrt{\phi_1}\tau\big)-1}{\mathcal{T}(\kappa)}\\&+\int_0^1 d\kappa\ \big[f_{\rm II}^-(\kappa)+f_{\rm II}^+(\kappa)\big]\int_0^{\mathcal{T}}d\tau\ \frac{2\,{\rm dn}^2\big(\kappa,\kappa\sqrt{\phi_1}\tau\big)-1}{\mathcal{T}(\kappa)}.\end{aligned} \tag{2.40}$$

The integral over τ can be taken analytically; using the integral tables of Gradshteyn and Ryzhik [53, pp 630], we obtain the following expression for the nonlinear dielectric function (Eq. 2.19):

$$\begin{aligned}\varepsilon\big(\bar{\mathcal{I}},\phi_1\big)=1+&\frac{2}{\phi_1}\int_1^\infty d\kappa\ \big[f_{\rm I}(\kappa)+f_{\rm III}(\kappa)\big]\left[2\kappa^2\frac{\mathscr{E}(1/\kappa)}{\mathscr{K}(1/\kappa)}+1-2\kappa^2\right]\\&+\frac{2}{\phi_1}\int_0^1 d\kappa\ \big[f_{\rm II}^+(\kappa)+f_{\rm II}^-(\kappa)\big]\left[2\frac{\mathscr{E}(\kappa)}{\mathscr{K}(\kappa)}-1\right].\end{aligned} \tag{2.41}$$

Requiring (2.41) to vanish gives an implicit relationship between ϕ_1 and $\bar{\mathcal{I}}$; to obtain an explicit expression for $\bar{\mathcal{I}}(\phi_1)$, we expand the nonlinear dielectric function for small changes

in $\bar{\mathcal{I}}$. For an initially Maxwellian plasma with no electrostatic field, the mean action in the moving frame is equal to the linear frequency ω_L, and we have the expansion:

$$0 = \varepsilon(\omega_L, \phi_1) + \left(\bar{\mathcal{I}} - \omega_L\right) \frac{\partial}{\partial \bar{\mathcal{I}}} \varepsilon\left(\bar{\mathcal{I}}, \phi_1\right)\Big|_{\bar{\mathcal{I}}=\omega_L} + \cdots . \tag{2.42}$$

Rewriting the Taylor expansion (2.42) yields the following expression for the mean frequency-shifted action in terms of potential amplitude:

$$\bar{\mathcal{I}} \approx \omega_L - \frac{\varepsilon(\omega_L, \phi_1)}{\frac{\partial}{\partial \omega_L} \varepsilon(\omega_L, \phi_1)}. \tag{2.43}$$

The equation (2.43) determines the mean frequency-shifted action $\bar{\mathcal{I}}$ required to support the potential of amplitude ϕ_1. In previous works, the right-hand side of (2.43) was identified as the frequency shift of the wave, not the change in action of the distribution. We will see that in the small ϕ_1 limit the change in action equals the change in the frequency. This is because the particle action J is essentially constant in this case, so that $\mathcal{I} \propto p$ implies that a change in $\mathcal{I}$ is due to a decrease in the phase velocity of the wave at fixed k [i.e., given by $\delta\omega(\tau)$]. As the wave amplitude becomes appreciable, however, the plasma bulk becomes excited and the particle action J begins to increase, so that $\delta\omega(\tau) < \bar{\mathcal{I}}(\tau) - \omega_L$ and (2.43) can no longer be considered to be simply equal to the frequency shift.

In subsequent sections we calculate the shift in mean action (2.43) analytically in the linear and small ϕ_1 limit, for which we find it convenient to integrate (2.41) by parts. The boundary terms at $\kappa = 0,\ \pm\infty$ vanish, while those at $\kappa = 1$ cancel, leaving us with the following expression for the dielectric function:

$$\begin{aligned} \varepsilon(\omega_L, \phi_1) = 1 &+ \int_1^\infty d\kappa\ \frac{h(\kappa)}{\mathcal{I}_s} \left\{ f_{\mathrm{I}}(\kappa)\Big[\mathcal{I}(\kappa) - \omega_L\Big] + f_{\mathrm{III}}(\kappa)\Big[\mathcal{I}(\kappa) + \omega_L\Big] \right\} \\ &+ \int_0^1 d\kappa\ \frac{q(\kappa)}{\mathcal{I}_s} \left\{ f_{\mathrm{II}}^-(\kappa)\Big[\mathcal{I}(\kappa) - \omega_L\Big] + f_{\mathrm{II}}^+(\kappa)\Big[\mathcal{I}(\kappa) + \omega_L\Big] \right\}, \end{aligned} \tag{2.44}$$

where

$$\begin{aligned} h(\kappa) &\equiv \frac{32}{3\pi^2\sigma^2}\Big[(2\kappa^3 - \kappa)\,\mathscr{E}(1/\kappa) - 2(\kappa^3 - \kappa)\,\mathscr{K}(1/\kappa)\Big] \\ q(\kappa) &\equiv \frac{32}{3\pi^2\sigma^2}\Big[(2\kappa^2 - 1)\,\mathscr{E}(\kappa) - (\kappa^2 - 1)\,\mathscr{K}(\kappa)\Big] \end{aligned}$$

and we take the convention that $\bar{\mathcal{I}} \to \omega_L$ in any of the distribution functions $f_s(\kappa)$ ($s =$ I, II, III) when evaluating (2.44). Taking the derivative of (2.44), we obtain

$$\begin{aligned}\frac{\partial}{\partial\omega_L}\varepsilon(\omega_L,\phi_1) = &\int_1^\infty d\kappa\ \frac{h(\kappa)}{\mathcal{I}_s}\left\{f_{\rm I}(\kappa)\left[\tfrac{(\mathcal{I}(\kappa)-\omega_L)^2}{\sigma^2}-1\right]-f_{\rm III}(\kappa)\left[\tfrac{(\mathcal{I}(\kappa)+\omega_L)^2}{\sigma^2}-1\right]\right\}\\ &+\int_0^1 d\kappa\ \frac{q(\kappa)}{\mathcal{I}_s}\left\{f_{\rm II}^-(\kappa)\left[\tfrac{(\mathcal{I}(\kappa)-\omega_L)^2}{\sigma^2}-1\right]-f_{\rm II}^+(\kappa)\left[\tfrac{(\mathcal{I}(\kappa)+\omega_L)^2}{\sigma^2}-1\right]\right\}.\end{aligned} \tag{2.45}$$

Finally, we obtain an explicit expression for the frequency shift in the Langmuir wave (2.24). To obtain $\delta\omega(\tau)$, we use the pendulum formula (2.34), which gives the momentum in terms of Jacobi elliptic functions and the frequency shift $\delta\omega(\tau)$. By definition, in the moving frame the average velocity of the trapped particles is zero [mathematically, the integral of $\mathrm{cn}(\kappa,x)$ from 0 to $4\,\mathscr{K}(\kappa)$ vanishes], and (2.24) can be written as

$$\omega_L+\delta\omega(\tau) = \int_1^\infty d\kappa\ \frac{f_{\rm I}(\kappa)-f_{\rm III}(\kappa)}{\mathcal{T}(\kappa)}\int_0^{\mathcal{T}} d\tau\ 2\kappa\sqrt{\phi_1}\ \mathrm{dn}\Big(1/\kappa,\kappa\sqrt{\phi_1}\tau\Big). \tag{2.46}$$

We can take the τ integral analytically using Gradshteyn and Ryzhik [53, pp 630]:

$$\delta\omega = \int_1^\infty d\kappa\ \frac{4\phi_1\kappa}{\sqrt{2\pi}\sigma}\left\{e^{-\frac{1}{2\sigma^2}\left[\mathcal{I}_s\kappa\,\mathscr{E}(1/\kappa)-\bar{\mathcal{I}}\right]^2}-e^{-\frac{1}{2\sigma^2}\left[\mathcal{I}_s\kappa\,\mathscr{E}(1/\kappa)+\bar{\mathcal{I}}\right]^2}\right\}-\omega_L. \tag{2.47}$$

From the formula for the mean frequency-shifted action (2.43), with the numerator and denominator given by (2.41) and (2.45), respectively, the equation for the frequency shift (2.47) completely determines the weakly-driven, BGK-type solution. In the next two sections we compare our results with previous calculations, discussing in what limits our results mirror those. We conclude this chapter with some numerical comparisons of our theoretical results with those obtained from particle simulations.

The dielectric function in the linear limit

Here, we present the linear limit of (2.43), i.e., the limit as $\phi_1 \to 0$. In this limit, the mean action is that corresponding to the phase velocity of the infinitesimal wave, $\bar{\mathcal{I}} \to \omega_L$. Since the denominator in (2.43) is well-behaved and (2.45) is neither zero nor infinite as

$\phi_1 \to 0$, the linear limit is characterized by

$$\lim_{\phi_1 \to 0} \varepsilon(\omega_L, \phi_1) = 0. \tag{2.48}$$

To evaluate this limit from the integral expression (2.44), some care must be taken. A cursory inspection of the integrals in (2.44) seems to indicate that the terms $\sim \mathcal{I}_{\rm s}$ vanish as $\sqrt{\phi_1}$, while the terms $\sim \omega_L$ cancel. While this does hold true for the trapped particles (the integral from 0 to 1), the infinite limit on the integral over the bulk of the distribution invalidates such naïve analysis. This is because when $\phi_1 \equiv 0$, the integrand $h(\kappa) \sim 1/\kappa$ for $\kappa \gg 1$, and the integral formally diverges. For this reason, we must work a little harder to obtain the appropriate $\phi_1 \to 0$ limit. Replacing the distributions $f_s(\kappa)$ with their definitions (2.37), we determine

$$\lim_{\phi_1 \to 0} \left\{ 1 + \int_1^\infty d\kappa \, \frac{h(\kappa)\, \mathscr{K}(1/\kappa)}{\sigma\sqrt{2\pi}} \left[\Big(\mathcal{I}_{\rm s} \kappa\, \mathscr{E}(1/\kappa) - \omega_L \Big) e^{-\frac{\{\mathcal{I}_{\rm s}\kappa\, \mathscr{E}(1/\kappa) - \omega_L\}^2}{2\sigma^2}} + \Big(\mathcal{I}_{\rm s} \kappa\, \mathscr{E}(1/\kappa) + \omega_L \Big) e^{-\frac{\{\mathcal{I}_{\rm s}\kappa\, \mathscr{E}(1/\kappa) + \omega_L\}^2}{2\sigma^2}} \right] \right\}. \tag{2.49}$$

To calculate (2.49), we note that as $\phi_1 \to 0$, the integrand vanishes exponentially for small κ. Thus, we consistently take $\kappa \gg 1$, for which we have

$$\sigma^2 h(\kappa)\, \mathscr{K}(1/\kappa) \approx \frac{1}{\kappa} + O\big(1/\kappa^3\big) \qquad\qquad \mathcal{I}_s \kappa\, \mathscr{E}(1/\kappa) \approx \sqrt{\phi_1}\big[2\kappa + O(1)\big]. \tag{2.50}$$

Defining the dummy variables x and y such that

$$\sigma x \equiv 2\kappa\sqrt{\phi_1} + \omega_L\,, \qquad\qquad \sigma y \equiv -2\kappa\sqrt{\phi_1} + \omega_L\,, \tag{2.51}$$

and using the large κ relations (2.50), we find that $\lim_{\phi_1 \to 0} \varepsilon(\omega_L, \phi_1) = 0$ yields

$$0 = \sigma^2 + 1 + \frac{\omega_L/\sigma}{\sqrt{2\pi}} \lim_{\phi_1 \to 0} \left\{ \int_{\frac{\omega_L}{\sigma} + 2\sqrt{\phi_1}}^{\infty} dx \, \frac{e^{-x^2/2}}{x - \omega_L/\sigma} + \int_{-\infty}^{\frac{\omega_L}{\sigma} - 2\sqrt{\phi_1}} dy \, \frac{e^{-y^2/2}}{y - \omega_L/\sigma} \right\}. \tag{2.52}$$

As we can see, the $\phi_1 \to 0$ limit gives a prescription for treating the resonant pole at $x = \omega_L/\sigma$: the symmetric limit is defined to be the Cauchy Principal Value. Note that this

is the standard pole occurring when the particle velocity equals the phase velocity of the wave (or, in our language, when the particle action equals that of the separatrix defined by the infinitesimal wave). Denoting the principal value by $\mathscr{P}$, we have shown that

$$\lim_{\phi_1 \to 0} \varepsilon(\omega_L, \phi_1) = 1 + \frac{1}{\sigma^2}\left[1 + \frac{\omega_L/\sigma}{\sqrt{2\pi}}\, \mathscr{P}\int_{-\infty}^{\infty} dx\, \frac{e^{-x^2/2}}{x - \omega_L/\sigma}\right] = 0. \tag{2.53}$$

The condition (2.53) is nothing more than the linear plasma dispersion relation as found by Vlasov [54]. While this is encouraging, one may wonder what happened to Landau damping. Mathematically, we see that our calculation and Landau's yield different prescriptions for treating the pole at the particle phase velocity in the plasma dispersion relation. The difference arises from our considering a distribution uniform in canonical angle with a small, self-consistent electric field, rather than treating the problem as an initial value problem (in the literature, these two assumptions are respectively referred to as the "adiabatic" and "sudden" approximations).

Physically, our lack of any damping appears because we have assumed that the distribution is completely phase-mixed near the separatrix. As shown by O'Neil [6], such phase-mixing causes linear Landau damping to be a transient effect that itself decays away on the bounce time scale $\sim 1/\sqrt{\phi_1}$, which diverges as $\phi_1 \to 0$. Thus, our analysis and the dispersion relation (2.53) apply to finite amplitude waves only after several bounce periods have passed. In this case, the distribution evolves to become nearly uniform in canonical angle so that Landau damping has been "washed out." This interpretation gains additional credence in light of the existence of small-amplitude Bernstein-Greene-Kruskal (BGK) waves [7]. As shown in [33] and [55], the dispersion relation of small amplitude, nearly sinusoidal BGK waves is that of Vlasov rather than Landau, and is identical to (2.53) derived here.

The mean frequency shifted action $\bar{\mathcal{I}}$ and the nonlinear frequency shift $\delta\omega$ in the small amplitude limit

In this subsection, we calculate the change in the mean action (2.43) and frequency shift (2.47) induced by the near-resonant particles, assuming the amplitude of the potential ϕ_1 is small. To make the expanded integrals of $\varepsilon(\omega_L, \phi_1)$ manifestly convergent, we start by first "rewriting the 1" in the expression for the dielectric function (2.44). Assuming the linear dispersion relation (2.53) is satisfied, in terms of the energy κ we have

$$1 = -\mathscr{P}\int_{-\infty}^{\infty} d\kappa \left[2\kappa\sqrt{\phi_1} - \omega_L\right] \frac{e^{-\frac{1}{2\sigma^2}\left(2\sqrt{\phi_1}\kappa - \omega_L\right)^2}}{\kappa\sqrt{2\pi}\sigma^3}. \tag{2.54}$$

By appropriately partitioning the κ integration, we express (2.54) as a sum of integrals whose limits are such that $1 \leq \kappa < \infty$ or $0 \leq \kappa \leq 1$. In this form, we can replace the σ^2 in the nonlinear dielectric function (2.44) by the integral expression (2.54). Thus, the nonlinear dielectric function is given by

$$\begin{aligned}
\varepsilon(\omega_L, \phi_1) = &\int_1^{\infty} d\kappa \left\{ \Big[\mathcal{I}(\kappa) - \omega_L\Big] h(\kappa) f_{\mathrm{I}}(\kappa) - \frac{2\kappa\sqrt{\phi_1} - \omega_L}{\kappa\sqrt{2\pi}\sigma^3} e^{-\frac{\left(2\kappa\sqrt{\phi_1} - \omega_L\right)^2}{2\sigma^2}} \right\} \\
&+ \int_1^{\infty} d\kappa \left\{ \Big[\mathcal{I}(\kappa) + \omega_L\Big] h(\kappa) f_{\mathrm{III}}(\kappa) - \frac{2\kappa\sqrt{\phi_1} + \omega_L}{\kappa\sqrt{2\pi}\sigma^3} e^{-\frac{\left(2\kappa\sqrt{\phi_1} + \omega_L\right)^2}{2\sigma^2}} \right\} \\
&+ \int_0^{1} d\kappa \left\{ \Big[\mathcal{I}(\kappa) - \omega_L\Big] q(\kappa) f_{\mathrm{II}}^{-}(\kappa) - \frac{2\kappa\sqrt{\phi_1} - \omega_L}{\kappa\sqrt{2\pi}\sigma^3} e^{-\frac{\left(2\kappa\sqrt{\phi_1} - \omega_L\right)^2}{2\sigma^2}} \right\} \\
&+ \int_0^{1} d\kappa \left\{ \Big[\mathcal{I}(\kappa) + \omega_L\Big] q(\kappa) f_{\mathrm{II}}^{+}(\kappa) - \frac{2\kappa\sqrt{\phi_1} + \omega_L}{\kappa\sqrt{2\pi}\sigma^3} e^{-\frac{\left(2\kappa\sqrt{\phi_1} + \omega_L\right)^2}{2\sigma^2}} \right\}.
\end{aligned} \tag{2.55}$$

The expression (2.55) is perfectly well-defined in the small amplitude limit, and this limit is simple to calculate numerically. Taylor expanding the first two integrals, we have the contribution

$$\begin{aligned}
&\int_1^{\infty} d\kappa \left[\frac{3\pi^3}{64} - h(\kappa)\kappa\,\mathscr{E}(1/\kappa)\,\mathscr{K}(1/\kappa)\right] \\
&\qquad \times \frac{256}{3\pi^3}\sqrt{\phi_1}\left(\frac{\omega_L^2}{\sigma^2} - 1\right)\frac{e^{-\omega_L^2/2\sigma^2}}{\sigma\sqrt{2\pi}} \approx -1.5016\sqrt{\phi_1}\left(\frac{\omega_L^2}{\sigma^2} - 1\right)\frac{\exp\left(\frac{-\omega_L^2}{2\sigma^2}\right)}{\sqrt{2\pi}\sigma^3},
\end{aligned}$$

while the last two integrals of (2.55) yield

$$\int_0^1 d\kappa \left\{ \frac{3\pi^3}{64} - \kappa q(\kappa)\,\mathscr{K}(\kappa)\big[\,\mathscr{E}(\kappa) + (\kappa^2-1)\,\mathscr{K}(\kappa)\big] \right\}$$

$$\times \frac{256}{3\pi^3}\sqrt{\phi_1}\left(\frac{\omega_L^2}{\sigma^2}-1\right)\frac{e^{-\omega_L^2/2\sigma^2}}{\sigma\sqrt{2\pi}} \approx 2.5905\sqrt{\phi_1}\left(\frac{\omega_L^2}{\sigma^2}-1\right)\frac{\exp\left(\frac{-\omega_L^2}{2\sigma^2}\right)}{\sqrt{2\pi}\sigma^3}.$$

Adding these contributions, we find that the small amplitude behavior of the nonlinear dielectric function is

$$\lim_{\phi_1\to 0}\varepsilon(\omega_L,\phi_1) = 1.089\sqrt{\phi_1}\left(\frac{\omega_L^2}{\sigma^2}-1\right)\frac{\exp\left(\frac{-\omega_L^2}{2\sigma^2}\right)}{\sqrt{2\pi}\sigma^3}. \tag{2.56}$$

A similar expression for the small amplitude dielectric function has been derived by a number of authors, although there is some variation in the $O(1)$ coefficient replacing our 1.089 pre-factor. Interestingly, our coefficient is identical to that of Dewar [25], who calculated the frequency shift assuming a small but finite sinusoidal wave that is adiabatically excited; other calculations in a similar regime have obtained values of 1.41 (Manheimer and Flynn [23]), 1.76 (Rose and Russell [35]) and 1.60 (Barnes [56]). It should be noted that these all differ slightly from the coefficient of 1.63 calculated by Morales and O'Neil [24] and separately by Dewar [25] for an instantaneously excited wave (i.e., the initial value problem starting from a Maxwellian plasma). The majority of these authors then determine the nonlinear frequency shift using an expression similar to (2.43); we will see that this yields accurate results provided that $\phi_1 \lesssim v_{th}^2/v_p^2 \equiv \sigma^2$.

To complete the small amplitude results for the change in the average action (2.43), we calculate $\lim_{\phi_1\to 0}\left[\frac{\partial}{\partial\omega_L}\varepsilon(\omega_L,\phi_1)\right]$, i.e., the small amplitude limit of (2.45). Differentiating the linear dielectric function (2.53) and integrating by parts, we obtain

$$\lim_{\phi_1\to 0}\frac{\partial}{\partial\omega_L}\varepsilon(\omega_L,\phi_1) = \frac{1}{\sqrt{2\pi}\sigma^3}\,\mathscr{P}\int_{-\infty}^{\infty} dx\,\frac{1-x^2}{x-\omega_L/\sigma}e^{-x^2/2} \tag{2.57}$$

$$= \frac{1}{\omega_L\sigma^2}\left(\omega_L^2 - 1 - \sigma^2\right), \tag{2.58}$$

and the second equality arises by enforcing the linear dispersion relation (2.53). Collecting the results (2.56) and (2.58) into (2.43), we find that, for small values of ϕ_1, the change in

the mean action is given by

$$\begin{aligned}\bar{\mathcal{I}}(\tau) - \omega_L &\approx -1.089\,\omega_L\sqrt{\phi_1}\,\frac{\left(\frac{\omega_L^2}{\sigma^2}-1\right)e^{-\omega_L^2/2\sigma^2}}{\left(\omega_L^2-1-\sigma^2\right)\sqrt{2\pi}\sigma} \\ &= -1.089\sqrt{\phi_1}\,\frac{\omega_L\sigma^2}{\omega_L^2-1-\sigma^2}f''(u)\Big|_{u=\omega_L}, \end{aligned} \tag{2.59}$$

with the distribution given by the Maxwellian $f(u) = \exp(-u^2/2\sigma^2)/\left(\sigma\sqrt{2\pi}\right)$.

We conclude by calculating the difference between the frequency-shifted average action and the frequency; in this limit, $\bar{\mathcal{I}} - (\omega_L + \delta\omega) = \bar{J}$, which we will show is $O(\phi_1^{3/2})$. Using the definition $\bar{\mathcal{I}} \equiv \langle\mathcal{I}\rangle$ and the expression for the frequency shift (2.47), we find that

$$\begin{aligned}\bar{\mathcal{I}} - \left(\omega_L + \delta\omega\right) = &\int_1^\infty d\kappa \left[\mathcal{I}(\kappa) - \frac{\pi\kappa\sqrt{\phi_1}}{\mathscr{K}(1/\kappa)}\right]\left[f_{\mathrm{I}}(\kappa) - f_{\mathrm{III}}(\kappa)\right] \\ &+ \int_0^1 d\kappa\,\mathcal{I}(\kappa)\left[f_{\mathrm{II}}^-(\kappa) - f_{\mathrm{II}}^+(\kappa)\right].\end{aligned}$$

It can be shown that both integrals separately vanish in the limit $\phi_1 \to 0$. Taylor expanding the integrals for small values of the potential ϕ_1, we find that

$$\begin{aligned}\bar{\mathcal{I}} - \left(\omega_L + \delta\omega\right) &\approx \frac{32}{\pi}\frac{\omega_L}{\sigma^2}\frac{e^{-\omega_L^2/2\sigma^2}}{\sigma\sqrt{2\pi}}\phi_1^{3/2}\left\{\int_1^\infty d\kappa\;\mathscr{E}(1/\kappa)\left[\frac{4\kappa^2}{\pi^2}\mathscr{E}(1/\kappa)\,\mathscr{K}(1/\kappa) - \kappa^2\right]\right. \\ &\qquad\left. + \int_0^1 d\kappa\,\frac{4\kappa}{\pi^2}\mathscr{K}(\kappa)\left[\mathscr{E}(\kappa) + (\kappa^2-1)\,\mathscr{K}(\kappa)\right]\right\} \\ &= \frac{64}{9\pi}\frac{\omega_L}{\sigma^2}\frac{e^{-\omega_L^2/2\sigma^2}}{\sigma\sqrt{2\pi}}\phi_1^{3/2}. \end{aligned} \tag{2.60}$$

Thus, we see that the average action $\bar{J}$ grows as $\phi_1^{3/2}$ for ϕ_1 small. For Langmuir wave amplitudes such that the right-hand side of (2.60) can be neglected, the frequency shift is equal to the change in the frequency-shifted action $\mathcal{I}$, and the canonical action is approximately conserved.

2.4 Comparison of theory with Vlasov simulations

In this section, we compare our theoretical results for the properties of the slowly-driven nonlinear Langmuir waves with those obtained from particle simulations. Before

discussing these examples, we make a few comments on the numerical methods. In these single-wavelength simulations, we numerically solve the equations of motion with periodic boundary conditions for the electrons and the electric field, driven by an external force. For a single wavelength with N macro-particles, an electron with coordinate $\zeta_j \equiv kz_j$ experiences the combined self-consistent electrostatic force and prescribed drive, giving rise to the following equation of motion:

$$\begin{aligned}\frac{d^2}{d\tau^2}\zeta_j(\tau) = \sum_{m=1}^{M}\frac{1}{N}\sum_{\ell=1}^{N}\frac{2}{m}\sin\big[m\zeta_j(\tau) - m\zeta_\ell(\tau)\big] \\ + \mathcal{V}(\tau)\cos(\omega_L\tau + \zeta_j) - \mathcal{E}_0(\tau),\end{aligned} \tag{2.61}$$

where we have expanded the electrostatic potential in M harmonics, each of which is a sum over the N macro-particles. This is a standard technique of the free electron laser community [57], although here we have also retained the DC field $\mathcal{E}_0$ [58], to be calculated using the longitudinal component of the Ampère-Maxwell law:

$$\frac{d}{d\tau}\mathcal{E}_0(\tau) = \frac{1}{N}\sum_{\ell=1}^{N}\frac{d}{d\tau}\zeta_\ell(\tau). \tag{2.62}$$

For the examples shown here, we use $N \approx 10^6$ particles and $M \approx 32$ harmonics. We solve the system (2.61-2.62) for a given drive potential $\mathcal{V}(\tau)$ using a symplectic operator-splitting scheme that is second-order accurate in time.

To compare the simulation results to our theory, we slowly turn on the ponderomotive drive, ramping the electrostatic field to a chosen amplitude, at which point we slowly turn the drive off. By taking the discrete Hilbert transform of the potential ϕ, we obtain the total frequency $(\omega_L + \delta\omega)$, from which we extract the frequency shift for a given amplitude ϕ_1. These results are shown in Fig. 2.7, where we compare the frequency shift extracted from simulation to the theory of Dewar [25] and Bénisti and Gremillet [42] using action invariance (dashed green line) and to our theory (solid red line) for four different values of $k\lambda_D \equiv \sigma$: $k\lambda_D = 0.4$ (a), $k\lambda_D = 0.3$ (b), $k\lambda_D = 0.2$ (c), and $k\lambda_D = 0.1$ (d). Furthermore, we include the lowest order results (orange dotted line) given by Morales and O'Neil [24] and Dewar [25], $\delta\omega \sim \sqrt{\phi_1}f''(\omega_L)$, expressed in (2.59). We obtain the green dashed line

corresponding to the nonlinear invariant action theory of the Dewar/Bénisti by solving the equations (2.21) and taking $\delta\omega = \bar{\mathcal{I}} - \omega_L$ of the untrapped particles. Our action *ansatz* theory (red line) then uses this expression for the mean area to determine the frequency shift via (2.24).

The range of ϕ_1 over which $\delta\omega$ was measured in Fig. 2.7 includes all electrostatic amplitudes that were attained via resonant excitation with the peak drive amplitude $\mathcal{V} = 0.01$ and frequency equal to ω_L. Further driving of the plasma results in a ringing of ϕ_1 that we interpret as resulting from the detuning of the nonlinear Langmuir wave from the external drive (as observed and explained numerically in Ref. [59]).

As we can see in Fig. 2.7, the Dewar/Bénisti theory agrees with our results assuming that $\phi_1 \ll \sigma^2$, but deviates at larger values of the potential. For warm plasmas such that $\sigma = 0.4$, Fig. 2.7(a) shows that the two theories closely agree over the entire range of attained values of ϕ_1, with the simulation results more or less lying on top of the two. In this case, the action J is nearly conserved, since its deviation (2.60) scales as $f'(v_p)\phi_1^{3/2} \ll \delta\omega$, and the pendulum results of Sec. 2.3.1 mimic all the essential features of the dynamics.

However, for colder plasmas that can be driven to larger amplitudes, the discrepancy between the theories becomes apparent. Fig. 2.7(b) indicates that while the qualitative features of the two theories are similar for $\sigma = 0.3$, their quantitative predictions can differ by nearly a factor of two. In this case, we see that the simulation results favor our action *ansatz* that the distribution remains invariant in the action difference $J - \bar{J}$ for the bulk and invariant in J for the trapped particles, rather than the direct invariant-in-action distribution theory of Dewar and Bénisti and Gremillet.

For the relatively cold plasmas with $\sigma = 0.2$ and $\sigma = 0.1$, Fig. 2.7(c)-(d) indicates that taking the distribution to be invariant in the presumably conserved action results in a positive value for the frequency shift. This positive $\delta\omega$ was predicted theoretically using action conservation in Ref. [60], although we see that this result is not borne out by the Vlasov simulations. On the other hand, the distribution corresponding to our action *ansatz* closely follows the simulation points of $\delta\omega$ for $k\lambda_D = 0.2$; for $k\lambda_D = 0.1$ our theory

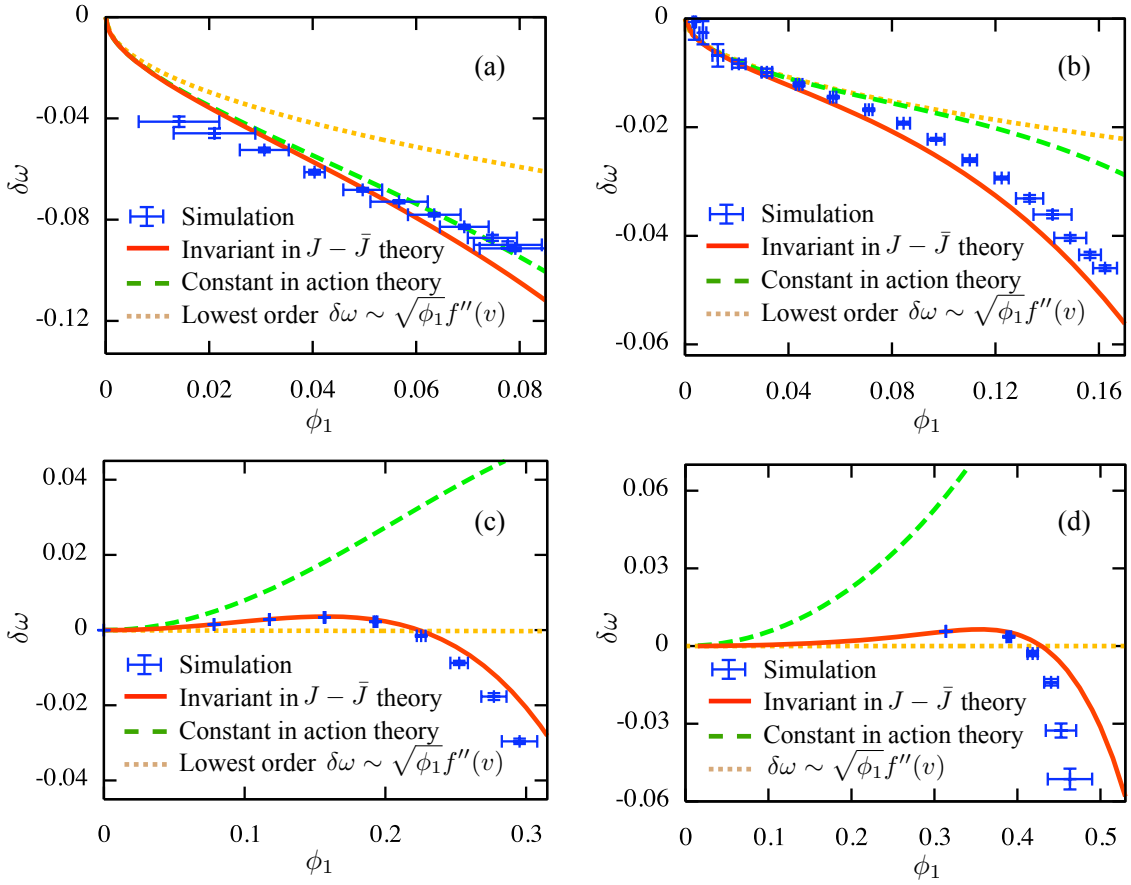

Figure 2.7: Nonlinear frequency shift for four different temperatures: $k\lambda_D = 0.4$ (a), $k\lambda_D = 0.3$ (b), $k\lambda_D = 0.2$ (c), and $k\lambda_D = 0.1$ (d). The points are obtained from particle simulations, with error bars indicating two standard deviations in the output. This "error" was due to uncertainty arising from the residual ringing in the electrostatic amplitude after the drive was turned off, along with oscillations in the measured frequency of the Langmuir wave. We see that the theoretical value of $\delta\omega$ from the action *ansatz* distribution (solid line) agrees quite well with the simulation results, which are only closely represented by the Dewar and Bénisti theory of constant action for $\phi_1 \ll \sigma^2$. To compare with the well known lowest order result $\delta\omega \sim f''(v)\sqrt{\phi_1}$ first given by Morales and O'Neil and Dewar, we also include the orange dotted line, whose equation is given by (2.59). To calculate our theoretical frequency shift (red line), we obtain f by solving the equations associated with a distribution invariant in $\mathcal{I} - \bar{\mathcal{I}}(\tau)$, (2.21), and use (2.24) to obtain $\delta\omega$.

is qualitatively the same, but some quantitative difference arises for the highest amplitude plasma waves, from which $\phi_1 \sim 0.45$.

The basic lesson of Fig. 2.7 is that assuming that the distribution in invariant in a constant action [i.e., $\bar{J}(\phi_1) = 0$] yields reliable results only if $\phi_1 \lesssim \sigma^2$. In this case, the electrostatic potential felt by an electron is less than its typical kinetic energy, so that the change in the action associated with the excited Langmuir wave is small, and can be neglected. However, as the coherent electrostatic field of the plasma wave grows, the change of the action resulting from the nearly-constant frequency of the particles in the plasma bulk[6] becomes appreciable. Thus, to obtain an accurate expression for the frequency shift for potentials $\phi_1 \gtrsim \sigma^2$, one must include the bulk change in action $\bar{J}$.

To clarify these arguments, we conclude this section by comparing the change in the canonical action $\bar{J}$ predicted by our distribution action *ansatz* with that obtained from our Vlasov simulations. To extract $\Delta\bar{J}$ from the simulations, we use the previously determined frequency shift to obtain the Hamiltonian for each particle (after the drive is turned off):

$$\mathcal{H}(p_j, \theta_j) = \tfrac{1}{2}\big(p_j + \delta\omega\big)^2 + \phi(\theta_j) = \tfrac{1}{2}\big(p_j + \delta\omega\big)^2 + \sum_{m=1}^{M} \frac{1}{N} \sum_{\ell=1}^{N} \cos(m\theta_j - m\theta_\ell). \qquad (2.63)$$

At any given time, (2.63) gives the particle energy H_j in terms of the numerical position and momentum; using the nonlinear potential, the average action is determined by

$$\bar{J} \equiv \frac{1}{N}\sum_{n=1}^{N} J_j = \frac{1}{N}\sum_{n=1}^{N} \frac{1}{2\pi} \oint d\theta_j \left\{ \sqrt{2[H_j + \phi(\theta_j)]} - \delta\omega \right\}. \qquad (2.64)$$

We compare the simulation points with those of our action *ansatz* theory for three different temperatures in Fig. 2.8. As we can see, the average action increases as the particles are excited in the Langmuir wave, becoming appreciable (of order $\delta\omega$) when $\phi_1 \gg \sigma^2$. As seen in Fig. 2.7, neglecting this change in $\bar{J}$ yields a significantly different frequency of the wave from that measured in the particle simulations.

[6] As mentioned earlier, while typical nonlinear oscillators have frequencies that are a function of the action, this nearly amplitude-independent frequency is a peculiarity of the (sufficiently cold, sufficiently nonrelativistic) nonlinear Langmuir wave. In this case, the dynamics are analogous those of the simple harmonic oscillator, in that a change in oscillator energy is accompanied by a change in its action.

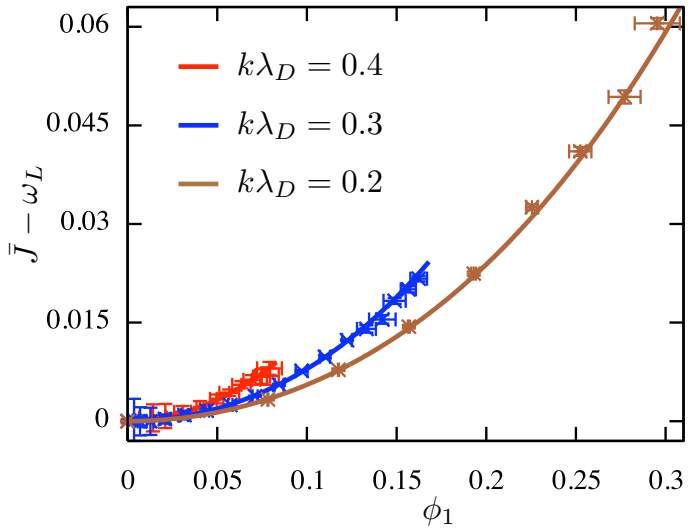

Figure 2.8: Growth of the average particle action $\bar{J}$ as a function of the potential for three different temperatures: $k\lambda_D = 0.4$ (red), $k\lambda_D = 0.3$ (blue), and $k\lambda_D = 0.2$ (brown). The points are obtained from particle simulations, with error bars indicating two standard deviations (again, basically arising due to the uncertainty associated with the ringing of the plasma wave amplitude and measured frequency). We see that the average action increases as the Langmuir wave amplitude increases. As discussed earlier, this corresponds to a nearly rigid shift of the distribution in the Ψ-J plane, and results from the nearly amplitude-independent frequency of the particles oscillating in the plasma bulk.

Structures similar to the BGK-type distributions have been seen in kinetic simulations of Raman backscatter [61, 62], while their generic physical properties (reduced Landau damping and the nonlinear frequency shift) have been used to interpret experiments investigating Raman backscatter in a plasma [15, 63, 16]. We will use various properties of these distributions in the following chapters to formulate a reduced description of Raman scatter in an under-dense plasma. Since nonlinear electrostatic waves arise in a variety of applications, the BGK-type distributions detailed in this chapter may have other applications as well.

Chapter 3

Extended Three-Wave Model of Stimulated Raman Scatter in a Plasma

When studying the Raman interaction of lasers in plasma it is convenient and often necessary to resort to reduced models. The utility of such simplified descriptions is two-fold: they illuminate the basic physics processes and are significantly less time-consuming to implement numerically. Of course, these models are only as valid as their underlying assumptions and reliable to the extent to which they capture the dominant physics. The simplest description of Raman scatter is that given by the ubiquitous three-wave model describing the lowest order coupling between nearly resonant modes [21, 64]. It can be thought of as an interaction through which a laser photon is converted to a frequency down-shifted photon and a longitudinal plasma oscillation in such a way as to satisfy the Planck-Einstein energy and momentum conservation relations:

$$\omega_0 = \omega_1 + \omega_2\,, \qquad\qquad \boldsymbol{k}_0 = \boldsymbol{k}_1 + \boldsymbol{k}_2, \tag{3.1}$$

where ω_0, $\boldsymbol{k}_0$ are the frequency and wave vector of the initial pump photon, while ω_1, $\boldsymbol{k}_1$ is that of the daughter photon, and $\omega_2 \approx \omega_p$, $\boldsymbol{k}_2$ characterize the Langmuir wave. Note that although we have used quantum-mechanical language, the conservation equations (3.1) can be understood in purely classical terms as resonance conditions. From the three-wave models a number of important physical insights have been made regarding the growth rates of the instability, the effects of plasma inhomogeneities, and novel nonlinear solutions in which the energy of one laser is efficiently transferred to an amplifying, narrowing pulse suitable for short-pulse, high intensity interactions [29, 65, 66].

Although the three-wave model is physically appealing, (somewhat) analytically tractable, and straightforward to implement numerically, it also neglects a host of other potentially important phenomena. Perhaps the most relevant physics that it does not include are the thermal and kinetic influences on the plasma wave. To completely address these issues, one must turn to a either particle-in-cell [67, 68, 69] or Vlasov codes (see, e.g., [62, 70, 71]). Even as computers increase in computational power, however, full-scale kinetic simulations in multiple dimensions are prohibitively time-consuming, even on state-of-the-art parallel computers. For this reason, there is much interest in developing three-wave type models that incorporate the relevant kinetic processes; we call such a description an extended three-wave model.

In this chapter, we develop the stimulated Raman backscatter equations beginning with Maxwell's equations coupled to plasma charges and currents. By assuming the field quantities vary slowly over a ponderomotive bucket, we suitably average the Vlasov-Maxwell equations in Sec. 3.1, thereby deriving a simplified coupled set of laser amplitude and plasma equations. This set of equations is not closed, however, as it involves higher order moments of the distribution function as well as nonlinear terms. Although not soluble in general, we consider two physically important limits in Sec. 3.2, in which the higher-order terms from the plasma envelope equation can be expressed in terms of the Langmuir wave amplitude, thereby closing the system. The first limit is obtained when the ponderomotive force initially interacts with the Langmuir wave, in which case the distribution

function is close to a Maxwellian and the linear oscillation has a natural frequency and damping given by the plasma dispersion relation evaluated along the Landau contour. The second limit is determined assuming that sufficient time has passed such that the electrons have effectively phase-mixed in the wave. In this case the natural frequency is that found in Ch. 2, and the Landau damping goes to zero.

The dynamics linking the initial value, linear problem to the asymptotic, phase-mixed state is complicated by particle trapping and phase-mixing in an evolving electrostatic wave. Rather than attempt to model this transition directly, in Sec. 3.3 we develop an approximate scheme to smoothly interpolate the evolution from the linear state to the phase-mixed state. The basis of this model is energy conservation: the decrease in wave energy due to Landau damping must equal the increase in particle kinetic energy. By associating this kinetic energy with that required to develop the phase-mixed distribution, we have a means of estimating the degree to which the distribution is phase-mixed. This in turn yields a tractable expression for the dynamic frequency and damping that depend on both the Landmuir wave amplitude and time. Finally, we write the complete, reduced three-wave model of Raman backscatter in a thermal plasma in Sec. 3.4, and briefly compare it to other results of Divol *et al.* [36] and that of Vu, DuBois, and Bezzerides [37].

3.1 Raman backscatter in a Vlasov plasma: governing equations

In this section, we develop the coupled mode equations relevant for stimulated Raman backscatter. To begin, we sacrifice some rigor for clarity and brevity when reducing the fully three-dimensional equations to a more manageable set[1] for which transverse dimensions appear only through the diffraction of the lasers. We carefully average these equations over the fast time-scales defined by the laser frequencies and the small spatial

[1]This set of equations is typically the starting point for the three-wave type analyses we have seen in the literature without apology or derivation; see, e.g., [34, 72].

scale defined by the laser beat wavelength; coupled mode equations then emerge. In the final sections in this chapter, we develop an approximate plasma model to close the set of equations.

3.1.1 From three to "nearly" one dimension

We begin our presentation by establishing under what assumptions and limits Raman scattering can be described as the propagation of paraxial lasers, coupled to the plasma response through an essentially one-dimensional, three-wave type interaction. To perform this reduction in a transparent manner, we use the cold-fluid model for the plasma. In Sec. 3.1.4 we replace the cold plasma response with that obtained from moments of the Vlasov equation, thereby including thermal and kinetic effects, assuming that the dominant contribution acts on the longitudinal (Langmuir wave) degrees of freedom. Thus, we start with the cold fluid continuity and momentum equations, coupled via Maxwell's equations:

$$\frac{\partial n_e}{\partial t} + \boldsymbol{\nabla}\cdot(n_e\boldsymbol{v}) = 0 \tag{3.2a}$$

$$\left[\frac{\partial}{\partial t} + \boldsymbol{v}\cdot\boldsymbol{\nabla}\right] m_e\boldsymbol{v} = e\boldsymbol{\nabla}\Phi + \frac{e}{c}\frac{\partial \boldsymbol{A}}{\partial t} - e\frac{\boldsymbol{v}}{c}\times(\boldsymbol{\nabla}\times\boldsymbol{A}) \tag{3.2b}$$

$$\boldsymbol{\nabla}^2\Phi = 4\pi e(n_e - n_0) \tag{3.2c}$$

$$\left[\frac{\partial^2}{\partial t^2} - c^2\boldsymbol{\nabla}^2\right]\boldsymbol{A} = -4\pi e c n_e\boldsymbol{v} - c\frac{\partial}{\partial t}\boldsymbol{\nabla}\Phi, \tag{3.2d}$$

where we have introduced the usual electromagnetic scalar and vector potentials, so that

$$\boldsymbol{E} \equiv -\boldsymbol{\nabla}\Phi - \frac{1}{c}\frac{\partial \boldsymbol{A}}{\partial t} \qquad\qquad \boldsymbol{B} \equiv \boldsymbol{\nabla}\times\boldsymbol{A}, \tag{3.3}$$

and we have assumed the Coulomb gauge condition $\boldsymbol{\nabla}\cdot\boldsymbol{A} = 0$. Rather than deal directly with the fluid quantities from (3.2), we simplify our presentation by introducing a special case of the Clebsch potential formulation of the cold plasma [73, 74] in which the canonical momentum $\boldsymbol{p}_c \equiv m_e\boldsymbol{v} - \frac{e}{c}\boldsymbol{A}$ is replaced by a scalar field. We take the curl of the momentum

equation (3.2b) and rearrange, obtaining

$$\frac{\partial}{\partial t}\boldsymbol{\nabla}\times\boldsymbol{p}_c+\boldsymbol{\nabla}\times[(\boldsymbol{\nabla}\times\boldsymbol{p}_c)\times\boldsymbol{v}]=0. \tag{3.4}$$

Eq. (3.4) is of the same form as that for the vorticity in an incompressible fluid, and Kelvin's theorem (see, e.g., [75]) guarantees that the "canonical vorticity" is carried by the flow. For an initially quiescent plasma, such that the "canonical vorticity" is everywhere zero, (3.4) implies that $\boldsymbol{\nabla}\times\boldsymbol{p}_c=0$ for all times, and the canonical momentum can be written as the gradient of a scalar. To simplify the subsequent equations, we will, for this section only, normalize variables with appropriate combinations of the speed of light c and the characteristic frequency of the lasers ω:

$$\check{t}\equiv\omega t \qquad \check{\boldsymbol{x}}\equiv\frac{\omega}{c}\boldsymbol{x} \qquad \varphi\equiv\frac{e}{m_ec^2}\Phi \qquad \boldsymbol{a}\equiv\frac{e}{m_ec^2}\boldsymbol{A} \qquad \boldsymbol{\nabla}_{\check{x}}\chi\equiv\frac{\boldsymbol{p}_c}{m_ec}. \tag{3.5}$$

We write the Maxwell-fluid system (3.2) in terms of the scaled variables (3.5). Dropping the háčeks from the coordinates, and defining the small parameter $\epsilon^2\equiv\omega_p^2/\omega^2\ll 1$, we have

$$\frac{\partial}{\partial t}\frac{\delta n}{n_0}+\boldsymbol{\nabla}\cdot\left[\left(1+\frac{\delta n}{n_0}\right)\boldsymbol{\nabla}\chi\right]+\boldsymbol{a}\cdot\boldsymbol{\nabla}\frac{\delta n}{n_0}=0 \tag{3.6a}$$

$$\frac{\partial\chi}{\partial t}+\frac{1}{2}\boldsymbol{a}^2+\boldsymbol{a}\cdot\boldsymbol{\nabla}\chi+\frac{1}{2}\left(\boldsymbol{\nabla}\chi\right)^2=\varphi+1 \tag{3.6b}$$

$$\boldsymbol{\nabla}^2\varphi=\epsilon^2\frac{\delta n}{n_0} \tag{3.6c}$$

$$\left[\frac{\partial^2}{\partial t^2}-c^2\boldsymbol{\nabla}^2\right]\boldsymbol{a}=-\epsilon^2\left(1+\frac{\delta n}{n_0}\right)(\boldsymbol{a}+\boldsymbol{\nabla}\chi)-\frac{\partial}{\partial t}\boldsymbol{\nabla}\varphi. \tag{3.6d}$$

We now make explicit use of the fact that the plasma is under-dense, i.e., $\omega_p^2/\omega^2\equiv\epsilon^2\ll 1$. In this case, there are two well-separated, natural time-scales in the problem: that associated with the laser frequencies, $\omega\sim 1$ and that associated with the plasma frequency $\omega_p\sim\epsilon$. In the one-dimensional limit, the former dominantly describes the lasers and the associated rapid transverse quiver of the electrons, while the latter is basically related to the longitudinal plasma waves and the back-reaction on the laser envelopes. Therefore, each field variable $\mathcal{Y}$ (i.e., $\delta n/n_0$, χ, φ, $\boldsymbol{a}$) consists of a "fast" and a "slow" component in

the following additive manner:

$$\mathcal{Y} = \mathcal{Y}^{\mathrm{f}} + \mathcal{Y}^{\mathrm{s}} \qquad \text{with} \qquad \frac{\partial \mathcal{Y}^{\mathrm{f}}}{\partial t} \sim \mathcal{Y}^{\mathrm{f}}, \quad \frac{\partial \mathcal{Y}^{\mathrm{s}}}{\partial t} \sim \epsilon \mathcal{Y}^{\mathrm{s}}. \tag{3.7}$$

The continuity equation (3.6a) has a rapidly oscillating component of both the density and the canonical momentum potential χ given by

$$\left(\frac{\partial n}{n_0}\right)^{\mathrm{f}} \sim \chi^{\mathrm{f}} \sim \boldsymbol{a}_\perp^{\mathrm{f}} \cdot \boldsymbol{\nabla}_\perp \left(\frac{\delta n}{n_0}\right)^{\mathrm{s}} + a_z^{\mathrm{f}} \frac{\partial}{\partial z}\left(\frac{\delta n}{n_0}\right)^{\mathrm{s}} \lesssim \frac{|\boldsymbol{a}_\perp^{\mathrm{f}}|}{R_\perp}, \tag{3.8}$$

where $R_\perp$ is the transverse scale length. We assume that the laser spot sizes are much greater than the plasma collisionless skin depth c/ω_p, so that $1/R_\perp^2 \ll \epsilon^2$. From the Poisson equation (3.6c) the fast component of the potential scales as:

$$\varphi^{\mathrm{f}} \sim \epsilon^2 \left(\frac{\delta n}{n_0}\right)^{\mathrm{f}} \sim \epsilon^2 \frac{|\boldsymbol{a}_\perp^{\mathrm{f}}|}{R_\perp}. \tag{3.9}$$

Using the scalings (3.8)-(3.9), the transverse part of the fast component of the current in the Ampère-Maxwell Law, i.e., the right-hand side of (3.6d), is seen to behave as

$$\begin{aligned} \epsilon^2 \left[1 + \left(\frac{\delta n}{n_0}\right)^{\mathrm{s}}\right]\left(\boldsymbol{a}_\perp^{\mathrm{f}} + \boldsymbol{\nabla}_\perp \chi^{\mathrm{f}}\right) + \epsilon^2 \left(\frac{\delta n}{n_0}\right)^{\mathrm{f}} \left(\boldsymbol{a}_\perp^{\mathrm{s}} + \boldsymbol{\nabla}_\perp \chi^{\mathrm{s}}\right) - \boldsymbol{\nabla}_\perp \frac{\partial \varphi^{\mathrm{f}}}{\partial t} \\ \sim \epsilon^2 \left\{ \left[1 + \left(\frac{\delta n}{n_0}\right)^{\mathrm{s}}\right]\left(\boldsymbol{a}_\perp^{\mathrm{f}} + \boldsymbol{\nabla}_\perp \chi^{\mathrm{f}}\right) + \frac{|\boldsymbol{a}_\perp|}{R_\perp^2} \right\}. \end{aligned} \tag{3.10}$$

The last term in (3.10) can be thought of as representing changes to the transverse profile of the lasers due to coupling with the plasma. As is apparent from (3.10), this effect is $O(\epsilon^2)$ smaller than that of the transverse Laplacian of the Ampère-Maxwell wave operator. Therefore, (3.10) indicates that, to lowest order, the lasers couple to a current given by $n_e c\, \boldsymbol{a}_\perp$ as one would have in the case of exact canonical momentum conservation. In this limit, the dominant three-dimensional physics is given simply by the vacuum diffraction operator $\boldsymbol{\nabla}_\perp^2$ acting on the laser field.

We similarly simplify the plasma response: the slow terms from the ponderomotive/convective derivative term on the left-hand side of the momentum-type equation (3.6b) scale as

$$\frac{1}{2}(\boldsymbol{a}^{\mathrm{f}})^2 + \boldsymbol{a}^{\mathrm{f}} \cdot \boldsymbol{\nabla} \chi^{\mathrm{f}} + \frac{1}{2}\left(\boldsymbol{\nabla} \chi^{\mathrm{s}}\right)^2 \approx \frac{1}{2}(\boldsymbol{a}_\perp^{\mathrm{f}})^2 + \frac{1}{2}\left(\frac{\partial \chi^{\mathrm{s}}}{\partial z}\right)^2 + O\left(\tfrac{|\boldsymbol{a}_\perp|}{R_\perp^2}\right), \tag{3.11}$$

while the slowly oscillating terms from the convective derivative in the continuity equation are given by

$$\boldsymbol{\nabla}\cdot\left[\left(1+\frac{\delta n}{n_0}\right)\boldsymbol{\nabla}\chi\right]^{\mathrm{s}}+\boldsymbol{a}^{\mathrm{f}}\cdot\boldsymbol{\nabla}\left(\frac{\delta n}{n_0}\right)^{\mathrm{f}}\approx\frac{\partial}{\partial z}\left(1+\frac{\delta n}{n_0}\right)^{\mathrm{s}}\frac{\partial\chi^{\mathrm{s}}}{\partial z}+O\Big(\tfrac{\chi}{R_\perp^2}\Big)+O\Big(\tfrac{|\boldsymbol{a}_\perp|^2}{R_\perp^2}\Big)\,. \quad (3.12)$$

Inspection of the nonlinear terms from the plasma response (3.11) and (3.12) shows that the plasma is, to $O(1/R_\perp^2)$, described by the slow pieces of the density perturbation and the z-derivative of the "canonical momentum potential" χ. Additionally, we can show that the slow part of $\frac{\partial}{\partial z}\chi$ is essentially the longitudinal velocity by considering the slow part of the transverse Ampère Maxwell Law:

$$\epsilon^2\boldsymbol{a}_\perp^{\mathrm{s}}\sim\epsilon^2\boldsymbol{\nabla}_\perp\chi^{\mathrm{s}}+\boldsymbol{\nabla}_\perp\varphi^{\mathrm{s}}\quad\Rightarrow\quad\boldsymbol{a}_\perp^{\mathrm{s}}\sim\frac{\chi^{\mathrm{s}}}{R_\perp}. \quad (3.13)$$

Using the Coulomb gauge condition, we obtain $a_z^{\mathrm{s}}\sim|\boldsymbol{a}|_\perp^{\mathrm{s}}/R_\perp$. Therefore, from the definition of (3.5) of the Clebsch potential, the slow part of $\frac{\partial}{\partial z}\chi$ is given by

$$\frac{\partial\chi^{\mathrm{s}}}{\partial z}\sim\tfrac{1}{c}v_z\left[1+O\Big(\tfrac{1}{R_\perp^2}\Big)\right]. \quad (3.14)$$

Therefore, in the limit that the plasma is under-dense ($\omega_p^2\ll\omega^2$) and the laser spot sizes are large (typically with waists much larger than c/ω_p), the Raman interaction can be consistently modeled by essentially transverse (paraxial) lasers that couple to the plasma through the current generated by the transverse quiver, and the Ampère-Maxwell Law (in terms of actual time and space) is given by

$$\left[\frac{\partial^2}{\partial t^2}-c^2\boldsymbol{\nabla}^2\right]\boldsymbol{a}_\perp=-\frac{\omega_p^2}{n_0}\,n_e\boldsymbol{a}_\perp. \quad (3.15)$$

Furthermore, in this approximation the transverse motion of the particles is given by the local quiver in the laser field, so that different transverse ribbons of the plasma only couple to each other via the lasers. We will use these facts in the next sections wherein we average the laser and plasma equations.

3.1.2 Paraxial, eikonal lasers in a plasma

We now generalize the fluid response in (3.15) to include longitudinal thermal and kinetic effects. To do this, we replace the fluid density n_e with its definition as the moment

of the electron distribution over velocity space

$$n_e \equiv \int d\boldsymbol{v}\ f_e(\boldsymbol{v}, z, \boldsymbol{r}_\perp; t). \tag{3.16}$$

Since we noted in the previous section that the fluid variables inherit their transverse structure from the laser profile, we will omit the explicit transverse spatial dependence of f_e in what follows. Thus, the Ampère-Maxwell equation (3.15) is written as

$$\left[\frac{\partial^2}{\partial t^2} - c^2\frac{\partial^2}{\partial z^2}\right]\boldsymbol{a}_\perp(z,t) = -\frac{\omega_p^2}{n_0}\,\boldsymbol{a}_\perp(z,t)\int d\boldsymbol{v}\ f_e(\boldsymbol{v}, z; t) \tag{3.17}$$

We further assume the transverse vector potential characterizes two linearly polarized lasers that are counter-propagating along the z-axis. In terms of the dimensionless root mean square amplitudes and phases, the lasers are given by

$$\boldsymbol{a}_\perp(\boldsymbol{x},t) = \frac{1}{\sqrt{2}}\left[a_0(\boldsymbol{x},t)e^{-i(\omega_0 t + k_0 z)} + a_1(\boldsymbol{x},t)e^{-i(\omega_1 t - k_1 z)}\right]\hat{\boldsymbol{x}} + c.c., \tag{3.18}$$

with the convention that each ω and k is positive, such that the "pump wave" $a_0(\boldsymbol{x},t)$ travels to the left, while the "seed wave" $a_1(\boldsymbol{x},t)$ travels to the right. Furthermore, the lasers are assumed to each satisfy the eikonal relations

$$\left|\frac{\partial}{\partial t}\ln a_{0,1}(\boldsymbol{x},t)\right| \ll \omega_{0,1}, \qquad\qquad \left|\frac{\partial}{\partial z}\ln a_{0,1}(\boldsymbol{x},t)\right| \ll k_{0,1}, \tag{3.19}$$

and the linear dispersion relations

$$\omega_0^2 = c^2k_0^2 + \omega_p^2, \qquad\qquad \omega_1^2 = c^2k_1^2 + \omega_p^2. \tag{3.20}$$

Using the counter-propagating laser vector potential (3.18) and the dispersion relations (3.20), Ampère's Law (3.17) becomes

$$\begin{aligned} &e^{-i(\omega_0 t + k_0 z)}\left[\omega_0\frac{\partial}{\partial t} - c^2k_0\frac{\partial}{\partial z} - \frac{ic^2}{2}\boldsymbol{\nabla}_\perp^2\right]a_0(\boldsymbol{x},t) + c.c. \\ &+ e^{-i(\omega_1 t - k_1 z)}\left[\omega_1\frac{\partial}{\partial t} + c^2k_1\frac{\partial}{\partial z} - \frac{ic^2}{2}\boldsymbol{\nabla}_\perp^2\right]a_1(\boldsymbol{x},t) + c.c. \\ &\qquad = -\frac{i\omega_p^2}{2n_0}\left[a_0e^{-i(\omega_0 t + k_0 z)} + a_1e^{-i(\omega_1 t - k_1 z)}\right]\left[\int d\boldsymbol{v}\ f_e(\boldsymbol{v}, z; t) - 1\right] + c.c., \end{aligned} \tag{3.21}$$

where, in light of the eikonal relations (3.19), we have dropped the second-order time and space derivatives. To obtain fully consistent amplitude equations for the lasers, we further average the equation (3.21) over the short spatial scale defined by the beat wavenumber $k_2 \equiv k_0 + k_1$, and then over the fast temporal scale given by the laser frequencies $\sim \omega_{0,1}$, yielding two equations for the counter-propagating amplitudes a_0 and a_1. Since these amplitudes vary smoothly and slowly (with respect to k_2) in space, they are driven by a smooth, averaged electron current. Thus, we are led to equations that couple the eikonal fields to averaged plasma quantities, for which we must also determine equations of motion.

3.1.3 The averaged transverse Ampère-Maxwell equation

Eliminating the spatial scale given by $1/k_2$ from the wave equation (3.21) requires a longitudinal averaging procedure that we will denote as $\langle\cdot\rangle_z$. To simplify notation, we introduce the dimensionless coordinate $\zeta \equiv k_2 z$, so that the spatial average of any function $\mathcal{X}(z,t)$ is given by

$$\left\langle \mathcal{X}(z',t)\right\rangle_z (z,t) \equiv \frac{k_2}{2\pi}\int\limits_{z-\frac{\pi}{k_2}}^{z+\frac{\pi}{k_2}} dz'\ \mathcal{X}(z',t) \equiv \frac{1}{2\pi}\int\limits_{\zeta-\pi}^{\zeta+\pi} d\zeta'\ \mathcal{X}(\zeta',t). \tag{3.22}$$

Note that, as indicated, removing the fine-scale structure still allows for variation in z on scales longer than k_2, although in what follows we will generally suppress this explicit dependence. To obtain an equation for the slowly-varying amplitude $a_0(z,t)$, we multiply (3.21) by the phase $e^{i(\omega_0 t + k_0 z)}$ and apply the londitudinal averaging operation (3.22). We address each term in turn; for those terms on the left-hand side of (3.18) involving a_0, we Taylor expand around the central point of the averaging operator $\langle\cdot\rangle_z$ to obtain

$$\begin{aligned}\left\langle a_0(\zeta',t)\right\rangle_z &= \left\langle a_0(\zeta,t) + (\zeta'-\zeta)\frac{\partial a_0}{\partial\zeta} + \tfrac{1}{2}(\zeta'-\zeta)^2\frac{\partial^2 a_0}{\partial\zeta^2} + \ldots\right\rangle_z \\ &= a_0(\zeta,t) + \frac{1}{6}\frac{\partial^2 a_0}{\partial\zeta^2} + \ldots,\end{aligned} \tag{3.23}$$

where we will only retain the first term, consistent with our previous omission of the second order derivatives. Alternatively, the terms involving a_1 can be wholly neglected

upon averaging, as seen by

$$\left\langle a_1(\zeta',t)e^{i\zeta'}\right\rangle_z = \left\langle e^{i\zeta'}\left[a_1(\zeta',t)+(\zeta'-\zeta)\frac{\partial a_1}{\partial\zeta'}+\ldots\right]\right\rangle_z = ie^{i\zeta}\frac{\partial}{\partial\zeta}a_1(\zeta,t)+\ldots \tag{3.24}$$

If our lasers were circularly polarized, the results (3.23) and (3.24) would be sufficient for the averaged right-hand side of (3.21). However, for linearly polarized light we still have two additional series of terms: those involving a_0^* and a_1^*. To appropriately eliminate these, we must also take the time average over the sum frequency $\omega_0+\omega_1$. Because the amplitude a_0 is essentially constant over this time scale, we have

$$\left\langle a_0(z,t')\right\rangle_t \equiv \frac{\omega_0+\omega_1}{2\pi}\int_{t-\frac{\pi}{\omega_0+\omega_1}}^{t+\frac{\pi}{\omega_0+\omega_1}} dt'\; a_0(z,t') = a_0(z,t)+\frac{\pi^2}{6(\omega_0+\omega_1)^2}\frac{\partial^2 a_0}{\partial t}+\ldots, \tag{3.25}$$

and only the first term on the right-hand side of (3.25) survives. On the other hand, since the time average commutes with the spatial average, for the terms involving a_1^* we consider

$$\left\langle a_1^*(z,t')e^{i(\omega_0+\omega_1)t'}\right\rangle_t = \frac{i}{\omega_0+\omega_1}\frac{\partial a_1^*}{\partial t}e^{i(\omega_0+\omega_1)t}+\ldots,$$

and these terms can be neglected. Finally, we calculate the lowest order terms involving a_0^*. First, we have

$$\left\langle a_0^*(\zeta',t)e^{i(2\omega_0 t+2k_0\zeta'/k_2)}\right\rangle_z = \frac{\sin(2\pi k_0/k_2)}{2\pi k_0/k_2}a_0^*(\zeta,t)e^{i(2\omega_0 t+2k_0/k_2)}+\ldots,$$

while the time average of this is

$$\begin{aligned}\frac{\sin(2\pi k_0/k_2)}{2\pi k_0/k_2}&\left\langle a_0^*(\zeta,t')e^{i(2\omega_0 t'+2k_0\zeta'/k_2)}\right\rangle_t \\ &= \frac{\sin[2\pi\omega_0/(\omega_0+\omega_1)]\sin(2\pi k_0/k_2)}{[2\pi\omega_0/(\omega_0+\omega_1)]2\pi k_0/k_2}a_0^*(\zeta,t)e^{i(2\omega_0 t+2k_0\zeta/k_2)}+\ldots\end{aligned} \tag{3.26}$$

To simplify (3.26), we note that

$$\frac{2\pi\omega_0}{\omega_0+\omega_1}\equiv\frac{2\pi\omega_0}{2\omega_0-(\omega_0-\omega_1)}\approx\pi\left(1+\frac{\omega_0-\omega_1}{2\omega_0}\right), \tag{3.27}$$

where we have assumed that the plasma is under-dense (i.e., $\omega_{0,1}^2 \gg \omega_p^2$) and that the frequency difference between the lasers is near resonance ($\omega_0-\omega_1\approx\omega_p$). These assumptions and the electromagnetic dispersion relations also lead to the following approximate

equation:

$$\frac{2\pi k_0}{k_2} \equiv \frac{2\pi k_0}{k_0 + k_1} \approx \pi\left(1 + \frac{k_0 - k_1}{2k_0}\right) \approx \pi\left(1 + \frac{\omega_0 - \omega_1}{2\omega_0}\right). \tag{3.28}$$

Using the approximate expressions (3.27) and (3.28), we find that

$$\left\langle a_0^* e^{i(2\omega_0 t' + 2k_0\zeta'/k_2)} \right\rangle_{z,t} \approx \left(\frac{\omega_0 - \omega_1}{2\omega_0}\right)^2 e^{i(2\omega_0 t + 2k_0\zeta/k_2)} a_0^*, \tag{3.29}$$

which is much smaller than the retained terms. Finally, we consider the course-grained current given by the temporal and spatial averaging of the right-hand side of (3.21). For this discussion, we proceed largely in analogy with those averages already computed, and use the general properties of the plasma response discussed in Ch. 2 to determine which terms survive the averaging procedure. To further simplify notation, we use the dimensionless longitudinal velocity $u \equiv k_2 v_z/\omega_p$ and the rescaled and marginalized (over the transverse velocities) distribution function f defined such that

$$\frac{1}{n_0}\int d\boldsymbol{v}\; f_e(\boldsymbol{v}, z; t) \equiv \int du\; f(u, z; t).$$

As indicated in Sec. 3.1, the Raman interaction in an under-dense plasma with large laser spots is essentially one-dimensional, so that this marginalization does not affect the relevant information. Furthermore, we recall that the distribution f is defined such that the dimensionless electron perturbation is

$$\frac{\delta n}{n_0} \equiv \frac{n_e - n_0}{n_0} \equiv \int du\; f(u, \zeta; \tau) - 1. \tag{3.30}$$

To simplify the plasma current, we use the fact that the natural response of the plasma has a frequency $\omega_p \approx \omega_0 - \omega_1$ and is dominantly driven[2] at the beat spatial length-scale $1/k_2$. Under these assumptions, averaging the terms in the current $\sim a_0^*$ and $\sim a_1$ is, in analogy with (3.29), given by

$$\left\langle a_0^* e^{i(2\omega_0 t' + 2k_0\zeta'/k_2)} \frac{\delta n}{n_0} \right\rangle_{z,t} \sim \left\langle a_1^* e^{i[(\omega_0+\omega_1)t' + (k_0 - k_1)\zeta'/k_2)} \frac{\delta n}{n_0} \right\rangle_{z,t} \sim \frac{\omega_p^2}{\omega_0^2} a_{0,1} e^{i(\omega_{0,1} + k_{0,1})}.$$

[2]To be complete, for now we also include long-scale spatial variation in the plasma wave that is relevant if the laser envelopes have longitudinal structure on the scale $\sim c/\omega_p \gg 1/k_2$.

while the term involving the initial velocity spread $v_x(0)$ is

$$\left\langle \left(1+\frac{\delta n}{n_0}\right)\frac{v_x(0)}{c}e^{i(\omega_0 t'+k_0 z')}\right\rangle_{z,t} \sim \frac{\omega_p^2}{\omega_0^2}\frac{v_x(0)}{c}e^{i(\omega_0 t+k_0 z)}. \tag{3.31}$$

Note that in order to obtain (3.31) we implicitly assumed that any variation in the initial perpendicular velocity was over spatiotemporal scales much longer that $1/\omega_0$ and $1/k_2$. While this is consistent with the eikonal assumptions in a pre-ionized plasma, it may fail to be true if either the pump or seed laser is providing the ionization energy. In this case, the transverse velocity is correlated with the laser phase, and (3.31) may not hold.

Neglecting those terms that have been "averaged away," we see that the averaged longitudinal current is given by

$$\frac{4\pi e}{m_e c}\left\langle \boldsymbol{J}_\perp\right\rangle_{z,t} = -\frac{i\omega_p^2}{2}\left[a_0(z,t)\left\langle\frac{\delta n}{n_0}\right\rangle_z + a_1(z,t)\left\langle e^{i[(\omega_0-\omega_1)t+\zeta]}\frac{\delta n}{n_0}\right\rangle_z\right]\hat{\boldsymbol{x}}, \tag{3.32}$$

where we have used expansions of the form (3.23) to take the eikonal fields outside of the averaging in z, and implicitly assumed that the currents change little over the time-scale given by $\omega_{0,1}$, thereby neglecting the explicit time average. For what follows, we assume that any long-range density perturbation is small, so that we may neglect the first term on the right-hand side of the averaged current (3.32). In this way, we have now completely determined the averaged equation for the eikonal field amplitude $a_0(z,t)$; by multiplying (3.21) by the phase $e^{i(\omega_1-k_1 z)}$ and carrying out the same averaging procedure we obtain a similar equation for the amplitude $a_1(z,t)$. Introducing the dimensionless time, frequency difference, and group velocities

$$\tau \equiv \omega_p t, \qquad \omega_2 \equiv \frac{\omega_0-\omega_1}{\omega_p}, \qquad u_0 \equiv \frac{k_2}{\omega_p}\frac{c^2 k_0}{\omega_0}, \qquad u_1 \equiv \frac{k_2}{\omega_p}\frac{c^2 k_1}{\omega_1},$$

the resulting set of equations is written as

$$\left[\frac{\partial}{\partial\tau} - u_0\frac{\partial}{\partial\zeta} - \frac{i\omega_p}{\omega_0}\boldsymbol{\nabla}_\perp^2\right]a_0(\zeta,\tau) = -\frac{i\omega_p}{2\omega_0}\,a_1\left\langle e^{i(\omega_2\tau+\zeta)}\left[\int du\; f(u,\zeta;\tau)-1\right]\right\rangle_z \tag{3.33a}$$

$$\left[\frac{\partial}{\partial\tau} + u_1\frac{\partial}{\partial\zeta} - \frac{i\omega_p}{\omega_1}\boldsymbol{\nabla}_\perp^2\right]a_1(\zeta,\tau) = -\frac{i\omega_p}{2\omega_1}\,a_0\left\langle e^{-i(\omega_2\tau+\zeta)}\left[\int du\; f(u,\zeta;\tau)-1\right]\right\rangle_z. \tag{3.33b}$$

The rest of this chapter will concern itself with the derivation of a simplified equation for $\left\langle e^{-i(\omega_2\tau+\zeta)}\left[\int du\ f-1\right]\right\rangle_z$, what is known in the free electron laser community as the bunching parameter. We proceed by forming a hierarchy of moments of the Vlasov equation, and then close this set of equations by formulating an approximate distribution function in the limit that the bunching changes slowly on the plasma time scale $1/\omega_p$.

3.1.4 Bunching parameter governing equation

In this section, we derive a governing equation for the phase-modulated density perturbation that couples the lasers a_0 and a_1 to each another. This is typically expressed either through a third wave equation to complete a three-wave model of stimulated Raman scatter, or through a kinetic response using either a particle or Vlasov model. The former has the advantage of elegant interpretation and numerical simplicity, while the latter more accurately models the thermal and kinetic effects in a realistic plasma. In what follows, we will try to incorporate some kinetic physics into a simple, extended three-wave type model. Before proceeding to this task, we find it convenient to define the following ponderomotive potential phase space average at fixed time (this is the slowly-varying generalization of the phase-space average in Ch. 2):

$$\left\langle \mathcal{X}(u,\zeta';\tau)\right\rangle_{\mathcal{PS}}(\zeta,\tau)\equiv\frac{1}{2\pi}\int_{\zeta-\pi}^{\zeta+\pi}d\zeta'\int_{-\infty}^{\infty}du\ f(u,\zeta';\tau)\mathcal{X}(u,\zeta';\tau).$$

To determine the plasma response relevant in Raman scattering, we must derive an equation for the bunching parameter[3]. We turn to the Vlasov equation for the electron distribution function. In terms of the dimensionless variables τ, ζ, and u, the Vlasov equation is given by

$$\left[\frac{\partial}{\partial\tau}+u\frac{\partial}{\partial\zeta}+\frac{du}{d\tau}\frac{\partial}{\partial u}\right]f(u,\zeta;\tau)=0, \tag{3.34}$$

where $du/d\tau$ is the dimensionless acceleration due to the normalized electrostatic and

[3]This derivation is similar in spirit to that used for the averaged particle equations in Ref. [76], but by not mixing Eulerian and Lagrangian coordinates, we feel that it is simpler.

ponderomotive potentials

$$\frac{du}{d\tau} = \frac{k_2}{\omega_p^2}\frac{dv}{dt} = \frac{k_2}{\omega_p^2}\left[\frac{e}{m_e}\frac{\partial \Phi}{\partial z} - \frac{e^2}{2m_e^2c^2}\frac{\partial \boldsymbol{A}_\perp^2}{\partial z}\right] \equiv \frac{\partial \phi}{\partial \zeta} - \frac{c^2k_2^2}{2\omega_p^2}\frac{\partial \boldsymbol{a}_\perp^2}{\partial \zeta}. \tag{3.35}$$

As in the previous chapter, the dimensionless electrostatic potential ϕ is obtained by scaling Φ by the kinetic energy associated with the nominal phase velocity ω_p/ck_2, so that $\phi \equiv e\Phi/[m_e(\omega_p/k_2)^2]$. It is determined via Poisson's equation:

$$\frac{\partial^2 \phi}{\partial \zeta^2} = \frac{e}{m_e\omega_p^2}\frac{\partial^2 \Phi}{\partial z^2} = \frac{4\pi e^2 n_0}{m_e^2\omega_p^2}\left[\int du\ f(u,\zeta;\tau) - 1\right] \equiv \frac{\delta n}{n_0}. \tag{3.36}$$

We begin by obtaining a relation between the zeroth and first order moments of the Vlasov equation. Integrating (3.34) over u and rearranging yields the following form of the continuity equation

$$-\frac{\partial}{\partial \zeta}\int du\ f(u,\zeta;\tau)u = \frac{\partial}{\partial \tau}\left[\int du\ f(u,\zeta;\tau) - 1\right] \equiv \frac{\partial}{\partial \tau}\frac{\delta n}{n_0}. \tag{3.37}$$

Multiplying the Vlasov equation (3.34) by u and integrating with respect to the velocity yields the dynamical equation for the first moment (i.e., the momentum equation)

$$\frac{\partial}{\partial \tau}\int du\ f(u,\zeta;\tau)u + \frac{\partial}{\partial \zeta}\int du\ f(u,\zeta;\tau)u^2 - \frac{du}{d\tau}\int du\ f(u,\zeta;\tau) = 0, \tag{3.38}$$

where we have integrated the last term (involving the acceleration) by parts. Taking $-\frac{\partial}{\partial \zeta}$ to the momentum equation (3.38), and using the continuity equation (3.37) and the acceleration (3.35), we have

$$\frac{\partial^2}{\partial \tau^2}\frac{\delta n}{n_0} + \frac{\partial^2 \phi}{\partial \zeta^2} - \frac{\partial^2}{\partial \zeta^2}\int du\ fu^2 + \frac{\partial}{\partial \zeta}\left[\frac{\partial \phi}{\partial \zeta}\frac{\delta n}{n_0}\right] = \frac{\partial}{\partial \zeta}\left[\frac{c^2k_2^2}{2\omega_p^2}\frac{\partial \boldsymbol{a}_\perp^2}{\partial \zeta}\left(1 + \frac{\delta n}{n_0}\right)\right],$$

from which, using Poisson's equation (3.36), we obtain

$$\frac{\partial^2}{\partial \tau^2}\frac{\delta n}{n_0} + \frac{\delta n}{n_0} - \frac{\partial^2}{\partial \zeta^2}\left[\int du f u^2 - \frac{1}{2}\left(\frac{\partial \phi}{\partial \zeta}\right)^2\right] = \frac{c^2k_2^2}{2\omega_p^2}\frac{\partial}{\partial \zeta}\left[\frac{\partial \boldsymbol{a}_\perp^2}{\partial \zeta}\left(1 + \frac{\delta n}{n_0}\right)\right]. \tag{3.39}$$

To make the averaging and eikonal approximations explicit, we rewrite this second-order (in time) equation for the real density perturbation as a first-order equation for a single complex wave-field $g(\zeta,\tau)$. This is in some ways similar to quantum field theory, for

which one typically defines k-dependent creation and annihilation operators that factor the Hamiltonian. Thus, we define

$$g(\zeta,\tau) \equiv \frac{1}{2}\left[1+\frac{i}{\omega_L}\frac{\partial}{\partial\tau}\right]\frac{\delta n}{n_0}, \tag{3.40}$$

where ω_L is the dimensionless linear resonant frequency, shifted shifted slightly from unity (the plasma frequency) due to thermal effects. Using the oscillator-type equation (3.39), we find that the wave-field $g(\zeta,\tau)$ satisfies the following partial differential equation

$$\begin{aligned}\frac{\partial g}{\partial\tau}+i\frac{\omega_L^2+1}{2\omega_L}g-\frac{i}{2\omega_L}\frac{\partial^2}{\partial\zeta^2}\left[\int du\; fu^2-\left(\frac{\partial\phi}{\partial\zeta}\right)^2\right]-i\frac{\omega_L^2-\omega_p^2}{2\omega_L}g^* \\ =\frac{i}{2\omega_L}\frac{\partial}{\partial\zeta}\left[\frac{c^2k_2^2}{2\omega_p^2}\frac{\partial \boldsymbol{a}_\perp^2}{\partial\zeta}\left(1+g+g^*\right)\right]\end{aligned} \tag{3.41}$$

Now, we expand the field $g(\zeta,\tau)$ in a Fourier-eikonal series about the resonant phase $(\zeta+\omega_L\tau)$ as follows

$$g(\zeta,\tau)=\frac{1}{2}\sum_{n\neq 0} g_n e^{-in(\zeta+\omega_L\tau)} \tag{3.42}$$

where we assume that the modes g_n are slowly-varying in space:

$$\left|\frac{\partial}{\partial\zeta}\ln|g_n(\zeta,\tau)|\right| \ll n. \tag{3.43}$$

Before proceeding, we remind ourselves that the eikonal laser equations (3.33) are coupled though the bunching parameter $\left\langle e^{i(\zeta+\omega_2\tau)}\frac{\delta n}{n_0}\right\rangle_z$. Apart from the phase difference $\omega_L-\omega_2$, we determine its relation to the modes g_n as

$$\begin{aligned}\left\langle e^{i(\zeta+\omega_L\tau)}\frac{\delta n}{n_0}\right\rangle_z &= \frac{1}{2\pi}\int_{\zeta-\pi}^{\zeta+\pi} d\zeta'\; e^{i(\zeta+\omega_L\tau)}\left[\int du f(u,\zeta;\tau)-1\right] \\ &= \frac{1}{2\pi}\int_{\zeta-\pi}^{\zeta+\pi} d\zeta'\; e^{i(\zeta+\omega_L\tau)}(g+g^*)=\frac{1}{2}\left(g_1+g_{-1}^*\right).\end{aligned} \tag{3.44}$$

Thus, we see that the lasers couple to the plasma modes g_1 and g_{-1}. To obtain their governing equations, we respectively multiply (3.41) by $e^{i(\zeta+\omega_L\tau)}$ and $e^{-i(\zeta+\omega_L\tau)}$ and integrate

over one wavelength. To simplify the second line in (3.41), we note that

$$\begin{aligned}\left\langle e^{i(\zeta+\omega_L\tau)}\frac{\partial^2}{\partial\zeta^2}\mathcal{X}(\zeta,\tau)\right\rangle_z &= e^{i\omega_L\tau}\left\langle \frac{\partial}{\partial\zeta}e^{i\zeta}\frac{\partial\mathcal{X}}{\partial\zeta} - ie^{i\zeta}\frac{\partial\mathcal{X}}{\partial\zeta}\right\rangle_z \\ &= e^{i\omega_L\tau}\left\langle \left[\frac{\partial^2}{\partial\zeta^2} - 2i\frac{\partial}{\partial\zeta} - 1\right]e^{i\zeta}\mathcal{X}(\zeta,\tau)\right\rangle_z \\ &= \left[\frac{\partial^2}{\partial\zeta^2} - 2i\frac{\partial}{\partial\zeta} - 1\right]\left\langle e^{i(\zeta+\omega_L\tau)}\mathcal{X}(\zeta,\tau)\right\rangle_z .\end{aligned}$$

Due to our eikonal assumptions (3.43), we can drop the second order ζ-derivatives in what follows. Thus, alternately multiplying (3.41) by $e^{i(\zeta+\omega_L\tau)}$ and $e^{-i(\zeta+\omega_L\tau)}$ and integrating over one wavelength, we find

$$\left[\frac{\partial}{\partial\tau} - i\frac{\omega_L^2-1}{2\omega_L}\right]g_1 - i\frac{\omega_L^2-1}{2\omega_L}g_{-1}^* - \left[\frac{1}{\omega_L}\frac{\partial}{\partial\zeta} - \frac{i}{2\omega_L}\right]\mathcal{Q}(\zeta,\tau) = \mathscr{F} \tag{3.45a}$$

$$\left[\frac{\partial}{\partial\tau} + i\frac{3\omega_L^2+1}{2\omega_L}\right]g_{-1} - i\frac{\omega_L^2-1}{2\omega_L}g_1^* + \left[\frac{1}{\omega_L}\frac{\partial}{\partial\zeta} + \frac{i}{2\omega_L}\right]\mathcal{Q}^*(\zeta,\tau) = \mathscr{F}^*, \tag{3.45b}$$

where we have defined

$$\mathcal{Q}(\zeta,\tau) \equiv \left\langle e^{i(\zeta'+\omega_L\tau)}\left[2\int du\; fu^2 - \left(\frac{\partial\phi}{\partial\zeta'}\right)^2\right]\right\rangle_z , \tag{3.46a}$$

$$\mathscr{F}(\zeta,\tau) \equiv \frac{i}{\omega_L}\left\langle e^{i(\zeta'+\omega_L\tau)}\frac{\partial}{\partial\zeta'}\left[\frac{c^2k_2^2}{2\omega_p^2}\frac{\partial\boldsymbol{a}_\perp^2}{\partial\zeta}(1+g+g^*)\right]\right\rangle_z . \tag{3.46b}$$

Simplification of the drive term $\mathscr{F}$ yields the desired lowest order coupling to the lasers. Integrating the average $\langle\cdot\rangle_z$ by parts results in

$$\mathscr{F}(\zeta,\tau) = \frac{1}{\omega_L}\left\langle e^{i(\zeta'+\omega_L\tau)}\left[\frac{c^2k_2^2}{2\omega_p^2}\frac{\partial\boldsymbol{a}_\perp^2}{\partial\zeta}(1+g+g^*)\right]\right\rangle_z + O\Big(\tfrac{\partial}{\partial\zeta}\mathscr{F}\Big). \tag{3.47}$$

From the assumed form (3.18) of the vector potential, the dominant contribution to the ponderomotive force $\frac{\partial}{\partial\zeta}\boldsymbol{a}_\perp^2$ is given by

$$\frac{\partial}{\partial\zeta}\boldsymbol{a}_\perp^2(\zeta,\tau) = -ia_0a_1^*e^{-i(\zeta+\omega_2\tau)} + ia_0^*a_1e^{i(\zeta+\omega_2\tau)} + \ldots .$$

The dots represent terms that are either small due to our eikonal assumptions or rapidly oscillating and would otherwise be subsequently averaged away. Using the Fourier-eikonal expansion (3.42) for $g(\zeta,\tau)$, and neglecting the higher order couplings, we see that

$$\mathscr{F}(\zeta,\tau) \approx -\frac{i}{\omega_L}\frac{c^2k_2^2}{2\omega_p^2}a_0(\zeta,\tau)a_1^*(\zeta,\tau)\,e^{-i(\omega_2-\omega_L)\tau}. \tag{3.48}$$

To further simplify the Langmuir wave equation, we now use results that will be obtained in subsequent analysis. In the following sections, we will show that in two limits (the initial, linear value problem and the asymptotic, phase-mixed case) $\mathcal{Q}(\zeta,\tau)$ can be written in the form:

$$\mathcal{Q}(\zeta,\tau) = (\omega^2 - 1)(g_1 + g_{-1}^*), \tag{3.49}$$

where the (possibly complex, possibly nonlinear) frequency ω will also be determined later. If we additionally assume that the dispersion relation remains of the Bohm-Gross form $\omega^2 = \omega_p^2 + \beta k^2$, we find that the scaled group velocity is

$$u_{\rm gr} = \frac{k}{\omega_p}\frac{d\omega}{dk} = \frac{\omega^2 - \omega_p^2}{\omega_p\,\omega}. \tag{3.50}$$

Finally, we assume that the time-scale set by the plasma frequency ω_p is much faster that that associated with the change in the Langmuir wave amplitude. In this, the so-called Raman limit of stimulated scattering, the temporal and spatial derivatives in (3.45b) can be neglected, and the resulting algebraic equation solved for g_1^*:

$$g_{-1}^* \approx \frac{\omega_L^2 - \omega^2}{3\omega_L^2 - \omega^2} g_1 + i\frac{2\omega_L}{3\omega_L^2 - \omega^2}\mathscr{F}. \tag{3.51}$$

Now, we combine the lowest order expressions for the slowly-evolving Langmuir wave, namely: the lowest order drive (3.48), the term $\mathcal{Q}$ given by (3.49), the group velocity (3.50), and the non-resonant Langmuir wave (3.51). Neglecting terms of order $(\omega_L - \omega)^3$ under the assumption that the plasma wave is nearly resonant, the system (3.45) simplifies to

$$\left[\frac{\partial}{\partial\tau} + i(\omega - \omega_L) - u_{\rm gr}\frac{\partial}{\partial\zeta}\right] g_1 = -\frac{ic^2k_2^2}{2\omega_L\omega_p^2} a_0 a_1^* e^{-i(\omega_2 - \omega_L)\tau}. \tag{3.52}$$

As mentioned previously, the rest of this chapter concerns itself with obtaining closed form expressions for the term $\mathcal{Q}(\zeta,\tau)$ in two limits: the first for an initial value problem with linear amplitudes, the second corresponding to the asymptotic, phase-mixed limit. As alluded to, we will find that in these two limits $\mathcal{Q}$ is given in the form (3.49), so that Eq. 3.52 holds. We then link these two limits with a physically motivated, albeit

heuristic, model to obtain a simplified, closed set of equations for the laser and plasma wave amplitudes.

3.2 Dynamic damping and frequency shift for the plasma wave equation

In this section, we determine simplified expressions of the plasma wave damping and frequency shift in two limits. The first limit is that of a linear, initial value problem, in which case the results are naturally expressible in terms of the plasma dispersion function [77]. The second limit corresponds to the asymptotic, phase-mixed state presented in Ch. 2 with its associated frequency shift and vanishing damping.

3.2.1 The envelope equation in the initial value, linear limit

In the linear, $\tau = 0$ limit, we assume that the distribution function can be written as a sum of the initial Maxwellian and a small perturbation:

$$f = \frac{e^{-u^2/2\sigma^2}}{\sigma\sqrt{2\pi}} + f_1 \equiv f_0 + f_1. \tag{3.53}$$

Taking the Fourier-Laplace transform of the Vlasov equation and using the expansion (3.53), we have

$$\big[\omega + v_z k\big]\tilde{f}_1(v_z,k,\omega) + k\tilde{\phi}(k,\omega)\frac{\partial f_0}{\partial v_z} = -\int d\omega' dk'\; k'\tilde{\phi}(k',\omega')\frac{\partial}{\partial v_z}\tilde{f}_1(v_z,k-k',\omega-\omega'), \tag{3.54}$$

where the tilde indicates the Fourier-Laplace transform[4], and we have omitted the ponderomotive drive. Assuming that the perturbation is small, i.e., $f_1 \ll f_0$, we neglect the convolution on the right-hand side of (3.54), and then solve for $\tilde{f}_1$ in terms of the potential and the unperturbed distribution:

$$\tilde{f}_1(k,\omega) = -\tilde{\phi}(k,\omega)\frac{\frac{\partial}{\partial v_z}f_0(v_z)}{v_z + \omega/k}, \tag{3.55}$$

[4]To more easily mesh with our choice of the plasma wave having carrier wave vector $-k_2 < 0$, the sign convention for the Fourier transform is opposite that of standard analysis.

To be consistent with the previous section, we write (3.55) in terms of the dimensionless frequency $\hat{\omega} \equiv \omega/\omega_p$ and the dimensionless wave vector $\hat{k} \equiv k/k_2$. In terms of these variables, the Poisson equation implies that the Fourier transform of the potential is approximately given by

$$\tilde{\phi}(\hat{k},\hat{\omega}) = -\frac{1}{\hat{k}^2}\frac{\delta\tilde{n}}{n_0} = -\frac{1}{\hat{k}^2}\left(\tilde{g}+\tilde{g}^*\right) \approx -\frac{1}{2}\sum_{n\neq 0}\frac{1}{\hat{k}^2}\Big[\tilde{g}_n\delta(\hat{k}+n)+\tilde{g}_n^*\delta(\hat{k}-n)\Big]. \tag{3.56}$$

We insert the linear relation (3.55) with the potential (3.56) into the nonlinear/thermal average (3.46a). Taking the inverse Fourier-Laplace transform and neglecting the higher-order nonlinear terms, we find

$$\mathcal{Q}(\zeta,\tau) \approx -\left(g_1+g_{-1}^*\right)\int_{\mathcal{C}} du \frac{u^2}{u+\omega}\frac{\partial f_0}{\partial u}, \tag{3.57}$$

where the velocity integration proceeds along the usual Landau contour $\mathcal{C}$, defined to lie below all the poles in the complex u-plane [3, 4]. To write (3.57) in the simplified form (3.49), we manipulate the integral as follows:

$$\begin{aligned}\int_{\mathcal{C}} du\,\frac{u^2}{u+\omega}\frac{\partial f_0}{\partial u} = \int_{\mathcal{C}} du\,\left[u-\omega+\frac{\omega^2}{u+\omega}\right]\frac{\partial f_0}{\partial u} &= -1-\omega^2\int_{\mathcal{C}} du\, f_0\frac{\partial}{\partial u}\frac{1}{u+\omega}\\ &= -1-\frac{\omega^2}{\sqrt{2\pi}\sigma}\frac{\partial}{\partial\omega}\int_{\mathcal{C}} du\,\frac{e^{-u^2/2\sigma^2}}{u+\omega},\end{aligned} \tag{3.58}$$

where we have taken the initial unperturbed distribution $f_0(u)$ to be Maxwellian. The second term in (3.58) is closely related to the linear susceptibility of the plasma, and therefore equal to -1 for ω satisfying the linear dispersion relation. To make this more explicit, we set $x \equiv u/\sigma$, $\alpha \equiv -\omega/\sigma$, obtaining

$$\mathcal{Q} = \left(g_1+g_{-1}^*\right)\left[-1+\omega^2\frac{1}{\sigma^2\sqrt{2\pi}}\frac{\partial}{\partial\alpha}\int_{\mathcal{C}} dx\,\frac{e^{-x^2/2}}{u-\alpha}\right].$$

Along the Landau contour, for a given temperature set by $k^2\lambda_D^2 \equiv \sigma^2$ and complex phase velocity α, the linear plasma dispersion relation is given by

$$\begin{aligned}1-\varepsilon(\sigma,\alpha) &= \frac{1}{\sigma^2\sqrt{2\pi}}\frac{\partial}{\partial\alpha}\int_{\mathcal{C}} dx\,\frac{e^{-x^2/2}}{u-\alpha}\\ &= \frac{1}{\sigma^2\sqrt{2\pi}}\frac{\partial}{\partial\alpha}\left[\mathscr{P}\int dx\,\frac{e^{-x^2/2}}{u-\alpha}+i\pi e^{-\alpha^2/2}\right] = 1.\end{aligned} \tag{3.59}$$

If desired, (3.59) can be directly written in terms of the so-called plasma dispersion function[5] [77]. Regardless, enforcing the Landau dispersion relation (3.59) yields the complex frequency frequency $\omega = \omega_r - i\nu_\ell$ of the electrostatic oscillation; this gives rise to the Landau damping associated with phase-mixing of the Case-van Kampen modes of the distribution function. Decomposing the natural frequency into its real and imaginary parts in this way, the Langmuir wave envelope equation (3.52) becomes

$$\left[\frac{\partial}{\partial\tau} + i(\omega_r - \omega_L) + \nu_\ell - u_{\rm gr}\frac{\partial}{\partial\zeta}\right] g_1 = -\frac{ic^2k_2^2}{2\omega_L\omega_p^2} a_0 a_1^* e^{-i(\omega_2-\omega_L)\tau}. \tag{3.60}$$

This Langmuir wave governing equation is as one might expect; in the linear limit, similar envelope equations (and related equations for the wave energy) can be derived by expanding the dielectric assuming eikonal wave fields (see, e.g., [78, 79]).

3.2.2 The envelope equation in the time asymptotic, BGK-type limit

Complementary to the initial value problem of the previous section, we consider here the case where the electrons have made many oscillations in the wave, producing the time-asymptotic, BGK-type limit presented in Ch. 2. In this case, we have seen that the Landau damping has been phase-mixed away while the flattening of $f(v)$ at the phase velocity (as described by the action *ansatz* distribution) gives rise to a nonlinear frequency shift. In analogy with our discussion of the initial value problem, we anticipate obtaining the following expression for the kinetic/nonlinear term $\mathcal{Q}(\zeta,\tau)$

$$\mathcal{Q} \to \left[(\omega_L + \delta\omega)^2 - 1\right](g_1 + g_{-1}^*). \tag{3.61}$$

Using the pendulum limit, for which the potential is assumed to have only one harmonic so that $\phi_n = 0$ for $n \geq 2$, we show this to be true analytically, while in the general case we resort to numerical analysis.

[5] With root finding software readily available, we find the explicit use of the plasma dispersion function $Z(\zeta)$, as it is ususally written, to be unnecessary, particularly since it is expressible in terms of other well-known functions, i.e., the complex error function. Thus, we choose not to use it.

Time asymptotic limit in the pendulum approximation

To consistently evaluate the single harmonic, pendulum limit, we first note that assuming a single harmonic potential and an action-invariant distribution induces a second (and third, etc.) harmonic. Using the bulk, trapped, and passing distributions $f_{\rm I}$, $f_{\rm II}$, and $f_{\rm III}$ defined in (2.37), the second harmonic is obtained via

$$\begin{aligned}\phi_2 &= -\tfrac{1}{2}\left\langle \cos 2\theta \right\rangle_z = -\tfrac{1}{2}\left\langle 8\cos^4(\theta/2) - 8\cos^2(\theta/2) + 1 \right\rangle_z \\ &= -\frac{1}{2}\int_1^\infty d\kappa\, \frac{f_{\rm I}(\kappa) + f_{\rm III}(\kappa)}{\mathscr{K}(\mu)} \int_0^{\mathscr{K}(\mu)} dx \left[8\,\mathrm{sn}^4(\mu,x) - 8\,\mathrm{sn}^2(\mu,x) + 1\right] \\ &\quad - \frac{1}{2}\int_0^1 d\kappa\, \frac{f_{\rm II}^-(\kappa) + f_{\rm II}^+(\kappa)}{\mathscr{K}(\kappa)} \int_0^{\mathscr{K}(\kappa)} dy \left[8\kappa^4\,\mathrm{sn}^4(\kappa,y) - 8\kappa^2\,\mathrm{sn}^2(\kappa,y) + 1\right].\end{aligned} \tag{3.62}$$

Since we have assumed a monochromatic potential described by ϕ_1, in future calculations we must also neglect terms of the form (3.62). In other words, retention of such terms would require consistent calculation of the dynamics using the potential described by ϕ_1 and ϕ_2, and is beyond our analysis here. To evaluate the integrals (3.62) and a similar one to follow, we make use of the identities [53, pp 629-630]

$$\mathrm{cn}^2(\kappa,x) = 1 - \mathrm{sn}^2(\kappa,x) \qquad \mathrm{dn}^2(\kappa,x) = 1 - \kappa^2\,\mathrm{sn}^2(\kappa,x) \tag{3.63a}$$

$$3\kappa^2 \int_0^{\mathscr{K}(\kappa)} dx\ \mathrm{sn}^4(\kappa,x) = \int_0^{\mathscr{K}(\kappa)} dx\ \left[2\left(1+\kappa^2\right)\mathrm{sn}^2(\kappa,x) - 1\right] \tag{3.63b}$$

$$\kappa^2 \int_0^{\mathscr{K}(\kappa)} dx\ \mathrm{sn}^2(\kappa,x) = \mathscr{K}(\kappa) - \mathscr{E}(\kappa). \tag{3.63c}$$

This gives

$$\begin{aligned}\phi_2 = &\int_1^\infty d\kappa \left[f_{\rm I}(\kappa) + f_{\rm III}(\kappa)\right]\left[\frac{16(\kappa^2-\kappa^4)-3}{6} + \frac{4(2\kappa^4-\kappa^2)}{3}\frac{\mathscr{E}(1/\kappa)}{\mathscr{K}(1/\kappa)}\right] \\ &+ \int_0^1 d\kappa \left[f_{\rm II}^+(\kappa) + f_{\rm II}^-(\kappa)\right]\left[\frac{5-8\kappa^2}{6} + \frac{4(2\kappa^2-1)}{3}\frac{\mathscr{E}(\kappa)}{\mathscr{K}(\kappa)}\right].\end{aligned} \tag{3.64}$$

Numerical evaluation of the integral (3.64) indicates that the second harmonic of the potential satisfies $\phi_2 \sim \frac{1}{4}\phi_1^2$, as to be anticipated from the warm fluid theory (see, e.g.,

[80, 81]). Keeping in mind that consistency of our approximation requires neglecting such terms, we proceed by evaluating the term $\mathcal{Q}(\zeta,\tau)$ using our assumed invariant-in-action distribution function. First, we note that in the pendulum limit, the contribution from the phase-weighted electrostatic energy is zero

$$\left\langle e^{i(\zeta'+\omega_L\tau)}\left(\frac{\partial\phi}{\partial\zeta'}\right)^2\right\rangle_z = \sum_{n=1}^{\infty}\frac{n(n+1)}{2}\phi_n\phi_{n+1}e^{i(\psi_n-\psi_{n+1})}\to 0.$$

Next, we calculate the first term in $\mathcal{Q}$, proportional to the phase-weighted kinetic energy:

$$\begin{aligned}2\left\langle u^2 e^{i(\zeta'+\omega_L\tau)}\right\rangle_{\mathcal{PS}} &= 2\left\langle (p-\omega_L)^2 e^{i(\zeta'+\omega_L\tau)}\right\rangle_{\mathcal{PS}}\\ &= 2e^{-i\psi}\left\langle \left(\tfrac{d\theta}{d\tau}\right)^2 e^{i\theta}\right\rangle_{\mathcal{PS}} - 4(\omega_L+\delta\omega)e^{-i\psi}\left\langle \tfrac{d\theta}{d\tau}e^{i\theta}\right\rangle_{\mathcal{PS}}\\ &\quad + (\omega_L+\delta\omega)^2\left(g_1+g_{-1}^*\right),\end{aligned} \tag{3.65}$$

where we have used $p=\frac{d}{d\tau}\theta-\delta\omega$ and replaced the bunching with the modes g_1, g_{-1}^*. In the limit of a fully phase-mixed distribution, the last term on the first line of (3.65) vanishes, while

$$\left\langle \left(\tfrac{d\theta}{d\tau}\right)^2 e^{i\theta}\right\rangle_{\mathcal{PS}} = \left\langle \left(\tfrac{d\theta}{d\tau}\right)^2\cos\theta\right\rangle_{\mathcal{PS}}. \tag{3.66}$$

Since (3.66) is real, it provides a pure nonlinear frequency shift of the wave; we note that we expect the terms $\sim i\sin\theta$ to provide damping, which should initially reproduce the Landau damping of the previous section, while at long times should asymptote to zero as appropriate for a fully phase-mixed distribution function. In subsequent sections, we provide a heuristic way to describe this dynamical process. Now, we turn to calculating (3.66) for our assumed BGK-type action distribution. Using the pendulum relations (2.31), (2.33), and (2.34), the phase-space average (2.39), and the coordinates $x\equiv\kappa\sqrt{\phi_1}\tau$, $y\equiv\sqrt{\phi_1}\tau$, and $\mu\equiv 1/\kappa$, we have

$$\begin{aligned}\left\langle \left(\tfrac{d\theta}{d\tau}\right)^2 e^{i\theta}\right\rangle_{\mathcal{PS}} &= \int_1^\infty d\kappa\,\left[f_{\mathrm{I}}(\kappa)+f_{\mathrm{III}}(\kappa)\right]\int_0^{\mathscr{K}(\mu)} dx\,\frac{4\phi_1\,\mathrm{dn}^2(\mu,x)}{\mu^2\,\mathscr{K}(\mu)}\left[2\,\mathrm{cn}^2(\mu,x)-1\right]\\ &\quad + \int_0^1 d\kappa\,\left[f_{\mathrm{II}}^-(\kappa)+f_{\mathrm{II}}^+(\kappa)\right]\int_0^{\mathscr{K}(\kappa)} dy\,\frac{4\kappa^2\phi_1\,\mathrm{cn}^2(\kappa,y)}{\mathscr{K}(\kappa)}\left[2\,\mathrm{dn}^2(\kappa,y)-1\right].\end{aligned} \tag{3.67}$$

We can perform the x and y integrals analytically with the tables of Gradshteyn and Ryzhik [53, pp 630]. Using the identities (3.63) and the expression for ϕ_2 (3.62) gives

$$\begin{aligned} 2\left\langle \left(\tfrac{d\theta}{d\tau}\right)^2 e^{i\theta}\right\rangle_{\mathcal{PS}} &= \int_1^\infty d\kappa\, \left[f_{\rm I}(\kappa)+f_{\rm III}(\kappa)\right]\frac{8\phi_1\kappa^2}{3}\left[2-2\kappa^2+\left(2\kappa^2-1\right)\frac{\mathscr{E}(1/\kappa)}{\mathscr{K}(1/\kappa)}\right] \\ &\quad + \int_0^1 d\kappa\, \left[f_{\rm II}^-(\kappa)+f_{\rm II}^+(\kappa)\right]\frac{8\phi_1}{3}\left[1-\kappa^2+\left(2\kappa^2-1\right)\frac{\mathscr{E}(\kappa)}{\mathscr{K}(\kappa)}\right] \\ &= \phi_1\big(1+2\phi_2\big). \end{aligned} \tag{3.68}$$

Poisson's equation relates (3.68) to the modes g_1 and g_{-1}:

$$\frac{\partial^2\phi}{\partial\zeta^2} = -\sum_{n=1}^\infty n^2\phi_n\cos[n(\zeta+\omega_L\tau)+\psi] = \frac{\delta n}{n_0} = \frac{1}{2}\sum_{n\neq 0} g_n e^{-in(\zeta+\omega_L\tau)}.$$

Multiplying by $e^{i(\zeta+\omega_L\tau)}$ and integrating over 2π in ζ yields

$$\phi_1 = -\left(g_1+g_{-1}^*\right)e^{i\psi}. \tag{3.69}$$

Thus, using (3.69) in (3.68), the phase-weighted kinetic energy (3.65) is given by

$$2\left\langle u^2 e^{i(\zeta'+\omega_L\tau)}\right\rangle_{\mathcal{PS}} = \left[(\omega_L+\delta\omega)^2-1\right](g_1+g_{-1}^*) = \mathcal{Q}(\zeta,\tau). \tag{3.70}$$

Again, we see that the kinetic/nonlinear term in the Langmuir envelope equation is given in the form $\sim(\omega^2-1)$, only in this case the frequency is purely real, but is also a nonlinear function of the plasma wave amplitude as determined in Sec. 2.2.4.

Langmuir envelope equation in the general, nonlinear, time asymptotic limit

We have shown that a single harmonic potential leads to a time-asymptotic nonlinear frequency shift of the Langmuir wave, as indicated by (3.70). For the fully nonlinear wave, one must numerically determine the distribution and potential via the system of equations (2.21), from which the averaged quantity $\mathcal{Q}$ can be determined. While this can be done in principle, it is complicated by the fact that the various terms comprising $\mathcal{Q}$ tend to be much larger than $\mathcal{Q}$ itself, so that very precise numerical calculations must be made at every step to obtain the appropriate cancelation between terms.

From previous arguments, we know that in the time asymptotic, fully phase-mixed limit, the plasma wave is stationary (not damped), and has a nonlinear frequency given by $\omega_L + \delta\omega$, where $\delta\omega$ is a function of the Langmuir amplitude, resulting from thermal and trapped particle effects. In the previous section, we showed that this frequency shift is precisely what appears in the Langmuir envelope equation. Numerical evaluations of $\mathcal{Q}$ indicate that in the general, nonlinear case, $\mathcal{Q}$ is similarly given by (3.61), so that the total contribution to the envelope equation is again the frequency shift $\delta\omega$; as mentioned earlier, however, it is difficult to obtain this result numerically with high precision. For these reasons, we take the following form for the Langmuir wave amplitude equation in the asymptotic, phase-mixed limit:

$$\left[\frac{\partial}{\partial\tau} + i\delta\omega - u_{\rm gr}\frac{\partial}{\partial\zeta}\right] g_1(\zeta,\tau) = -\frac{ic^2k_2^2}{2\omega_L\omega_p^2} a_0(\zeta,\tau)a_1^*(\zeta,\tau)\, e^{-i(\omega_2-\omega_L)\tau}, \tag{3.71}$$

where the purely real, nonlinear frequency shift $\delta\omega$ is obtained via (2.24) using the phase-mixed distribution and potential determined by (2.21). We have found that over the wide range of temperatures and amplitudes investigated here, namely $0.4 \le k_2\lambda_D \le 0.1$ and $0 \le |g_1| \le 0.5$, this frequency shift is approximately given by an analytic expression:

$$\begin{aligned}\delta\omega \approx -\frac{e^{-\omega_L^2/2\sigma^2}}{\sqrt{2\pi}\sigma}\Bigg[&1.09\,\frac{\omega_L\left(\frac{\omega_L^2}{\sigma^2}-1\right)}{\omega_L^2-1-\sigma^2}\sqrt{|g_1|} + 40\,|g_1| + 7.8\frac{\omega_L^2}{\sigma^4}\,|g_1|^2 \\ &+ 0.115\frac{(\omega_L^2-8\sigma^2)^2}{\sigma^{11}}\,|g_1|^4\Bigg] + 6\sigma^2\Big(|g_1|^2 + 3\,|g_1|^4 - 250\,|g_1|^8\Big)\,.\end{aligned} \tag{3.72}$$

The expression (3.72) can be roughly considered as consisting of two contributions: the first, in square brackets, arises from the resonant and near-resonant particles (and thus is proportional to the number particles near the phase velocity, $\sim e^{-\omega_L^2/2\sigma^2}$); the second, in parentheses, can be thought of as resulting from the fluid nonlinearities, and scales as the temperature σ^2. We reiterate that, while quite complicated, (3.72) is widely applicable, roughly valid for $0.1 \le k_2\lambda_D \le 0.4$. If one is only interested in warmer plasmas, simpler expressions with fewer terms can be fit to $\delta\omega$, but we do not pursue that further here.

3.2.3 The extended three-wave equations

In this section, we complete the derivation of our model coupling the two laser amplitudes to that of the Langmuir wave envelope via an extended three-wave model. To do this, we must collect various results that are scattered throughout the text. We begin with the equations governing the lasers (3.33). Replacing the bunching $\left\langle \frac{\delta n}{n_0} e^{i(\omega_2\tau+\zeta)} \right\rangle_z$ with our Langmuir modes $g_{\pm 1}$ using the relation (3.44):

$$\left[\frac{\partial}{\partial\tau} - u_0\frac{\partial}{\partial\zeta} - \frac{i\omega_p}{\omega_0}\boldsymbol{\nabla}_\perp^2\right] a_0(\zeta,\tau) = -\frac{i\omega_p}{4\omega_0} a_1(\zeta,\tau)\left[g_1 + g_{-1}^*\right] e^{i(\omega_2-\omega_L)\tau} \tag{3.73a}$$

$$\left[\frac{\partial}{\partial\tau} + u_1\frac{\partial}{\partial\zeta} - \frac{i\omega_p}{\omega_1}\boldsymbol{\nabla}_\perp^2\right] a_1(\zeta,\tau) = -\frac{i\omega_p}{4\omega_1} a_0(\zeta,\tau)\left[g_1^* + g_{-1}\right] e^{-i(\omega_2-\omega_L)\tau}. \tag{3.73b}$$

Again, we eliminate the mode g_{-1} with the slowly-varying approximation (3.51). At this point, we could introduce the wave actions for the pump laser, seed laser, and Langmuir wave, along with the wave coupling $\mathcal{W}$

$$a \equiv \sqrt{\tfrac{\omega_0}{\omega_p}} a_0, \qquad b \equiv \sqrt{\tfrac{\omega_1}{\omega_p}} a_1,$$

$$\rho \equiv \sqrt{\omega_L}\frac{i\omega_p}{\sqrt{2}ck_2} g_1\, e^{e^{i(\omega_2-\omega_L)\tau}}, \qquad \mathcal{W} \equiv \frac{ck_2}{2\sqrt{2\omega_0\omega_1\omega_L}},$$

to write the equations in manifest wave-action form. However, we find that this will require a change in notation that does unnecessary violence to our attempts at coherency across the chapters. For this reason, we only make a minor change, by introducing the phase-shifted Langmuir wave amplitude

$$\mathcal{G} \equiv -ig_1 e^{i(\omega_2-\omega_L)\tau}. \tag{3.74}$$

We use this definition, the laser equations (3.73) with g_{-1}^* eliminated, and the Langmuir wave equations (3.60) and (3.71), to obtain the following three coupled-mode equations:

$$\left[\frac{\partial}{\partial\tau} - u_0\frac{\partial}{\partial\zeta} + i\frac{c^2k_2^2\,|a_1|^2}{32\omega_p\omega_0\omega_L^2} - \frac{i\omega_p}{\omega_0}\boldsymbol{\nabla}_\perp^2\right] a_0(\zeta,\tau) = \quad \frac{\omega_p}{4\omega_0} a_1(\zeta,\tau)\mathcal{G}(\zeta,\tau) \tag{3.75a}$$

$$\left[\frac{\partial}{\partial\tau} + u_1\frac{\partial}{\partial\zeta} + i\frac{c^2k_2^2\,|a_0|^2}{32\omega_p\omega_1\omega_L^2} - -\frac{i\omega_p}{\omega_1}\boldsymbol{\nabla}_\perp^2\right] a_1(\zeta,\tau) = -\frac{\omega_p}{4\omega_1} a_0(\zeta,\tau)\mathcal{G}^*(\zeta,\tau) \tag{3.75b}$$

$$\left[\frac{\partial}{\partial\tau} - u_{gr}\frac{\partial}{\partial\zeta} + i\big(\omega-\omega_2\big) + \nu\right]\mathcal{G}(\zeta,\tau) = -\frac{c^2k_2^2}{2\omega_L\omega_p^2} a_0(\zeta,\tau)a_1^*(\zeta,\tau). \tag{3.75c}$$

Here, the frequency ω and damping ν have the initial, linear expression indicated in (3.60), while asymptotically appear as in (3.71). The question remains how the initial, complex frequency $\omega_r - i\nu_\ell$ of the Landau dispersion relation (3.59) evolves into the nonlinear, real frequency $\omega_L + \delta\omega$ associated with the asymptotically phase-mixed distribution. Schematically, as time progresses we have

$$\omega(t=0) = \omega_r \to \omega(t=\infty) = \omega_L + \delta\omega, \qquad \nu(t=0) = \nu_\ell \to \nu(t=\infty) = 0. \tag{3.76}$$

The dynamics encapsulated within the arrows in (3.76) are complicated, involving orbit modification, phase-mixing, and trapping of many particles with widely disparate initial conditions in a changing Langmuir wave. In the simplified case of an initial plasma wave whose amplitude does not change dramatically before particles phase-mix in the wave, a dynamic expression for the damping was first calculated by O'Neil in his pioneering work on nonlinear Landau damping [6], while a similar expression for the frequency shift was given later by Morales and O'Neil [24]. The latter work indicates that the nonlinear Landau damping oscillates with a period of order the bounce period while asymptotically approaching zero, while the frequency shift oscillates (with decreasing amplitude) at approximately twice the bounce frequency about its asymptotic value. After about 3-5 bounce periods, both the damping and the frequency have attained their respective asymptotic values. While these results serve to illuminate the process, they do not directly apply to a driven Langmuir wave. Furthermore, we anticipate that any attempt to generalize these (already complicated[6]) expressions would lead to a dramatic increase in the complexity of the system, which is against the spirit of our reduced description. For this reason, in the next section we present a simple model describing the process (3.76) based on energy conservation: the electrostatic energy that is "lost" due to Landau damping is equal to the kinetic energy gain associated with particle phase-mixing.

[6]The dynamic damping given in Ref. [6] involves an infinite sum over complicated integrals involving trigonometric functions whose arguments are elliptic functions. The dynamic frequency shift is not in any readily accessible source, although [24] indicates that it involves multiple sums over similar integrals.

3.3 Phase-mixing as a means to formulate a simplified model of nonlinear Landau damping

Our model owes much to the asymptotic result obtained by O'Neil in his landmark paper on nonlinear Landau damping [6]. After first deriving the evolution of the Langmuir wave in the regime where the damping is much smaller than the bounce period (so that the wave amplitude changes little before Landau damping has been "washed out"), Ref. [6] proceeds to show that the loss in electrostatic energy from Landau damping is equal to the increase in kinetic energy of the particles. This is a simple consequence of energy conservation and illuminates the "irreversible" nature of Landau damping, since in essence it states that the originally "coherent" electrostatic energy of the plasma wave is converted to the "incoherent" kinetic energy of the phase-mixed distribution. It must be stressed that because the Vlasov equation conserves the plasma entropy, this notion of phase-mixed, incoherent energy is only viable in a course-grained sense; nevertheless, in Ref. [6] O'Neil showed that because nearby particles have different frequencies in the wave, the phase-space area over which one must course-grain goes to zero as $t \to \infty$. Thus, in the long-time limit any macroscopic measure of the entropy increases, and one has a consistent notion of this transfer from coherent to incoherent energy in the plasma wave[7].

Although the basic physics (energy conservation in nonlinear Landau damping) of our model is quite similar to O'Neil's, our analysis also has much in common with the work of Dewar [10], who adopted the ideas of particle trapping and subsequent phase-mixing to serve as a nonlinear saturation mechanism of plasma instabilities. In particular, Dewar used momentum conservation to equate the increase in wave momentum of the growing, unstable mode to that of the trapped particles, thereby obtaining an expression for the saturated electrostatic potential. To determine the trapped particle momentum

[7]Note that these arguments are adopted from the general ideas underlying "irreversibility" in many-degree-of-freedom Hamiltonian systems. Although the dynamics of each particle may be time-reversible, macroscopic averages of these particles typically do not respect this symmetry (i.e., for many initial conditions there is one final state) and time has a "natural" direction.

and saturated Langmuir wave amplitude, Dewar used the distribution function assuming a constant particle action that he introduced in [25]. We will find that our theory reproduces his analytic result in the small amplitude limit, much like was found Sec. 2.3. For larger amplitude potentials, however, our asymptotic phase-mixed distribution described in Ch. 2 results in a mean shift in canonical action, and the two theories give quite different answers (see Fig. 2.7).

In this section, we calculate the phase-mixed (i.e., incoherent) energy required to develop the invariant-in-action-difference distribution introduced in Ch. 2. Since we assume that the source of this energy is the electrostatic wave, we thereby obtain the total amount of energy to be lost by (nonlinear) Landau damping as a function of the wave amplitude ϕ_1. We will then use this in Sec. 3.4 to formulate an extended three-wave model of Raman backscatter in a plasma.

3.3.1 The Langmuir wave action and associated incoherent energy

In this section, we derive two equations for the Langmuir wave action (i.e., plasmon number in quantum mechanical language): the first from the envelope equation of the Langmuir wave (3.75c), and the second directly from the Vlasov equation. Equating the resulting expressions leads to energy conservation: associated with the loss of coherent Langmuir wave energy due to the nonlinear damping coefficient $\nu(\phi_1, t)$ is an equal increase in phase-mixed (incoherent) kinetic energy of the particles. We begin with the Langmuir wave equation (3.75c):

$$\left[\frac{\partial}{\partial\tau} - u_{gr}\frac{\partial}{\partial\zeta} + i\big(\omega - \omega_2\big) + \nu\right]\mathcal{G} = -\frac{c^2k_2^2}{2\omega_L\omega_p^2}a_0a_1^*. \tag{3.77}$$

Multiplying (3.77) by $\omega_L^2\mathcal{G}^*$ and adding to the resulting equation its complex conjugate, we have

$$\left[\frac{\partial}{\partial\tau} - u_{\rm gr} + 2\nu(|\mathcal{G}|,\tau)\right]\left(\omega_L^2\,|\mathcal{G}|^2\right) = -\omega_L\frac{c^2k_2^2}{2\omega_p^2}\big(a_0^*a_1\mathcal{G} + a_0a_1^*\mathcal{G}^*\big). \tag{3.78}$$

Since the wave energy is given by the product of the wave action (or quanta) $\omega_L|\mathcal{G}|^2$ with its associated excitation energy ω_L, (3.78) describes how the wave energy evolves in time.

The second term on the left-hand side changes the local wave energy via advection in space, while the third term decreases the energy through a (possibly nonlinear) Landau-type damping; the right-hand side affects the Langmuir energy by coupling it to the lasers. This can be interpreted as inverse Joule heating via $J_{\rm PM}E_z$, where $J_{\rm PM}$ is an effective ponderomotive (longitudinal) current. To eliminate the driving term in favor of an expression involving only the Langmuir wave amplitude, we multiply the Vlasov equation (3.34) by u^2:

$$\frac{\partial}{\partial\tau}\left(fu^2\right)+\frac{\partial}{\partial\zeta}\left(fu^3\right)+\frac{\partial}{\partial u}\left(\frac{du}{d\tau}u^2f\right)-2\frac{du}{d\tau}uf=0. \tag{3.79}$$

We integrate (3.79) over all u and over a single wavelength in ζ, assuming that the energy flux is small, consistent with our assumptions that the plasma is slowly-varying on the laser beat scale. Using the expression (3.35) to replace the acceleration in favor of the electrostatic and ponderomotive forces, we obtain

$$\frac{1}{2}\frac{\partial}{\partial\tau}\int d\zeta du\; fu^2+\frac{1}{2}\frac{\partial}{\partial\zeta}\int d\zeta du\; fu^3=\int d\zeta du\; fu\frac{\partial\phi}{\partial\zeta}-\frac{c^2k_2^2}{2\omega_p^2}\int d\zeta du\; fu\frac{\partial\boldsymbol{a}_\perp^2}{\partial\zeta}. \tag{3.80}$$

We now simplify the right-hand side of (3.80). First, we use the longitudinal component of the Ampère-Maxwell law (2.22) to relate the longitudinal current to the potential:

$$\begin{aligned}\int d\zeta\;\frac{\partial\phi}{\partial\zeta}\int du\; fu=-\int d\zeta\;\frac{\partial\phi}{\partial\zeta}\frac{\partial^2\phi}{\partial\zeta\partial\tau}=-\frac{1}{2}\frac{\partial}{\partial\tau}\int d\zeta\;\left(\frac{\partial\phi}{\partial\zeta}\right)^2\\ \approx-\frac{1}{4}\left|\mathcal{G}\right|^2-\frac{1}{4}\sum_{n=2}^{\infty}n^2\left|\phi_n\right|^2\end{aligned} \tag{3.81}$$

Next, we integrate by parts the term involving the ponderomotive force on the right-hand side of (3.80), and use the continuity equation (3.37) to obtain

$$\int d\zeta\;\frac{\partial\boldsymbol{a}_\perp^2}{\partial\zeta}\int du\; fu=-\int d\zeta\;\boldsymbol{a}_\perp^2\frac{\partial}{\partial\zeta}\int du\; fu=\int d\zeta\;\boldsymbol{a}_\perp^2\frac{\partial}{\partial\tau}\int du\; f. \tag{3.82}$$

Finally, we replace the time derivative of the density with our electrostatic modes using (3.40), the Fourier expansion (3.42) and the definition (3.74). We then insert the ponderomotive laser drive $\boldsymbol{a}_\perp^2$ from (3.18) and neglect those terms that vary on the fast time

scales; the dominant result is given by

$$\frac{c^2k_2^2}{2\omega_p^2}\int d\zeta\ \boldsymbol{a}_\perp^2\,\frac{\partial}{\partial\tau}\int du\ f \approx -i\omega_L\frac{c^2k_2^2}{2\omega_p^2}a_0^*a_1\int d\zeta\ e^{i(\omega_2\tau+\zeta)}\big(g-g^*\big) - c.c.$$
$$\approx -\omega_L\frac{c^2k_2^2}{2\omega_p^2}\big(a_0^*a_1\mathcal{G}+a_0a_1^*\mathcal{G}^*\big). \tag{3.83}$$

Collecting the expressions (3.81) and (3.83) in the second moment equation (3.80), we obtain

$$\frac{\partial}{\partial\tau}\left\{\frac{1}{2}\left\langle u^2\right\rangle_{\mathcal{PS}}+\frac{1}{4}\left|\mathcal{G}\right|^2+\sum_{n=2}^{\infty}\frac{n^2}{4}\left|\phi_n\right|^2\right\}+\frac{1}{2}\frac{\partial}{\partial\zeta}\left\langle u^3\right\rangle_{\mathcal{PS}}=\omega_L\frac{c^2k_2^2}{4\omega_p^2}\big(a_0^*a_1\mathcal{G}+a_0a_1^*\mathcal{G}^*\big). \tag{3.84}$$

This is another expression for the change in the energy of the Langmuir wave. In this case, the sum of the kinetic and electrostatic energy in the plasma can be either advected via the last term on the left-hand side of (3.84) or changed by the inverse Joule heating on the right-hand side. Comparing (3.84) to the previous result involving the Langmuir wave energy (3.78), we can eliminate the coupling to the ponderomotive drive, obtaining

$$\frac{\partial}{\partial\tau}\left\{\frac{1}{2}\left\langle u^2\right\rangle_{\mathcal{PS}}-\frac{1}{2}\left(\omega_L^2-\tfrac{1}{2}\right)\left|\mathcal{G}\right|^2+\sum_{n=2}^{\infty}\frac{n^2}{4}\left|\phi_n\right|^2\right\}=\nu\,\omega_L^2\left|\mathcal{G}\right|^2. \tag{3.85}$$

Integrating in time, and assuming that initially $\mathcal{G}=\phi_n=0$ and $\left\langle u^2\right\rangle_{\mathcal{PS}}=\sigma^2$, we find that the integrated damped energy is given by the following relation

$$\omega_L^2\int_0^\tau d\tau'\ \nu(\tau')\left|\mathcal{G}\right|^2=\underbrace{\frac{1}{2}\Big[\left\langle u^2\right\rangle_{\mathcal{PS}}-\sigma^2\Big]}_{(1)}+\underbrace{\frac{1}{4}\left[\left|\mathcal{G}\right|^2+\sum_{n=2}^{\infty}n^2\left|\phi_n\right|^2\right]}_{(2)}-\underbrace{\frac{1}{2}\omega_L^2\left|\mathcal{G}\right|^2}_{(3)}. \tag{3.86}$$

We interpret the damped energy (3.86) as the incoherent energy associated with particle phase-mixing in the (nearly) sinusoidal potential. To be more explicit, we divide up the right-hand side into three parts: (1) is the change in kinetic energy of the particles; (2) consists of the total electrostatic energy; while (3) represents the wave energy. Thus, the incoherent, phase-mixed energy is given by the difference between the total [kinetic (1) plus potential (2)] and the wave energy (3). The latter wave energy can be understood as the coherent energy (in the form of the resonant Langmuir wave) of both the particles and potential. In the cold, linear limit, the scaled frequency $\omega_L\to 1$, and (3.86) indicates

that the wave energy is equal to twice the electrostatic energy. Furthermore, in this limit the electrostatic and kinetic energies are equal, so that their sum is precisely that given by the wave energy $\frac{1}{2}\omega_L^2 |\mathcal{G}|^2$ (in agreement with standard results, see, e.g., Nicholson [82, Sec. 6.6]).

The right-hand side of (3.86) can be evaluated for a given potential $\phi_1 = |\mathcal{G}|$ using the asymptotic, action *ansatz* distribution. We will find that this damped/phase-mixed energy, to lowest order, behaves as $\sim \nu_\ell |\mathcal{G}|^{3/2}$, where ν_ℓ is the linear Landau damping exponent. This implies that the damping coefficient is approximately that given by linear Landau damping for a time on the order of the bounce period in the wave, $\tau_B = 1/\sqrt{\phi_1}$. For times beyond the bounce period, particles have nearly completed an oscillation in the wave, and the damping has "phase-mixed away". This is precisely the effect that O'Neil discussed in [6], and we will show that our result for the right-hand side of (3.86) is similar to his asymptotic result for small amplitude waves. This saturation of Landau damping is also closely related to the saturation of plasma instabilities by particle trapping as studied by Dewar [10]. In fact, we obtain an identical expression for the saturated wave amplitude as that found by Dewar in the small amplitude limit $\phi_1^2 \ll \sigma^2$, only in our case the linear instability growth rate of [10] is replaced by the Landau damping rate. However, our analysis extends the saturation energy beyond this small amplitude regime, and it may be applicable to the nonlinear saturation of other plasma instabilities.

3.3.2 Small amplitude damped energy

In this section, we calculate the integrated, phase-mixed energy in the small amplitude limit. In this case, the higher harmonics are neglegible, i.e., $\phi_n = 0$ for $n \geq 2$, so that we again assume that the particles move in a pendulum-like potential. As previously mentioned, we find the right-hand side of (3.86) to be $\sim \phi^{3/2} = |\mathcal{G}|^{3/2}$, so that its small amplitude limit can be derived via

$$\lim_{\phi_1 \to 0} \frac{\omega_L^2}{\phi_1^{3/2}} \int_{-\infty}^{\infty} d\tau \; \nu(\tau)\phi_1(\tau)^2 = \lim_{\phi_1 \to 0} \frac{\langle u^2 \rangle_{\mathcal{PS}} - \sigma^2}{2\phi_1^{3/2}}.$$

We concentrate on the calculation of the numerator, keeping only those terms $\sim \phi_1^{3/2}$. In coordinates co-moving at the phase velocity of the wave, the average of the kinetic energy in terms of the canonical coordinates (2.6) is given by

$$\big\langle u^2 \big\rangle_{\mathcal{PS}} = \big\langle (p-\omega_L)^2 \big\rangle_{\mathcal{PS}} = \Big\langle \big(\tfrac{d\theta}{d\tau}\big)^2 \Big\rangle_{\mathcal{PS}} - \big(\omega_L + \delta\omega\big)^2. \tag{3.87}$$

In terms of integrals over the invariant-in-action distribution (in the pendulum limit), the average in (3.87) becomes

$$\begin{aligned}
\Big\langle \big(\tfrac{d\theta}{d\tau}\big)^2 \Big\rangle_{\mathcal{PS}} &= \int_1^\infty d\kappa \ \big[f_{\rm I}(\kappa) + f_{\rm III}(\kappa)\big] \frac{4\kappa^2\phi_1}{\mathscr{K}(1/\kappa)} \int_0^{\mathscr{K}(1/\kappa)} dx \ \mathrm{dn}^2(1/\kappa, x) \\
&\quad + \int_0^1 d\kappa \ \big[f_{\rm II}^-(\kappa) + f_{\rm II}^+(\kappa)\big] \frac{4\kappa^2\phi_1}{\mathscr{K}(\kappa)} \int_0^{\mathscr{K}(\kappa)} dy \ \mathrm{cn}^2(\kappa, y)
\end{aligned} \tag{3.88}$$

$$\begin{aligned}
&= 4\phi_1 \int_1^\infty d\kappa \ \big[f_{\rm I}(\kappa) + f_{\rm III}(\kappa)\big] \frac{\kappa^2\, \mathscr{E}(1/\kappa)}{\mathscr{K}(1/\kappa)} \\
&\quad + 4\phi_1 \int_0^1 d\kappa \ \big[f_{\rm II}^-(\kappa) + f_{\rm II}^+(\kappa)\big] \frac{\mathscr{E}(\kappa) + (\kappa^2-1)\,\mathscr{K}(\kappa)}{\mathscr{K}(\kappa)},
\end{aligned} \tag{3.89}$$

where the small amplitude distributions f_s are given by (2.37), and the integration over τ was performed, as in (2.40), using Gradshteyn and Ryzhik [53, pp 630]. We simplify the integrals of the first line in (3.89) by integrating by parts, obtaining

$$\begin{aligned}
\int_1^\infty d\kappa \ \big[f_{\rm I}(\kappa) + f_{\rm III}(\kappa)\big] \frac{4\phi_1\kappa^2\, \mathscr{E}(1/\kappa)}{\mathscr{K}(1/\kappa)} &= \bar{\mathcal{I}} \int_1^\infty d\kappa \ \big[f_{\rm I}(\kappa) - f_{\rm III}(\kappa)\big] \frac{\pi\kappa\sqrt{\phi_1}}{\mathscr{K}(1/\kappa)} \\
&\quad + \int_1^\infty d\kappa \ \big[f_{\rm I}(\kappa) + f_{\rm III}(\kappa)\big] \frac{\sigma^2\pi^2\kappa^2\, \mathscr{E}(1/\kappa)}{4(\kappa^2-1)\,\mathscr{K}(1/\kappa)^3} \\
&\equiv \bar{\mathcal{I}}\big(\omega_L + \delta\omega\big) + \int_1^\infty d\kappa \ \big[f_{\rm I}(\kappa) + f_{\rm III}(\kappa)\big] \frac{\sigma^2\pi^2\kappa^2\, \mathscr{E}(1/\kappa)}{4(\kappa^2-1)\,\mathscr{K}(1/\kappa)^3}.
\end{aligned} \tag{3.90}$$

Combing the expressions (3.89) and (3.90) with the average of the kinetic energy (3.87), we find that in the small amplitude limit the total change in kinetic energy is given by

$$\begin{aligned}\big\langle u^2\big\rangle_{\mathcal{PS}} - \sigma^2 = \big(\omega_L + \delta\omega\big)\big[\bar{\mathcal{I}} - \big(\omega_L + \delta\omega\big)\big] \\ + \sigma^2 \int_1^\infty d\kappa \, \frac{\big[f_{\rm I}(\kappa) + f_{\rm III}(\kappa)\big]\,\pi^2\kappa^2\,\mathscr{E}(1/\kappa)}{4(\kappa^2-1)\,\mathscr{K}(1/\kappa)^3} - \sigma^2 \\ + 4\phi_1 \int_0^1 d\kappa \, \big[f_{\rm II}^-(\kappa) + f_{\rm II}^+(\kappa)\big]\,\frac{\mathscr{E}(\kappa) + (\kappa^2-1)\,\mathscr{K}(\kappa)}{\mathscr{K}(\kappa)}.\end{aligned} \tag{3.91}$$

We have already calculated the small amplitude expression for the first line (3.91), which is the difference between the frequency shifted average action and the frequency, namely, the change in the average action $\bar{J}$; the expression is given in Sec. 2.3 by (2.60), in which we see that $\bar{J} \sim \phi_1^{3/2}$. Since the frequency shift $\delta\omega \sim \sqrt{\phi_1}$, it is of higher order in ϕ_1, and the first line of (3.91) is given by

$$\big(\omega_L + \delta\omega\big)\big[\bar{\mathcal{I}} - \big(\omega_L + \delta\omega\big)\big] \approx \omega_L\big(\bar{\mathcal{I}} - \omega_L\big) \approx \frac{64}{9\pi}\frac{\omega_L^2}{\sigma^2}\frac{e^{-\omega_L^2/2\sigma^2}}{\sigma\sqrt{2\pi}}\phi_1^{3/2}. \tag{3.92}$$

Next, we calculate the two terms proportional to σ^2 from the second line in (3.91). From our normalization of the distribution function we have $\sigma^2 = \big\langle\sigma^2\big\rangle_{\mathcal{PS}}$, so that the terms proportional to σ^2 can be written as

$$\sigma^2 \int_1^\infty d\kappa \left[\frac{\pi^2\kappa^2\,\mathscr{E}(1/\kappa)}{4(\kappa^2-1)\,\mathscr{K}(1/\kappa)^3} - 1\right]\big[f_{\rm I}(\kappa) + f_{\rm III}(\kappa)\big] - \sigma^2 \int_0^1 d\kappa \, \big[f_{\rm II}^-(\kappa) + f_{\rm II}^-(\kappa)\big].$$

Again, these integrals vanish in the limit $\phi_1 \to 0$; to find the small amplitude approximation we Taylor expand the distributions:

$$\begin{aligned}\frac{\sigma e^{-\omega_L^2/2\sigma^2}}{\sqrt{2\pi}} \int_1^\infty d\kappa \left[\frac{\pi^2\kappa^2\,\mathscr{E}(1/\kappa)}{4(\kappa^2-1)\,\mathscr{K}(1/\kappa)^2} - \mathscr{K}(1/\kappa)\right] \\ \times \left[\frac{8\sqrt{\phi_1}}{\pi} + \frac{64\phi_1^{3/2}}{\pi^3\sigma^2}\left(\tfrac{\omega_L^2}{\sigma^2} - 1\right)\kappa^2\,\mathscr{E}(1/\kappa)^2\right] \\ - \frac{\sigma e^{-\omega_L^2/2\sigma^2}}{\sqrt{2\pi}} \int_0^1 d\kappa\,\kappa\,\mathscr{K}(\kappa)\left\{\frac{8\sqrt{\phi_1}}{\pi} + \frac{64\phi_1^{3/2}}{\pi^3\sigma^2}\left(\tfrac{\omega_L^2}{\sigma^2} - 1\right)\big[\mathscr{E}(\kappa) + (\kappa^2-1)\,\mathscr{K}(\kappa)\big]^2\right\}.\end{aligned} \tag{3.93}$$

The terms $\sim \sqrt{\phi_1}$ in (3.93) can be shown to cancel:

$$\int_1^\infty d\kappa \left[\frac{\pi^2\kappa^2\,\mathscr{E}(1/\kappa)}{4(\kappa^2-1)\,\mathscr{K}(1/\kappa)^2} - \mathscr{K}(1/\kappa)\right] - \int_0^1 d\kappa\;\kappa\,\mathscr{K}(\kappa)$$
$$= \left[\frac{\pi^2\kappa}{4\,\mathscr{K}(1/\kappa)} - \kappa\,\mathscr{E}(1/\kappa)\right]_{\kappa=1}^{\infty} - \Big[\,\mathscr{E}(\kappa) + (\kappa^2-1)\,\mathscr{K}(\kappa)\Big]_{\kappa=0}^{1} = 0,$$

while the terms $\sim \phi_1^{3/2}$ in (3.93) can be integrated analytically. For the integral such that $1 \le \kappa < \infty$, we integrate by parts, so that the piece $\sim\phi_1^{3/2}$ is given by

$$\int_1^\infty d\kappa \left[\frac{\pi^2\kappa^2\,\mathscr{E}(1/\kappa)}{4(\kappa^2-1)} - \mathscr{K}(1/\kappa)^3\right] \frac{\kappa^2\,\mathscr{E}(1/\kappa)^2}{\mathscr{K}(1/\kappa)^2}$$
$$= \frac{\kappa^3}{4}\left[\frac{\pi^2\,\mathscr{E}(1/\kappa)^2}{4\,\mathscr{K}(1/\kappa)} - \mathscr{E}(1/\kappa)^3\right]_{\kappa=1}^{\infty} - \int_1^\infty d\kappa\;\frac{\kappa^2}{2}\left[\frac{\pi^2}{4}\,\mathscr{E}(1/\kappa) - \mathscr{K}(1/\kappa)\,\mathscr{E}(1/\kappa)^2\right]$$
$$= 1 - \frac{2}{3}\left\{\frac{\pi^2\kappa}{12}\left[(4\kappa^2-2)\,\mathscr{E}(1/\kappa) - (\kappa^2-1)\,\mathscr{K}(1/\kappa)\right] - \kappa^3\,\mathscr{E}(1/\kappa)^3\right\}_{\kappa=1}^{\infty}$$
$$= \frac{1}{3} + \frac{\pi^2}{9}. \tag{3.94}$$

Integration of the second term proportion to $\phi_1^{3/2}$ (for which $0 \le \kappa \le 1$) yields

$$\int_0^1 d\kappa\;\kappa\,\mathscr{K}(\kappa)\big[\mathscr{E}(\kappa) + (\kappa^2-1)\,\mathscr{K}(\kappa)\big]^2 = \frac{1}{3}\left[\mathscr{E}(\kappa) + (\kappa^2-1)\,\mathscr{K}(\kappa)\right]^3\Big|_{\kappa=0}^{1} = \frac{1}{3}. \tag{3.95}$$

Taking the difference of (3.95) from (3.94), we find that (3.93) [i.e., the second line of (3.91)] is

$$\sigma^2\int_1^\infty d\kappa \frac{\pi^2\kappa^2\,\mathscr{E}(1/\kappa)}{4(\kappa^2-1)\,\mathscr{K}(1/\kappa)^3}\left[f_{\rm I}(\kappa) + f_{\rm III}(\kappa)\right] - \sigma^2 \approx \frac{64}{9\pi}\frac{e^{-\omega_L^2/2\sigma^2}}{\sigma\sqrt{2\pi}}\left(\frac{\omega_L^2}{\sigma^2} - 1\right)\phi_1^{3/2}. \tag{3.96}$$

Finally, we calculate the last integral of (3.91), which is the contribution of the trapped particles to the damped energy. Taylor expanding $f_{\rm II}$ to lowest order, the last term in (3.91) gives the contribution

$$\frac{32}{\pi}\frac{e^{-\omega_L^2/2\sigma^2}}{\sigma\sqrt{2\pi}}\phi_1^{3/2}\int_0^1 d\kappa\;\kappa\big[\,\mathscr{E}(\kappa) + (\kappa^2-1)\,\mathscr{K}(\kappa)\big]$$
$$= \frac{32}{\pi}\frac{e^{-\omega_L^2/2\sigma^2}}{\sigma\sqrt{2\pi}}\phi_1^{3/2}\left\{\frac{1}{9}\Big[(4\kappa^2-2)\,\mathscr{E}(1/\kappa) + (3\kappa^4-5\kappa^2+2)\,\mathscr{K}(1/\kappa)\Big]\right\}_{\kappa=0}^{1}$$
$$= \frac{64}{9\pi}\frac{e^{-\omega_L^2/2\sigma^2}}{\sigma\sqrt{2\pi}}\phi_1^{3/2}. \tag{3.97}$$

Combining (3.92), (3.96), and (3.97), we find that

$$\frac{1}{2}\left[\left\langle u^2\right\rangle_{\mathcal{PS}} - \sigma^2\right] = \frac{\pi}{2}\frac{\omega_L^2}{\sigma^2}\frac{e^{-\omega_L^2/2\sigma^2}}{\sigma\sqrt{2\pi}}\frac{128}{9\pi^2}\phi_1^{3/2} \equiv \nu_\ell \frac{128}{9\pi^2}\phi_1^{3/2}. \tag{3.98}$$

The physical interpretation of (3.98) is clear: the increase in the particle kinetic energy is that dissipated by Landau damping (parametrized by the coefficient ν_ℓ) over a time of order the bounce period $1/\sqrt{\phi_1}$. As previously mentioned, this expression is similar to that derived by O'Neil [6] for the initial value problem; his $O(1)$ coefficient (Eq. 34 in [6]) can be numerically integrated to approximately yield 1.96, which is 40% larger than our value $\frac{128}{9\pi^2} \approx 1.44$. Furthermore, our expression (3.98) can be obtained from Dewar's [10] equation for the momentum of the trapped particles due to the saturation of an instability. Multiplying Eq. 10 from Ref. [10] by the characteristic energy of the trapped particles moving at the phase velocity of the wave, $\frac{1}{2}\omega_L^2$, we obtain (3.98), with Dewar's linear instability growth rate γ replaced by the linear Landau damping coefficient ν_ℓ.

3.3.3 The fully nonlinear damped energy and maximal damping rate

While the expression for the damped energy (3.98) is attractive both because it is analytic and because it has a clear, physical interpretation, it will fail to be an accurate expression for the phase-mixed energy when the amplitude of the potential becomes sufficiently large. In this case, we again must resort to the fully nonlinear realizations of the distribution function and electrostatic potential, from which we then calculate the average of the kinetic energy. To obtain the invariant-in-action-difference distribution of Ch. 2 and the corresponding potential, we solve the system of equations [from (2.21)]

$$\bar{\mathcal{I}}^{j+1} = \bar{\mathcal{I}}^j - \frac{\varepsilon\left(\bar{\mathcal{I}}^j;\phi^j\right)}{\frac{\partial}{\partial\bar{\mathcal{I}}^j}\varepsilon\left(\bar{\mathcal{I}}^j;\phi^j\right)}, \tag{3.99a}$$

$$\phi_n^{j+1} = -\frac{2}{n^2}\left\langle \cos(n\theta)\right\rangle_{\mathcal{PS}}. \tag{3.99b}$$

For the distribution obtained using (3.99), we determine the phase-mixed, incoherent (i.e., Landau damped) energy [from (3.86), with $|G| = \phi_1$]:

$$\omega_L^2 \int_0^\tau d\tau' \, \nu(\tau') \, |\mathcal{G}|^2 = \frac{1}{2}\Big[\big\langle u^2 \big\rangle_{\mathcal{PS}} - \sigma^2 \Big] - \frac{\omega_L^2}{2}\phi_1^2 + \frac{1}{4}\sum_{n=1}^{\infty} n^2 \phi_n^2 \equiv U_{\rm incoh}. \tag{3.100}$$

While we have obtained a fully nonlinear expression for the phase-mixed energy inherent in the asymptotic distribution function, we have yet to relate this to an instantaneous damping coefficient. As a first step, we consider the maximal damping rate associated with a plasma wave whose asymptotic, phase-mixed energy is $U_{\rm incoh}$. We proceed by analogy with the small amplitude case, in which we interpreted this energy to be proportional to the electrostatic energy $\sim \phi_1^2$ damped over a bounce period $\sim 1/\sqrt{\phi_1}$, so that the behavior of the Landau damped energy (3.100) is given by

$$\omega_L^2 \int_0^\tau d\tau' \, \nu(\tau') \, |\mathcal{G}|^2 \;\sim\; \int_0^{1/\sqrt{\phi_1}} d\tau \, \nu_{\rm max} \phi_1^2 \;\sim\; \nu_{\rm max}(\phi_1)\phi_1^{3/2} \;\sim\; U_{\rm incoh}. \tag{3.101}$$

Thus, we see that the maximal damping of the plasma wave is proportional to $U_{\rm incoh}/\phi_1^{3/2}$. In the small amplitude limit, the maximal damping $\nu_{\rm max}$ should reproduce linear Landau damping. Inspection of the small amplitude result for the incoherent energy (3.98) implies that this matching is satisfied by taking

$$\nu_{\rm max}(\phi_1) = \frac{U_{\rm incoh}}{\frac{128}{9\pi^2}\phi_1^{3/2}}.$$

By numerically solving for the average action and nonlinear potential (3.99), and then using the resulting distribution to calculate the incoherent energy (3.100), we can obtain curves for the maximal damping as a function of the potential amplitude for different temperatures. We have fit these curves to the following approximate analytic expression

$$U_{\rm incoh}(\phi_1) \approx \frac{128}{9\pi^2}\nu_\ell \, \phi_1^{3/2}\left(1 + \tfrac{1.3}{\sigma^2}\,\phi_1\right) + 2.45\,\sigma^2\phi_1^{5/2}(1 + 59\,\phi_1^2), \tag{3.102a}$$

$$\nu_{\rm max}(\phi_1) \approx \nu_\ell\big(1 + \tfrac{1.3}{\sigma^2}\,\phi_1\big) + 1.7\,\sigma^2\phi_1(1 + 59\,\phi_1^2). \tag{3.102b}$$

These equations have been found to fit the numerically determined averages to within a few percent for the range of temperatures $0.1 \le k_2\lambda_D \le 0.4$ and wave amplitudes

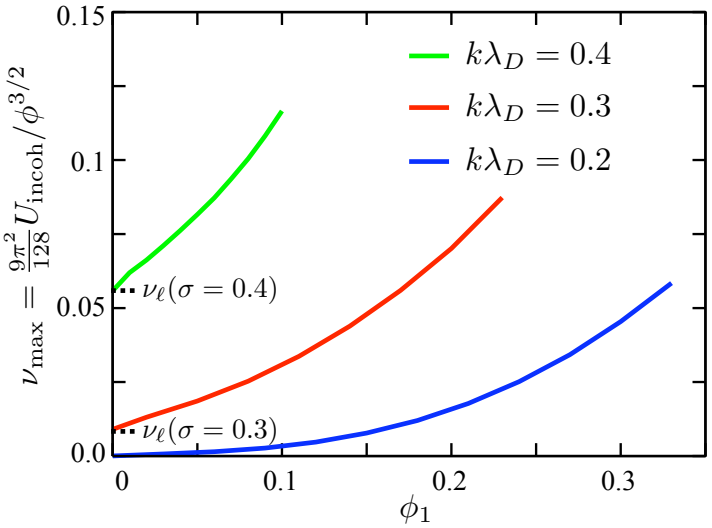

Figure 3.1: Maximal nonlinear damping $\nu_{\max} \equiv U_{\rm incoh}/\phi_1^{3/2}$ as a function of the electrostatic potential for three different temperatures. For vanishing ϕ_1 the lines asymptote to the linear Landau damping rate ν_ℓ, as marked on the figure for $\sigma = 0.4$ and $\sigma = 0.3$. As the wave grows, so does the damping rate; for the relatively cold plasma with $k\lambda_D = 0.2$ it can increase by several orders of magnitude.

$0 \le \phi_1 \lesssim 0.5$. From the formula (3.102b) we see that if the electrostatic potential is much less than the thermal energy of the plasma, $\phi_1 \ll \sigma^2$, then the damping decrement is close to the linear Landau level ν_ℓ. When the electrostatic potential is larger than the thermal spread, however, there is a significant increase in the damped energy over the lowest-order expression (3.98), suggesting that the effective damping rate is an increasing function of the electrostatic potential. This phenomenon has a straightforward explanation: as the Langmuir wave grows, it resonantly interacts with a larger number of electrons from the plasma bulk, nearly all of which (in an initially Maxwellian plasma) will be accelerated and take energy from the wave. Consequently, the corresponding electrostatic damping is more rapid than that obtained in the linear limit, a result that qualitatively agrees with the calculation of Sugihara *et al.* [83] (although the specifics are quite distinct). We will provide further comparison to their findings at the end of this section.

To explicitly show this effect, we plot the maximum Langmuir wave damping $\nu_{\max}$ as a function of the wave amplitude for three different temperatures in Fig. 3.1. For a

vanishingly small value of ϕ_1, we see that the damping asymptotes to the Landau damping value ν_ℓ for the given temperature. As the plasma wave amplitude grows, the phase-mixed, asymptotic energy required to sustain the invariant-in-action-difference distribution increases, and the corresponding damping of the plasma wave also increases. For warm plasmas with $k\lambda_D = 0.4$, the initial linear Landau levels are rather large, and Fig. 3.1 indicates that the maximal plasma damping increases by an factor of order one. For cold plasmas with $k\lambda_D = 0.2$, the initial linear damping $\nu_\ell \approx 6 \times 10^{-5}$, but can increase by several orders-of-magnitude as the plasma wave grows to $\phi_1 \sim 0.3$.

For these large amplitude plasma waves, the incoherent energy is of the same order as the kinetic energy of all trapped particles moving at the phase velocity of the wave. Thus, this additional nonlinear Landau-type damping can be thought of as associated with the transfer of coherent wave energy to that of the trapped particles moving at the phase velocity of the large amplitude wave. Note that while it may be a useful interpretation of the nonlinear damping for high-amplitude waves, this correspondence fails for small ϕ_1, in which the trapped particle fraction is given by

$$\int_{-\mathcal{I}_s}^{\mathcal{I}_s} d\mathcal{I}\, \frac{1}{\sigma\sqrt{2\pi}} e^{-(\mathcal{I}-\omega_L)^2/2\sigma^2} = \frac{1}{2}\left\{ \mathrm{erf}\left[\tfrac{1}{\sqrt{2}\sigma}\left(\tfrac{4\sqrt{\phi_1}}{\pi} - \omega_L\right)\right] + \mathrm{erf}\left[\tfrac{1}{\sqrt{2}\sigma}\left(\tfrac{4\sqrt{\phi_1}}{\pi} + \omega_L\right)\right]\right\}$$
$$\approx \frac{8}{\pi}\frac{e^{-\omega_L^2/2\sigma^2}}{\sigma\sqrt{2\pi}}\sqrt{\phi_1} + \ldots \tag{3.103}$$

so that the energy associated with the trapped particles appears to scale $\sim \sqrt{\phi_1}$. Since we have explicitly shown that the total energy of phase-mixing $\sim \phi_1^{3/2}$ for $\phi_1 \ll \sigma^2$, there must be additional contributions to the phase-mixed energy due to near-resonant particles that cannot, in general, be neglected. Furthermore, even in the large amplitude limit we do not claim that the incoherent energy is equal to the product of the trapped particle fraction and their kinetic energy $\sim \frac{1}{2}\omega_L^2$, but rather that this is the dominant contribution as the Langmuir wave becomes quite large, i.e., in the limit $\phi_1 \gg \sigma^2$.

Finally, we note that our result for the maximal damping (3.102b) is rather different from the expressions of Sugihara *et al.* [83], who perturbatively calculated the corrections to

the linear damping rate assuming an initially prescribed, large amplitude Langmuir wave. In this analysis, Ref. [83] found the large-amplitude corrections to the damping became super-exponential for large amplitude waves, such that the wave amplitude decreased $\sim e^{-t^2}$ and $\sim e^{-t^4}$. However, since phase-mixing happens rapidly in such large amplitude waves, the expressions of [83] are only valid over some short time scale characterized by the bounce period $1/\sqrt{\phi_1}$, at which time the damping becomes negligible. In a similar way, (3.102b) is to be understood as approximating the maximal damping coefficient, which, as time progresses, decreases from (3.102b) to zero in such a way that the total damped energy is given by (3.102a) over a time $\sim 1/\sqrt{\phi_1}$. For either driven or large amplitude waves, we find that it is this dynamical decrease in damping that is the dominant physics, so that the quantitative discrepancies between (3.102b) and the expression of [83] are largely irrelevant. In the following section, we will present a simple model that, while not computing the true dynamics, nevertheless yields the correct physics involved in this complicated process.

3.4 The extended three-wave model of Raman backscatter in a plasma

In the previous sections of this chapter, we derived various components of an extended three-wave model relevant to Raman backscatter in a plasma. By averaging the transverse Ampère-Maxwell equation, we first derived equations for the counter-propagating laser amplitudes, coupled via the bunching parameter of the plasma wave. Since the bunching parameter is closely related to the natural modes of the Langmuir wave, we then turned to the Vlasov equation, from which governing equations for the natural modes can be derived. These equations in turn involve higher moments of the distribution, and hence do not form a closed set of equations. In two limits, however, a natural closure is available: initially, the higher order terms can be equated to the natural frequency and damping given by the linear Langmuir dispersion relation along the Landau contour; in the time-asymptotic limit

these terms can be written as the frequency shift associated with the BGK-type nonlinear distribution function of Ch. 2.

In this section, we develop a technique for making the transition from the initial to asymptotic limits of the envelope equation by using the incoherent energy (3.102a) associated with the phase-mixed distribution. By comparing this energy to that damped by the envelope equations, we have a means of estimating the degree to which the distribution has phase-mixed as a function of time. As the distribution becomes more phase-mixed, we smoothly take the (real) frequency from ω_r to $\omega_L + \delta\omega$, while also taking the nonlinear damping from $\nu_{\max}(\phi_1)$ to zero. Although our choice for this transition is rather *ad hoc*, we have found that the envelope equation is not strongly dependent on its precise functional form. The model thus obtained, while heuristic, is well-grounded in physical principles, efficient to implement numerically, and agrees well with single-wavelength Vlasov simulations using a non-evolving laser drive. We will show such comparisons in the next chapter.

3.4.1 Dynamic damping and frequency of the Langmuir wave

In the previous section we saw how the damped and phase-mixed energy are related, and obtained the total incoherent energy required to develop the asymptotic, phase-mixed distribution. As this phase-mixing progresses, the maximal (Landau-type) plasma wave damping coefficient (3.102b) should smoothly asymptote to zero as the total damped/phase-mixed energy approaches (3.102a). At the same time, particle trapping and other kinetic effects will cause the natural frequency of the wave to decrease from its linear value ω_r to the nonlinear, BGK-type frequency $\omega_L + \delta\omega$. Since these effects result from the degree to which the distribution is phase-mixed, we will take them to be a function of the ratio of the total energy damped by the (nonlinear) Landau damping to the total incoherent

energy required to yield the asymptotic distribution:

$$\nu(\phi_1, \Lambda) = \Upsilon_\nu(\Lambda)\nu_{\max}(\phi_1) \tag{3.104a}$$

$$\omega(\phi_1, \Lambda) = \Upsilon_\omega(\Lambda)\,\omega_r + \big[1 - \Upsilon_\omega(\Lambda)\big]\big[\omega_L + \delta\omega(\phi_1)\big] \tag{3.104b}$$

$$\text{where } \Lambda \equiv \frac{U_{\text{damp}}(\phi_1, \tau)}{U_{\text{incoh}}(\phi_1)}; \qquad \Upsilon_\nu(0) = \Upsilon_\omega(0) = 1; \qquad \Upsilon_\nu(1) = \Upsilon_\omega(1) = 0. \tag{3.104c}$$

Note that the damping $\nu_{\max}$, frequencies ω_r and $\omega_L + \delta\omega$, and incoherent, phase-mixed energy U_{incoh} have analytic expressions in the text, while the damped energy U_{damp} is a single number easily obtained from the numerical implementation. Thus, we have only to determine the functions Υ_ν and Υ_ω, both of which are a measure of the degree to which the distribution function has phase-mixed. Since the argument of these functions is the ratio of the damped to incoherent energy, we have $0 \leq \Lambda \leq 1$. At the two extremes, $\Lambda = 0$ indicates no phase-mixing, while $\Lambda = 1$ represents a perfectly phase-mixed, asymptotic distribution. Beyond these limits, our discussion thus far provides no particular guidance regarding the precise functional form. We found that the resulting model is rather independent of the exact form for Υ, provided only that it smoothly and monotonically satisfies (3.104c); for simplicity, we choose

$$\Upsilon_\nu(\Lambda) = \Upsilon_\nu(\Lambda) = \Upsilon(\Lambda) = \tfrac{1}{2}\left\{1 - \tanh\big[7\,(\Lambda - 0.5)\big]\right\}. \tag{3.105}$$

The numerical coefficients were chosen such that the appropriate $\Lambda \to 0$ and $\Lambda \to 0$ limits are satisfied; we note that making the replacement $7 \to 8$ or $0.5 \to 0.4$ has little discernable effect on the Langmuir wave evolution.

We now have a closed set of envelope equations for Raman scatter in a plasma including some thermal and kinetic corrections to the Langmuir wave evolution. Collecting the coupled-mode equations (3.75), the nonlinear frequency shift (3.72) and damping (3.102b), and the phase-mixed energy (3.102a) and interpolating function (3.105), we write the

complete extended three-wave model here:

$$\left[\frac{\partial}{\partial\tau} - u_0\frac{\partial}{\partial\zeta} + i\frac{c^2k_2^2\,|a_1|^2}{32\omega_p\omega_0\omega_L^2} - \frac{i\omega_p}{\omega_0}\boldsymbol{\nabla}_\perp^2\right] a_0(\zeta,\tau) = \quad \frac{\omega_p}{4\omega_0}a_1(\zeta,\tau)\mathcal{G}(\zeta,\tau), \tag{3.106a}$$

$$\left[\frac{\partial}{\partial\tau} + u_1\frac{\partial}{\partial\zeta} + i\frac{c^2k_2^2\,|a_0|^2}{32\omega_p\omega_1\omega_L^2} - \frac{i\omega_p}{\omega_1}\boldsymbol{\nabla}_\perp^2\right] a_1(\zeta,\tau) = -\frac{\omega_p}{4\omega_1}a_0(\zeta,\tau)\mathcal{G}^*(\zeta,\tau), \tag{3.106b}$$

$$\left[\frac{\partial}{\partial\tau} - u_{gr}\frac{\partial}{\partial\zeta} + i\big(\omega-\omega_2\big) + \nu\right]\mathcal{G}(\zeta,\tau) = -\frac{c^2k_2^2}{2\omega_L\omega_p^2}a_0(\zeta,\tau)a_1^*(\zeta,\tau), \tag{3.106c}$$

where, for $|\mathcal{G}| \equiv \phi_1$, we have

$$\nu(\phi_1,\Lambda) = \Upsilon(\Lambda)\nu_{\max}(\phi_1), \tag{3.107a}$$

$$\omega(\phi_1,\Lambda) = \Upsilon(\Lambda)\,\omega_r + \big[1-\Upsilon(\Lambda)\big]\big[\omega_L + \delta\omega(\phi_1)\big], \tag{3.107b}$$

$$\Lambda(\phi_1,\tau) \equiv \frac{U_{\rm damp}}{U_{\rm incoh}} = \frac{U_{\rm damp}(\tau)}{\frac{128}{9\pi^2}\nu_{\max}\phi_1^{3/2}}, \tag{3.107c}$$

and

$$\nu_{\max} = \nu_\ell\big(1+\tfrac{1.3}{\sigma^2}\,\phi_1\big) + 1.7\,\sigma^2\phi_1(1+59\,\phi_1^2), \tag{3.108a}$$

$$\delta\omega = -\frac{e^{-\omega_L^2/2\sigma^2}}{\sqrt{2\pi}\sigma}\left[1.09\,\frac{\omega_L\left(\frac{\omega_L^2}{\sigma^2}-1\right)}{\omega_L^2-1-\sigma^2}\sqrt{\phi_1} + 40\,\phi_1 + 7.8\frac{\omega_L^2}{\sigma^4}\phi_1^2 + 0.115\frac{(\omega_L^2-8\sigma^2)^2}{\sigma^{11}}\phi_1^4\right] + 6\sigma^2\big(\phi_1^2+3\phi_1^4-250\,\phi_1^8\big)\,. \tag{3.108b}$$

In the model above, the (real) frequencies ω_r and ω_L are given by the Landau and Vlasov dispersion relations, (3.59) and (2.53) respectively, ν_ℓ is the damping decrement given by (3.59), and the total damped energy $U_{\rm damp}$ is tracked during the numerical integration.

Our set of equations bears some resemblance to that by Divol *et al.* [36] and that of Vu, DuBois, and Bezzerides [37]. Both of these models consider the competition between trapping (which tends to decrease Landau damping while yielding a nonlinear frequency shift) and collisions (which will tend to de-trap particles and return the plasma to a Maxwellian). Although their exact calculations are rather different, both [36] and [37] rely on the smallness of the electrostatic amplitude, and use the physical intuition given by Zakharov and Karpman [84] and O'Neil [6] to obtain thresholds for when to eliminate

Landau damping, and when to use a frequency shift that is chosen to match, within factors of $O(1)$, that of Morales and O'Neil [24]. As we have seen, the model we have deriven is qualitatively similar, but obtained with a consistent and uniform set of equations and assumptions, and is applicable to larger amplitude Langmuir waves. For problems involving longer time-scales, however, our analysis will need to be generalized to include the collisional relaxation of the plasma. We leave this to future research.

Chapter 4

Modeling thermal effects in Raman backscatter

In Chapter 2, we developed a simplified distribution function to describe thermal, one-dimensional electron plasmas that are weakly-driven on or near resonance. We found that the distribution was invariant in canonical action for the trapped particles, while invariant in the difference $J - \bar{J}$ for the untrapped distribution, where $\bar{J}$ is the slowly-evolving mean determined via self-consistency with the Poisson equation. From this distribution, we extracted a nonlinear frequency shift of the Langmuir wave due to thermal and kinetic effects, which agreed quite well with particle simulations for $0.1 \leq k\lambda_D \leq 0.4$.

We then developed a simplified model of Raman backscatter in a plasma in Chapter 3, deriving three coupled-mode equations for the pump, seed, and Langmuir wave envelope, under the assumptions that these envelopes varied over spatial scales much longer than the wavelength of the laser beat ($\sim 1/k_2$) and over time scales much greater than that given by the plasma frequency, $(1/\omega_p)$. As is characteristic of any set of moment equations, however, the equation for the plasma response included higher-order velocity moments of the distribution function; in order to close these equations, we derived two limits of these higher-moment terms, one valid for a linear initial value problem and the other valid in the

time-asymptotic limit. In the former, the plasma wave is described by a natural, complex frequency given by the Landau dispersion relation, while in the latter limit the damping vanishes and the natural frequency is given by the real, nonlinear value obtained in Ch. 2. To interpolate between these two extremes, we introduced the idea of the phase-mixed energy required for the time-asymptotic limit, and argued that as the damped energy approaches the phase-mixed energy, the damping smoothly goes to zero while the real part of the frequency is smoothly decreased from its linear value to the nonlinear level.

In this Chapter, we compare the Langmuir wave evolution as predicted by this reduced envelope model to that obtained via Vlasov simulations. Because some of these comparisons involve effects that are strongly dependent on the tails of the distribution (most notably, the nonlinear Landau damping of very weakly-driven plasmas), we developed an Eulerian Vlasov solver to complement the particle code discussed in Sec. 2.4. We continue this Chapter with Sec. 4.1, in which we discuss some basic aspects of this Vlasov code, and then show, as an example, results obtained for the nonlinear Landau damping of an initially prescribed plasma wave. We proceed in Sec. 4.2 to compare the results of this code to those predicted by the extended three-wave model of Ch. 3. In Sec. 4.2.1, we compare results for Langmuir wave evolution in a strongly damped plasma, for which linear theory predicts a steady state plasma wave amplitude given roughly by the ratio of the drive to damping, whereas our model and the Vlasov code indicate an increase in the plasma wave levels due to particle phase-mixing. We then address the regime of more strongly-driven thermal plasmas in Sec. 4.2.2, for which our model predicts saturation of Raman scattering through the nonlinear frequency shift due to resonant particle effects. Having verified our model of the Langmuir wave response in the case of a prescribed, external ponderomotive drive, we then turn to the full three-wave model, in which feedback and, hence, laser amplification and depletion are possible. Finally, we conclude with some preliminary discussions concerning the use of this code as a simulation tool for modeling an ongoing experiment of the plasma-based Raman amplifier at Princeton University.

4.1 An Eulerian Vlasov code for Raman scatter in a plasma

To complement the particle code previously discussed, we developed a single-wavelength, one-dimensional Vlasov-Poisson solver with external forcing. To solve the Vlasov equation

$$\frac{\partial f_e}{\partial t} + v\frac{\partial f_e}{\partial z} + \frac{F_z}{m_e}\frac{\partial f_e}{\partial v} = 0, \tag{4.1}$$

we use the standard Cheng-Knorr algorithm [85] for advecting the incompressible phase-space "fluid" on an Eulerian grid. This operator splitting scheme divides the integration along the characteristics (which are the single particle orbits) for any time step into three pieces as shown schematically in Fig. 4.1. The first part (a) entails an advection for a half-step in v by an amount $\frac{F_z}{m_e}\frac{\Delta t}{2}$, followed by advecting f_e in z by an amount $v\Delta t$ in (b), and concluding in (c) with a final half time step in v. Note that during the simulation, substeps (c) from one step and (a) from the next can usually be grouped together into one step in v by an amount $\frac{F_z}{m_e}\Delta t$. The value of the updated distribution function for each step is determined by looking "back in time" along the characteristic, as indicated by the blue arrows in Fig. 4.1. In general, these updates require the value of the distribution function that is between the Eulerian grid points, so that we must interpolate f_e from the grid; we do this by fitting f_e with (1D) cubic splines along either v for the substeps (a) and (c) or z for step (b).

To solve for the self-consistent electrostatic fields, we use the longitudinal $\hat{\boldsymbol{z}}$ component of the Ampère-Maxwell law, given by

$$\frac{\partial E_z}{\partial t} = -\frac{4\pi}{c}J_z = \frac{4\pi e}{c}\int dv\; f_e(v,z;t)\, v. \tag{4.2}$$

Thus, in this model E_z is considered a dynamical variable that must be incorporated in the split-step scheme in such a manner as to leave the entire method second order accurate. To do this, we add two more steps to our operator split scheme in Fig. 4.1, advancing E_z by one half time step between (a) and (b) and between (b) and (c).

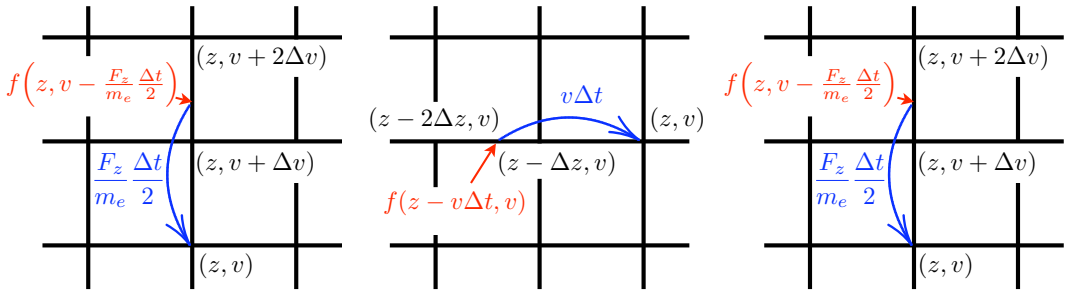

(a) Advect along v at constant z by $\frac{F_z}{m_e}\frac{\Delta t}{2}$

(b) Advect along z at constant v by $v\Delta t$

(c) Advect along v at constant z by $\frac{F_z}{m_e}\frac{\Delta t}{2}$

Figure 4.1: A schematic representation of the Cheng-Knorr split-step algorithm for solving the Vlasov equation on an Eulerian grid [85]. Each time step is divided into three sub-steps: advecting in v for a half time-step, followed by a full step advection in z, and concluding with a half time-step advection in v. To obtain the value of f_e between the grid points, we interpolate with cubic splines.

4.1.1 Numerical example of nonlinear Landau damping

We benchmarked the Vlasov code with many basic plasma physics problems; as one example most relevant to this chapter, and to illuminate the nonlinear saturation of Landau damping, we present some examples for an initially prescribed Langmuir wave. In [6], O'Neil showed that the dynamic damping drops to zero in the limit that the product of the linear Landau damping rate and the bounce period $1/\sqrt{\phi_1}$ is small, i.e., $\nu_\ell \tau_B \ll 1$. Physically, this means that the trapped particles execute many oscillations in the wave before its amplitude changes significantly, so that phase-mixing occurs before the wave is damped away. Building upon these ideas, Oei and Swanson [86] included the lowest order change of the electrostatic potential to show that waves with an initial value $\nu_\ell \tau_B \lesssim 0.6$ damp away to zero, while larger initial potentials will survive, approaching a steady-state, BGK-type wave.

Since these theoretical papers and the first numerical work [87], the idea that there may be a critical initial amplitude below which Langmuir waves are destined to be damped to zero while above which they are may persist as BGK-type steady-states with non-zero electrostatic amplitude has received some attention in the literature, with both theoretical [88, 89] and numerical papers [90, 91] seeming to indicate different scalings and relevant

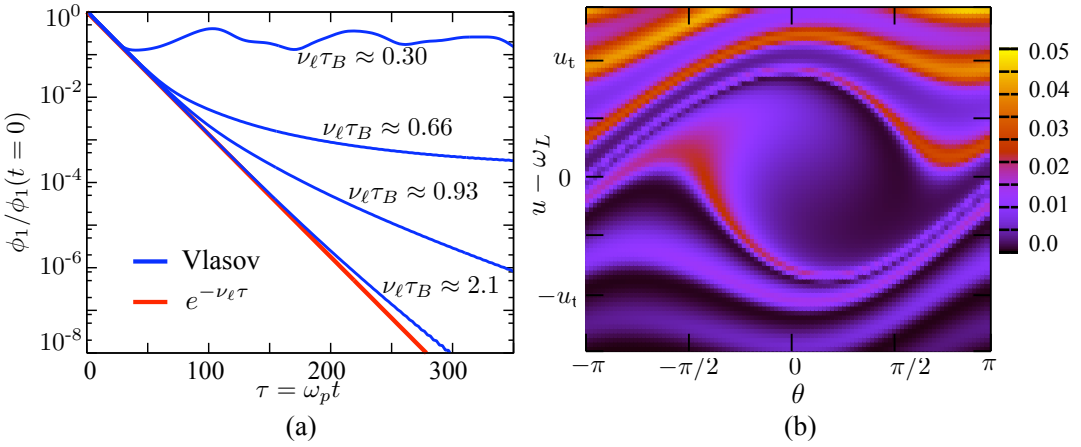

Figure 4.2: Nonlinear Landau damping in a warm plasma with $k\lambda_D = \sigma = 0.4$, for which $\nu_\ell \approx 0.066$. To make this example, we initialize the plasma wave at various amplitudes, as indicated in (a). As the product of the initial bounce period and the linear Landau damping $\nu_\ell/\sqrt{\phi_1} = \nu_\ell\tau_B$ decreases, the damping rate of the potential decreases over time; for $\nu_\ell\tau_B(0) \approx 0.3$, we see that the wave amplitude approaches a steady state. This is associated with particle trapping, as shown by the phase space plot at $\tau = 90$ in (b).

physics. We believe that the BGK-type waves and their associated phase-mixed energy presented in Chs. 2 and 3 may provide additional insight into this "critical phenomenon" that has been associated with phase space, and leave this for future work.

Returning to the Vlasov code, we initialized standing Langmuir waves using an initial sinusoidal density variation of various amplitudes in a plasma with $k\lambda_D = 0.4$. We plot the evolution of the maximum amplitude (scaled by its initial value) in Fig. 4.2. After an initial transient over a plasma oscillation or two (not visible), we see that the wave initially damps at the linear Landau levels. For very small initial amplitudes, say $\phi_1(0) = 10^{-3}$ and $\nu_\ell\tau_B \approx 2$, the damping is nearly constant for 300 plasma oscillations. For larger initial amplitudes, the damping rate decreases with time, until at $\phi_1(0) = 0.05$ and $\nu_\ell\tau_B \approx 0.3$, the wave oscillates about a steady, finite value. This is associated with trapping and phase-mixing in the Langmuir wave, as can be seen from the phase-space portrait at $\tau = 90$ shown in Fig. 4.2(b), where, for $\nu_\ell\tau_B \approx 0.3$, ϕ_1 is growing. Finally, we note that while this example demonstrates the utility of the Vlasov code, and illuminates some interesting nonlinear physics, there are important differences in the case of a *driven* wave, as is relevant

to Raman backscatter. In this case, there is an external source of energy for the phase-mixing, so that the damping decreases to zero even for very small waves after times of order one bounce period.

4.2 Comparison of the Langmuir envelope model to driven Vlasov and particle simulations

As the first step in verifying our extended three-wave model, we tested the simplified kinetic model of the plasma wave, namely the Langmuir envelope equation (3.106c) with its dynamic, nonlinear damping and frequency given by (3.107) and (3.108). To this end, we performed a number of single-wavelength particle and Vlasov simulations using the following prescribed ponderomotive drive:

$$\frac{c^2k_2^2}{2\omega_L\omega_p^2}\left[a_0(\tau)a_1(\tau)^*e^{i(\zeta+\omega_L\tau)}+c.c.\right]=\frac{c^2k_2^2}{\omega_L\omega_p^2}\,a_0(\tau)a_1(\tau)\cos(\zeta+\omega_L\tau)$$
$$\equiv\mathcal{V}(\tau)\cos(\zeta+\omega_L\tau), \tag{4.3}$$

where $\mathcal{V}(\tau)$ is slowly-varying with respect to the time $1/\omega_L$, typically taken to slowly ramp from zero to a fixed value that is much less than unity. We then compare the evolution of the Langmuir wave in these fully kinetic simulations to that obtained with the envelope equation (3.106c).

4.2.1 Small amplitude Langmuir waves in a strongly damped plasma

We first tested our model for very weakly-driven Langmuir waves in a warm plasma, for which sufficiently high levels of (constant) Landau damping are expected to disrupt the Raman instability. In this, the strong damping limit, the Langmuir wave becomes entrained to the ponderomotive drive; neglecting the derivatives from the envelope equation (3.106c) in comparison with the damping, the Langmuir wave becomes an algebraic function of the

laser amplitudes:

$$\left[\frac{\partial}{\partial\tau} + i(\omega_r - \omega_2) + \nu_\ell\right]\mathcal{G} \;\;\rightarrow\;\; \nu_\ell\,\mathcal{G} = \frac{c^2k_2^2}{2\omega_L\omega_p^2}a_0a_1^*e^{i(\omega_2-\omega_r)} = \frac{\mathcal{V}}{2\omega_L}e^{i(\omega_2-\omega_r)}. \tag{4.4}$$

Under this simplification, the standard three-wave model is reduced to two, for which Chu and Karney [92] determined closed form solutions. As we have discussed, however, since the Landau damping is not a constant, but rather dynamically decreases as the particles phase-mix in the Langmuir wave (and develop the velocity-space plateau), (4.4) cannot hold for arbitrarily long times. The subsequent increase in Langmuir wave amplitude and concomitant laser scatter beyond the linear, strong damping prediction has become known in the inertial confinement fusion community as "kinetic inflation" [61, 62] or "kinetic enhancement" [71], and has been seen in a variety of experiments [93, 15]. Because these researchers are looking to maximize laser fluence on target, the potential increase in laser scatter due to these kinetic effects could pose serious difficulties for ignition.

To properly determine the degree to which Raman scattering deleteriously affects the on-target laser power, one must consider a number of additional effects. Although it is not the purpose of this thesis to address this overarching question facing the fusion community, we will include a few basic ideas to try and put our model in some perspective. In inertial confinement fusion, the laser-plasma interactions of interest take place in a "hot-spot" of the drive laser, which can be thought of as a high intensity filament within which the laser-plasma couplings tend to be largest. Within this hot-spot, our 1D assumptions are largely valid (see, e.g., [35]), the main difference arising from those particles that leave or enter the hot-spot along the transverse directions (referred to as "side-loss"). Since the surrounding region essentially contains a Maxwellian reservoir of plasma, these transverse effects tend to thermalize the plasma, thereby providing a competing effect to the phase-mixing and subsequent decrease in Landau damping that we have discussed. Our analysis will not address the impact of this competition, but is rather focused on trying to properly model just the latter component, i.e., the decrease of Landau damping and commensurate increase in Langmuir wave amplitude, which may then saturate via the nonlinear detuning

Parameter	σ	ν_ℓ	ω_r	ω_L	ω_2	$\mathcal{V}$
Description	$k\lambda_D$	Landau damping	"Resonant" Landau frequency	BGK/ Vlasov frequency	Driving frequency	Driving amplitude
Value	0.352	0.0354	1.223	1.214	1.223	10^{-5}–10^{-4}

Table 4.1: Plasma and drive parameters for the weakly-driven, warm plasma simulations testing the disappearance of Landau damping and subsequent saturation through detuning from the resonant ponderomotive drive.

from the resonant ponderomotive drive.

The essential physics intrinsic to the "kinetic enhancement" of Langmuir wave evolution is modeled by the changing Landau damping coefficient (3.107a) and (3.108a) of the Langmuir wave envelope. Thus, testing our envelope model in situations when the plasma wave is strongly damped provides a test both of the maximal, nonlinear damping coefficient $\nu_{\max}$ and of the manner in which we model the phase-mixing, namely, the ratio of the damped to incoherent energy $\Lambda \equiv U_{\rm damp}/U_{\rm incoh}$ from (3.107c). Since these comparisons involve small perturbations in the tails of the velocity distribution, for which particle codes tend to suffer from excessive levels of noise, we used the single wavelength Vlasov code as our reference kinetic model for comparison.

We used a weakly-driven, strongly damped set of plasma parameters adopted from [71]; a summary of the relevant numbers is given in Table 4.1. In this table, the saturated Langmuir wave amplitude $|G|_{\rm steady}$ is obtained by solving (4.4), and is given by

$$|G|_{\rm steady} = \frac{\mathcal{V}}{2\omega_L \nu_\ell}. \tag{4.5}$$

Of course, (4.5) assumes that the Landau damping coefficient is constant.

We present a comparison of the Vlasov simulation with that of our Langmuir wave envelope equation in Fig. 4.3. In Fig. 4.3(a) we plot the evolution of the potential (density perturbation) as a function of time $\omega_p t$ for three different drive strength, obtained both from the Vlasov simulation (dotted lines) and the extended three-wave model (solid lines). We see that the growth of ϕ_1 slows after some time, and that the duration of this plateau

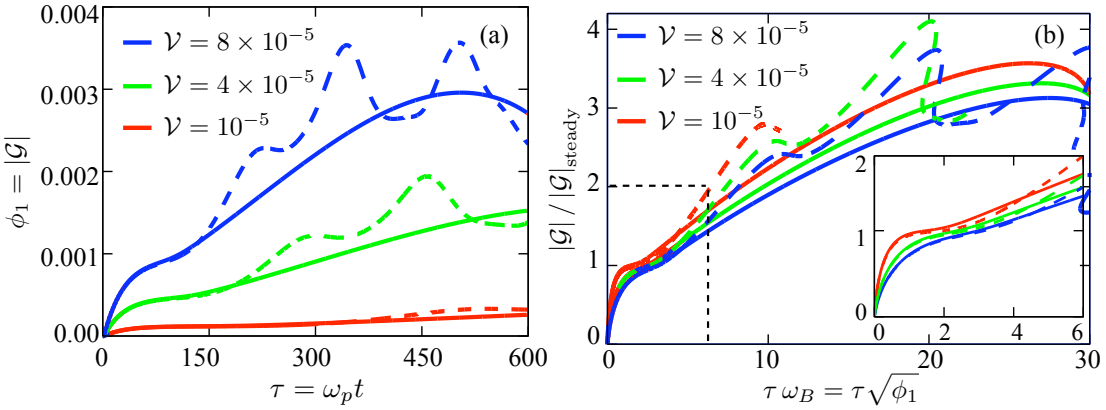

Figure 4.3: Evolution of the Langmuir wave for a strongly damped plasma, with $\nu_\ell \approx 0.035\,\omega_p$. In (a), we compare the evolution in physical units for the Vlasov simulation (dotted lines) and the extended three-wave model (solid lines) for three different drive strengths. The model reliably predicts the final amplitude about which the Vlasov evolution oscillates, from which we conclude that the final saturation is due to the nonlinear frequency shift from the resonant drive. We re-plot the evolution in (b), but with time scaled by the bounce frequency and the electrostatic amplitude by the theoretical steady state value (4.5). The Langmuir wave evolution plateaus near the theoretical value $|\mathcal{G}|_{\text{steady}}$, but after a time of order the bounce period begins to increase, consistent with O'Neil's theory. Furthermore, the extended three-wave model well predicts the initial strong-damping saturation and subsequent rise as the Landau damping vanishes due to particle trapping and phase-mixing.

increases with decreasing drive strength (and, therefore, decreasing Langmuir wave amplitude). Rather than saturating, however, after some period of time, $\omega_p t \sim 100 - 300$, the plasma wave begins to grow again, only to saturate at some rather larger value. Furthermore, the extended three-wave model captures the critical physics involved in the saturation (or lack thereof): it predicts an initial plateau in the Langmuir wave growth, followed by subsequent amplification to larger amplitudes. After the initial linear Landau-damping-induced plateau, the extended three-wave model accurately predicts the later saturation observed with the Vlasov code, which we can now attribute to the nonlinear frequency shift from the resonant drive due to the trapped and near-trapped particles.

To further illuminate this dynamical process, we plot the same data in Fig. 4.3(b), only in this case[1] we scale the time $\tau = \omega_p t$ by the bounce frequency $\omega_B = \sqrt{\phi_1}$, while we normalize the electrostatic amplitude by the strong damping, steady state value $|\mathcal{G}|_{\text{steady}}$ given by Eq. 4.5. In this case, the physics becomes clear: the "plateau" in the growth of ϕ_1 is at an amplitude given by the steady state value, and the duration of this plateau is approximately a few bounce periods. After this time, Landau damping has been decreased through the process of particle phase-mixing, and the driven wave can grow to larger amplitudes. In this case, the Langmuir wave saturates at a value three or four times that predicted by the strongly damped limit (4.5).

Additionally, while the extended three-wave model accurately portrays the generic behavior of the evolution, the Vlasov simulations indicate some oscillations about the reduced model predictions. From Fig. 4.3(b), we see that these oscillations have a frequency of order the bounce frequency, and we therefore interpret these effects as being related to trapped oscillations of electrons in the Langmuir wave. Since the envelope model has effectively averaged over this bounce time scale, we do not expect it to reproduce these amplitude oscillations.

[1]We thank D. J. Strozzi for communicating his finding that this scaling causes the disparate curves to collapse onto a nearly universal form, thus clearly illuminating the physics.

$\sigma = k\lambda_D$	ν_ℓ	ω_r	ω_L	ω_2	$\mathcal{V}$
0.4	0.066	1.285	1.256	ω_r	0.01
0.3	0.0126	1.156	1.158	ω_r	0.01
0.2	5.5×10^{-5}	1.064	1.064	ω_r	0.01
0.1	10^{-14}	1.015	1.015	ω_r	0.01

Table 4.2: Plasma and drive parameters for the weakly-driven, warm plasma simulations used to compare the Langmuir wave evolution predicted by our Vlasov and extended three-wave codes. These parameters are used in the runs shown Figs. 4.4 and 4.6, while the results in Fig. 4.7 use drive amplitudes of twice and one-half that given here.

4.2.2 Saturation of large amplitude Langmuir waves via nonlinear frequency shifts

In the previous section, we presented evidence that our simple model for the dynamic damping in a plasma yields the basic evolution of a driven plasma wave. This indicates that for a given electrostatic amplitude ϕ_1, the linear Landau damping smoothly goes to zero as the damped energy approaches that required to sustain a phase-mixed, BGK-type wave with potential ϕ_1, and that it does so in a manner consistent with a simple, tanh-type interpolation given by Eq. (3.105). We also saw evidence that the subsequent saturation of the Langmuir wave amplitude can be associated with detuning from the resonant drive due to the nonlinear frequency shift of the wave. To test this final saturation mechanism further, we performed additional simulations using larger amplitude ponderomotive drives over a wide range of temperatures, as summarized in Table 4.2.

We present in Fig. 4.4 the amplitude evolution for large amplitude driven Langmuir waves in a plasma with temperature such that $0.1 \leq k\lambda_D \leq 0.4$. For these simulations, we slowly turn on the drive near $\tau = 0$ to a constant value $\mathcal{V} = 0.01$; as a result, the plasma wave grows to some maximum amplitude, from which it subsequently performs (slightly damped) oscillations. We compare in Fig 4.4 the reduced model (red) and the Vlasov evolution (blue) for times up to $\omega_p t = 350$, corresponding to many bounce periods (approximately 80 for $k\lambda_D = 0.4$, and nearly 250 for $k\lambda_D = 0.1$). The reduced model

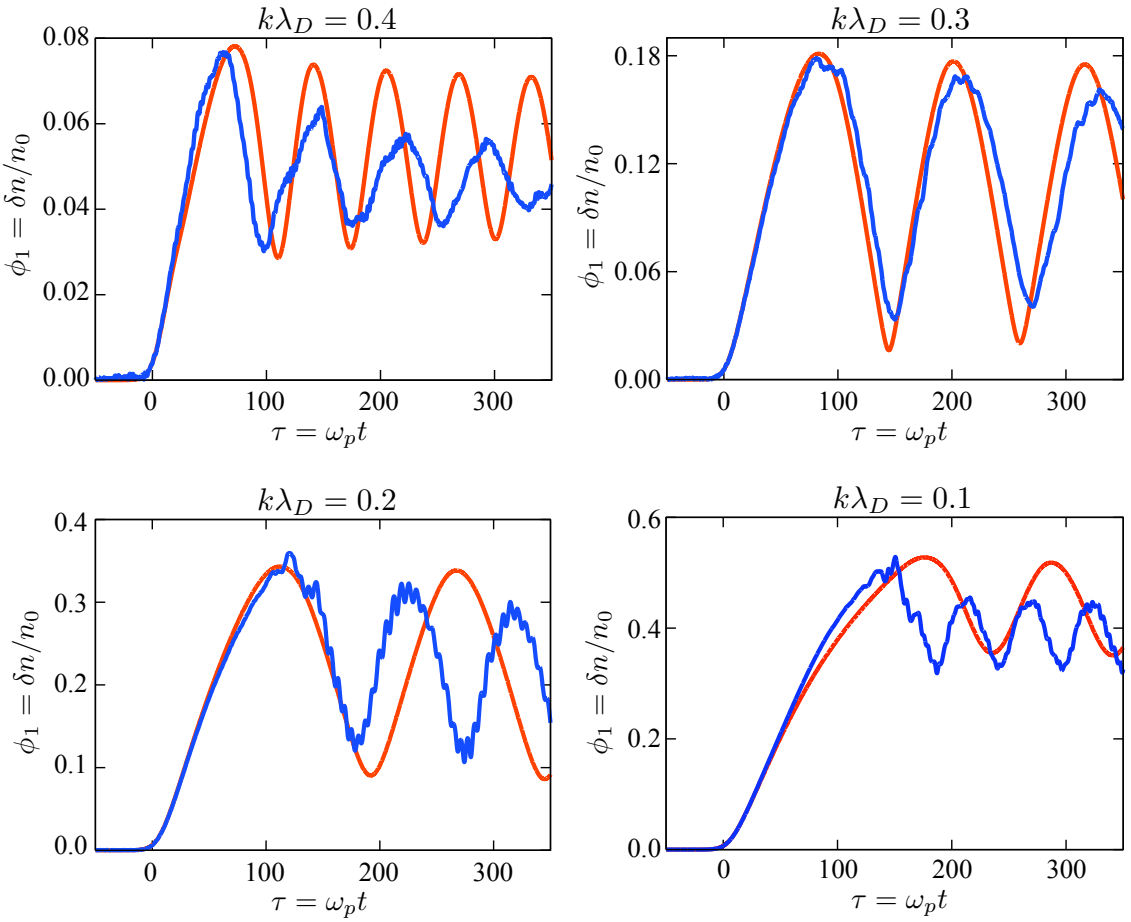

Figure 4.4: Comparison of the extended three-wave model (red curve) and Vlasov simulation (blue curves) for the evolution of the Langmuir wave amplitude using four different temperatures. We see that the Langmuir wave saturation level is well-predicted by the reduced model for $0.1 \leq k\lambda_D \leq 0.4$. Since the dominant saturation mechanism occurs via detuning from the fixed-frequency drive, this indicates that the dynamic, nonlinear frequency shift is well represented up to saturation. After the maximum amplitude is reached, the subsequent dynamics are qualitatively reproduced by the reduced model, with quantitative agreement for the middle range of temperatures near $k\lambda_D = 0.3$.

accurately predicts both the initial evolution and the Langmuir wave saturation amplitude over the entire range of temperature $0.1 \leq k\lambda_D \leq 0.4$. Furthermore, the amplitude and average value of the subsequent oscillations predicted by the reduced model agree quite well with those seen in the Vlasov simulations, although the frequency of these oscillations is more poorly represented. We believe that most of this discrepancy after wave saturation is due to the fact that as the Langmuir wave amplitude becomes smaller, the once-trapped particles again cross the separatrix. While the majority of these particles were trapped from the bulk (and initially above the separatrices), once phase-mixing has taken place they exit the trapping region symmetrically, as predicted by slow separatrix crossing theory [47, 46]. As a result, some particles that were initially above the separatrices will subsequently populate the region below the separatrices, and the corresponding form of the BGK-type action distribution will be flatter around the trapping region than that of a purely growing wave of the same amplitude, as shown in Fig. 4.5(a). Here, we imagine that the potential has decreased from its maximal value corresponding to the separatrix action $J_{\rm sep}^{\rm peak}$ to the present level. For a symmetric de-trapping of the particles, the distribution below the separatrices ($-J_{\rm sep}^{\rm peak} \geq J \geq J_{\rm sep}$) gets an excess of particles from the bulk, as indicated in Fig. 4.5(a). We note that this distribution will be disrupted by collisions, and may cause additional instabilities[2], and therefore will only be a useful description over some limited time-scale.

Because the distribution of the shrinking Langmuir wave in Fig. 4.5(a) is different than that of the purely growing wave, the associated frequency shift $\delta\omega$ is not a single valued function of ϕ_1, as shown in Fig. 4.5(b). To include hysteresis in $\delta\omega$, we solve the iterated equations (2.21) for the mean action $\bar{J}$, but with the distribution chosen to be symmetric about the separatrices for those particles that were at one time trapped in the wave. Since this necessarily requires knowledge of the peak amplitude of the wave, we presently have no means of determining a simple curve fit as was presented for $\delta\omega$

[2]Unlike spatially uniform plasmas, for which the Penrose criterion can be used to determine stability, the nonlinear stability of BGK-type modes has no general theory.

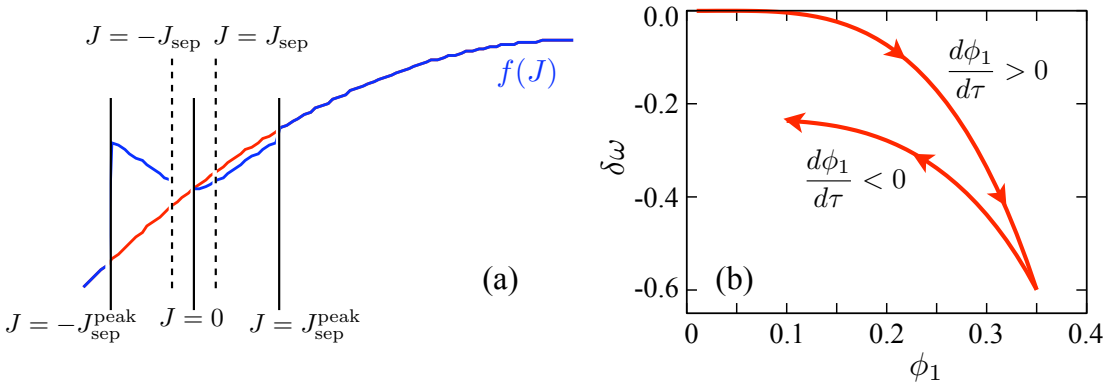

Figure 4.5: Physics associated with a shrinking Langmuir wave. In (a), we schematically plot the distribution in J for a decreasing Langmuir wave, for which the maximal electrostatic potential had the associated separatrix action $J_{\rm sep}^{\rm peak}$. As the wave shrinks, symmetric de-trapping leads to an excess of particles below the separatrices that were originally in the plasma bulk. This leads to hysteresis in the nonlinear frequency shift $\delta\omega$, as shown for a plasma with $k\lambda_D = 0.2$ in (b).

in (3.108b), but rather calculate the hysteresis effect within the envelope model. As an example of the hysteresis in $\delta\omega$, we plot the frequency shift as a function of the amplitude in Fig. 4.5(b) for $k\lambda_D = 0.2$. One general finding is that the frequency shift is a nearly single-valued function of ϕ_1 for warm plasmas, in agreement with the findings of Bénisti and Gremillet [42], while there can be considerable hysteresis as $k\lambda_D$ becomes small. We leave improvements and simplifications for future work.

To properly couple the laser and plasma modes, prediction of the Langmuir amplitude is insufficient, as one must also properly model the phase of the Langmuir mode $\mathcal{G}(\zeta,\tau)$. Mathematically, we compare the real part of $\mathcal{G}$ with the cosine transform of $\phi(\zeta)$, while the imaginary part of $\mathcal{G}$ corresponds to the sine transform of $\phi(\zeta)$. Physically, this divides the plasma response into two quadrature components: the absorptive component that is $\pi/2$ out of phase with the drive (the real/cosine part), and the elastic component that is in phase with the drive (the imaginary/sine part). Since the energy transfer to the plasma is given by

$$J_{\rm PM}E_z \sim a^2\frac{\partial\phi_1}{\partial\zeta} \sim \mathcal{V}\cos(\omega_L\tau)\frac{\partial\phi}{\partial\zeta}, \tag{4.6}$$

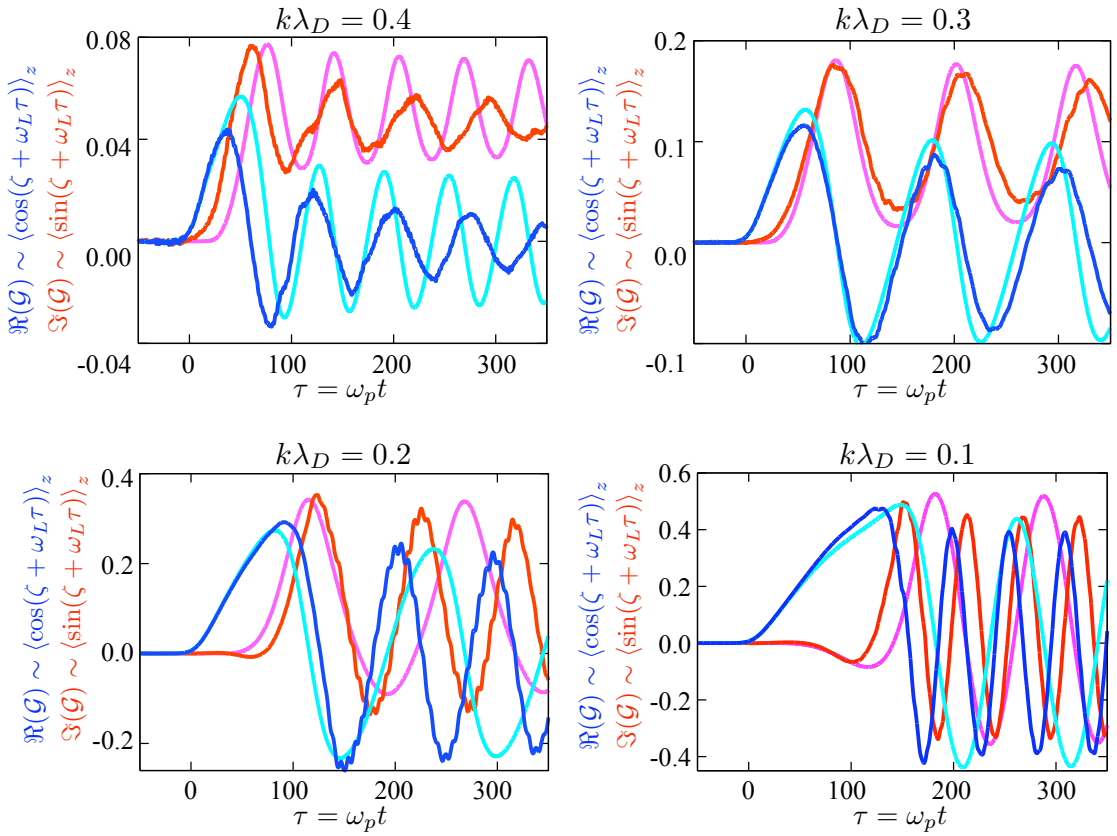

Figure 4.6: Comparison of the driven Langmuir wave phase evolution in the extended envelope model to that of particle simulations. The real part of the Langmuir mode $\mathcal{G}$ is plotted in blue (dark blue for the particle simulation, cyan for the reduced description), while the imaginary part of $\mathcal{G}$ is in red (dark red for the particle result, magenta for the reduced model). We see that up to saturation, the real and imaginary parts are in good agreement, especially for $k\lambda_D \leq 0.3$. After that, the dynamics are complicated by the subsequent trapping and de-trapping in the evolving Langmuir wave. Nevertheless, the simplified envelope equations still yield reasonable agreement.

we see that the absorptive plasma response ($\pi/2$ out of phase with the drive) will tend to extract energy from (or return it to) the drive, whereas the in-phase portion will typically result in no time-averaged energy transfer, but is associated with the frequency shift of the Langmuir wave.

We plot in Fig. 4.6 the real and imaginary parts of the Langmuir response $\mathcal{G}$ for parameters identical to those of Fig. 4.4, and compare these to the cosine and sine transforms of the electrostatic potential ϕ_1. As was found in Fig. 4.4 for the amplitude, Fig. 4.6 shows that the extended envelope model well describes the phase of the Langmuir wave up to saturation. Furthermore, the growth of the imaginary (in-phase) response is correlated to the wave saturation, and hence is further indication that the Langmuir wave saturation is due to the nonlinear frequency shift of the wave.

After saturation, the envelope model only captures the generic features of the subsequent oscillations of the in-phase (elastic) and out-of-phase (absorptive) components. At the high end of the temperatures measured here, $k\lambda_D = 0.4$, the envelope model neglects some small residual damping of the wave while predicting a large-scale oscillation frequency about 15% larger than that seen in the particle simulation. On the other end of the temperature scale, the extended envelope model yields a post-saturation oscillation frequency that is approximately 50% that seen in the particle code for $k\lambda_D = 0.1$, while correctly predicting its amplitude. Between these two extremes, the oscillation frequency and damping are more closely represented by the extended envelope equation, so that for $k\lambda_D = 0.3$, the waveforms are nearly identical.

Finally, we plot the Langmuir wave amplitude for two different magnitudes of the ponderomotive drive in Fig. 4.7: one for which $\mathcal{V}$ is twice that of Figs. 4.4 and 4.6, while the other that is one-half its size. Again, we see that the extended three-wave model accurately predicts the saturation amplitude of the Langmuir wave, while having similar deficiencies predicting the subsequent post-saturation oscillations for hot and cold plasmas as previously discussed. Furthermore, while increasing the drive strength significantly changes the final saturation amplitude for the warm plasmas, its influence decreases as

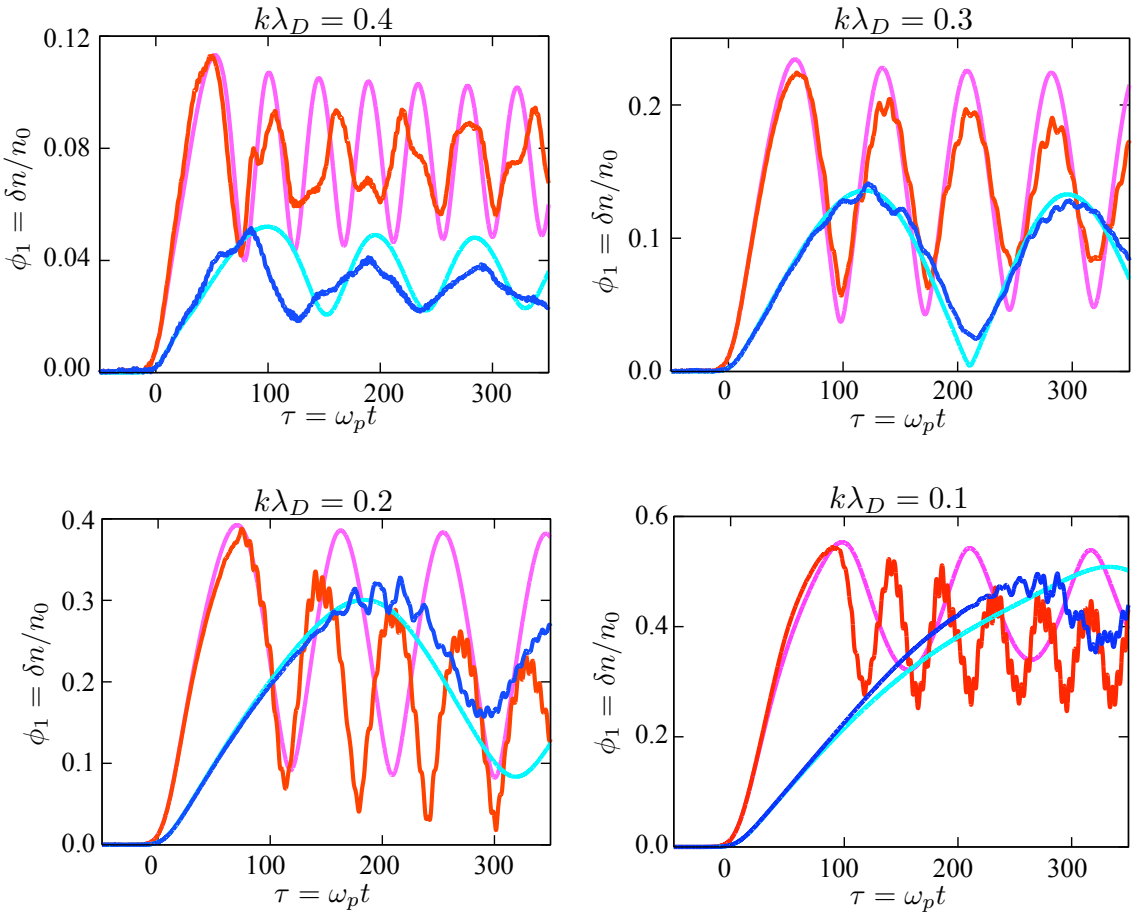

Figure 4.7: Comparison of the reduced envelope model and full particle simulations for the same plasma parameters as Fig 4.4, but with different drive amplitudes. The red is Langmuir wave amplitude evolution obtained from the particle simulation with $\mathcal{V} = 0.02$ (twice that previously) while the magenta is that predicted by the envelope model. Similarly, the dark blue line gives the electrostatic evolution obtained from the particle simulation for $\mathcal{V} = 0.005$, to be compared with the reduced model plotted in cyan. We can see that in all cases the agreement is quite good.

$k\lambda_D$ decreases, such that for $k\lambda_D = 0.1$ the saturated plasma wave amplitude is nearly independent of the drive strength. We interpret this result as follows. For very cold plasmas, we recall from Fig. 2.7 that the nonlinear frequency shift remains small over a broad range of wave amplitudes, beyond which it steeply dives toward large negative values. Therefore, the Langmuir wave is detuned from the drive at the nearly same electrostatic amplitude regardless of the drive strength. One may wonder if this is in some way related to wave-breaking in the plasma. For nonrelativistic plasma oscillations, Coffey [28] used the water bag model to show that the wave-breaking amplitude is given by

$$\max|\phi| = \sqrt{1 - \tfrac{3}{2}\sigma^2 - \tfrac{8}{3^{3/4}}\sqrt{\sigma} + 2\sqrt{3}\,\sigma}\ . \tag{4.7}$$

For $\sigma = 0.1$, Coffey's formula (4.7) gives $\max|\phi| \approx 0.47$. Note that this is close to, but actually less that the wave amplitude seen in Fig. 4.7, which has $\max|\phi| \approx 0.55$. Furthermore, while "wave-breaking" is usually associated with a sudden and dramatic loss of wave coherence, this does not appear to happen to our driven plasma waves.

4.3 Raman amplification in a plasma: numerically modeling the Princeton experiment

In this section we present a brief application of our extended three-wave model to recent experiments at Princeton University on Raman laser amplification by Fisch, Suckewer, and co-workers [30, 94]. The idea is to transfer energy from a long, low-amplitude pump laser to a short, high-amplitude, down-shifted seed pulse using Raman backscatter in an under-dense plasma. Under appropriate initial conditions, the three-wave equations lead to solutions in which nearly all the pump energy can be transfered into the seed pulse whose energy and inverse width increases linearly with interaction distance (the so-called "transient regime," see, e.g., [29, 65, 95, 96]). Applying this transient regime of Raman scatter to a plasma, Malkin, Shvets, and Fisch [29] find that under certain conditions such an amplification scheme may become competitive with the standard chirped pulse ampli-

fication [97], particularly at smaller wavelengths, and may obviate the need for some large and costly gratings.

4.3.1 The theory of pulse compression in a plasma

The basic theory derives from the three-wave equations in a cold plasma; we will only give the briefest review; for more detailed analysis see [98] and the references cited therein. To make the presentation more concise, we introduce the wave action amplitudes for the pump, seed, and plasma wave, along with the coupling $\mathcal{W}$:

$$a \equiv \sqrt{\tfrac{\omega_0}{\omega_p}}\, a_0 \qquad\qquad b \equiv \sqrt{\tfrac{\omega_1}{\omega_p}}\, a_1 \tag{4.8a}$$

$$\rho \equiv \frac{\omega_p}{ck_2}\frac{\mathcal{G}}{\sqrt{2}} \qquad\qquad \mathcal{W} \equiv \frac{ck_2}{2\sqrt{2\omega_0\omega_1}}. \tag{4.8b}$$

Next, we employ coordinates co-moving with the seed pulse (along $+\hat{\boldsymbol{z}}$ with velocity c), and scale these coordinates with the linear Raman growth rate given by $\mathcal{W}\bar{a}$, where $\bar{a}$ is some characteristic (or average) value of the pump:

$$T \equiv \mathcal{W}\bar{a}\left(\omega_p t - \tfrac{\omega_p}{c} z\right) = \mathcal{W}\bar{a}\left(\tau - \tfrac{\omega_p}{ck_2}\zeta\right) \qquad Z \equiv \mathcal{W}\bar{a}\,\tfrac{\omega_p}{c} z = \mathcal{W}\bar{a}\,\tfrac{\omega_p}{ck_2}\zeta \tag{4.9}$$

In terms of the variables (4.8) and coordinates (4.9), the three-wave equations (3.106) with $\nu = u_{\rm gr} = (\omega - \omega_2) = \boldsymbol{\nabla}_\perp = 0$ are

$$2\frac{\partial a}{\partial T} - \frac{\partial a}{\partial Z} = +b\rho \qquad \frac{\partial b}{\partial Z} = -a\rho^* \qquad \frac{\partial \rho}{\partial T} = -ab^*. \tag{4.10}$$

In the highly nonlinear regime of pulse amplification, the pump develops a sharp leading edge in the moving frame as it becomes nearly depleted; in this case $\partial_T a \gg \partial_Z a$ and we can negect the Z-derivative in the pump equation from (4.10); this approximation together with the plasma wave equation leads to a simplified Manley-Rowe conservation equation

$$\frac{\partial}{\partial T}\left[|a|^2 + \tfrac{1}{2}|\rho|^2\right] = 0. \tag{4.11}$$

We assume that the pump is initially flat, which in our variables scaled by $\bar{a}$ implies $a(T \to -\infty) = 1$, and that the plasma wave is initially zero, i.e., $\rho(T \to -\infty) = 0$. Noting

this, the conservation law (4.11) implies that we can make the definitions

$$a = \cos(u/2) \qquad\qquad \rho = \sqrt{2}\sin(u/2).$$

By defining u to be proportional to the integrated area under the seed pulse, namely

$$u(T, Z) \equiv \sqrt{2}\int_{-\infty}^{T} dT'\; b(T', Z), \tag{4.12}$$

we find that the integrated seed area u obeys the sine-Gordon equation

$$\frac{\partial^2 u}{\partial T\,\partial Z} - \sin(u) = 0. \tag{4.13}$$

There are many well-known solutions of the sine-Gordon equation. As suggested by the work in [65], we will look for a particular "self-similar" solution of (4.13) that is a function only of the coordinate $\eta \equiv 2\sqrt{TZ}$. At the end of the calculation, we will also find that these solutions will satisfy our assumption $\partial_T a \gg \partial_Z a$. Making the substitution $\eta \equiv 2\sqrt{TZ}$ in (4.13), we now have the ordinary differential equation

$$\frac{d^2 u}{d\eta^2} + \frac{1}{\eta}\frac{du}{d\eta} - \sin(u) = 0. \tag{4.14}$$

Qualitatively, (4.14) is a damped pendulum equation with a nonlinear damping coefficient $1/\eta$. Here, the values $u = 2n\pi, n \in \mathbb{R}$ represent the unstable fixed points (a physical pendulum pointing up), while $u = (2n+1)\pi$ are the stable fixed points (a pendulum hanging down). Thus, we expect u to oscillate about its fixed point $u = \pi$, approaching it slowly as $\eta \to \infty$. We also note that as $u \to \pi$, the pump $a \to 0$, and is completely depleted. Examples of the solutions to (4.14) are plotted in Fig. 4.8. On the left are scaled intensities of the pump, plasma wave, and seed in terms of the similarity variable, while the right panel of Fig. 4.8 is a realization of the pulses in the co-moving variable after some particular propagation distance. As this distance increases, the seed energy can be seen to increase while the width decreases. This can be understood by considering the location of the similarity variable $\eta = \eta_{\mathrm{M}}$ at which the seed reaches a maximum. Converting to the physical variables, the seed duration D is approximately given by

$$\eta_{\mathrm{M}}^2(\zeta) \equiv 2(\tau - \zeta)_{\mathrm{M}}\zeta \sim D\zeta \quad \Rightarrow \quad D \sim \frac{\eta_{\mathrm{M}}^2}{\zeta}, \tag{4.15}$$

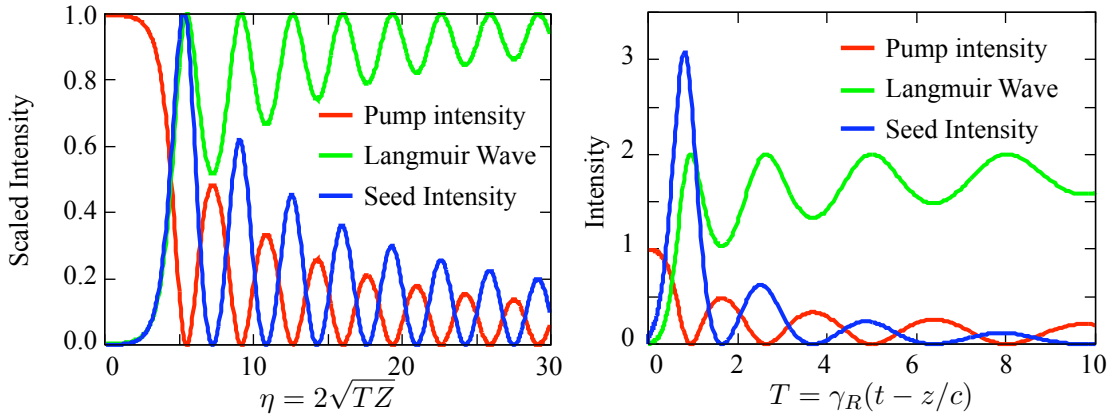

Figure 4.8: Self-similar solution of an amplifying, shortening pulse in the three-wave model. The left panel shows the scaled pump, plasma, and seed intensities in terms of the similarity variable η. In a frame comoving with the seed, these solutions appear as those given in the right panel. The seed energy increases linearly with the interaction length while the width is inversely proportional to this same distance.

and the pulse length scales as the inverse interaction length. Furthermore, because the complete wave action transfer occurs over an ever-decreasing spatial extent, the integrated Manley-Rowe relations

$$\int d\zeta \left(|a|^2 + |b|^2 \right) = \text{constant} \tag{4.16}$$

imply that the amplified seed pulse energy is proportional to the interaction length (i.e., that all the pump energy has been swept up by the seed).

4.3.2 The Princeton experiment on Raman amplification

As numerous theoretical studies [72, 99, 100] have demonstrated the apparent robustness of the plasma-based Raman amplifier, an experimental effort to demonstrate pulse amplification and compression in an physical device was begun by the Suckewer group at Princeton University. The first significant experimental result was obtained using a broad-band seed pulse, for which energy gains of order 50-100 were observed [94]. However, since only a small fraction of the broad-band seed was actually resonant with and amplified by the plasma, the overall efficiency was very low. Since that time, a narrow band, resonant seed pulse has been implemented, and significant pulse amplification $\sim$1-5$\times 10^3$ has been

	Plasma			
Density	$n_0 = 10^{19}$ cm^{-3}		$\omega_p/\gamma_R = 70$	
Length	2-3 mm		15-25 gain lengths	
Temperature	50 eV		$k\lambda_D = 0.25$	
	Pump laser		**Seed laser**	
Wavelength	800 nm	$\omega_0/\omega_p = 12$	870 nm	$\omega_0/\omega_p = 13$
Intensity	10^{14} W/cm^2	$a_0 = 0.005$	10^{12} W/cm^2	$a_1 = 0.0005$
FWHM	15 ps	30 gain lengths	500 fs	1 gain length
Spot	50 μm	30 c/ω_p	40 μm	25 c/ω_p

Table 4.3: Representative parameters for the Princeton experiment, in both physical and scaled units.

achieved for very small amplitude seed pulses, while larger amplitude lasers experienced gain of order 60. The efficiency was still rather low, however, $\sim$1-2 %. In order to help guide the experiment to improve this figure of merit, a more complete account of physics beyond the resonant three-wave model is required. By properly understanding such effects as density fluctuations, thermal and kinetic physics, and transverse effects in simulations and experiments, one can hope to benchmark codes and design future experiments and devices.

Typical parameters for the laser amplification experiment are given in Table 4.3, where we include both the physical parameters of the experiment and the normalized quantities that we have introduced. We see that the experimental parameters have been chosen such that the laser frequency is much greater than the plasma frequency which, in turn, is much greater than the Raman growth length. While the temperature is not large, it is also not negligible; furthermore, while the transverse spot size is large enough to justify a nearly one-dimensional approach, diffraction and the transverse variation in the growth length are probably not negligible. Thus, a two-dimensional simulation including kinetic effects is probably required to properly model the experiment.

We have performed an initial study to address these issues, starting with the averaged particle-in-cell code aPIC [69] and now with the extended three-wave model. We plot the results of the energy amplification for the approximate parameters of Table 4.3 in Fig. 4.9.

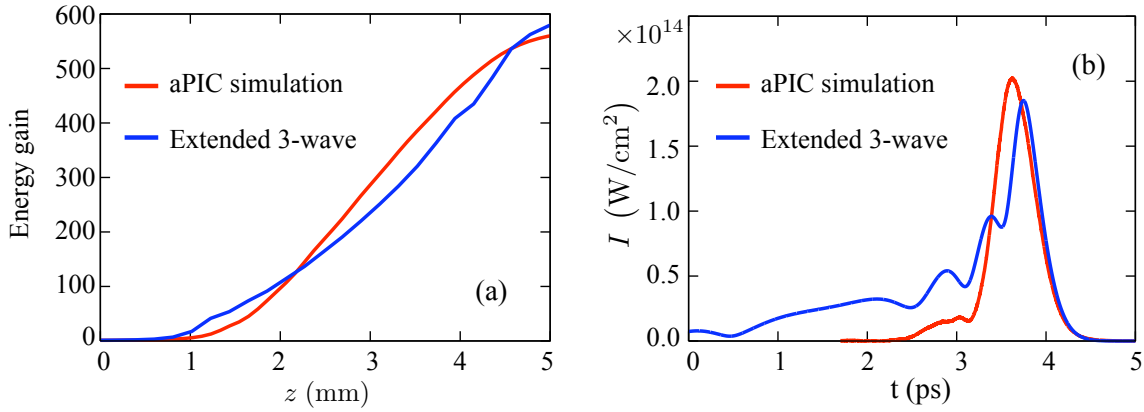

Figure 4.9: Comparison of the aPIC and extended three-wave code for parameters relevant to the Princeton laser amplification experiment [30]. We plot in (a) the energy gain as a function of the interaction length, for which similar results are predicted by both models. The experimental data indicate an amplification of ~ 60, which would correspond to an effective one-dimensional plasma length of 1.75mm as predicted by aPIC, while 1.5 mm as measured for the three-wave model. In (b) we plot the intensity profiles of the seed pulses assuming that the interaction proceeds for the full 2 mm of plasma. In this case, the energy gain is predicted to be 95 and 105 by aPIC and the three-wave model, respectively, while both models predict a final seed intensity larger than that of the pump. At this point in the interaction, the local energy depletion of the pump is $\sim 40\%$.

We see that the two curves approximately follow each other, and note that they consistently over-estimate the actual amplification seen in the experiment. For the approximately 2-3 mm plasma, 4.9(a) indicates gain of the order 100-300, while that observed in the experiment is $\sim$60. We see that this corresponds to an effective one-dimensional plasma length of order 1.5-1.75 mm. Furthermore, significant discrepancy is found with the standard three-wave model (4.10), which predicts gain that is 2-5 times greater still than that seen in either the aPIC or extended three-wave simulations. Nevertheless, determining which of the various limiting factors (thermal, plasma inhomogeneities, or transverse effects) is dominant requires additional investigation. We leave such analysis, including extensions to two dimensional dynamics, to future work.

Chapter 5

Some aspects of plasma fluid models in one dimension

In this chapter, we describe some aspects of one-dimensional plasma fluid models that have arisen during our study of basic plasma processes. We begin with a new (to our knowledge) canonical and Hamiltonian warm fluid description of a plasma, in which the coordinates are standard fluid variables (the velocity and electric fields). We then apply this Hamiltonian formulation to cold plasma waves, showing that the canonical action of a nonlinear, nonrelativistic plasma wave is proportional to its energy, verifying that the dependence of the natural frequency of the Langmuir wave on its amplitude arises solely from thermal and relativistic effects[1], as previous analyses have indicated [80, 64].

In the next section, we present a careful analysis of the Langmuir wave in Eulerian (fixed frame) variables, arriving at an intuitive, geometric description of the velocity field, from which the fluid variables in a nonlinear wave have analytic (but parametric) representations. We identify the velocity field as a curtate cycloid whose amplitude depends upon the field strength, while the electric field is described by a closely related curve that,

[1]This is an unusual state of affairs, in that the convective derivative nonlinearity from the continuity equation is cancelled by that of the force equation when determining the oscillation frequency, while the fields themselves are not purely sinusoidal.

to our knowledge, does not have a name. We then use the parametric representation of the potential to calculate the frequency of test particles moving in the Langmuir wave potential, for which we find a family of orbits (that we call the cold orbits) whose frequency is independent of the particle energy. These orbits are parameterized by the electrostatic amplitude and have a canonical action that is proportional to their energy. We conclude by showing that the electrostatic fields described by the cold theory closely approximates those that dynamically arise in the slowly driven thermal plasmas of Ch. 2. This suggests that warm plasmas also have an evolving orbit whose frequency is energy-independent, in accord with our finding in Ch. 2 that the mean action of the distribution function evolves as the plasma wave grows.

Although both Hamiltonian fluid theories and Langmuir waves have been studied extensively and for a long time, we have failed to find these results in any of the literature. We believe that the former has a simple explanation - the Hamiltonian formulation of a warm plasma found here is specific to one dimension. While one may consider this is to be rather restrictive constraint, many basic plasma phenomena were first detailed and described using one-dimensional approximations, and we have found that this additional Hamiltonian structure has made some of these calculations much simpler to perform.

5.1 Canonical Hamiltonian warm fluid theory for Eulerian plasmas in one dimension

The Hamiltonian structure of fluid models is well known (see, for example, the review by Morrison [101] and references cited therein). While material, or Lagrangian, fluid variables often permit canonical Hamiltonian structures (see, e.g., [102]) Eulerian descriptions of infinite-dimensional systems in terms of physically meaningful variables generally involve non-canonical formulations. Examples include the KdV equation [103], the one dimensional compressible fluid [104], and three dimensional plasma-fluid dynamics [105, 106]. Associated with these degenerate, noncanonical structures are Casimir invariants, which

are kinematic invariants built into the phase space evolution under consideration, and, as such, limit the dynamics to what are referred to as sympletic leaves. In the charged-fluid example under consideration, one of these Casimirs leads to the continuity equation, and as such may be related to the constrained variational principles for the associated Lagrangian given by Brizard [107]. In what follows, we present a one-dimensional, Eulerian Hamiltonian for a warm plasma that is both described in terms of physical variables and fully canonical.

To obtain our Hamiltonian model, we begin by taking velocity moments of the Vlasov equation. The first two moments yield the Eulerian fluid equations

$$\frac{\partial}{\partial t} n_e + \frac{\partial}{\partial z}(n_e v_z) = 0 \tag{5.1a}$$

$$\frac{\partial}{\partial t}(n_e v_z) + \frac{\partial}{\partial z}(n_e v_z^2) + \frac{\partial}{\partial z}\mathscr{P} + \frac{F_z}{m_e} n_e = 0, \tag{5.1b}$$

where n_e, v_z, and $\mathscr{P}$ are the fluid density, velocity, and pressure defined respectively as the zeroth, first, and centered second-order moment of the electron distribution function f_e with respect to the velocity:

$$n_e \equiv \int dv\ f_e(v,z;t), \quad n_e v_z \equiv \int dv\ f_e(v,z;t) v, \quad \mathscr{P} \equiv \int dv\ f_e(v,z;t)(v-v_z)^2. \tag{5.2}$$

The force F_z is given by the sum of the electric and ponderomotive forces

$$F_z = -eE_z + \frac{e^2}{2m_e^2 c^2}\frac{\partial \boldsymbol{A}_\perp^2}{\partial z}, \tag{5.3}$$

which in turn evolve according to Maxwell's equations

$$\frac{\partial \mathcal{E}}{\partial z} = \quad 4\pi e(n_0 - n_e) \tag{5.4a}$$

$$\left[\frac{\partial^2}{\partial t^2} - c^2\frac{\partial^2}{\partial z^2}\right]\boldsymbol{A}_\perp = -\tfrac{4\pi e^2}{m_e} n_e \boldsymbol{A}_\perp. \tag{5.4b}$$

As it stands, the equations are not complete, as the pressure $\mathscr{P}$ is given in terms of higher order velocity moments of the distribution function. In gas dynamics, closure is typically achieved via the Chapman-Enskog-type expansion assuming that the dynamics

is dominated by collisions. In certain laser-plasma interactions, however, the typical collision relaxation time can be much longer than the relevant time-scales for the processes of interest, so that collisional closures are inappropriate. One alternative is to invoke an equation of state $\mathscr{P} = \mathscr{P}(n_e, T_e)$, typically taken to be either isothermal ($\mathscr{P} = n_e T_e/m_e$) or adiabatic $\left[\mathscr{P} = n_e^3 T_e/\left(n_0^2 m_e\right)\right]$; another common method is to close the system with the so-called "water-bag" model [108, 109], in which the incompressible phase-space distribution function is taken to be a constant between two boundaries (that depend on z and t), while zero outside of this region. In this case f_e is parametrized by only two numbers at every point in z (the water bag centroid and its width, i.e., mean velocity and pressure), which closes the fluid equations. A final scheme, the "warm fluid" model [110, 111], is an asymptotic closure based on the assumption that the distribution is, in some sense, narrow in width, so that the higher order centered moments (third, fourth, etc.) can be neglected. Interestingly, in the nonrelativistic limit, the last three closure methods (adiabatic, water bag, and warm fluid) all give the same expression for the pressure:

$$\mathscr{P} = v_{\text{th}}^2 \frac{n_e^3}{n_0^2}, \tag{5.5}$$

where $m_e v_{\text{th}}^2 \equiv T_e$. We will use the closure (5.5). To simplify the equations, we normalize time by the plasma frequency, $\tau \equiv \omega_p t$, and the longitudinal coordinate by some characteristic wavevector[2] k, so that $\zeta \equiv kz$. These dimensionless coordinates lead naturally to the normalized field variables

$$\frac{\delta n}{n_0} \equiv \frac{n_e - n_0}{n_0} \qquad u \equiv \frac{\omega_p}{k} v_z \tag{5.6a}$$

$$\mathcal{E} \equiv \frac{m_e \omega_p^2}{ek} E_z \qquad \boldsymbol{a}_\perp \equiv \frac{e}{m_e c^2} \boldsymbol{A}_\perp, \tag{5.6b}$$

[2]Two "natural" choices for the wavevector k are the inverse collisionless skin depth ω_p/c or that associated with the Debye length, $2\pi/\lambda_D$; since our previous chapters normalized z using the laser beat wavevector k_2, for now we will choose to leave k unspecified.

and the Maxwell-fluid system (5.1)-(5.4) becomes

$$\frac{\partial}{\partial\tau}\frac{\delta n}{n_0}+\frac{\partial}{\partial\zeta}\left[u\left(1+\frac{\delta n}{n_0}\right)\right]= 0 \tag{5.7a}$$

$$\frac{\partial u}{\partial\tau}+u\frac{\partial u}{\partial\zeta}+3\sigma^2\left[1+\frac{\delta n}{n_0}\right]\frac{\partial}{\partial\zeta}\frac{\delta n}{n_0}= \mathcal{E}+\frac{c^2k^2}{2\omega_p^2}\frac{\partial}{\partial\zeta}\boldsymbol{a}_\perp^2 \tag{5.7b}$$

$$\frac{\partial}{\partial\zeta}\mathcal{E}=-\frac{\delta n}{n_0} \tag{5.7c}$$

$$\left[\frac{\partial^2}{\partial\tau^2}-c^2\frac{\partial^2}{\partial\zeta^2}\right]\boldsymbol{a}_\perp=-\left(1+\frac{\delta n}{n_0}\right)\boldsymbol{a}_\perp. \tag{5.7d}$$

To put the system (5.7) into a form from which we can deduce the canonical coordinates and the generating Hamiltonian, we use the Poisson equation (5.7c) to eliminate the density perturbation from the continuity equation (5.7a):

$$\frac{\partial}{\partial\zeta}\left[\frac{\partial\mathcal{E}}{\partial\tau}+u\frac{\partial\mathcal{E}}{\partial\zeta}-u\right]=0 \quad\Rightarrow\quad \frac{\partial\mathcal{E}}{\partial\tau}+u\frac{\partial\mathcal{E}}{\partial\zeta}-u=h(\tau), \tag{5.8}$$

where $h(\tau)$ is some spatially uniform function of time; consistency with the longitudinal component of the Ampère-Maxwell Law implies $h(\tau)=0$:

$$\frac{\partial\mathcal{E}}{\partial\tau}=\left(1+\frac{\delta n}{n_0}\right)u=u-u\frac{\partial\mathcal{E}}{\partial\zeta}. \tag{5.9}$$

Thus, our system reduces to

$$\frac{\partial u}{\partial\tau}+u\frac{\partial u}{\partial\zeta}=-\mathcal{E}+3\sigma^2\left[1-\frac{\partial\mathcal{E}}{\partial\zeta}\right]\frac{\partial^2\mathcal{E}}{\partial\zeta^2}-\frac{1}{2}\frac{\partial\boldsymbol{a}_\perp^2}{\partial\zeta} \tag{5.10a}$$

$$\frac{\partial\mathcal{E}}{\partial\tau}+u\frac{\partial\mathcal{E}}{\partial\zeta}=u \tag{5.10b}$$

$$\left[\frac{\partial^2}{\partial\tau^2}-\frac{\partial^2}{\partial\zeta^2}+1\right]\boldsymbol{a}_\perp=\boldsymbol{a}_\perp\frac{\partial\mathcal{E}}{\partial\zeta}. \tag{5.10c}$$

In one dimension, the warm, nonrelativistic charged fluid system of equations (5.10) has a canonical Hamiltonian structure. While this is readily apparent for the electromagnetic fields, to our knowledge this is the first time a canonical Hamiltonian has been identified with the warm plasma response in "physical" Eulerian coordinates. In this case, the electric field $\mathcal{E}$ is identified with the fluid generalized coordinate, while the velocity u is its conjugate momentum. Thus, we define the phase space coordinates

$$(\boldsymbol{p};\,\boldsymbol{q})=(p,\boldsymbol{\pi}_\perp;\,\mathcal{E},\boldsymbol{a}_\perp), \tag{5.11}$$

with $\boldsymbol{\pi}_\perp$ the conjugate to the vector potential $\boldsymbol{a}_\perp$. In terms of the phase space variables (5.11) the warm electrodynamic fluid system (5.10) can be derived from the functional Hamiltonian

$$\mathcal{H}\big[\boldsymbol{p}(\zeta,\tau);\, \boldsymbol{q}(\zeta,\tau)\big] = \int d\zeta'\, \mathscr{H}\big(\boldsymbol{p}(\zeta',\tau);\, \boldsymbol{q}(\zeta',\tau)\big) \tag{5.12}$$

where the Hamiltonian density $\mathscr{H}(\boldsymbol{p}(\zeta',\tau);\boldsymbol{q}(\zeta',\tau))$ is given by

$$\begin{aligned}\mathscr{H}(p,\pi_\perp;\, \mathcal{E},\boldsymbol{a}_\perp) = \frac{1}{2}p^2 + \frac{1}{2}\mathcal{E}^2 + \frac{3\sigma^2}{2}\left(\frac{\partial \mathcal{E}}{\partial \zeta}\right)^2 \\ - \frac{1}{2}p^2\frac{\partial \mathcal{E}}{\partial \zeta} + \frac{\sigma^2}{2}\left(\frac{\partial \mathcal{E}}{\partial \zeta}\right)^3 \\ + \frac{1}{2}\boldsymbol{\pi}_\perp^2 + \frac{1}{2}\left(\frac{\partial \boldsymbol{a}_\perp}{\partial \zeta}\right)^2 + \frac{1}{2}\boldsymbol{a}_\perp^2 \\ - \frac{1}{2}\mathcal{E}\frac{\partial \boldsymbol{a}_\perp^2}{\partial \zeta},\end{aligned} \tag{5.13}$$

and the evolution of any phase space observable $\mathcal{Z}$ is given by Hamilton's equations with the canonical Poisson bracket $\{\cdot\,,\,\cdot\}$:

$$\frac{\partial}{\partial \tau}\mathcal{Z}(\zeta,\tau) = \int d\zeta'\, \big\{\mathcal{Z}(\zeta,\tau),\, \mathscr{H}\big(\boldsymbol{p}(\zeta',\tau);\, \boldsymbol{q}(\zeta',\tau)\big)\big\} \tag{5.14a}$$

$$\big\{\mathcal{E}(\zeta,\tau),\, \mathcal{E}(\zeta',\tau)\big\} = \big\{p(\zeta,\tau),\, p(\zeta',\tau)\big\} = 0 \tag{5.14b}$$

$$\big\{\mathcal{E}(\zeta,\tau),\, p(\zeta',\tau)\big\} = \delta(\zeta-\zeta'). \tag{5.14c}$$

The Hamiltonian density naturally divides into four pieces

$$\mathscr{H} = \mathscr{H}_{\rm p}^0 + \mathscr{H}_{\rm p}^1 + \mathscr{H}_{\rm EM}^0 + \mathscr{H}_{\rm p,EM}^{\rm couple}, \tag{5.15}$$

where $\mathscr{H}_{\rm p}^0$ is that of the warm, linear plasma wave, $\mathscr{H}_{\rm p}^1$ describes the fluid and thermal nonlinearities, $\mathscr{H}_{\rm EM}^0$ gives the electromagnetic radiation (with the $\frac{1}{2}\boldsymbol{a}_\perp^2$ yielding the linear change in dispersion due to the plasma), and $\mathscr{H}_{\rm p,EM}^{\rm couple}$ describes the ponderomotive coupling between the lasers and the plasma.

As a simple application of this formalism, we use the Lagrangian associated with (5.13) to investigate the cold, nonrelativistic plasma wave. Although this has been well-studied, we feel that we might offer a modest addition with respect to understanding how

the (seemingly) nonlinear Eulerian plasma wave has a frequency that is independent of its amplitude in the cold case. To this end, we first write the Hamiltonian density for a cold plasma ($\sigma \equiv k\lambda_D = 0$)

$$\mathscr{H}(p, \pi_\perp; \mathcal{E}, \boldsymbol{a}_\perp) = \frac{1}{2}p^2 + \frac{1}{2}\mathscr{E}^2 - \frac{1}{2}p^2\frac{\partial \mathcal{E}}{\partial \zeta} + \frac{1}{2}\boldsymbol{\pi}_\perp^2 + \frac{1}{2}\left(\frac{\partial \boldsymbol{a}_\perp}{\partial \zeta}\right)^2 + \frac{1}{2}\boldsymbol{a}_\perp^2 - \frac{1}{2}\mathcal{E}\frac{\partial \boldsymbol{a}_\perp^2}{\partial \zeta}. \quad (5.16)$$

Note that (5.16) has an appealing interpretation as the energy density: grouping the first and third terms together we have $\frac{1}{2}\left(1 - \frac{\partial \mathcal{E}}{\partial \zeta}\right)p^2 = \frac{1}{2}np^2$, i.e., the kinetic energy density, while the second term $\frac{1}{2}\mathcal{E}^2$ is the electrostatic energy density. Although one could construct the Lagrangian density $\mathscr{L}$ associated with $\mathscr{H}$ in terms of the coordinates $\mathcal{E}$ and $\boldsymbol{a}_\perp$, we find it convenient to first make a canonical transformation that exchanges the roles of p and q for the plasma wave (i.e., the velocity u and the electric field $\mathcal{E}$). Denoting the new variables with háčeks, we use the mixed generating function [52]

$$F(q_1, \boldsymbol{q}_2; \check{q}_1, \check{\boldsymbol{p}}_2) = \mathcal{E}\check{q} + \boldsymbol{a}_\perp \check{\boldsymbol{\pi}}_\perp, \quad (5.17)$$

which, through the relations

$$p = \frac{\partial F}{\partial \mathcal{E}} = \check{q}, \qquad \check{p} = -\frac{\partial F}{\partial \check{q}} = -\mathcal{E},$$
$$\boldsymbol{\pi}_\perp = \frac{\partial F}{\partial \boldsymbol{a}_\perp} = \check{\boldsymbol{\pi}}_\perp, \qquad \check{\boldsymbol{a}}_\perp = \frac{\partial F}{\partial \check{\boldsymbol{\pi}}_\perp} = \boldsymbol{a}_\perp,$$

has the effect of exchanging the position and momentum roles of the plasma coordinates, while keeping the laser coordinates fixed. Dropping the háčeks on the "new" laser variables, and making substitution of the generalized coordinate $\check{q} = u$ we have

$$\mathscr{H}(\check{p}, \pi_\perp; u, \boldsymbol{a}_\perp) = \frac{1}{2}\check{p}^2 + \frac{1}{2}u^2 - \check{p}u\frac{\partial u}{\partial \zeta} + \frac{1}{2}\boldsymbol{\pi}_\perp^2 + \frac{1}{2}\boldsymbol{a}_\perp^2 + \frac{1}{2}\left(\frac{\partial \boldsymbol{a}_\perp}{\partial \zeta}\right)^2 + \frac{1}{2}\check{p}\frac{\partial \boldsymbol{a}_\perp^2}{\partial \zeta}. \quad (5.18)$$

The Lagrangian density associated with (5.18) is found via the Legendre transform. We have

$$\mathscr{L} = \frac{\partial \boldsymbol{q}}{\partial \tau} \cdot \boldsymbol{p} - \mathscr{H} \qquad \frac{\partial \boldsymbol{q}}{\partial \tau} = \frac{\partial \mathscr{H}}{\partial \boldsymbol{p}}, \quad (5.19)$$

so that

$$\begin{aligned}\mathscr{L} = &\frac{1}{2}\left(\frac{\partial u}{\partial \tau}\right)^2 - \frac{1}{2}u^2 + u\frac{\partial u}{\partial \zeta}\frac{\partial u}{\partial \tau} + \frac{1}{2}u^2\left(\frac{\partial u}{\partial \zeta}\right)^2 \\ &+ \frac{1}{2}\left[\left(\frac{\partial \boldsymbol{a}_\perp}{\partial \tau}\right)^2 - \left(\frac{\partial \boldsymbol{a}_\perp}{\partial \zeta}\right)^2 - \boldsymbol{a}_\perp^2\right] + \frac{1}{2}\left(\frac{\partial u}{\partial \tau} + u\frac{\partial u}{\partial \zeta}\right)\frac{\partial \boldsymbol{a}_\perp^2}{\partial \zeta},\end{aligned} \tag{5.20}$$

which, again, can be divided into the linear and nonlinear pieces associated with the free plasma wave, the free electromagnetic piece (with the linear renormalization due to the plasma medium), and the ponderomotive coupling between the two.

5.2 The cold, nonrelativistic plasma frequency

Up to this point, we have used Eulerian variables to describe the plasma response. This basically amounts to considering the fluid quantities (such as density, velocity, pressure, etc.) to be defined at fixed locations in space, so that the governing equations describe the local fluxes and time rates of change. In this way, the Eulerian viewpoint is analogous to sitting on the bank of a river and watching the flow proceed. Generally, we find these variables to be the most convenient, but there is one case in which the alternate, Lagrangian perspective leads to the most transparent analysis, namely, in determining the frequency of a cold plasma.

In the Lagrangian viewpoint, one follows individual fluid elements as they are subjected to forces. In this way, the Lagrangian perspective is more analogous to a boat riding with the flow, and thus complementary to the Eulerian river-bank approach. From the Lagrangian perspective it is easy to show that, neglecting relativity, the local force on each plasma electron is proportional to its displacement (below wave-breaking), so that each electron undergoes simple harmonic motion with constant frequency given ω_p [49]. Since this piece of physics must be independent of the means of analysis, it must also be true that an Eulerian analysis of the Langmuir wave reveals an amplitude independent frequency ω_p. Since in the Eulerian perspective the fluid fields are governed by nonlinear equations (specifically, they include the convective derivative $\frac{d}{d\tau} + u\frac{d}{d\zeta}$), it is not obvious that the

nonlinear solutions have amplitude-independent frequencies.

In fact, various analyses of the cold, Eulerian fluid equations have given rise to conflicting results in the literature. The first such analyses, pioneered by Akhiezer and Lyubarskii [112] and Akheizer and Polovin [113], were quasi-static, in which the wave is assumed to depend only on the variable co-moving at the plasma wave phase velocity. These papers showed that changes to the Langmuir wave frequency were due solely to relativistic effects, in agreement with the Lagrangian analyses. Nevertheless, in the mid 1980's perturbation expansions of the one-dimensional fluid equations resulted in several differing formulae for the nonlinear frequency of Langmuir waves. Using a consistent expansion, the source of these various discrepancies was finally resolved by McKinstrie and Forslund [81], who recovered the result of [113].

In this section, we use the Eulerian, Hamiltonian formulation of a cold, one-dimensional plasma to demonstrate the constancy of the frequency in a nonlinear, nonrelativistic Langmuir wave. Furthermore, these equations yield a simple, geometric picture of the nonlinear fields, clearly relating them to the single-particle (Lagrangian) motion. Finally, we calculate the frequency of an electron moving in the cold fields, showing that it is independent of the Langmuir wave amplitude for the fluid orbit of a cold plasma, as required.

5.2.1 Cold plasma in the Lagrangian viewpoint

In a one-dimensional cold plasma, the only force acting of individual fluid elements is the local electrostatic field, so that Newton's third law for a fluid element is given by

$$\frac{d^2}{dt^2} z(z_0, t) = -\frac{e}{m_e} E_z[z(z_0, t), t]. \tag{5.21}$$

Here we have parametrized each fluid element by its initial position z_0 at time $t = 0$. Assuming that these one-dimensional charge sheets do not cross (i.e., that the fluid motion remains below wave-breaking), this parameterization is unique. The self-consistent electric field evaluated at $z = z(z_0, t)$ at time t is determined via Poisson's equation:

$$\frac{d}{dz} E_z = -4\pi e \left[n_e(z, t) - n_0 \right]. \tag{5.22}$$

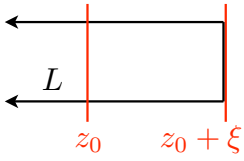

$$E_z(z,t) = 4\pi Q/A = 4\pi e n_0 \big[\overbrace{(L+\xi)}^{\text{ions}} - \overbrace{L}^{\text{electrons}}\big]$$
$$= 4\pi e n_0 \xi(z_0, t)$$

Figure 5.1: Gauss's Law for a Lagrangian element in a cold plasma below wave-breaking. The electric field is proportional to the displacement $\xi(z_0, t)$ from equilibrium.

In the Lagrangian viewpoint we follow individual fluid elements that may deform (being stretched or squeezed in the z direction), but always contain the same fluid. This is encapsulated by the particle conservation equation

$$n_e[z(z_0,t),t]dz = n_e(z_0)dz_0 \equiv n_0\, dz_0. \tag{5.23}$$

Solving (5.23) for the density n_e and using this in the Poisson equation (5.22), we find

$$\frac{d}{dz}E_z = 4\pi e n_0 \left[1 - \frac{dz_0}{dz}\right]. \tag{5.24}$$

In this form, we see that for a cold, one dimensional plasma below wave-breaking, the Poisson equation can be trivially integrated:

$$E_z[(z(z_0,t),t] = 4\pi e n_0 [z(z_0,t) - z_0] \equiv 4\pi e n_0\, \xi(z_0,t), \tag{5.25}$$

where we have introduced the electron displacement $\xi \equiv z - z_0$. From (5.25), we see that the electric field is proportional to the fluid displacement from its equilibrium position. This can be understood as a consequence of Gauss's Law from the stationary ion column; because the electron charge sheets are assumed not to cross, in this geometry the displacement of a fluid element results in a capacitor-like charge separation, as depicted in Fig. 5.1. A simple application of Gauss's Law as in Fig. 5.1 results in (5.25); this model of one-dimensional electron charge sheet moving in a stationary, neutralizing background was introduced by Dawson [49], and is valid below cold wave-breaking, i.e., for $E_z \leq E_0 \equiv \frac{mc\omega_p}{e}$, beyond which the electron displacement is greater than the characteristic wavelength, and the charge sheets cross.

Since the restoring force is proportional to the displacement, using (5.25) in the force equation (5.21) results in the simple harmonic oscillator equation

$$\frac{d^2}{dt^2}\xi(z_0,t) + \omega_p^2\,\xi(z_0,t) = 0. \tag{5.26}$$

In general, one might expect the natural frequency of the plasma to have nonlinear contributions as the plasma wave grows, but as indicated in (5.26), the nonrelativistic one-dimensional plasma has no such frequency shift. Indeed, the relativistic counterpart to (5.26), for which the momentum $\frac{d}{dt}\xi \to \gamma\frac{d}{dt}\xi$ was used by Rosenbluth and Liu [20] to show that the nonlinear dependence of the frequency on the amplitude arises solely from relativistic corrections in the cold plasma.

The Lagrangian perspective clearly shows that each fluid element undergoes simple harmonic motion. It is not obvious, however, that the nonlinear Eulerian fluid equations similarly yield this result. Indeed, this created some confusion and controversy in the literature, with some published results in conflict with the Lagrangian conclusions. While more careful perturbation expansions have resolved this conflict in the weakly nonlinear regime and numerical solutions indicates no (nonrelativistic) nonlinear frequency shift, there as yet seems no general analytic proof (other than appeals to Lagrangian-Eulerian equivalence). In the next section, we derive two such proofs, hopefully illuminating the somewhat unusual Eulerian nature of this independence fluid fields.

5.2.2 The cold plasma in the Eulerian perspective

In this section, we investigate the cold plasma waves discussed in the previous section, only through the use of Eulerian coordinates. This will necessarily involve some transformations and subsequent approximations; to manifestly preserve the Hamiltonian/Lagrangian structure discussed in Sec. 5.1, we apply all such simplifications directly to the Lagrangian density (5.20) rather than directly to the equations of motion. Since we will look for traveling wave solutions, we make a Galilean coordinate change to a frame moving at the phase

velocity of the wave using the coordinates

$$\theta \equiv \tau + \zeta \equiv \omega_p[t + z/v_p], \qquad \tau \equiv \omega_p t, \tag{5.27}$$

where $v_p \equiv \omega_p/k$ is the phase velocity of the wave. Assuming that there is no laser field, the Lagrangian density (5.20) can be expressed in terms of the coordinates θ and τ as

$$\mathscr{L} = \frac{1}{2}(1+u)^2\left(\frac{\partial u}{\partial \theta}\right)^2 - \frac{1}{2}u^2 + \left[\frac{1}{2}\frac{\partial u}{\partial \tau} + (1+u)\frac{\partial u}{\partial \theta}\right]\frac{\partial u}{\partial \tau}. \tag{5.28}$$

To find the (stationary) traveling wave solutions, we take the quasi-static limit of (5.28), for which we assume that the dynamics are essentially independent of time τ in the frame moving at the wave phase velocity. Thus, in the quasi-static approximation we neglect the time derivatives in (5.28), in which case we find that the quasistatic Langmuir wave equation can be obtained from the Lagrangian

$$\mathcal{L}(u, u') = \tfrac{1}{2}(1+u)^2 u'^2 - \tfrac{1}{2}u^2, \tag{5.29}$$

where we denote the co-moving derivative $\frac{d}{d\theta}u = u'$. Again, we note that the linearization of $\mathcal{L}(u, u')$ yields the Lagrangian of a simple harmonic oscillator $\frac{1}{2}(u'^2 - u^2)$. Applying the Euler-Lagrange equations to (5.29), we obtain the second-order nonlinear oscillator equation for the velocity field:

$$(1+u)^2 u'' + (1+u)u'^2 + u = 0. \tag{5.30}$$

The nonlinearity in (5.30) derives from the convective derivative $\frac{\partial}{\partial \tau} + u\frac{\partial}{\partial \zeta}$ which, in the co-moving frame under the quasi-static approximation, is simply $(1+u)\frac{d}{d\theta}$.

This equation is straightforward to solve numerically, assuming the normalized velocity $|u| < 1$. We show some numerical solutions to the equations (5.30) in Fig. 5.2, where we have determined the electric field via the definitions (5.9):

$$\mathcal{E} = -(1+u)u'. \tag{5.31}$$

Note that while the nonlinearities do give rise to steepening velocity fields and sawtooth electric field profiles as $u_{\max}$ increases, they do not appear to yield any shift in the natural frequency, in agreement with the analysis in Lagrangian (or material) coordinates.

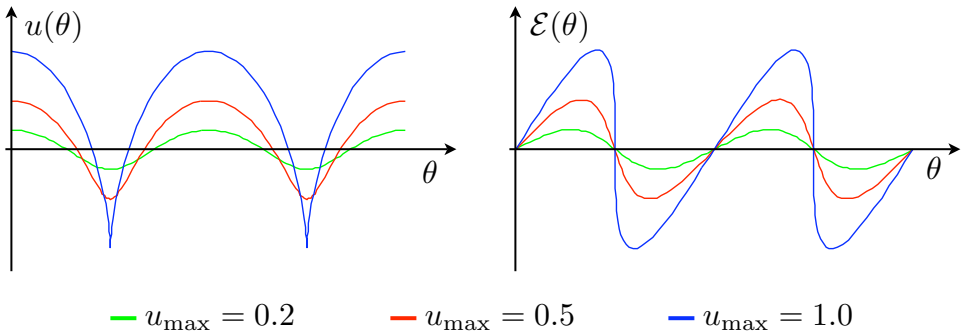

Figure 5.2: Nonlinear Eulerian velocity and electric field profiles for three different amplitudes. Note that although the profiles steepen as $u_{\max}$ increases, their wavelength remains constant.

To make this analytically aparent, we first calculate the canonical action of the plasma wave, and then show that the frequency is independent of the wave amplitude. While this result is sufficient to show the Eulerian-Lagrangian correspondence, it does not (in our opinion) illuminate the connection between the simple harmonic motion observed in the Lagrangian perspective and the nonlinear Eulerian fields of Fig. 5.2. To better understand the dynamics, we conclude this section with a parameterization of the nonlinear fields that makes explicit the connection between the two viewpoints.

The Langmuir wave action

To determine the canonical action of the Langmuir wave, we use the Legendre transformation to obtain the Hamiltonian associated with the Lagrangian (5.29):

$$p \equiv \frac{\partial \mathcal{L}}{\partial u'} = (1+u)^2 u', \qquad \mathcal{H}(p,u) = pu - \mathcal{L}[u'(p,u),u], \tag{5.32}$$

from which we obtain

$$\mathcal{H}(p,u) = \frac{p^2}{2(1+u)^2} + \frac{u^2}{2}. \tag{5.33}$$

Neglecting nonlinear terms, the Hamiltonian (5.33) is that of a simple harmonic oscillator, and the frequency is constant. What is less obvious, however, is that the frequency is independent of the amplitude even when one includes the nonlinear terms. To show this

fact, we calculate the canonical action of the plasma wave:

$$\mathcal{J}(H) = \frac{1}{2\pi}\oint du\, p(u,H) = \frac{1}{2\pi}\oint du\, (1+u)\sqrt{2H-u^2}, \tag{5.34}$$

where the integral is evaluated along the particle orbit with energy H. To calculate (5.34), note that $p = 0$ at the turning points $u_\pm$, so that $u_\pm = \pm\sqrt{2H}$. The action integral is then

$$\mathcal{J}(H) = \frac{1}{\pi}\int_{-\sqrt{2H}}^{\sqrt{2H}} du\, (1+u)\sqrt{2H-u^2} = \frac{2H}{\pi}\int_{-\pi/2}^{\pi/2} d\theta\, \cos^2\theta(1+\sin\theta) = H. \tag{5.35}$$

Thus, in canonical action-angle variables, the Hamiltonian $\mathcal{H}(\mathcal{J},\Psi) = \mathcal{J}$, and the frequency (the time derivative of the angle) is equal to unity:

$$\frac{d}{d\theta}\Psi = \frac{\partial\mathcal{H}}{\partial\mathcal{J}} = 1. \tag{5.36}$$

The canonical formalism shows that the frequency is independent of the Langmuir wave amplitude for arbitrary levels of excitation, just as was found in the Lagrangian analysis.

While this is the desired explicit confirmation of what logic dictated must be true, it does not further illuminate the correspondence between the simple harmonic motion of any one plasma electron (or Lagrangian fluid element) and the manifestly nonlinear Eulerian fields shown in Fig. 5.2. We remedy this in the following section.

Geometrical picture of the Eulerian fields

The second-order system (5.30) is analytically solvable, although only in an implicit manner that does not immediately illuminate the nature of the problem. With a little physical intuition, however, this solution can be sensibly interpreted. To aid this intuition, we begin by writing two first-order equations for the fluid velocity and electric field. Using the equation for the electric field (5.31), we see that the second order oscillator equation (5.30) is equivalent to the system

$$\frac{du}{d\theta} = -\frac{\mathcal{E}}{1+u} \tag{5.37a}$$

$$\frac{d\mathcal{E}}{d\theta} = \frac{u}{1+u}. \tag{5.37b}$$

Multiplying (5.37a) by u and (5.37b) by $\mathcal{E}$, adding the two equations and integrating yields the first integral

$$u^2 + \mathcal{E}^2 = u_{\max}^2. \tag{5.38}$$

Using (5.38) to eliminate $\mathcal{E}$ from (5.37a), we find

$$\frac{1+u}{\sqrt{u_{\max}^2 - u^2}} du = -d\theta. \tag{5.39}$$

Integrating this equation, the velocity field $u(\theta)$ is given by the implicit relation

$$\sqrt{1 - \frac{u^2}{u_{\max}^2}} - \sin\left(\frac{u}{u_{\max}}\right) = \theta. \tag{5.40}$$

In general, such a formal solution is not particularly helpful. However, in this case (5.40) describes a curtate cycloid, where the ratio between inner and outer radius is $u_{\max}$, as shown in Fig. 5.3. Furthermore, at the wave-breaking limit, where the charge sheets are just about to cross, $u_{\max} = 1$ and the velocity field is precisely a cycloid. By analogy, increasing the amplitude beyond wave-breaking results in a prolate cycloid for which the velocity is double-valued near $u_{\max} = -1$. This would violate the assumptions inherent in the cold plasma model.

The cycloidic nature of the nonlinear plasma wave also clearly emerges from the Lagrangian picture, in which each particle undergoes simple harmonic motion with amplitude $u_{\max}$ in the (stationary) laboratory frame. In the Eulerian frame moving at the phase velocity of the wave, this simple harmonic motion is given parametrically by

$$\theta(\mathfrak{s}) = \mathfrak{s} + u_{\max} \sin \mathfrak{s} \tag{5.41}$$

$$u(\mathfrak{s}) = u_{\max} \cos \mathfrak{s}. \tag{5.42}$$

These are the parametric equations for a curtate cycloid and therefore for the Eulerian velocity field. We note that there is a clear correspondence between the time τ for any Lagrangian fluid element in the co-moving frame and the parameterization of the Eulerian fields by $\mathfrak{s}$ above. Since the electric field is out of phase with the "displacement" θ, the

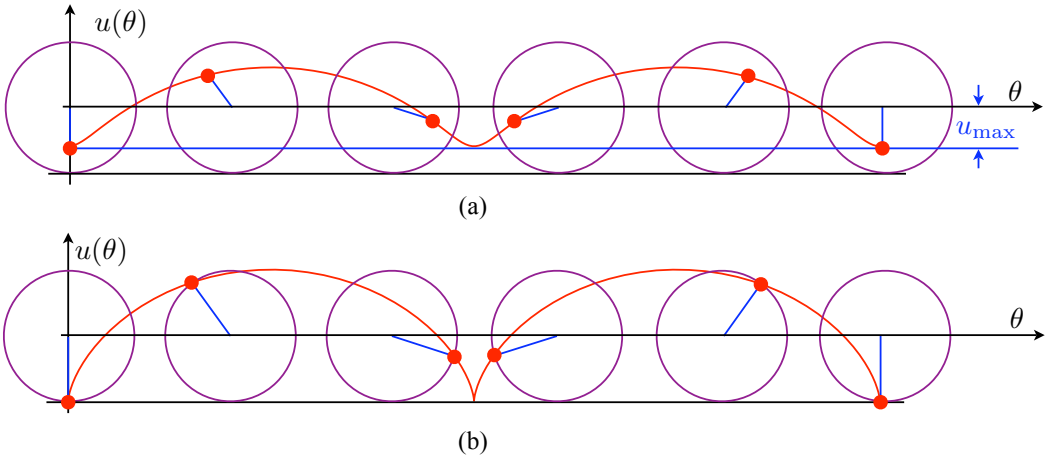

Figure 5.3: Phase space trajectory of a charged particle in the moving Eulerian frame. In this frame, (a) shows that the plasma electrons map out a curtate cycloid, with the ratio to the inner and outer radius given by the ratio of the maximum velocity to the phase velocity, $u_{\max} \leq 1$. At wave breaking ($u_{\max} = 1$) the motion is on a cycloid as in (b).

parametric solutions for the Eulerian velocity and electric fields are given by

$$\theta(\mathfrak{s}) = \mathfrak{s} + u_{\max} \sin \mathfrak{s} \tag{5.43a}$$

$$u(\mathfrak{s}) = u_{\max} \cos \mathfrak{s} \tag{5.43b}$$

$$\mathcal{E}(\mathfrak{s}) = u_{\max} \sin \mathfrak{s}. \tag{5.43c}$$

This parametric representation trivially satisfies (5.37):

$$(1+u)\frac{du}{d\theta} = (1+u)\frac{\frac{du}{d\mathfrak{s}}}{\frac{d\theta}{d\mathfrak{s}}} = (1+u_{\max}\cos\mathfrak{s})\,\frac{-u_{\max}\sin\mathfrak{s}}{1+u_{\max}\cos\mathfrak{s}} = -u_{\max}\sin\mathfrak{s} = -\mathcal{E}(\mathfrak{s})$$

$$(1+u)\frac{d\mathcal{E}}{d\theta} = (1+u)\frac{\frac{d\mathcal{E}}{d\mathfrak{s}}}{\frac{d\theta}{d\mathfrak{s}}} = (1+u_{\max}\cos\mathfrak{s})\,\frac{u_{\max}\cos\mathfrak{s}}{1+u_{\max}\cos\mathfrak{s}} = u_{\max}\cos\mathfrak{s} = u(\mathfrak{s}).$$

We note that parametric equations for the nonlinear Langmuir wave similar to these were discussed by [114], but this simple interpretation was not realized[3]. In this way, we have determined an exact, parametric set of equations giving the Eulerian velocity field $u(\theta)$ and electric field $\mathcal{E}(\theta)$ for the nonlinear, nonrelativistic plasma wave. Plotting the parametric equations (5.43) faithfully reproduce the nonlinear fields in Fig. 5.2.

[3]Their resulting equations were in terms of infinite sums, obtained using the Bessel-Anger equality. Further investigation is required to determine to what extent these are equivalent.

5.2.3 Canonical action in the nonlinear Langmuir wave potential

The phase of a particle in the weakly-driven plasma wave satisfies the equations of motion

$$\frac{d}{d\tau}\theta = \frac{\partial}{\partial p}\frac{p^2}{2}, \qquad \frac{d}{d\tau}p = \frac{\partial}{\partial \theta}\big[\phi(\theta,\tau) - \mathcal{V}(\tau)\sin\theta\big]. \tag{5.44}$$

The system of equations (5.44) can be obtained from the Hamiltonian

$$\mathcal{H}(p,\theta;\tau) = \frac{1}{2}p^2 - \phi(\theta,\tau) + \mathcal{V}(\tau)\sin\theta. \tag{5.45}$$

To make contact with the Lagrangian description discussed previously, we determine the period of the unperturbed ($\mathcal{V} \to 0$) Hamiltonian associated with the undriven Langmuir wave. The period is obtained from the canonical action J in the usual manner

$$\mathcal{T}(H) = \frac{2\pi}{\omega(H)} = 2\pi\frac{\partial J}{\partial H} = \frac{\partial}{\partial H}\oint d\theta\, p(\theta,H) = \oint d\theta \frac{1}{\sqrt{2\,[H+\phi(\theta)]}} \tag{5.46}$$

We use the parametric representation for the Eulerian fields (5.43) given in the previous section to calculate $\mathcal{T}(H)$. From the equation for the electric field (5.43c), the potential is

$$\begin{aligned} \frac{\partial\phi}{\partial\theta} = \frac{d\mathfrak{s}}{d\theta}\frac{d\phi}{d\mathfrak{s}} = \frac{1}{1+u_{\max}\cos\mathfrak{s}}\frac{d\phi}{d\mathfrak{s}} = -\mathcal{E}(\mathfrak{s}) = -u_{\max}\sin\mathfrak{s} \\ \Rightarrow\ \phi(\mathfrak{s}) = u_{\max}\cos\mathfrak{s} + \tfrac{1}{2}u_{\max}^2\cos^2\mathfrak{s} - \tfrac{1}{2}\big(1+u_{\max}^2\big)\,, \end{aligned} \tag{5.47}$$

where the constant term is added for future convenience. Furthermore,

$$\frac{d\theta}{d\mathfrak{s}} = 1 + u_{\max}\cos\mathfrak{s}, \tag{5.48}$$

and the period (5.46) is given by

$$\begin{aligned} \mathcal{T}(H) &= \oint d\theta \frac{1}{\sqrt{2\,[H+\phi(\theta)]}} = \oint d\mathfrak{s}\,\frac{d\theta}{d\mathfrak{s}}\frac{1}{\sqrt{2\,[H+\phi(\mathfrak{s})]}} \\ &= 2\int_0^\pi d\mathfrak{s}\,\frac{1+u_{\max}\cos\mathfrak{s}}{\sqrt{2\left[H - \frac{1}{2}(1+u_{\max}^2) + u_{\max}\cos\mathfrak{s} + \frac{1}{2}u_{\max}^2\cos^2\mathfrak{s}\right]}}\,. \end{aligned} \tag{5.49}$$

To calculate the integral (5.49), we change variables to $x \equiv \cos\mathfrak{s}$, and factor the term under the square root, obtaining

$$\mathcal{T}(H) = \frac{2}{u_{\max}} \int_{-1}^{1} dx \, \frac{1 + u_{\max} x}{\sqrt{2\left[(1-x)(x+1)(x-x_+)(x-x_-)\right]}}, \tag{5.50}$$

where the roots $x_\pm$ are defined as

$$x_\pm \equiv \frac{1}{u_{\max}} \left[-1 \pm \sqrt{2 + u_{\max}^2 - 2H} \right]. \tag{5.51}$$

The integral (5.50) can be evaulated analytically using Gradshteyn and Ryzhik [53, pp 242-3]:

$$\mathcal{T}(H, u_{\max}) = \frac{4}{\sqrt{(1-x_+)(-1-x_-)}} \left\{ \left(\tfrac{1}{u_{\max}} + x_- \right) \mathscr{K}(\beta) + (1 - x_-)\, \Pi(\alpha, \beta) \right\}, \tag{5.52}$$

with

$$\beta \equiv \sqrt{\frac{2(x_+ - x_-)}{(1-x_+)(-1-x_-)}}, \qquad \alpha \equiv \frac{-2}{-1-x_-}, \tag{5.53}$$

and the elliptic integral of the third kind defined as usual by

$$\Pi(\alpha, \beta) \equiv \int_0^{\pi/2} dx \, \frac{1}{\left(1 + \alpha \sin^2 x\right) \sqrt{1 - \beta^2 \sin^2 x}}. \tag{5.54}$$

The cold plasma orbit is characterized by the energy $H = 1 + \frac{1}{2} u_{\max}^2$, with corresponding roots $x_+ = x_- = -1/u_{\max}$. For this family of orbits, we have

$$\beta = 0, \qquad \alpha = -\frac{2u_{\max}}{1 - u_{\max}}, \tag{5.55a}$$

$$\mathscr{K}(\beta) = \frac{\pi}{2}, \qquad \Pi(\alpha, \beta) = \sqrt{\frac{1 - u_{\max}}{1 + u_{\max}}}, \tag{5.55b}$$

and the period reduces to a constant:

$$\mathcal{T}(H) = 2\pi. \tag{5.56}$$

Thus, we have again explicitly demonstrated what was previously determined in the Lagrangian formalism: the cold plasma has a period (or frequency) that is independent of the energy. From the canonical equations

$$1 = \omega(H) \equiv \frac{d\Psi}{d\tau} = \frac{\partial \mathcal{H}}{\partial J}, \tag{5.57}$$

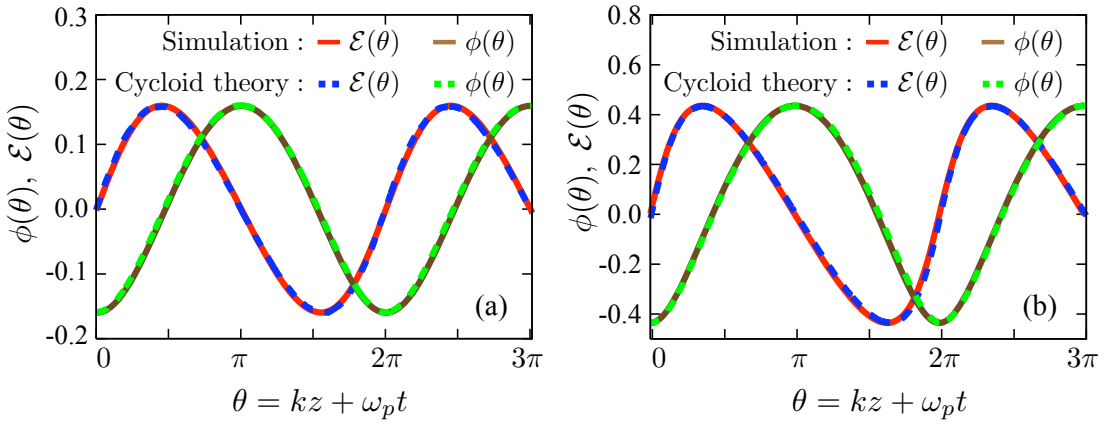

Figure 5.4: Comparison of the cold cycloidic electric field (5.43c) and electrostatic potential (5.47) to the simulation results of a slowly driven warm plasma which are taken from the particle code of Ch. 2. (a) shows a plasma with $k\lambda_D = 0.3$ and $\phi_1 \approx 0.15$, while (b) has $k\lambda_D = 0.1$ and $\phi_1 \approx 0.45$. The differences in both cases are too small to see here, of order a few percent.

we see that for this orbit $\mathcal{H} = J$, and changing the energy of the orbit requires a commensurate change in the action. Although this may appear to be a very specific finding, in Fig. 5.4 we compare the cold electrostatic potential and electric field with that measured in the driven simulation examples of Ch. 2. As shown in Fig. 5.4, the cold electrostatic fields closely approximate those of a warm plasma. This indicates that the warm plasma also has a (dynamically evolving) orbit for which the action is directly proportional to the energy, namely, the orbit whose energy is $H = 1 + \frac{1}{2}u_{\max}^2$. While this orbit does not necessarily correspond to that of the warm fluid velocity, its presence indicates that the distribution action changes under slow evolution, as found in Ch. 2.

Chapter 6

Conclusions and outlook

The central results of this thesis concerned the nonlinear, BGK-type distribution function describing weakly-driven Langmuir wave, and its application to devising a reduced model of kinetic effects in Raman scatter: the so-called extended three-wave model of Raman backscatter. We showed that the distribution function of a weakly-driven plasma is approximately invariant in the action-angle plane, but with small translations in J to self-consistently support the electrostatic potential. We then calculated both the nonlinear frequency and the incoherent energy associated with the particle phase-mixing in the wave, and used these to model a dynamic frequency and damping of the Langmuir wave appropriate for an envelope model of the Langmuir wave. Finally, we presented some novel aspects of one-dimensional warm fluid models and Langmuir waves.

There remain several questions and extensions of this work for future study. We suggest some here, starting with the more straightforward extensions and proceeding with more speculative applications.

The distribution as the wave shrinks: While we have indicated how the distribution evolves as the Langmuir wave decreases in amplitude, we have not performed a careful study and have only included its effect in the extended three wave model in a very rudimentary manner. Therefore, while it should be rather straightforward, a more

detailed analysis of this effect is warranted.

Collisional effects: Collisions lead to diffusion in velocity-space that will tend to destroy the BGK-type nonlinear distribution function and return the plasma to a Maxwellian equilibrium. In this way, a competition will arise between the formation of the nonlinear wave and the relaxation of the distribution to equilibrium. This in turn will lead to heating of the plasma, modifying the distribution further. We think this could lead to a rich interplay of additional physics that might nonetheless be tractable to further analysis.

Trapped particle instability: The oscillations of the trapped particles in the electrostatic well can give rise to the growth of side-bands whose frequency is basically $\omega_p \pm \omega_B$, with ω_B the bounce frequency in the wave. This instability leads to coalescence of neighboring phase-space buckets and a break-up of the plasma wave. On the one hand, this is yet another competing mechanism for Raman scatter saturation as proposed in Ref. [70], whose relative import must be compared with the effects discussed in this thesis. On the other hand, our description of the nonlinear BGK-type wave might form the basis for a more quantitative theory of the trapped particle instability. The present analytical predictions of the instability growth rate are based on a very crude model [26] for which the trapped particles are treated as one macro-particle[1]. As has been noted Ref. [115], experimental measurements of this instability in non-neutral plasmas were only in qualitative agreement with the predictions of [26]. The BGK-type waves presented in Ch. 2 could be used as an equilibrium distribution from which a perturbative analysis may yield a more quantitatively predictive theory.

Nonlinear saturation of instabilities: Our results may find applications in extending the work of Dewar regarding the saturation of general plasma instabilities through nonlinear phase mixing. This is a rather vague suggestion, based on the success in

[1]This was also the paper that first described this effect theoretically.

extending O'Neil's theory on nonlinear Landau damping and on the fact that in the small amplitude limit, we reproduced Dewar's predictions.

Hamiltonian analysis: To our mind, we have only laid out the Hamiltonian framework, and some work remains to expound its features. First, one might be able to make the Lagrangian-to-Eulerian coordinate transformation explicit, thereby illuminated to what extent this might be generalizable. Further, there is a cold relativistic Hamiltonian formulation, and some indications that Eulerian Hamiltonians can be generalized to include relativistic effects. We speculate there may be a warm fluid Hamiltonian in Eulerian coordinates that is fully relativistic.

Relativistic plasma waves: There may be analogs of the nonlinear distribution including relativity that may have relevance to the large amplitude, high phase-velocity waves used to accelerate particles. In this case, they may be useful to illuminate some aspects of particle self-trapping, dark current, and wave-breaking in these plasma-based acceleration structures.

Nonlinear Landau damping as a "critical phenomenon": There have been a number of fairly recent papers [88, 89, 90, 91] discussing the possibility of describing nonlinear Landau damping as a critical phenomenon. In this case, the critical parameter is the initial electric field: if the electrostatic field begins below some critical value Landau damping prevails and the asymptotic electric field vanishes, while if it above this parameter the field attains some final, steady state value. We speculate that the asymptotic, BGK-type distribution and its associated phase-mixed energy may provide some additional insight into this subject.

Appendix A

"Adiabatic" separatrix crossing

In this appendix we summarize and clarify the work by various authors [46, 47, 48, 116, 117, 118] on the slow crossing of separatrices, collecting various findings in a (hopefully) more transparent manner and, in some cases, completing and correcting some results. In style of presentation, we follow the recent work of Chow and Young [116], but use some ideas and results from the first publication of general separatrix crossings given by Neishatdt [46] and, independently and at the same time, by Cary, Escande, and Tennyson [47, 117]. Similar results and findings have also been published by Hannay [48], and Henrard [118]; the first work on slow separatrix crossing (for the symmetric case) was by Timofeev [45].

First, we present how near-separatrix motion can be analytically described in slowly-varying systems. We then use this description (referred to in [41] as neo-adiabatic motion) to calculate the change in the action of a particle as it slowly approaches, crosses, and finally retreats from a separatrix. Furthermore, we will include some results regarding its phase, for which there have been some discrepancy (between, for example, the paper of Cary and Skodje [40] and that of Elskens and Escande [41]). Finally, we apply these results to the slowly-varying pendulum, and discuss how this relates to particles being trapped in a slowly-varying Langmuir wave (our focus in Chapters 2 and 3).

The style of this appendix is comprehensive: while many of the results have been

published elsewhere, we felt a careful collection of the details involved in these calculations might be of general use. Those readers interested in the physics without getting bogged down in various manipulations might do well to basically skip sections A.3.3 through A.3.5. The central results of relevance to slow crossing in symmetric Hamiltonians (i.e., the case for particles being trapped in Langmuir waves) are given in Eqs. (A.103) and by Fig A.3.

A.1 Slow separatrix crossing: an introduction

Our discussion centers on a non-autonomous, one degree of freedom Hamiltonian system. We parametrize the time dependence with the order one parameter λ, setting $\lambda \equiv \varepsilon t$ for some small ε such that $0 \leq \varepsilon \ll 1$. Thus, the dynamical system is described by the Hamiltonian function $\mathcal{H}(p, q; \lambda)$, and the equations of motion are given by

$$\frac{d}{dt}q \equiv \dot{q} = \frac{\partial \mathcal{H}}{\partial p} \qquad \frac{d}{dt}p \equiv \dot{p} = -\frac{\partial \mathcal{H}}{\partial q} \qquad \frac{d}{dt}\mathcal{H} \equiv \dot{\mathcal{H}} = \epsilon \frac{\partial \mathcal{H}}{\partial \lambda} \tag{A.1}$$

Although our presentation owes much to [46, 47, 116], this Appendix will consider a general Hamiltonian with a "cat-eye" phase portrait as shown in Fig. A.1, rather than the typical figure-eight separatrix. While the resulting phase spaces are topologically equivalent (with our "trapped region" corresponding to that outside of the figure eight separatrices), our choice is more directly relevant for the trapping calculations of the Langmuir wave discussed in Ch. 2

To further simplify our discussion, we choose a specific realization of separatrix crossing, from which generalized results are easily obtainable. Much like the bulk of particles in the Langmuir wave of previous chapters, we assume that trajectories begin above the separatrices in region a of Fig. A.1[1], and that the separatrices slowly increase in size, such that eventually the separatrix intersects the initial, unperturbed orbit. When this happens, the period logarithmically diverges and traditional adiabatic theory breaks down, so that "near-separatrix" or "neo-adiabatic" motion must be considered. The basic physics

[1] This is an unfortunate change in notation from the previous chapters, but due to other numerical sub- and superscripts introduced here, we feel that it is unavoidable.

of approximating the motion when traditional adiabatic theory breaks down is contained in the following two statements:

1. The motion near the x-point is described by a hyperbolic Hamiltonian system with linear equations of motion.

2. The motion outside of the linearized region near the x-point approximately proceeds along the separatrix.

In what follows, we quote a few rigorous proofs relevant to the previous two statements. We then use these results to determine the action evolution and the asymptotic distribution in canonical angle (assuming that it is initially uniform) as one nears and crosses a separatrix. We have found the analysis and derivation given by Chow and Young [116] to be pedagogically appealing, although their actual results are not completely correct nor generalizable. Nevertheless, we keep our presentation much in their spirit, and explain how this work relates to the physics literature [40, 41, 46, 47, 48], and clear up a few discrepancies therein.

A.1.1 Near-separatrix motion in the autonomous system

We begin by applying the formalism of near-separatrix motion to the autonomous ($\varepsilon = 0$) system. In this case, of course, the system is integrable and λ is merely a constant parameterizing the system; this presentation serves primarily as an introduction to our notation. We take as convention that the energy is negative between the separatrices and positive outside, such that the energy increases as the orbits explore larger regions of phase space. In some small neighborhood of the hyperbolic equilibrium of Fig A.1, we can describe the dynamics as a linear system in the usual way. We align the coordinate axes along the stable and unstable directions: the y-axis along the unstable eigenvector with eigenvalue $+\mu(\lambda)$, and the x-axis along the stable eigenvector with eigenvalue $-\mu(\lambda)$. Using this construction, there exists a canonical transformation $\mathcal{H}(p, q; \lambda) \rightarrow h(x, y; \lambda)$

such that the Hamiltonian is given locally about the x-point by

$$h(x, y; \lambda) = \mu(\lambda) xy, \tag{A.2}$$

with linearized equations of motion

$$\dot{y} = \frac{\partial h}{\partial x} = \mu y \qquad\qquad \dot{x} = -\frac{\partial h}{\partial y} = -\mu x. \tag{A.3}$$

Within this locally linear neighborhood, we make the following convenient construction. First, we inscribe the square $\mathscr{D}$ as shown in Fig A.1, within which the linear equations (A.3) hold. The boundary of $\mathscr{D}$, denoted Σ, is given by

$$\Sigma : \left\{ \left(y = \pm d,\, |x| \leq d\right) \cup \left(x = \pm d,\, |y| \leq d\right) \right\}. \tag{A.4}$$

The absolute value of the energy at the corners of the square is

$$H \equiv \max_{\mathscr{D}} |h| = \mu d^2. \tag{A.5}$$

Inside $\mathscr{D}$, the dynamics is simple hyperbolic motion. The trajectories join adjacent segments of the boundary Σ along hyperbolae of constant h. For each trajectory there is a point of closest approach, defined as the point along the flow whose Euclidean distance to the x-point is a minimum [in terms of (x, y)]. Using the equations of motion (A.3), one can easily show that the set of points of closest approach form the lines $|x| = |y|$, and are represented as the dotted lines in Fig A.1 labeled $\mathcal{C}$; these lines are defined via

$$\mathcal{C} : \left\{ \left(x = y,\, \mu x^2 \leq H\right) \cup \left(x = -y,\, \mu x^2 \leq H\right) \right\}. \tag{A.6}$$

Armed with this construction (the linearized region $\mathscr{D}$ with boundary Σ and the lines of closest approach $\mathcal{C}$), we proceed to describe the dynamics of the trajectories near the separatrix. Inside the region $\mathscr{D}$, the physics we require is captured by two maps induced by the flow: the map from the boundary Σ to the line of closest approach $\mathcal{C}$, and the subsequent map from $\mathcal{C}$ to Σ. Since energy is conserved by the linearized system, these maps are functions of the single parameter h, denoted by

$$L_{\Sigma\to\mathcal{C}}(h) : \Sigma \to \mathcal{C} \text{ at constant } h \qquad L_{\mathcal{C}\to\Sigma}(h) : \mathcal{C} \to \Sigma \text{ at constant } h. \tag{A.7}$$

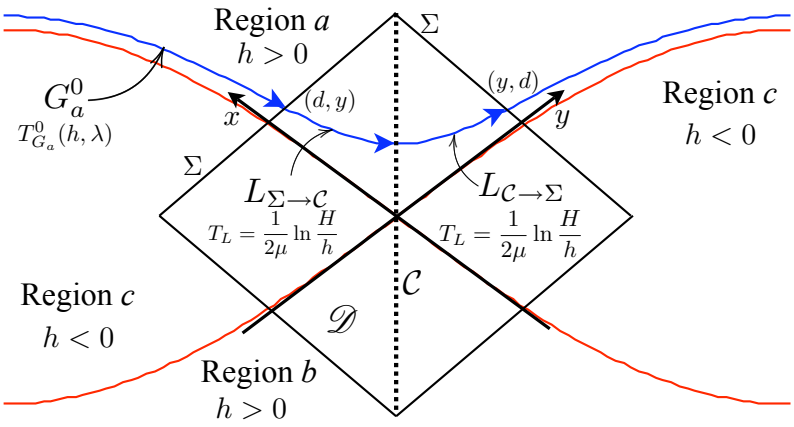

Figure A.1: Autonomous dynamics near a "cat-eye" (pendulum-like) separatrix. L maps points through the linearized region $\mathscr{D}$, while the unperturbed global map G_a^0 maps points between the boundaries Σ about the separatrix.

As an example, in Fig A.1, the map $L_{\Sigma\to\mathcal{C}}(h)$ takes the point (d,y) to the point $\left(\sqrt{dy},\sqrt{dy}\right)$, the energy being $h=\mu y d$ at both points. Similarly, $L_{\mathcal{C}\to\Sigma}(h)$ maps the point $\left(\sqrt{dy},\sqrt{dy}\right)$ to (y,d). Another property of the linear maps L that we require is the time it takes the flow to be mapped according to (A.7). This can easily be determined by integrating the equations of motion (A.3) for the transition $(d,y)\mapsto\left(\sqrt{dy},\sqrt{dy}\right)$; due to symmetry, the other transit times will be equal. Integrating the hyperbolic equations of motion, we find that the period for the maps L describing the linearized motion (A.7) are both

$$T_L(h)=\frac{1}{\mu}\ln\sqrt{\frac{d}{y}}=\frac{1}{2\mu}\ln\frac{\mu d^2}{\mu dy}=\frac{1}{2\mu}\ln\frac{H}{|h|}. \tag{A.8}$$

At this stage there is no apparent reason not to concatenate the linear maps L into one mapping amongst the boundaries $\Sigma\to\Sigma$ (indeed, this is done by [116]). However, as tacitly recognized in the physics literature [46, 47], defining the maps between the points of closest approach is the simplest way in which to include the order ε correction to the action near the separatrix. This correction is crucial for deriving consistent results.

Outside of the region $\mathscr{D}$, the flow proceeds close to the separatrix. In this case, we content ourselves with the mapping amongst the boundaries Σ. For $\varepsilon=0$, conservation of energy again implies that points along one boundary are mapped to the next at an

identical distance from the axes. In Fig. A.1, a point beginning at (d, y) is mapped to the point (y, d) by the flow. Since energy is not conserved in the non-autonomous system, we define the unperturbed global maps G_r^0, with the superscript indicating that $\varepsilon = 0$, and the subscript denoting the region in which the orbit lives, to be given by

$$G_a^0 : (x, d) \mapsto (d, x) \qquad\qquad G_b^0 : (-x, -d) \mapsto (-d, -x). \tag{A.9}$$

The period of a global circuit of the separatrix will depend on the particular form of the Hamiltonian $\mathcal{H}(p, q; \lambda)$. For now, we will use the function $T_{G_r}(h, \lambda)$ to denote the transit time required for the trajectories to map a point about the separatrix according to G_r^0. Later, we will relate the function T_{G_r} to quantities involving the unperturbed Hamiltonian.

Next, we construct the mappings that describe one closed orbit in phase space, i.e., those that increase the canonical angle by 2π. We take these revolution maps R to start and end on the line of closest approach $\mathcal{C}$, the form of which differ depending on the sign of the energy h. For $h > 0$, the orbit is either above or below the separatrices; for a circuit in region a or b the map is formed by composing the maps L and G_r^0 in the following way

$$R_a^0(h) : L_{\Sigma\to\mathcal{C}}(h) \circ G_a^0(h) \circ L_{\mathcal{C}\to\Sigma}(h) \quad r = a,\, b \tag{A.10a}$$

$$R_b^0(h) : L_{\Sigma\to\mathcal{C}}(h) \circ G_b^0(h) \circ L_{\mathcal{C}\to\Sigma}(h). \tag{A.10b}$$

When $h < 0$, the orbit traces along both separatrices, but may start by first revolving near region a or b depending upon which half of $\mathcal{C}$ it originated. Thus, these maps are given by the following compositions of the maps from (A.10)

$$R_{ab}^0(h) : R_b^0(h) \circ R_a^0(h) \qquad\qquad R_{ba}^0(h) : R_a^0(h) \circ R_b^0(h). \tag{A.11}$$

Note that the map $R_{ab}(h)$ first traces the orbit along the separatrix between region c and a, and then between region c and b, while the opposite is true for the map $R_{ba}(h)$. Later, we will refer to the maps depicting one nearly (for $\varepsilon \neq 0$) periodic orbit, (A.10) and (A.11), as one revolution or step. Using the periods T_L and T_{G_r} of the maps composing (A.10)

and (A.11), we see that the period $T(h)$ of the motion is given by

$$T_{R_r}(h>0) = T_{G_r} + \frac{1}{\mu}\ln\frac{H}{|h|} \tag{A.12a}$$

$$T_R(h<0) = T_{G_a} + T_{G_b} + \frac{2}{\mu}\ln\frac{H}{|h|}. \tag{A.12b}$$

Finally, we calculate the action $J(h)$ associated with a near-separatrix orbit of energy h. To begin, we use the identity

$$\frac{dJ}{dh} = \frac{dJ}{dt}\frac{dt}{dh} = \frac{\partial h}{\partial\theta}\left(\frac{\partial h}{\partial t}\right)^{-1} = \left(\frac{d\theta}{dt}\right)^{-1} = \frac{1}{\omega(h)} = \frac{1}{2\pi}T(h), \tag{A.13}$$

from which we obtain a differential equation for the action $J(h)$:

$$\frac{dJ}{dh} = \frac{1}{2\pi}T(h). \tag{A.14}$$

Using the period of the unperturbed system (A.12), we can easily integrate the differential equation $(A.14)$ from the separatrix to an orbit of energy h. For $h>0$, we have

$$\int_{Y_r}^{I} dJ' = \frac{1}{2\pi}\int_0^h dh'\, T_{R_r}(h') \approx \frac{1}{2\pi}\left[hT_{G_r} + \frac{h}{\mu}\left(1+\ln\frac{H}{|h|}\right)\right]. \tag{A.15}$$

The case with $h<0$ is similarly derived. Rearranging the expression above, we find that the action associated with an orbit of energy h of near-separatrix motion is:

$$J(h>0) = Y_r(\lambda) + \frac{h}{2\pi}\left[T_{G_r} + \frac{1}{\mu}\left(1+\ln\frac{H}{|h|}\right)\right], \qquad r = a \text{ or } b \tag{A.16a}$$

$$J(h<0) = Y_a(\lambda) + Y_b(\lambda) + \frac{h}{2\pi}\left[T_{G_a} + T_{G_b} + \frac{2}{\mu}\left(1+\ln\frac{H}{|h|}\right)\right] \tag{A.16b}$$

A.2 Near-separatrix motion in the drifting system

Having introduced our notation and some aspects of near-separatrix motion using the autonomous system, we now permit $\mathcal{H}(p,q;\lambda)$ to be a slow function of time, assuming that $\dot{\lambda} = \varepsilon$ for some small but non-zero ε. In this case, one might expect the motion to be similarly separable into a linearized system near the hyperbolic equilibrium and near-separatrix motion far from the x-point, and this is indeed the case. Although neither the

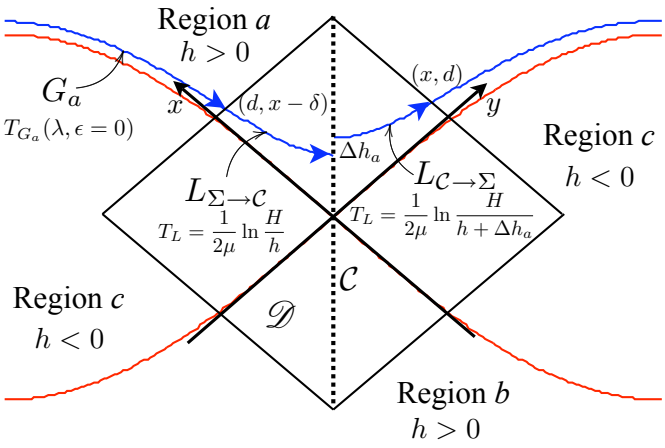

Figure A.2: Diagram of near-separatrix motion in the drifting ($\varepsilon \neq 0$) system. The linear maps L give the transit through region $\mathscr{D}$ at constant h, while the global map G_a about the separatrix changes the energy by the amount Δh_a.

stable and unstable manifolds nor the locally linear coordinates in the perturbed system will, in general, be identical to those for which $\varepsilon = 0$, linear equations of motion similar to (A.3) still hold inside an analogous region $\mathscr{D}$, and locally linear maps L with identical properties can be constructed, as indicated in Fig A.2. Since the energy is no longer conserved outside of the region $\mathscr{D}$, however, motion along the separatrix will not return to $\mathscr{D}$ with the same energy. Thus, the distance from the axes will change due to a revolution along the separatrix, as indicated by the offset δ in Fig A.2, and the perturbed maps G_r will have different properties than the unperturbed G_r^0.

First, we address the motion near the x-point, where we expect locally linear and hyperbolic motion. To be more rigorous, we include a statement of a theorem proved by Chow and Young [116] (similar results were also derived in [41, 47, 118]):

Theorem 1 *Suppose that for each λ of the unperturbed ($\varepsilon = 0$) Hamiltonian $\mathcal{H}(p, q; \lambda)$ there exists hyperbolic equilibria at the x-points $(p^*_\lambda, q^*_\lambda)$ with associated eigenvalues $\pm\mu(\lambda)$. Then, there exists a finite neighborhood about the perturbed x-points $(p^*_\lambda, q^*_\lambda)$ for which a smooth canonical coordinate change and reparametrization of time puts $\mathcal{H}$ into the locally hyperbolic form: $\mathcal{H}(p, q; \lambda) \to h(x, y; \lambda) = \mu(\lambda)xy$.*

While this theorem does not, in and of itself, indicate how one might perform the required transformation[2], it does tell us that we can apply the results for the autonomous system to the time-dependent case near the hyperbolic equilibrium. Thus, in the region $\mathscr{D}$, the expressions for the locally linear maps L and the periods T_L are:

$$L_{\Sigma\to\mathcal{C}}(h):\Sigma\to\mathcal{C} \text{ at constant } h \qquad T_L(h)=\frac{1}{2\mu}\ln\frac{H}{|h|} \tag{A.17a}$$

$$L_{\mathcal{C}\to\Sigma}(h):\mathcal{C}\to\Sigma \text{ at constant } h \qquad T_L(h)=\frac{1}{2\mu}\ln\frac{H}{|h|}. \tag{A.17b}$$

On the other hand, the motion away from the hyperbolic region $\mathscr{D}$ changes for the drifting Hamiltonian, as does the form of the maps G_r between boundaries. Since the energy is no longer conserved, the maps G_r will no longer close upon themselves. Instead, G_r will depend, in general, on ε and λ. Likewise, the periods T_{G_r} for the motion along the separatrix will also become functions of ε and λ. Thus, the maps and the transit times for the global motion take the form

$$G_a:(d,y)\mapsto(y-\delta(\varepsilon,\lambda),\,d) \qquad T_{G_a}=T_{G_a}(h,\varepsilon,\lambda) \tag{A.18a}$$

$$G_b:(-d,-y)\mapsto(-y+\delta(\varepsilon,\lambda),\,-d) \qquad T_{G_b}=T_{G_b}(h,\varepsilon,\lambda). \tag{A.18b}$$

As it now stands, the results obtained for the autonomous system do not appear to be directly applicable. Nevertheless, it was shown in [46, 47, 116] that the mapping G_r and the functions T_{G_r} in (A.18) can be considered constant to lowest order in ε during the separatrix crossing. We summarize the series of proofs in [116] with the theorem:

Theorem 2 *Suppose that the action of the separatrix is given by Y, with slow variation given by $\dot{Y}=\varepsilon\frac{d}{d\lambda}Y$. Then, the following limit holds:*

$$\lim_{\varepsilon\to0}\frac{\delta(\varepsilon,\lambda)}{\varepsilon}=-\frac{2\pi}{\mu d}\frac{dY}{d\lambda} \tag{A.19}$$

Furthermore, in the limit $\varepsilon\to0$, the size of the domain $\mathscr{D}$ vanishes, so that in this limit, the functions $\delta(\varepsilon,\lambda)$, $\frac{d}{d\lambda}Y$, and $T_G(h,\lambda,\varepsilon)$ can be considered constant during the approach, cross, and departure from the separatrix.

[2]Henrard [118] describes how such a transformation can be affected in a general system. He finds that the error terms in the transformation $\mathcal{H}\to h$ scale as $|h|^2\ll|h|$; in this work we will not concern ourselves with error analysis, concentrating instead on the lowest order results.

The boundaries of the global return maps G_r are identified with the Hamiltonian $h = \mu x d$. In this way, a change in the coordinate x by δ due to the map G has an associated change in the energy given by $\Delta h = -\mu d\delta$. Thus, we see that in the limit $\varepsilon \to 0$, the global return maps G_r result in a change in energy given by

$$G_a : \Sigma \to \Sigma \text{ such that } \Delta h \equiv \Delta h_a = -2\pi\varepsilon \frac{dY_a}{d\lambda} \tag{A.20a}$$

$$G_b : \Sigma \to \Sigma \text{ such that } \Delta h \equiv \Delta h_b = -2\pi\varepsilon \frac{dY_b}{d\lambda}. \tag{A.20b}$$

Note that the sign in (A.20) is such that for separatrices increasing in size, the energy decreases. Thus, orbits initially rotating in region a, for example, will slowly lose energy until they are trapped and librate in region c. Furthermore, the result (A.20) corresponds to the energy change given by Eq. (4) from [46]. It also identical to Eq. (45a) from [47], while the constancy of the parameters agrees with Eq. (56)[3].

A.2.1 Revolution mappings in the drifting system

As the separatrix changes size, we assume that trajectories will eventually enter the region $\mathscr{D}$ near the corner with energy $H \geq |h| > H - |\Delta h|$. The near-separatrix motion proceeds via a series of revolutions about the separatrix. Following previous authors, we will refer to these as steps, with each step starting and ending on the line of closest approach $\mathcal{C}$ (the dotted lines in Fig. A.2 where $|x| = |y|$). In this way, we have four different steps, corresponding to the simple generalizations of (A.10) and (A.11):

$$R_a(h>0): \quad L_{\Sigma\to\mathcal{C}}(h+\Delta h_a) \circ G_a(h) \circ L_{\mathcal{C}\to\Sigma}(h): \quad \mathcal{C}\big[h\big] \mapsto \mathcal{C}\big[h+\Delta h_a\big] \tag{A.21a}$$

$$R_b(h>0): \quad L_{\Sigma\to\mathcal{C}}(h+\Delta h_b) \circ G_b(h) \circ L_{\mathcal{C}\to\Sigma}(h): \quad \mathcal{C}\big[h\big] \mapsto \mathcal{C}\big[h+\Delta h_b\big] \tag{A.21b}$$

$$R_{ab}(h<0): \quad R_b(h+\Delta h_a) \circ R_a(h): \quad \mathcal{C}\big[h\big] \mapsto \mathcal{C}\big[h+\Delta h_a+\Delta h_b\big] \tag{A.21c}$$

$$R_{ba}(h<0): \quad R_a(h+\Delta h_b) \circ R_b(h): \quad \mathcal{C}\big[h\big] \mapsto \mathcal{C}\big[h+\Delta h_a+\Delta h_b\big]. \tag{A.21d}$$

Note that the change in energy Δh_r resulting from the global map G_r is reflected in the definitions (A.21). Furthermore, (A.21) represents an important departure from the work

[3] In [47] Cary *et al.* express everything in terms of areas rather than actions; some later work by the same authors change this convention.

of Chow and Young [116]. They defined a step as the map between the boundaries Σ; for example, in our notation, they would have $R_a(h)$ begin with the map $L_{\Sigma\to\mathcal{C}}(h)$. As alluded to earlier this difference (reflected in the physics literature [46, 47]), while subtle, is important to obtain consistent [to $O(\varepsilon)$] results. Finally, we include the transit time of the revolution map $R_r(h)$. This is simply a sum of the composing maps from (A.21):

$$T_{R_r} = T_L(h) + T_{G_r} + T_L(h+\Delta h_r) = \frac{1}{2\mu}\ln\frac{H}{|h|} + T_{G_r} + \frac{1}{2\mu}\ln\frac{H}{|h+\Delta h_r|}. \tag{A.22a}$$

$$T_{R_{ab}} = \frac{1}{2\mu}\ln\frac{H}{|h|} + T_{G_a} + \frac{1}{\mu}\ln\frac{H}{|h+\Delta h_a|} + T_{G_b} + \frac{1}{2\mu}\ln\frac{H}{|h+\Delta h_a+\Delta h_b|} \tag{A.22b}$$

$$T_{R_{ba}} = \frac{1}{2\mu}\ln\frac{H}{|h|} + T_{G_b} + \frac{1}{\mu}\ln\frac{H}{|h+\Delta h_b|} + T_{G_a} + \frac{1}{2\mu}\ln\frac{H}{|h+\Delta h_b+\Delta h_a|} \tag{A.22c}$$

A.2.2 The adiabatic invariant through order ε

We will find that as a trajectory approaches, crosses, and departs from a separatrix, there in an induced shift of the action by an amount $O(\varepsilon)$. In order to be consistent, we must therefore calculate the adiabatic invariant through order ε, i.e., we must find the lowest order correction to the action. By neglecting such a correction, the work of Chow and Young [116] is not directly applicable to general Hamiltonians, while their expressions for the change in action due to either the approach or the departure are incorrect even for symmetric Hamiltonians. In this case, they find that the action changes by an amount $\sim \ln N$, where N is the number of steps, while we find no such dependence[4]. This discrepancy arises because the authors in Ref. [116] calculate the change in the action between successive intersections of the boundary Σ, rather than the line of closest approach $\mathcal{C}$ as we (and the works [46, 47]) do. While in the symmetric Hamiltonian the $O(\varepsilon)$ correction to J vanishes along $\mathcal{C}$, it does make a contribution along the boundary Σ that is neglected in [116].

To calculate the adiabatic invariant through first order in ε, we use the results of Cary, Escande, and Tennyson [47] who, in their Appendix A, show how the first order correction is related to the unperturbed Hamiltonian. Rather than repeat their arguments, we just

[4]The terms $\sim \ln N$ from the approach and departure cancel in [116], so that their expression for the total change in action is correct.

quote the result, with the appropriate factors of 2π to change their areas to actions; the improved invariant $\mathcal{J}$ at the point of closest approach $\mathcal{C}$ is given by

$$\mathcal{J} = J + \varepsilon\pi \frac{\partial J}{\partial h}\frac{\partial J}{\partial \lambda} - \frac{\varepsilon}{2\pi}\oint dq\ \frac{\partial p}{\partial h}(q,h;\lambda)\int_{q_\mathcal{C}}^{q} dq'\ \frac{\partial p}{\partial \lambda}(q',h;\lambda), \tag{A.23}$$

where the integrals proceed along the unperturbed flow, the lower limit $q_\mathcal{C}$ has been chosen to be the coordinate along the line of closest approach, and the momentum is obtained by solving the unperturbed Hamiltonian $\mathcal{H}(p,q;\lambda) = E_Y + h$, with E_Y equal to the energy of the separatrix. The expression (A.23) can be simplified according to whether the trajectory is untrapped/rotating ($h > 0$) or trapped/librating ($h < 0$). For this calculation, we will find it convenient to introduce the coordinate q_s, defined to be the "half-way point" such that the action mapped out by the unperturbed orbit between the point of closest approach $q_\mathcal{C}$ and q_s is one-half the action of the unperturbed orbit:

$$\frac{1}{2\pi}\int_{q_\mathcal{C}}^{q_s} dq\ p = \frac{1}{2\pi}\int_{q_s}^{q_\mathcal{C}} dq\ p = \frac{1}{4\pi}\oint dq\ p \equiv \frac{1}{2}J(h,\lambda). \tag{A.24}$$

Using this definition, the expression for $\mathcal{J}$ in (A.23) can be simplified by breaking up the loop integral into two "halves" as

$$\frac{1}{2\pi}\oint dq\ \frac{\partial p}{\partial h}\int_{q_\mathcal{C}}^{q} dq'\frac{\partial p}{\partial \lambda} = \frac{1}{2\pi}\int_{q_\mathcal{C}}^{q_s} dq\ \frac{\partial p}{\partial h}\int_{q_\mathcal{C}}^{q} dq'\ \frac{\partial p}{\partial \lambda}\ + \frac{1}{2\pi}\int_{q_s}^{q_\mathcal{C}} dq\ \frac{\partial p}{\partial h}\int_{q_\mathcal{C}}^{q} dq'\ \frac{\partial p}{\partial \lambda}. \tag{A.25}$$

The second integral in (A.25) can be simplified outside the separatrices by noting that

$$\begin{aligned}\frac{1}{2\pi}\int_{q_s}^{q_\mathcal{C}} dq\ \frac{\partial p}{\partial h}\int_{q_\mathcal{C}}^{q} dq'\ \frac{\partial p}{\partial \lambda} &= \frac{1}{2\pi}\int_{q_s}^{q_\mathcal{C}} dq\ \frac{\partial p}{\partial h}\int_{q_\mathcal{C}}^{q_\mathcal{C}} dq'\ \frac{\partial p}{\partial \lambda}\ - \frac{1}{2\pi}\int_{q_s}^{q_\mathcal{C}} dq\ \frac{\partial p}{\partial h}\int_{q}^{q_\mathcal{C}} dq'\ \frac{\partial p}{\partial \lambda} \\ &\equiv \pi\frac{\partial J}{\partial h}\frac{\partial J}{\partial \lambda} - \frac{1}{2\pi}\int_{q_s}^{q_\mathcal{C}} dq\ \frac{\partial p}{\partial h}\int_{q}^{q_\mathcal{C}} dq'\ \frac{\partial p}{\partial \lambda},\end{aligned} \tag{A.26}$$

where we used the definition of q_s (A.24) and J. With the simplifications (A.25) and (A.26), the expression for the improved adiabatic invariant becomes

$$\mathcal{J} = J - \frac{\varepsilon}{2\pi}\int_{q_\mathcal{C}}^{q_s} dq\ \frac{\partial p}{\partial h}\int_{q_\mathcal{C}}^{q} dq'\ \frac{\partial p}{\partial \lambda}\ + \frac{\varepsilon}{2\pi}\int_{q_s}^{q_\mathcal{C}} dq\ \frac{\partial p}{\partial h}\int_{q}^{q_\mathcal{C}} dq'\ \frac{\partial p}{\partial \lambda}. \tag{A.27}$$

We see that the first integral in (A.27) is over the first "half" of the orbit, while reversing the limits of the second integral yields the same integration, only over the second orbit "half." Thus, the correction to the action between the separatrices is given by a number that is non-zero only if some asymmetry causes the two integrals in (A.27) to be different. The final simplification can be made by setting $h = 0$ in the integrals in (A.27), which implies the integration proceeds along the separatrix, so that $q_{\mathcal{C}} = 0$. Cary *et al.* have shown that this introduces a small error of $O(h)$, consistent with Theorem 2. Thus, in regions a and b, the invariant can be written through $O(\varepsilon)$ as

$$r = a,\, b: \quad \mathcal{J}_r = J_r + \varepsilon D_r, \tag{A.28}$$

where D_r is a constant obtained by integrating along the flow:

$$\begin{aligned} D_r = &-\frac{1}{2\pi}\int_0^{q_r} dq\, \frac{\partial p}{\partial h}(q, h=0;\lambda) \int_0^{q} dq'\, \frac{\partial p}{\partial \lambda}(q', h=0;\lambda) \\ &+ \frac{1}{2\pi}\int_{q_r}^{0} dq\, \frac{\partial p}{\partial h}(q, h=0;\lambda) \int_{q}^{0} dq'\, \frac{\partial p}{\partial \lambda}(q', h=0;\lambda), \end{aligned} \tag{A.29}$$

In the trapped region c, the expression for the invariant is given by (A.23) with the action J_c being the sum along the two separatrices. Furthermore, we include the fact that region c has two points of closest approach $q_{\mathcal{C}}$ with subscripts 1 and 2, and assume for the present that the flow proceeds from $q_{\mathcal{C}_1} \to q_{\mathcal{C}_2}$ adjacent to region b, while the flow $q_{\mathcal{C}_2} \to q_{\mathcal{C}_1}$ is along region a. This will be what we require for a crossing from region a into region c. Between the separatrices, (A.23) is

$$\begin{aligned} \mathcal{J} = J_a + J_b + \varepsilon\pi &\left(\frac{\partial J_a}{\partial h} + \frac{\partial J_b}{\partial h}\right)\left(\frac{\partial J_a}{\partial \lambda} + \frac{\partial J_b}{\partial \lambda}\right) \\ &- \frac{\varepsilon}{2\pi}\oint dq\, \frac{\partial p}{\partial h}(q, h;\lambda) \int_{q_{\mathcal{C}_1}}^{q} dq'\, \frac{\partial p}{\partial \lambda}(q', h;\lambda). \end{aligned} \tag{A.30}$$

We simplify the integral in (A.30) by breaking it up over the two (upper and lower) halves. Remembering that the integral from $q_{\mathcal{C}_1} \to q_{\mathcal{C}_2}$ is along region b while $q_{\mathcal{C}_2} \to q_{\mathcal{C}_1}$ is along

region a, we have, suppressing the dependence of p on q, h and λ,

$$\oint dq\,\frac{\partial p}{\partial h}\int_{q_{c_1}}^{q} dq'\,\frac{\partial p}{\partial \lambda} = \int_{q_{c_1}}^{q_{c_2}} dq\,\frac{\partial p}{\partial h}\int_{q_{c_1}}^{q} dq'\,\frac{\partial p}{\partial \lambda} + \int_{q_{c_2}}^{q_{c_1}} dq\,\frac{\partial p}{\partial h}\int_{q_{c_1}}^{q} dq'\,\frac{\partial p}{\partial \lambda}$$
$$= \int_{q_{c_1}}^{q_{c_2}} dq\,\frac{\partial p}{\partial h}\int_{q_{c_1}}^{q} dq'\,\frac{\partial p}{\partial \lambda} + (2\pi)^2\frac{\partial J_a}{\partial h}\frac{\partial J_b}{\partial \lambda} + \int_{q_{c_2}}^{q_{c_1}} dq\,\frac{\partial p}{\partial h}\int_{q_{c_2}}^{q} dq'\,\frac{\partial p}{\partial \lambda}. \tag{A.31}$$

The integrals in (A.31) can be simplified in the same manner as was done for trajectories outside region c, resulting in the following expression for $\mathcal{J}$ in the trapped region

$$\mathcal{J}_c = J_a + J_b + \varepsilon\left[\pi\left(\frac{\partial J_b}{\partial h}\frac{\partial J_a}{\partial \lambda} - \frac{\partial J_a}{\partial h}\frac{\partial J_b}{\partial \lambda}\right) + D_a + D_b\right]. \tag{A.32}$$

The formula (A.32) can be further evaluated by using the expressions for the near separatrix actions (A.16). At lowest order, (A.16) yields the following:

$$\frac{\partial J_r}{\partial h} = \frac{1}{2\pi}\left[T_{G_r} + \frac{1}{\mu}\ln\frac{H}{|h|}\right] \qquad\qquad \frac{\partial J_r}{\partial \lambda} = \frac{dY_r}{d\lambda} \tag{A.33}$$

which can be inserted into (A.32). Collecting the results for the improved [to $O(\varepsilon)$] invariant both outside the separatrices [(A.28) and (A.29)], and between the separatrices [(A.32) and (A.33)], with the near-separatrix actions (A.16), we have

$$\mathcal{J}(h>0) = Y_r(\lambda) + \frac{h}{2\pi}\left[T_{G_r} + \frac{1}{\mu}\left(1+\ln\frac{H}{|h|}\right)\right] + \varepsilon D_r \tag{A.34a}$$

$$\mathcal{J}(h>0) = Y_a(\lambda) + Y_b(\lambda) + \frac{h}{2\pi}\left[T_{G_a} + T_{G_b} + \frac{2}{\mu}\left(1+\ln\frac{H}{|h|}\right)\right] + \frac{\varepsilon}{2\mu}\frac{dY_a}{d\lambda}\left[\mu T_{G_b} + \ln\frac{H}{|h|}\right] - \frac{\varepsilon}{2\mu}\frac{dY_b}{d\lambda}\left[\mu T_{G_a} + \ln\frac{H}{|h|}\right] + \varepsilon(D_a + D_b), \tag{A.34b}$$

with the constant D_r defined by the following integrals along the flow:

$$D_r = -\frac{1}{2\pi}\int_0^{q_r} dq\,\frac{\partial p}{\partial h}(q, h=0;\lambda)\int_0^{q} dq'\,\frac{\partial p}{\partial \lambda}(q', h=0;\lambda) + \frac{1}{2\pi}\int_{q_r}^{0} dq\,\frac{\partial p}{\partial h}(q, h=0;\lambda)\int_q^{0} dq'\,\frac{\partial p}{\partial \lambda}(q', h=0;\lambda). \tag{A.35}$$

These results are in agreement with those of Neishtadt [46], who parametrizes (A.34) with the letters a, b_i, and d_i, (corresponding to our quantities μ, T_{G_r}, and D_r, respectively).

A.2.3 Definitions and notation for the separatrix crossing

To analyze the approach and crossing of the separatrix, we take as initial conditions a particle with a given action $\mathcal{J} = \mathcal{J}_-$ and variable canonical angle Ψ before the trajectory enters the region $\mathscr{D}$. Once the energy $|h| \leq H$, the evolution proceeds according to the aforementioned near-separatrix motion. In this case, we track how the invariant $\mathcal{J}$ evolves as a trajectory successively intersects the line of closest approach $\mathcal{C}$. In other words, we calculate the change in action $\mathcal{J}$ from each step of the revolution map R_a (or R_b, R_{ab}, R_{ba}). Furthermore, we will (approximately) calculate the final phase of the particle.

According to (A.20), a trajectory experiences a change in energy equal to Δh_a after one revolution in region a. Thus, each orbit first crosses the line of closest approach $\mathcal{C}$ in $\mathscr{D}$ with energy $H - |\Delta h_a| \leq h < H$. Furthermore, we see that a set of trajectories whose initial energies span an interval of $|\Delta h_a|$ along $\mathcal{C}$ is mapped by R_a to an adjacent interval along $\mathcal{C}$, also of size Δh_a. For this reason, we will find it useful during the approach to separate the energy of a trajectory into its whole and fractional parts of Δh_a:

$$h_{-n} \equiv (n + \xi)\Delta h_a, \quad n \in \mathbb{Z}^+, \ \xi \in (0, 1], \tag{A.36}$$

and set the maximal energy to be an integral multiple of Δh_a

$$H \equiv (N + 1)\,|\Delta h_a|\,, \quad N \in \mathbb{Z} \gg 1. \tag{A.37}$$

From the definitions (A.36) and (A.37), we see that a trajectory approaching the separatrix first crosses $\mathcal{C}$ with energy given by $h_{-N} = -(N+\xi)\Delta h_a$. Furthermore, after N revolutions (corresponding to N steps of the map R_a), the set of first crossings with energies in the range given by h_{-N} will be mapped to the interval right near the separatrix: $|\Delta h_a| \geq |h_0| = \xi\,|\Delta h_a| > 0$. In the next step, these trajectories will cross; the specifics are described by the parameter $\xi \in (0, 1]$. For this reason, we refer to ξ as the *crossing parameter*. We will also see that the crossing parameter is related to the initial phase of the trajectory, and hence we refer to quantities that depend on ξ as phase-dependent.

In the spirit of the definition (A.36), we use subscripts of negative integers and zero to label quantities during the approach, while positive integral subscripts label steps of the departure. These all depend on the crossing parameter ξ [see, e.g., (A.36)]. When possible, however, we wish to express the various calculations in terms of ξ-independent (i.e., phase-independent) quantities. For this reason, we define the pseudo-crossing time t_x as the time when the action of the separatrix equals that of the initial trajectory. Another phase-independent quantity is the initial action $\mathcal{J}(t_-) = \mathcal{J}_-$, while we will show that the asymptotic action $\mathcal{J}_+$ at the "end" of the crossing depends on ξ. As some examples of the notation, we include:

$$t_x : Y_a(t_x) = J(t_-) = J_-$$

$$t_- < t_{-N} < t_{-(N-1)} < \cdots < t_{-1} < t_0 < t_x < t_1 < \cdots < t_N < t_+$$

$$h_n = h(t_n),\ \mathcal{J}_n = \mathcal{J}(h_n),\ \lambda_n = \varepsilon t_n, \quad \big\{n \in \mathbb{Z} : -N \le n \le N\big\}.$$

Note that quantities subscripted by integers depend on the crossing parameter, while J_-, $Y_a(t_x)$, and t_x do not. Further, for $n \in [1, N]$, after $N - n$ revolutions a trajectory with initial energy h_{-N} is mapped to one of energy h_{-n}:

$$\underbrace{R_a\big(h_{-(n-1)}\big) \circ R_a\big(h_{-(n-2)}\big) \circ \cdots \circ R_a\big(h_{-N}\big)}_{N-n \text{ times}} : \mathcal{C}\big[h_{-N}\big] \mapsto \mathcal{C}\big[h_{-n}\big]. \tag{A.38}$$

To simplify our derivation of the change in the adiabatic invariant, we separate the crossing into the approach to the separatrix, the crossing of the separatrix, and the departure from the separatrix. Thus, for the total change in the action $\Delta\mathcal{J}$, we have

$$\Delta\mathcal{J} \equiv \mathcal{J}_+ - \mathcal{J}_- = \underbrace{(\mathcal{J}_+ - \mathcal{J}_N)}_{\text{match final}} + \underbrace{(\mathcal{J}_N - \mathcal{J}_1)}_{\text{depart}} + \underbrace{(\mathcal{J}_1 - \mathcal{J}_0)}_{\text{cross}} + \underbrace{(\mathcal{J}_0 - \mathcal{J}_{-N})}_{\text{approach}} + \underbrace{(\mathcal{J}_{-N} - \mathcal{J}_-)}_{\text{match initial}}.$$

We will show that the first and last "matching" terms are negligible, while the approach and departure depend on ξ and are of order ε. The crossing term is also ξ-dependent, and is $O(\varepsilon)$ or, in the asymmetric case, $O(\varepsilon \ln \varepsilon)$. Finally, we will determine the degree to which an initially phase-mixed distribution remains phase-mixed. We do this by relating

the time required for the crossing to the angle; in analogy with the action, we determine

$$\Delta t \equiv t_N - t_- = \underbrace{(t_N - t_1)}_{\text{depart}} + \underbrace{(t_1 - t_0)}_{\text{cross}} + \underbrace{(t_0 - t_{-N})}_{\text{approach}} + \underbrace{(t_{-N} - t_-)}_{\text{initial}}.$$

We will see that the time difference determines, to zeroth order, the degree to which an initially uniform in canonical angle distribution of trajectories remains uniform in angle.

A.2.4 The period T_{G_r}, the maximal energy H, and previous work on slow crossing theory

To conclude the introductory remarks, we will make a few comments on the heretofore unspecified quantities: the global period T_G and the maximal energy H. While the physics literature makes some reference to T_G (these are the b_i parameters of Neishtadt [46], they are specified as an integral by Cary *et al.* [47]), no clear reference is made to the energy H. Furthermore, the number of steps N is either not clearly denoted (as in [46]) or taken to infinity (by [47]). In this section we express these quantities in terms of the unperturbed Hamiltonian $\mathcal{H}$, and then relate them to the various definitions in [46] and [47].

We express the number of steps N in terms of H by summing the changes in energy over the N steps of the approach and the one step of the crossing. Since we assume the parameters to be constant, summing (A.20) yields

$$2\pi\varepsilon \sum_{n=0}^{N} \left| \frac{dY_a}{d\lambda} \right| = 2\pi\varepsilon(N+1) \left| \frac{dY_a}{d\lambda} \right| = \sum_{n=1}^{N+1} |\Delta h_a| = (N+1)|\Delta h_a| \equiv H$$

Thus, we see that

$$N + 1 = \frac{1}{2\pi} \left| \frac{dY_a}{d\lambda} \right|^{-1} \left(\frac{H}{\varepsilon} \right), \tag{A.39}$$

and the number of steps is $O(H/\varepsilon)$. Neishtadt indicates that $H \sim O(\sqrt{\varepsilon}/\ln\varepsilon)$, implying that $N \sim O(\ln\varepsilon/\sqrt{\varepsilon}) \gg 1$, while Elskens and Escande take $N \sim O(\varepsilon^{-1/3})$, and Cary *et al.* claim $N \sim O(\varepsilon^{-1/5})$, although we do not agree with Cary's error analysis.

Rather than determine an expression for the global period $T_G(h)$, we use the fact (to be demonstrated) that the period T_G and the number of steps N appear in final expressions

Description	This work	Neishtadt	Cary *et al.*
Separatrix actions	Y_r	$\frac{1}{2\pi}S_i$	$\frac{1}{2\pi}Y_\alpha$
Linearized frequency	μ	a	ω
Global period	T_{G_r}	b_i	???
Period of $R(h>0)$	T_{R_r}	T_i	T_α
$O(\varepsilon)$ correction	D_r	d_i	g_α
$\Delta\mathcal{J}$ parameter	$He^{\mu T_{G_r}}$	???	$h_\alpha \equiv \lim_{h\to 0} he^{T_\alpha(h)}$
Crossing parameter	$\xi \in (0,1]$	ξ_i, ξ^*	M_α

Table A.1: Comparison of parameter definitions for slow separatrix crossing

in the following manner:

$$\Delta\mathcal{J} \sim \varepsilon\big[\ln(N+1) + \mu T_{G_a}\big] = \varepsilon\ln\big[(N+1)e^{\mu T_{G_a}}\big] = \varepsilon\ln\big(He^{\mu T_{G_a}}\big) - \varepsilon\ln\big(2\pi\varepsilon\,\big|\tfrac{d}{d\lambda}Y_a\big|\big)\,,$$

where we have used (A.39). Thus, only the combination $He^{\mu T_G}$ is required to express the change in the invariant. Since the period for small h diverges as $\ln|h|$, we could follow Cary *et al.* and define the $O(1)$ parameter h_α as they do $h_\alpha \equiv \lim_{h\to 0} he^{\mu T_{G_\alpha}}$, but we feel like this obscures the physics in our discussion. For now we leave it unspecified, but note that the period can be obtained using

$$\frac{2\pi}{T_{G_a}} = \left.\frac{\partial\mathcal{H}}{\partial J}\right|_{\mathcal{H}=E_{Y_a}-H} \qquad \frac{2\pi}{T_{G_b}} = \left.\frac{\partial\mathcal{H}}{\partial J}\right|_{\mathcal{H}=E_{Y_b}-H}, \tag{A.40}$$

where E_Y is the energy the separatrix. Finally, we gather in Table A.1 the various quantities that arise in our work and that of Neishtadt [46] and Cary *et al.* We denote by (???) those quantities that either do not arise (in the case of [46]), or, are defined in terms of other things that we have not specified (as in Ref. [47]).

Thus far, our discussion has been general in that it will serve to describe separatrix crossing from one region to another due to an arbitrary combination of the separatrices along region a and b slowly growing or shrinking. We have found that to continue down this path of full generality leads to a confusion of notation that only obscures the physics

and subsequent results. Therefore, we choose to analyze the particular case of a trajectory beginning in region a that crosses the separatrix to become trapped in region c due to a slow growth of both separatrices. The generalizations to other configurations is straightforward, but omitted.

A.3 Action-angle evolution as trajectories approach, cross, and depart from the separatrix

In this section we calculate the change in the action and the angle due to a slow separatrix crossing. Here, we assume that trajectories begin in region a, and that both separatrices increase in time such that as $t \to +\infty$, all orbits are trapped in region c. The order of the calculation is as follows. First, we discuss the change in the invariant $\mathcal{J}$ due to one revolution in region a, and the corresponding time over which this occurs. Second, we use these results to show that the invariant changes negligibly as one enters the near-separatrix region (matching to $\mathcal{J}$ to $\mathcal{J}_-$), and show that the initial canonical angle is linearly related to the crossing parameter. Third, we sum the changes in the invariant and calculate the time elapsed during the approach to the separatrix. Fourth, we calculate the invariant change due to the crossing of the separatrix, along with the required time for such a crossing. Fifth, we sum the changes in the invariant and calculate the time elapsed over the departure from the separatrix. Adding the changes to $\mathcal{J}$ gives the final action, while the elapsed time yields the distribution in the canonical angle.

A.3.1 Change in the invariant and time elapsed from one step by R_a

Here, we discuss how the invariant of a trajectory changes due to one step in region a, i.e., the change in $\mathcal{J}(h)$ due to the revolution map $R_a(h)$. The invariant of a frozen orbit is given by (A.34a). As indicated by (A.38), an orbit with initial energy h_{-N} has an energy h_{-n} along $\mathcal{C}$ after $(N-n)$ steps of the map R_a. Using this frozen energy, along with the definitions (A.36) and (A.37), we see that $(N-n)$ revolutions result in a trajectory with

frozen first order invariant given by

$$\begin{aligned}\mathcal{J}(h_{-n}) &= Y_a(\lambda_{-n}) - (n+\xi)\frac{\Delta h_a}{2\pi\mu}\left[\mu T_{G_a} + 1 + \ln\frac{N+1}{n+\xi}\right] + \varepsilon D_a \\ &= Y_a(\lambda_{-n}) + (n+\xi)\frac{\varepsilon}{\mu}\frac{dY_a}{d\lambda}\left[\mu T_{G_a} + 1 + \ln\frac{N+1}{n+\xi}\right] + \varepsilon D_a, \end{aligned} \tag{A.41}$$

where we have used (A.20) to eliminate Δh_a in favor $\frac{d}{d\lambda}Y_a$. After an additional revolution, $\mathcal{J}$ is given by (A.41), with $n \to (n-1)$:

$$J\big(h_{-(n-1)}\big) = Y_a\big(\lambda_{-(n-1)}\big) + (n-1+\xi)\frac{\varepsilon}{\mu}\frac{dY_a}{d\lambda}\left[\mu T_{G_a} + 1 + \ln\frac{N+1}{n-1+\xi}\right] + \varepsilon D_a. \tag{A.42}$$

Furthermore, the action of the separatrix Y_a after step $(N-n+1)$ above can be related to that of step $(N-n)$ by Taylor expansion:

$$Y_a\big(\lambda_{-(n-1)}\big) = Y_a(\lambda_{-n}) + \varepsilon\big[t_{-(n-1)} - t_{-n}\big]\frac{dY_a}{d\lambda}. \tag{A.43}$$

This equation can be simplified by noting that the time difference in (A.43) is simply the period of revolution for an orbit starting with energy h_{-n}. In other words, it is the transit time of the map $R_a(h_{-n})$ given by (A.22a):

$$t_{-(n-1)} - t_{-n} = T_{R_a}(h_{-n}) = \frac{1}{2\mu}\left[\ln\frac{N+1}{n+\xi} + \ln\frac{N+1}{n-1+\xi}\right] + T_{G_a}. \tag{A.44}$$

Next, we calculate the change in invariant due to the $(N-n+1)^{\text{st}}$ step. To do this, we subtract the invariant after step $(N-n)$ given by (A.41) from that of the subsequent step, given by (A.42) with the Taylor expansion (A.43) and the time difference (A.44). Thus, we find that associated with the change in energy $h_{-n} \to h_{-(n-1)}$ from the step $N-n+1$, we have the change in the adiabatic invariant $\mathcal{J}$ given by

$$\Delta\mathcal{J}_{-(n-1)} \equiv \mathcal{J}\big(h_{-(n-1)}\big) - \mathcal{J}(h_{-n}) = \frac{\varepsilon}{\mu}\frac{dY_a}{d\lambda}\left[-1 + \big(n - \tfrac{1}{2} + \xi\big)\ln\frac{n+\xi}{n-1+\xi}\right]. \tag{A.45}$$

Note that the terms of (A.45) are $O(1/N^2)$ for large n (for which $|h| \approx H$), implying that the sum of terms, i.e., the total change in the action during the approach, will be convergent. This is different from the result in Ref. [116], in that their terms are $O(1/N)$, and their sum diverges as $\varepsilon \ln N$. As stated earlier, this is related to their choice of definition of a step and neglect of the higher order correction (in their work, the D_a evaluated on the boundary Σ is not constant, and, hence, also contributes).

A.3.2 Matching to the invariant action and initial canonical angle

As a necessary step in calculating the total change in the invariant, we must match $\mathcal{J}_-$ to the invariant in region $\mathscr{D}$. Furthermore, this illuminates the phase evolution across a separatrix, and yields the distribution of the canonical phase. Before we do that, we show that the change in the $\mathcal{J}$ for the first step, $\Delta\mathcal{J}_{-(N-1)}$, is negligible in the limit $N \gg 1$. From the expression (A.45), we have

$$\Delta\mathcal{J}_{-(N-1)} = \frac{\varepsilon}{\mu}\frac{dY_a}{d\lambda}\left[-1 + \left(N - \tfrac{1}{2} + \xi\right)\ln\frac{N+\xi}{N-1+\xi}\right] \approx \frac{1}{N^2}\frac{\varepsilon}{\mu}\frac{dY_a}{d\lambda}\Big[\left(\tfrac{13}{4} - \xi\right) + O\left(\tfrac{1}{N}\right)\Big].$$

Thus, in the limit $N \gg 1$, $\mathcal{J}$ is still a good invariant for the first few revolutions. In terms of the canonical action-angle coordinates, our initial conditions are the phase point with coordinates $(\mathcal{J}_-, \Psi_-)$, where $\mathcal{J}_- = J(h_-)$ and $\Psi \in (-2\pi, 0]$, chosen such that $\Psi = 0$ corresponds to the first crossing of $\mathcal{C}$. Defining the initial time t_- to be that when the frozen orbit just touches the corner of the region $\mathscr{D}$, i.e., when the energy of the frozen orbit $|h_-| = H$, we have $\mathcal{J}_- \approx \mathcal{J}(h_{-N})$. This observation permits us to relate the crossing parameter ξ to the initial phase Ψ_-. Using the near separatrix formula (A.41), we have

$$\mathcal{J}(h_{-N}) = Y_a(\lambda_{-N}) + \varepsilon(N+\xi)\frac{1}{\mu}\frac{dY_a}{d\lambda}\left[\mu T_{G_a} + 1 + \ln\frac{N+1}{N+\xi}\right] + \varepsilon D_a, \tag{A.46}$$

while our choice for t_- such that $h_- = -(N+1)\Delta h_a$ implies

$$\mathcal{J}_- = Y_a(\lambda_-) + \varepsilon(N+1)\frac{1}{\mu}\frac{dY_a}{d\lambda}\big[\mu T_{G_a} + 1\big] + \varepsilon D_a. \tag{A.47}$$

The initial action of the separatrix can be related to its value when the particle reaches the first crossing of the line $\mathcal{C}$ by Taylor expansion

$$Y_a(\lambda_-) = Y_a(\lambda_{-N}) + \varepsilon\frac{dY_a}{d\lambda}(t_- - t_{-N}). \tag{A.48}$$

Furthermore, since the invariant $\mathcal{J}$ is conserved [to $O(1/N^2)$] for the energy h_{-N}, the canonical action-angle variables are described by the equations of motion

$$\mathcal{J}(t) = \mathcal{J}_- \qquad\qquad \Psi(t) = \Psi_- + \frac{2\pi}{T}(t - t_-)\,.$$

When the phase point first intersects the line of closest approach $\mathcal{C}$, the time is t_{-N} and the angle $\Psi(t_{-N}) = 0$. Furthermore, the orbit period $T = T_{G_a} + T_L(h_{-N})$, so that

$$(t_- - t_{-N}) = \frac{\Psi_-}{2\pi}\left[T_{G_a} + \frac{1}{2\mu}\ln\frac{N+1}{N+\xi}\right]. \tag{A.49}$$

Finally, we set the invariant $\mathcal{J}(h_{-N}) = \mathcal{J}_-$, i.e., we equate (A.46) with (A.47), and use the expressions for the Taylor expansion (A.48) and (A.49) to obtain

$$(1+\mu T_{G_a})\,\xi + (N+\xi)\ln\frac{N+1}{N+\xi} = 1 + \left[\mu T_{G_a} + \tfrac{1}{2}\ln\frac{N+1}{N+\xi}\right]\frac{\Phi_-}{2\pi}. \tag{A.50}$$

Expanding the logarithms for large N, we find

$$\Big[2\pi\big(\xi-1\big) - \Psi_-\Big]\Big[\mu T_{G_a} + \tfrac{1}{2N}(1-\xi)\Big] + O\big(\tfrac{1}{N^2}\big) = 0.$$

Thus, the initial phase of the canonical angle is proportional to the crossing parameter:

$$-2\pi(1-\xi) = \Psi_- : \{\Psi_- \in (-2\pi, 0],\ \xi \in (0,1]\}. \tag{A.51}$$

A.3.3 Approach to the Separatrix

During the approach to the separatrix, there are N steps of the map R_a, taking the energy from $h_{-N} = -(N+\xi)\Delta h_a$ to $h_0 = -\xi\Delta h_a$. Furthermore, each step yields an associated change in the invariant $\mathcal{J}$; that due to step $(N-n+1)$ is given by (A.45). Summing these over the N steps of the approach, the total change in action is

$$\sum_{n=1}^{N}\Delta\mathcal{J}_{-(n-1)} = \frac{\varepsilon}{\mu}\frac{dY_a}{d\lambda}\left[-N + \sum_{n=1}^{N}\big(n - \tfrac{1}{2} + \xi\big)\ln\frac{n+\xi}{n-1+\xi}\right]. \tag{A.52}$$

We simplify the sum in expression (A.52) as follows. First, we write the log of the quotient as the difference of the logs, and then rearrange the sums to find

$$\begin{aligned}\sum_{n=1}^{N}\big(n-\tfrac{1}{2}+\xi\big)\ln(n+\xi) - \sum_{n=0}^{N-1}\big(n+\tfrac{1}{2}+\xi\big)\ln(n+\xi)& \\ = \big(N-\tfrac{1}{2}+\xi\big)\ln(N+\xi) - \big(\tfrac{1}{2}+\xi\big)\ln\xi - \sum_{n=1}^{N-1}\ln(n+\xi).&\end{aligned} \tag{A.53}$$

The final sum in (A.53) can be written in terms of the Gamma function, and approximated for large N using Stirling's approximation:

$$\sum_{n=1}^{N-1} \ln(n+\xi) = \ln \prod_{n=1}^{N} (n+\xi) = \ln\big[\Gamma(N+\xi)\big] - \ln\big[\Gamma(1+\xi)\big]$$
$$\approx \big(N - \tfrac{1}{2} + \xi\big) \ln(N-1+\xi) - (N-1+\xi) + \ln \frac{\sqrt{2\pi}}{\Gamma(1+\xi)}.$$

Combining this with (A.53) and (A.52), we find that, during the approach to the separatrix, the change in the invariant $\mathcal{J}$ is given by

$$\sum_{n=1}^{N} \Delta\mathcal{J}_{-(n-1)} = \frac{\varepsilon}{\mu} \frac{dY_a}{d\lambda} \left[\xi - \big(\tfrac{1}{2} + \xi\big) \ln \xi + \ln \frac{\Gamma(1+\xi)}{\sqrt{2\pi}} \right]. \tag{A.54}$$

We also calculate the time required to approach the separatrix, which will be used to determine the asymptotic phase distribution. Summing the periods of the maps $R_a(h)$ (A.44):

$$\sum_{n=1}^{N} \big[t_{-(n-1)} - t_{-n}\big] = \sum_{n=1}^{N} T_{R_a}(h_h) = \sum_{n=1}^{N} \left[T_{G_a} + \frac{1}{2\mu} \ln \frac{N+1}{n+\xi} + \frac{1}{2\mu} \ln \frac{N+1}{n-1+\xi} \right]$$
$$= N T_{G_a} + \frac{1}{\mu} \left[N \ln(N+1) + \frac{1}{2} \ln \frac{\Gamma(\xi)\Gamma(1+\xi)}{\Gamma(N+1+\xi)\Gamma(N+\xi)} \right]$$
$$= N T_{G_a} + \frac{1}{\mu} \left[N \ln(N+1) - \frac{1}{2} \ln[\xi(N+\xi)] + \ln \frac{\Gamma(1+\xi)}{\Gamma(N+\xi)} \right], \tag{A.55}$$

where we have used the Gamma function identities

$$\Gamma(N+1+\xi) = (N+1)\Gamma(N+\xi) \qquad\qquad \Gamma(\xi) = \frac{\Gamma(1+\xi)}{\xi}.$$

Using Stirling's approximation for the Gamma function, the approach time (A.55) becomes

$$t_0 - t_{-N} = N T_{G_a} + \frac{1}{\mu} \left[N \ln \frac{N+1}{N+\xi} - \xi \ln(N+\xi) + N + \xi + \ln \frac{\Gamma(1+\xi)}{\sqrt{2\pi\xi}} \right]. \tag{A.56}$$

A.3.4 The separatrix crossing

After the N steps of the approach, the next revolution sends the trajectory across the separatrix, mapping the point with energy $h_0 = -\xi\Delta h_a$ on the line of closest approach $\mathcal{C}$ inside region a to a point with energy $h_1 = (1-\xi)\Delta h_a$ along $\mathcal{C}$ between the separatrices.

During the crossing, the invariant $\mathcal{J}$ has a discontinuous jump from the change in orbit topology, since the area of the frozen trajectory now has a contribution as it traces along the separatrix of region b. This jump in $\mathcal{J}$ can be seen in the formulae (A.16); in terms of the aforementioned energies h_1 and h_0, we have

$$\mathcal{J}(h_0) = Y_a(\lambda_0) + \xi\frac{\varepsilon}{\mu}\frac{dY_a}{d\lambda}\left[1 + \mu T_{G_a} + \ln\frac{N+1}{\xi}\right] + \varepsilon D_a \tag{A.57a}$$

$$\begin{aligned}\mathcal{J}(h_1) &= Y_a(\lambda_1) + Y_b(\lambda_1) + \varepsilon(\xi-1)\frac{dY_a}{d\lambda}\left[T_{G_a} + T_{G_b} + \frac{2}{\mu} + \frac{2}{\mu}\ln\frac{N+1}{1-\xi}\right] \\ &\quad + \varepsilon(D_a + D_b) + \frac{\varepsilon}{2}\left[T_{G_b}\frac{dY_a}{d\lambda} - T_{G_a}\frac{dY_b}{d\lambda} + \frac{1}{\mu}\left(\frac{dY_a}{d\lambda} - \frac{dY_b}{d\lambda}\right)\ln\frac{N+1}{1-\xi}\right] \\ &= Y_a(\lambda_0) + Y_b(\lambda_0) - \frac{\varepsilon}{2\mu}\frac{dY_b}{d\lambda}\left[T_{G_a} + \ln\frac{N+1}{1-\xi}\right] + \varepsilon(D_a + D_b) \\ &\quad + \frac{\varepsilon}{\mu}\left(\frac{dY_a}{d\lambda} + \frac{dY_b}{d\lambda}\right)\left[\mu T_{G_a} + \frac{1}{2}\ln\frac{N+1}{1-\xi} + \frac{1}{2}\ln\frac{N+1}{\xi}\right] \\ &\quad + \frac{\varepsilon}{\mu}\frac{dY_a}{d\lambda}\left[(\xi-1)(2+\mu T_{G_a}) + \left(\xi - \tfrac{1}{2}\right)\left(\mu T_{G_b} + 2\ln\frac{N+1}{1-\xi}\right)\right],\end{aligned} \tag{A.57b}$$

where we use the time difference $(t_1 - t_0)$ from (A.44) to Taylor expand the separatrix actions $Y(\lambda_1)$. To obtain the change in $\mathcal{J}$, we subtract (A.57a) from (A.57b), yielding

$$\begin{aligned}\Delta\mathcal{J}_1 &= Y_b(\lambda_0) + \frac{\varepsilon}{2\mu}\frac{dY_b}{d\lambda}\left[\mu T_{G_a} + \ln(N+1) - \ln\xi\right] + \varepsilon D_b \\ &\quad + \frac{\varepsilon}{\mu}\frac{dY_a}{d\lambda}\left[\xi - 2 + \left(\xi - \tfrac{1}{2}\right)\left(\mu T_{G_b} + \ln\frac{N+1}{1-\xi} + \ln\frac{\xi}{1-\xi}\right)\right].\end{aligned} \tag{A.58}$$

As written, the quantity $Y_b(\lambda_0)$ in (A.58) depends on the crossing parameter ξ in a way that has yet to be determined. To rectify this situation, we write Y_b in terms of the ξ-independent pseudo-crossing time t_x[5]. We start with the simple expansion

$$Y_b(\lambda_0) = Y_b(\lambda_x) - \varepsilon(t_x - t_0)\frac{dY_b}{d\lambda}. \tag{A.59}$$

Now, we have shifted the difficulty to calculating the time difference $(t_x - t_0)$. This can be done by relating the separatrix action Y_a at the pseudo-crossing time with that at the

[5]We find the literature to be confusing regarding this point; although we believe such a calculation is required, it does not seem to appear in previous work.

beginning of the crossing:

$$\begin{aligned} Y_a(t_x) - Y_a(t_{-N}) &= \varepsilon \frac{dY_a}{d\lambda}\left[(t_x - t_0) + (t_0 - t_{-1}) + \cdots + \left(t_{-(N-1)} - t_{-N}\right)\right] \\ &= \varepsilon \frac{dY_a}{d\lambda}(t_x - t_0) + \varepsilon \frac{dY_a}{d\lambda} \sum_{n=1}^{N} \left(t_{-(n-1)} - t_{-n}\right). \end{aligned} \tag{A.60}$$

We eliminate the separatrix action $Y_a(t_{-N})$ by rearranging the equation (A.46) for the invariant $\mathcal{J}(t_{-N})$, finding that

$$Y_a(t_{-N}) = J(t_{-N}) - (N+\xi)\frac{\varepsilon}{\mu}\frac{dY_a}{d\lambda}\left[\mu T_{G_a} + 1 + \ln\frac{N+1}{N+\xi}\right]. \tag{A.61}$$

Using the definition of the pseudo-crossing time, $Y_a(t_x) = J(t_{-N})$, the equations (A.60) and (A.61) imply that

$$\mu(t_x - t_0) = (N+\xi)\left[\mu T_{G_a} + 1 + \ln\frac{N+1}{N+\xi}\right] - \sum_{n=1}^{N} \mu\left[t_{-(n-1)} - t_{-n}\right]. \tag{A.62}$$

The sum over the periods of successive mappings by R_a is given by (A.56), namely, the time required to approach the separatrix. Substituting (A.56) in the expression (A.60), we see that the difference between the pseudo-crossing time and the time of last crossing $\mathcal{C}$ is

$$\mu(t_x - t_0) = \mu T_{G_a}\xi + \xi\ln(N+\xi) - \ln\frac{\Gamma(1+\xi)}{\sqrt{2\pi}} + \frac{1}{2}\ln\xi. \tag{A.63}$$

Finally, we use the expansion (A.59) with time difference (A.63) in the expression (A.58). Using the definition of N in terms of H (A.39), we find that the change of the invariant $\mathcal{J}$ due to the separatrix crossing is

$$\begin{aligned} \Delta\mathcal{J}_1 = Y_b(\lambda_x) &+ \frac{\varepsilon}{\mu}\frac{dY_a}{d\lambda}\Big[\xi - 2 + (1-2\xi)\ln(1-\xi) + \left(\xi - \tfrac{1}{2}\right)\ln\xi\Big] \\ &+ \frac{\varepsilon}{\mu}\frac{dY_b}{d\lambda}\left[\ln\Gamma(1+\xi) - \ln\sqrt{2\pi} - \ln\xi\right] \\ &+ \left(\xi - \tfrac{1}{2}\right)\frac{\varepsilon}{\mu}\left[\frac{dY_a}{d\lambda}\ln\frac{He^{\mu T_{G_b}}}{2\pi\varepsilon\left|\frac{d}{d\lambda}Y_b\right|} - \frac{dY_b}{d\lambda}\ln\frac{He^{\mu T_{G_a}}}{2\pi\varepsilon\left|\frac{d}{d\lambda}Y_a\right|}\right] + \varepsilon D_b \end{aligned} \tag{A.64}$$

Finally, although we have already used the crossing time in the Taylor expansion to arrive at (A.57b), we write its explicit expression here:

$$t_1 - t_0 = T_{G_a} + \frac{1}{2\mu}\left[\ln\frac{N+1}{\xi} + \ln\frac{N+1}{1-\xi}\right]. \tag{A.65}$$

A.3.5 The Departure

After the trajectory crosses the separatrix, it alternately follows the two separatrices during the departure, first along b, then along a, and so on. Thus, the mapping of an orbit back to the same line of closest approach $\mathcal{C}$ is accomplished by the map R_{ba} from (A.21d), starting with $R_{ba}(h_1)$ and proceeding, for $n \in \mathbb{Z}^+$, as

$$\underbrace{R_{ba}(h_n) \circ R_{ba}(h_{n-1}) \circ \cdots \circ R_{ba}(h_2) \circ R_{ba}(h_1)}_{n \text{ times}} : \mathcal{C}\big[h_1\big] \mapsto \mathcal{C}\big[h_{n+1}\big] \tag{A.66}$$

The values of h in (A.66) are given by adding to the initial energy, $h_1 = (1-\xi)\Delta h_a$, to the net increase $\Delta h_a + \Delta h_b$, corresponding to successive maps adjacent to region b and then region a. For $n \in \mathbb{Z}^+$, the values of the energy are given by

$$h_n \equiv (n-\xi)\Delta h_a + (n-1)\Delta h_b. \tag{A.67}$$

Using the equation for the adiabatic invariant (A.34b) with the energy (A.67), $\mathcal{J}$ is given at each step by

$$\begin{aligned}\mathcal{J}(h_n) = Y_a(\lambda_n) + Y_b(\lambda_n) + \frac{h_n}{2\pi}\left[T_{G_a} + T_{G_b} + \frac{2}{\mu}\left(1 + \ln\frac{H}{|h_n|}\right)\right] \\ + \frac{\varepsilon}{2}\left[T_{G_b}\frac{dY_a}{d\lambda} - T_{G_a}\frac{dY_b}{d\lambda} + \frac{1}{\mu}\left(\frac{dY_a}{d\lambda} - \frac{dY_b}{d\lambda}\right)\ln\frac{H}{|h_n|}\right] + \varepsilon(D_a + D_b),\end{aligned}$$

so that the change in action for each step of R_{ba} during the departure is

$$\begin{aligned}\Delta\mathcal{J}_{n+1} \equiv \mathcal{J}(h_{n+1}) - \mathcal{J}(h_n) = \big[Y_a(\lambda_{n+1}) + Y_b(\lambda_{n+1})\big] - \big[Y_a(\lambda_n) + Y_b(\lambda_n)\big] \\ + \frac{h_{n+1} - h_n}{2\pi}\left[T_{G_a} + T_{G_b} + \frac{2}{\mu}\left(1 + \ln\frac{H}{|h_{n+1}|}\right)\right] \\ + \frac{h_n}{\pi\mu}\ln\frac{h_n}{h_{n+1}} + \frac{\varepsilon}{2\mu}\left(\frac{dY_b}{d\lambda} - \frac{dY_a}{d\lambda}\right)\ln\frac{h_{n+1}}{h_n}.\end{aligned} \tag{A.68}$$

The first line of (A.68) can be evaluated by Taylor expansion:

$$Y_a(\lambda_{n+1}) - Y_a(\lambda_n) + Y_b(\lambda_{n+1}) - Y_b(\lambda_n) = \varepsilon(t_{n+1} - t_n)\left(\frac{dY_a}{d\lambda} + \frac{dY_b}{d\lambda}\right), \tag{A.69}$$

where the time difference $(t_{n+1} - t_n)$ is nothing more than the transit time $T_{R_{ba}}(h_n)$ of the map $R_{ba}(h_n)$; from (A.22c),

$$T_{R_{ba}}(h_n) = \frac{1}{2\mu}\ln\frac{H}{|h_n|} + T_{G_b} + \frac{1}{\mu}\ln\frac{H}{|h_n + \Delta h_b|} + T_{G_a} + \frac{1}{2\mu}\ln\frac{H}{|h_{n+1}|}. \tag{A.70}$$

The term in brackets from the second line of (A.68) can be simplified by noting that during the departure the change in energy after one step is $\Delta h_a + \Delta h_b$, and by relating the step in energy to the change in the separatrix action [from (A.20)]:

$$h_{n+1} - h_n = \Delta h_a + \Delta h_b = -2\pi\varepsilon \left(\frac{dY_a}{d\lambda} + \frac{dY_b}{d\lambda} \right). \tag{A.71}$$

Finally, the first term on the second line of (A.68) can be written, using the definition (A.67) as

$$\frac{h_n}{\pi\mu} \ln \frac{h_n}{h_{n+1}} = \frac{\varepsilon}{\mu} \left[2(n-\xi) \frac{dY_a}{d\lambda} + 2(n-1) \frac{dY_b}{d\lambda} \right] \ln \frac{h_{n+1}}{h_n}. \tag{A.72}$$

The change in the adiabatic invariant (A.68) is then

$$\begin{aligned} \Delta\mathcal{J}_{n+1} = {} & \frac{\varepsilon}{\mu} \frac{dY_a}{d\lambda} \left[-2 + 2\left(n - \xi\right) \ln \frac{h_{n+1}}{h_n} + \ln \frac{h_{n+1}}{h_n + \Delta h_b} \right] \\ & + \frac{\varepsilon}{\mu} \frac{dY_b}{d\lambda} \left[-2 + 2\left(n - \tfrac{1}{2}\right) \ln \frac{h_{n+1}}{h_n} + \ln \frac{h_{n+1}}{h_n + \Delta h_b} \right]. \end{aligned} \tag{A.73}$$

Calculating the amount by which $\mathcal{J}$ changes as it moves away from the separatrix is a messy endeavor; to simplify notation, we define the ratio ρ of the energy steps, and the energy in terms of ρ, by

$$\rho \equiv \frac{\Delta h_b}{\Delta h_a} = \frac{\frac{d}{d\lambda} Y_b}{\frac{d}{d\lambda} Y_a} \qquad\qquad h_n = \Delta h_a (1+\rho) \left(n - \frac{\xi + \rho}{1+\rho} \right). \tag{A.74}$$

Using (A.74), Eq. A.73 becomes

$$\Delta\mathcal{J}_n = (1+\rho) \frac{\varepsilon}{\mu} \frac{dY_a}{d\lambda} \left[-2 + \left(2n - \frac{2\xi + \rho}{1+\rho} \right) \ln \frac{n + \frac{1-\xi}{1+\rho}}{n - \frac{\rho+\xi}{1+\rho}} + \ln \frac{n + \frac{1-\xi}{1+\rho}}{n - \frac{\xi}{1+\rho}} \right]. \tag{A.75}$$

To obtain the total shift in the invariant, we must sum (A.75) over the $N/2$ steps of the departure. This calculation is rather long, and we therefore attack the problem in pieces. First, we evaluate the sum over the term $\sim (\xi + \rho) \ln n$:

$$\begin{aligned} -\frac{2\xi + \rho}{1+\rho} \sum_{n=1}^{N/2} \ln \frac{n + \frac{1-\xi}{1+\rho}}{n - \frac{\rho+\xi}{1+\rho}} &= -\frac{2\xi + \rho}{1+\rho} \sum_{n=1}^{N/2} \left[\ln\left(n + 1 - \tfrac{\rho+\xi}{1+\rho} \right) - \ln\left(n - \tfrac{\rho+\xi}{1+\rho} \right) \right] \\ &= -\frac{2\xi + \rho}{1+\rho} \left[\ln\left(\tfrac{1}{2}N + \tfrac{1-\xi}{1+\rho} \right) - \ln\left(\tfrac{1-\xi}{1+\rho} \right) \right]. \end{aligned} \tag{A.76}$$

Next, we calculate the sum over the term $\sim n \ln n$ from (A.75). This yields

$$\begin{aligned}\sum_{n=1}^{N/2} 2n \ln \frac{n+\frac{1-\xi}{1+\rho}}{n-\frac{\rho+\xi}{1+\rho}} &= \sum_{n=1}^{N/2} \Big[2(n+1)\ln\Big(n+1-\tfrac{\rho+\xi}{1+\rho}\Big) - 2\ln\Big(n+\tfrac{1-\xi}{1+\rho}\Big) - 2n\ln\Big(n-\tfrac{\rho+\xi}{1+\rho}\Big)\Big] \\ &= (N+2)\ln\Big(\tfrac{1}{2}N+\tfrac{1-\xi}{1+\rho}\Big) - 2\ln\Big(\tfrac{1-\xi}{1+\rho}\Big) - \sum_{n=1}^{N/2} 2\ln\Big(n+\tfrac{1-\xi}{1+\rho}\Big). \end{aligned} \tag{A.77}$$

Combining the sum in (A.77) with the final sum from (A.75), we evaluate the following:

$$\begin{aligned}&\sum_{n=1}^{N/2}\Big[-\ln\Big(n-\tfrac{\xi}{1+\rho}\Big) - \ln\Big(n+\tfrac{1-\xi}{1+\rho}\Big)\Big] \\ &\quad= \ln\Big[\Gamma\Big(\tfrac{1+\rho-\xi}{1+\rho}\Big)\Big] - \ln\Big[\Gamma\Big(\tfrac{1}{2}N+1-\tfrac{\xi}{1+\rho}\Big)\Big] + \ln\Big[\Gamma\Big(\tfrac{2+\rho-\xi}{1+\rho}\Big)\Big] - \ln\Big[\Gamma\Big(\tfrac{1}{2}N+1+\tfrac{1-\xi}{1+\rho}\Big)\Big] \\ &\quad\approx \ln\Big[\Gamma\Big(\tfrac{1+\rho-\xi}{1+\rho}\Big)\Big] + \ln\Big[\Gamma\Big(\tfrac{1-\xi}{1+\rho}\Big)\Big] + \ln\Big(\tfrac{1-\xi}{1+\rho}\Big) + N + \frac{1-2\xi}{1+\rho} - \ln 2\pi \\ &\qquad- \Big(\tfrac{1}{2}N+\tfrac{1+\rho-2\xi}{2(1+\rho)}\Big)\ln\Big(\tfrac{1}{2}N-\tfrac{\xi}{1+\rho}\Big) - \Big(\tfrac{1}{2}N+\tfrac{1+\rho-2\xi}{2(1+\rho)}\Big)\ln\Big(\tfrac{1}{2}N-\tfrac{\xi}{1+\rho}\Big),\end{aligned} \tag{A.78}$$

where we have used Stirling's formula and the gamma function identity

$$\Gamma\Big(\tfrac{2+\rho-\xi}{1+\rho}\Big) = \Gamma\Big(1+\tfrac{1-\xi}{1+\rho}\Big) = \Big(\tfrac{1-\xi}{1+\rho}\Big)\Gamma\Big(\tfrac{1-\xi}{1+\rho}\Big).$$

The last term in the sum (A.75) is constant, and gives the contribution

$$\sum_{n=1}^{N/2}(-2) = -N. \tag{A.79}$$

Now, we collect the various sums to evaluate the total change in the invariant during the departure. We add (A.78) to the first part of (A.77), along with the contribution of the constant term (A.79). The result is

$$\begin{aligned}\sum_{n=1}^{N/2}\Delta\mathcal{J}_n &= (1+\rho)\frac{\varepsilon}{\mu}\frac{dY_a}{d\lambda}\left\{\Big(\tfrac{1}{2}N+\tfrac{1+\rho-2\xi}{2(1+\rho)}\Big)\ln\left(\frac{1+\frac{2}{N}\frac{1-\xi}{1+\rho}}{1-\frac{2}{N}\frac{\xi}{1+\rho}}\right) + \frac{1-2\xi}{1+\rho}\right. \\ &\qquad\left. + \frac{2\xi-1}{1+\rho}\ln\Big(\tfrac{1-\xi}{1+\rho}\Big) + \ln\Big[\tfrac{1}{2\pi}\Gamma\Big(\tfrac{1-\xi}{1+\rho}\Big)\Gamma\Big(\tfrac{2-\xi}{1+\rho}\Big)\Big]\right\} \\ &\approx (1+\rho)\frac{\varepsilon}{\mu}\frac{dY_a}{d\lambda}\left\{\frac{2(1-\xi)}{1+\rho} + \frac{2\xi-1}{1+\rho}\ln\Big(\tfrac{1-\xi}{1+\rho}\Big) + \ln\Big[\tfrac{1}{2\pi}\Gamma\Big(\tfrac{1-\xi}{1+\rho}\Big)\Gamma\Big(\tfrac{2-\xi}{1+\rho}\Big)\Big]\right\}\end{aligned} \tag{A.80}$$

In a more straightforward notation, the change in the action during the departure is

$$\begin{aligned}\sum_{n=1}^{N/2}\Delta\mathcal{J}_n = \frac{\varepsilon}{\mu}\frac{dY_a}{d\lambda}\Big[(2-2\xi) + (2\xi-1)\ln\Big(\tfrac{1-\xi}{1+\rho}\Big)\Big] \\ + \frac{\varepsilon}{\mu}\left(\frac{dY_a}{d\lambda}+\frac{dY_b}{d\lambda}\right)\ln\Big[\tfrac{1}{2\pi}\Gamma\Big(\tfrac{1-\xi}{1+\rho}\Big)\Gamma\Big(\tfrac{2-\xi}{1+\rho}\Big)\Big]\end{aligned} \tag{A.81}$$

Finally, we calculate the time required for the departure, obtained by summing the periods of the map R_{ba} given in (A.70). To do this properly, we need an improved expression for the number of steps of the map R_{ba} (note that this was not required for $\Delta\mathcal{J}$ since (A.81) is independent of the number of steps, provided that $N \gg 1$). We want N' steps to take the energy from h_1 to $h_{N'+1}$. Requiring $H \geq |h_{N'+1}|$, (A.67) implies that

$$H = (N'+1)\,|\Delta h_a| + N'\,|\Delta h_b| \;\Rightarrow\; N' = \frac{N}{1+\rho}. \tag{A.82}$$

Note that in the symmetric case, $\rho = 1$ and $N' = N/2$; if $\rho = 0$ only one separatrix is changing, and $N' = N$ while if $\rho \leq -1$, so that Y_b is shrinking as fast as Y_a is growing, there are no steps in region c since all the trajectories escape to region b. Summing the transit times (A.70) over N' steps, the departure time is

$$\sum_{n=1}^{N'} T_{R_{ba}} = N'\,(T_{G_a} + T_{G_b}) + \frac{1}{2\mu}\sum_{n=1}^{N'}\left[\ln\frac{N'+\frac{1}{1+\rho}}{n-\frac{\rho+\xi}{1+\rho}} + 2\ln\frac{N'+\frac{1}{1+\rho}}{n-\frac{\xi}{1+\rho}} + \ln\frac{N+\frac{1}{1+\rho}}{n+\frac{1-\xi}{1+\rho}}\right]. \tag{A.83}$$

The middle term of the sum can be expressed in a manner similar to that used to determine the approach time, namely

$$\sum_{n=1}^{N'}\ln\frac{N'+\frac{1}{1+\rho}}{n-\frac{\xi}{1+\rho}} = \frac{1}{2}\sum_{n=1}^{N'}\left[\ln\frac{N'+\frac{1}{1+\rho}}{n+\frac{1+\rho-\xi}{1+\rho}} + \ln\frac{N'+\frac{1}{1+\rho}}{n-1+\frac{1+\rho-\xi}{1+\rho}}\right] + \frac{1}{2}\ln\frac{N'+\frac{1+\rho-\xi}{1+\rho}}{1-\frac{\xi}{1+\rho}}. \tag{A.84}$$

The sum in (A.84) is of the same form as the approach (A.55), with $N \to N' - \frac{\rho}{1+\rho}$ and $\xi \to \frac{1+\rho-\xi}{1+\rho}$. Similarly, the first and last terms in the sum for the departure (A.83) can be obtained from (A.55), with $N \to N' - \frac{\rho}{1+\rho}$ and $\xi \to \frac{1-\xi}{1+\rho}$. Thus, the calculation for the departure time is much the same as that for the approach; using the gamma function identity $\Gamma(x+1) = x\Gamma(x)$ and N [from (A.82)], we find that

$$\begin{aligned} t_{N'} - t_1 = {} & \frac{N}{1+\rho}(T_{G_a} + T_{G_b}) + \frac{1}{\mu}\frac{N}{1+\rho}\ln\frac{(N+1)(N+1)}{(N+1-\xi)(N+1+\rho-\xi)} \\ & - \frac{1}{\mu}\left[\frac{1+\rho-2\xi}{2(1+\rho)}\ln(N+1+\rho-\xi) + \frac{1-\xi}{1+\rho}\ln(N+1-\xi)\right] \\ & + \frac{1}{\mu}\left[\frac{2N+2+\rho-2\xi}{1+\rho} + \frac{1-2\xi}{1+\rho}\ln(1+\rho) - \ln 2\pi\right] \\ & + \frac{1}{\mu}\ln\left[(1-\xi)^{1/2}\,\Gamma\left(\tfrac{1}{1+\rho} - \tfrac{\xi}{1+\rho}\right)\Gamma\left(1 - \tfrac{\xi}{1+\rho}\right)\right]. \end{aligned} \tag{A.85}$$

A.3.6 Matching to the final canonical action and angle

Asymptotically matching the action $\mathcal{J}_N$ to the value outside of the linearized region $\mathscr{D}$ $\mathcal{J}_+$ proceeds much as the initial matching in Sec. A.3.2. Again, we see that the difference induced by the final step, $\Delta\mathcal{J}_{N/2}$ from (A.75) is negligible (in the limit $N \gg 1$):

$$\begin{aligned}\Delta\mathcal{J}_{N/2} &= (1+\rho)\frac{\varepsilon}{\mu}\frac{dY_a}{d\lambda}\left[-2+\left(N-\frac{2\xi+\rho}{1+\rho}\right)\ln\frac{N+\frac{2(1-\xi)}{1+\rho}}{N-\frac{2(\rho+\xi)}{1+\rho}}+\ln\frac{N+\frac{2(1-\xi)}{1+\rho}}{N-\frac{2\xi}{1+\rho}}\right]\\ &\approx \frac{\varepsilon}{N^2}\frac{dY_a}{d\lambda}\left[\frac{2(1-\rho+\rho^2)}{3\mu(1+\rho)^3}+O\left(\tfrac{1}{N}\right)\right]. \end{aligned} \tag{A.86}$$

To obtain information about the canonical angle, we invoke the equations of motion away from the separatrix. Setting the origin of the canonical angle in region c to be at the line $\mathcal{C}$ intersected at time $t_{N'}$, we have

$$\begin{aligned}\Psi(t) = \frac{2\pi}{T}(t-t_{N'}) &= \frac{2\pi}{T_{G_a}+T_{G_b}}\left[t-(t_{N'}-t_{-N})+(t_--t_{-N})-t_-\right]\\ &= \frac{2\pi\,(t-t_-)}{T_{G_a}+T_{G_b}}+\frac{T_{G_a}}{T_{G_a}+T_{G_b}}\Psi_-+\frac{2\pi}{T_{G_a}+T_{G_b}}(t_{N'}-t_{-N}).\end{aligned} \tag{A.87}$$

The terms in (A.87) have a simple interpretation: the first being the time evolution of the angle (t_- is ξ-independent); the second corresponding to a rigid mapping of the angle in region a to that in region c, evenly distributed according to the ratio of the length of the separatrix dividing region a and c to that dividing region c from both regions a and b; the third represents the degree of phase mixing, in that if it is independent of ξ the final angle evenly fills the fraction of phase space given by $\frac{T_{G_a}}{T_{G_a}+T_{G_b}}$ (that then rotates in region c), while strong phase mixing results if this term takes initially close values of ξ to widely disparate final times. We will find that for symmetric Hamiltonians the situation is generically between these two extremes.

A.4 Separatrix crossing for the symmetric Hamiltonian

In the symmetric case, where the two "halves" of the trapped region are of the same size and grow at the same rate, the expressions for both the change in action and the total

crossing time simplify dramatically. In this case, during the approach the action changes according to

$$\sum_{n=1}^{N} \Delta\mathcal{J}_{-(n-1)} = \frac{\varepsilon}{\mu}\frac{dY_a}{d\lambda}\left[\xi - \left(\tfrac{1}{2}+\xi\right)\ln\xi + \ln\frac{\Gamma(1+\xi)}{\sqrt{2\pi}}\right]. \tag{A.88}$$

The change in $\mathcal{J}$ (A.64) due to crossing the separatrix is

$$\Delta\mathcal{J}_1 = Y_a(\lambda_x) + \frac{\varepsilon}{\mu}\frac{dY_a}{d\lambda}\left[\xi - 2 + (1-2\xi)\ln(1-\xi) + \left(\xi - \tfrac{3}{2}\right)\ln\xi + \ln\frac{\Gamma(1+\xi)}{\sqrt{2\pi}}\right]. \tag{A.89}$$

And the change in the invariant due to the departure of the separatrix (A.81)

$$\sum_{n=1}^{N/2} \Delta\mathcal{J}_n = \frac{\varepsilon}{\mu}\frac{dY_a}{d\lambda}\left[2 - 2\xi + (2\xi-1)\ln\frac{1-\xi}{2} + 2\ln\frac{\Gamma\left(1-\frac{1}{2}\xi\right)\Gamma\left(\frac{1}{2}-\frac{1}{2}\xi\right)}{2\pi}\right]. \tag{A.90}$$

We can simplify (A.90) by using the duplication formula of the gamma function

$$\Gamma(2x) = \frac{4^x}{2\sqrt{\pi}}\Gamma(x)\Gamma\left(\tfrac{1}{2}+x\right) \Rightarrow \Gamma\left(\tfrac{1}{2}-\tfrac{1}{2}\xi\right)\Gamma\left(1-\tfrac{1}{2}\xi\right) = \frac{2\sqrt{\pi}}{2^{1-\xi}}\Gamma(1-\xi), \tag{A.91}$$

so that (A.90) becomes

$$\sum_{n=1}^{N/2} \Delta\mathcal{J}_n = \frac{\varepsilon}{\mu}\frac{dY_a}{d\lambda}\left[2 - 2\xi + (2\xi-1)\ln(1-\xi) + 2\ln\frac{\Gamma(1-\xi)}{\sqrt{2\pi}}\right]. \tag{A.92}$$

Adding the symmetric expression for the change in the action (A.88), (A.89), and (A.92) expressions, we see that the total change in the action in the symmetric case is

$$\sum_{n=-N}^{N/2} \Delta\mathcal{J}_n = Y_a(\lambda_x) + 2\frac{\varepsilon}{\mu}\frac{dY_a}{d\lambda}\ln\frac{\Gamma(1-\xi)\Gamma(1+\xi)}{2\pi\,\xi}. \tag{A.93}$$

Using the gamma function identities

$$\Gamma(-x)\Gamma(1+x) = \frac{\pi}{\sin(-\pi x)}, \qquad \Gamma(1-x) = x\Gamma(-x), \tag{A.94}$$

we see that

$$\Gamma(1-\xi)\Gamma(1+\xi) = \xi\Gamma(-\xi)\Gamma(1+\xi) = \frac{\pi\,\xi}{\sin(\pi\xi)}, \tag{A.95}$$

so that the final action is

$$\mathcal{J}_+ = \mathcal{J}_- + Y_a(\lambda_x) - \frac{2\varepsilon}{\mu}\frac{dY_a}{d\lambda}\ln\left[2\sin(\pi\xi)\right]. \tag{A.96}$$

Calculating the crossing time proceeds in a similar manner. Adding the times associated with the approach (A.56), crossing (A.65), and departure (A.85) with $\rho = 1$, $T_{G_a} = T_{G_b}$, and expanding the logarithms assuming $N \gg 1$, we obtain

$$t_{N'} - t_{-N} = (2N+1)T_{G_a} + \frac{2N+2}{\mu} - \frac{\xi}{\mu}\ln 2 + \frac{1}{\mu}\ln\frac{\Gamma\left(\frac{1}{2}-\frac{\xi}{2}\right)\Gamma\left(1-\frac{\xi}{2}\right)\Gamma(1+\xi)}{2(\pi)^{3/2}\xi} \quad \text{(A.97)}$$

The expression for the total crossing time (A.97) can be simplified using the duplication formula (A.91) and the identity (A.95). We find that

$$t_{N'} - t_{-N} = (2N+1)T_{G_a} + \frac{1}{\mu}(2N+2) - \frac{1}{\mu}\ln\big[2\sin(\pi\xi)\big]. \quad \text{(A.98)}$$

The first thing to note about the time (A.98) is that it indicates where the separatrix crossing theory breaks down: when this time becomes $O(1/\varepsilon)$, our assumption that the parameters of the Hamiltonian are constant is violated, for which

$$\varepsilon\mu(t_{N'} - t_{-N}) = L < \varepsilon(2N+1)\mu T_{G_a} + 2\varepsilon\mu(N+1) - \varepsilon\ln\big[2\sin(\pi\xi)\big], \quad \text{(A.99)}$$

where $L \sim O(1)$. The first two terms vanish as $\varepsilon \to 0$ (although slowly), so that the separatrix crossing theory does not hold for particle such that

$$\sin(\pi\xi) < e^{-L/\varepsilon}e^{C/\varepsilon^{\alpha}}, \quad \text{(A.100)}$$

where $L, C \sim O(1)$ and, depending on whose error analysis one trusts, $\frac{1}{3} \lesssim \alpha \lesssim \frac{1}{2} < \frac{4}{5}$. Thus, we see that for slow evolution, the separatrix crossing theory applies for all particles except the exponentially few whose crossing parameters are very close to 1 or 0. These are the particles that pass very close to the hyperbolic equilibrium, spending arbitrary amounts of time tracing the stable manifolds.

The final conclusion we obtain from the crossing time (A.98) is the final canonical angle of the particles from (A.87):

$$\Psi(t) = \frac{\pi(t-t_-)}{T_{G_a}} + \pi(\xi-1) + \pi(2N+1) + \frac{2\pi(N+1)}{\mu T_{G_a}} - \frac{\pi}{\mu T_{G_a}}\ln\big[2\sin(\pi\xi)\big]. \quad \text{(A.101)}$$

The first term in (A.101) gives the dynamic evolution; the second results in the rigid mapping of evenly spaced particles over 2π above the separatrices to half that between the

separatrices; the third and fourth are uniform displacements in the angle for all particles due to the crossing; while the final term yields the degree to which the particles have phase-mixed. Since the period $T_{G_a} \sim \ln|H| \sim \ln\varepsilon$, this term does, strictly speaking, vanish in the $\varepsilon \to 0$, but too slowly to be neglected for most of physical situations, and certainly for any of the scenarios envisioned in Ch. 2 (for which $0.1 \gtrsim \varepsilon \gtrsim 0.0001$). Thus, we are led to the conclusions that although the results in Elskens and Escande [41] (who claim that the particles are essentially rigidly mapped across the separatrix as $\varepsilon \to 0$) are formally correct, the analytical and numerical work of Cary and Skodje [39, 40] (indicating that there is some residual phase mixing as $\varepsilon \to 0$) is more useful from a practical standpoint.

To illuminate these results on the evolution of the canonical action and angle under slow separatrix crossing, we have performed some numerical simulations of the slowly-varying pendulum, with Hamiltonian

$$\mathcal{H}(p,q;\lambda) = \frac{1}{2}p^2 + \phi(\lambda)\big[1-\cos(q)\big]. \tag{A.102}$$

As we have seen in Chapter 2, this Hamiltonian is qualitatively similar to that describing electrons in a slowly growing wave, and therefore can yield some insight on the evolution of the canonical action and angle as the particles cross the separatrix. Rewriting the expressions (A.96) and (A.101), we have the following expressions for the action and angle after a symmetric separatrix crossing:

$$\mathcal{J} = \mathcal{J}_- + Y_a(\lambda_x) - \frac{2\varepsilon}{\mu}\frac{dY_a}{d\lambda}\ln\big[2\sin(\pi\xi)\big] \tag{A.103a}$$

$$\Psi = \Psi_0 + \pi(\xi-1) - \frac{\pi}{\mu T_{G_a}}\ln\big[2\sin(\pi\xi)\big], \tag{A.103b}$$

with Ψ_0 an unspecified constant. We compare the analytic expressions (A.103) with simulations of the slowly-varying pendulum in Fig. A.3, for $\varepsilon = 0.005$. In the simulations, we initialize a number of particles uniformly over Ψ, with the potential $\phi(0) = 0$. We then slowly increase the amplitude of the potential, saving the final particle positions at a time after the particles have crossed, and moved a certain distance away from, the separatrix.

In Fig. A.3(a), we compare the resulting final positions in the Ψ-J plane of this initially

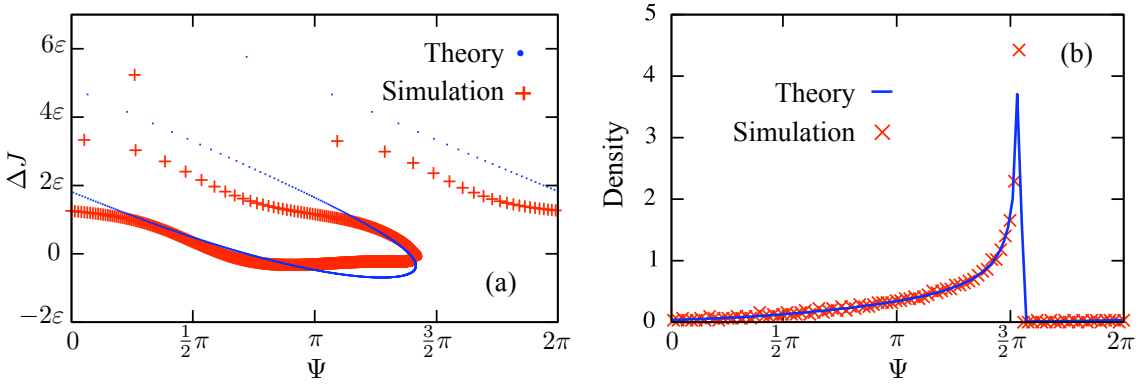

Figure A.3: Final distribution after crossing the separatrix of a set of particles that is initially distributed uniformly over Ψ, for $\varepsilon = 0.005$. In (a), we compare the resulting set of particles from the slowly-varying simulation (red crosses), to that predicted by (A.103). We see that the change in action is confined to $O(\varepsilon)$, with the J of some particles increasing and others decreasing, while the distribution in the canonical angle Ψ is not uniform. To make this more concrete, we present in (b) the phase-space density in Ψ, integrated over the action. We see a cusp that is associated with the "folding over" near $\Psi = 3\pi/2$ in panel (a), while the remainder of the distribution is spread across the rest of 2π. We note that this structure only slowly changes as $\varepsilon \to 0$.

uniform set of particles from the slowly-varying simulation (red crosses), to that predicted by (A.103). We see that final positions of the particles is well-predicted by the theory (note that the absolute phase Ψ_0 is not determined by the theory, and must be fit to the simulation). Furthermore, the change in action is confined to a narrow width $\sim O(\varepsilon)$, with the J of some particles increasing and others decreasing, such that the average ΔJ over all the particles is observed to be approximately zero.

Additionally, the distribution in the canonical angle Ψ is not uniform. We show this more definitively in Fig. A.3(b), in which we plot the integrated (in J) phase-space density of the particles in the canonical angle Ψ. We see a sharp enhancement in the density near $\Psi = 3\pi/2$ that is associated with the "folding over" in J of the set of particles in panel (a). The density decreases monotonically from $\Psi = 3\pi/2$, but remains nonzero for all $0 \leq \Psi < 2\pi$. We note that since this structure only vanishes logarithmically as $\varepsilon \to 0$, it remains the dominant feature for $\varepsilon \gtrsim 10^{-9}$. For our problems of interest, this implies

that from a practical standpoint the distribution is neither uniformly distributed over the entire range 2π in Ψ in the trapped region (full phase-mixing), nor is it evenly spread over only π (the "primitive" result as indicated by [41]).

Bibliography

[1] L. Tonks and I. Langmuir. Oscillations in ionized gases. *Physical Review*, 33(2):25–34, 1929.

[2] D. Pines and D. Bohm. A collective description of electron interactions: II. Collective vs. individual particle aspects of the interactions. *Physical Review*, 85(2):338–353, 1952.

[3] L. Landau. On the vibrations of the electronic plasma. *Journal of Physics (USSR)*, 10(1):25–34, 1946.

[4] J. D. Jackson. Longitudinal plasma oscillations. *Journal of Nuclear Energy, Part C: Plasma Physics*, 1:171–189, 1960.

[5] J. D. Dawson. On Landau damping. *Physics of Fluids*, 4(7):869–874, 1962.

[6] T. M. O'Neil. Collisionless damping of nonlinear plasma oscillations. *Physics of Fluids*, 8(12):2255–2262, 1965.

[7] I. B. Bernstein, J. M. Greene, and M. D. Kruskal. Exact nonlinear plasma oscillations. *Physical Review*, 108(3):546–550, 1957.

[8] L. M. Altshul' and V. I. Karpman. Theory of nonlinear oscillations in a non-collisional plasma. *Soviet Physics - JETP*, 22(2):1045 1058, 1966.

[9] T. M. O'Neil, J. H. Winfrey, and J. H. Malmberg. Nonlinear interaction of a small cold beam and a plasma. *Physics of Fluids*, 14(6):1204–1212, 1971.

[10] R. L. Dewar. Saturation of kinetic plasma instabilities by particle trapping. *Physics of Fluids*, 16(3):431–435, 1973.

[11] D. Montgomery and G. Joyce. Shock-like solutions of the electrostatic Vlasov equation. *Journal of Plasma Physics*, 3(1):1–11, 1969.

[12] H. Schamel. Electron holes, ion holes and double layers - Electrostatic phase space structures in theory and experiment. *Physics Reports - Review Section of Physics Letters*, 140(3):161–191, 1986.

[13] C. B. Warton, J. Malmberg, and T. M. O'Neil. Nonlinear effects of large-amplitude plasma waves. *Physics of Fluids*, 11(8):1761–1763, 1968.

[14] W. Bertsche, J. Fajans, and L. Friedland. Direct excitation of high-amplitude chirped bucket-BGK modes. *Physical Review Letters*, 91(26):265003/1–4, 2003.

[15] D. S. Montgomery, R. J.. Focia, H. A. Rose, D. A. Russell, J. .A. Cobble, J. C. Fernandez, and R. P. Johnson. Observation of stimulated electron-acoustic wave scattering. *Physical Review Letters*, 87(15):155001/1–4, 2001.

[16] D. H. Froula, L. Divol, A. A. Offenberger, N.. Meezan, T. Ao., G. Gregori, C. Niemann, D. Price, C. A. Smith, and S. H. Glenzer. Direct observation of the saturation of stimulated Brillouin scattering by ion-trapping-induced frequency shifts. *Physical Review Letters*, 93(3):035001/1–4, 2004.

[17] R. E. Ergun, C. W. Carlson, J. P. McFadden, F. S. Mozer, L. Muschietti, I. Roth, and R. J. Strangeway. Debye-scale plasma structures associated with magnetic-field-aligned electric fields. *Physical Review Letters*, 81(4):826–829, 1998.

[18] S. D. Bale, A. Hull, D. E. Larson, R. P. Lin, L. Muschietti, P. J. Kellogg, K. Goetz, and S. J. Monson. Electrostatic turbulence and Debye-scale structures associated with electron thermalization at collisionless shocks. *Astrophysical Journal*, 575(1):L25–L28, 2002.

[19] M. V. Goldman and D. F. DuBois. Stimulated incoherent scattering of light from plasmas. *Physics of Fluids*, 8(7):1404–1405, 1965.

[20] M. N. Rosenbluth and C. S. Liu. Excitation of plasma waves by two laser beams. *Physical Review Letters*, 29(11):701–705, 1972.

[21] J. F. Drake, P. K. Kaw, Y. C. Lee, G. Smidt, C. S. Liu, and M. N. Rosenbluth. Parametric instabilities of electromagnetic waves in plasmas. *Physics of Fluids*, 17(4):778–795, 1974.

[22] W. L. Kruer. *The Physics of Laser Plasma Interactions*. Westview Press, Boulder, CO, 2003.

[23] W. M. Manheimer and R. W. Flynn. Formation of stationary large amplitude waves in plasma. *Physics of Fluids*, 14(11):2393–2396, 1971.

[24] G. J. Morales and T. M. O'Neil. Nonlinear frequency shift of nonlinear plasma oscillations. *Physical Review Letters*, 28(7):417–420, 1972.

[25] R. L. Dewar. Frequency shift due to trapped particles. *Physics of Fluids*, 15(4):712–714, 1972.

[26] W. L. Kruer, J. M. Dawson, and R. N. Sudan. Trapped-particle instability. *Physical Review Letters*, 23(15):838–841, 1969.

[27] J. M. Dawson. Nonlinear electron oscillations in a cold plasma. *Physical Review*, 113(383):383–387, 1959.

[28] T. P. Coffey. Breaking of large amplitude plasma oscillations. *Physics of Fluids*, 14(7):1402–1406, 1971.

[29] V. M. Malkin, G. Shvets, and N. J. Fisch. Fast compression of laser beams to highly overcritical powers. *Physical Review Letters*, 82(22):4448–4451, 1999.

[30] W. Cheng, Y. Avitzour, Y. Ping, S. Suckewer, N. J. Fisch, M. S. Hur, and J. S. Wurtele. Reaching the nonlinear regime of Raman amplification of ultrashort laser pulses. *Physical Review Letters*, 94(4):045003/1–4, 2005.

[31] N. G. Van Kampen. On the theory of stationary waves in plasmas. *Physica*, 21:949–943, 1955.

[32] K M. Case. Plasma oscillations. *Annals of Physics*, 7:349–364, 1959.

[33] J. P. Holloway and J. J. Dorning. Undamped plasma waves. *Physical Review A*, 44(6):3856–3868, 1991.

[34] R. L. Berger, C. H. Still, E. A. Williams, and A. B. Langdon. On the dominant and subdominant behavior of stimulated Raman and Brillouin scattering driven by nonuniform laser beams. *Physics of Plasmas*, 5(12):4337–4356, 1998.

[35] H. A. Rose and D. A. Russell. A self-consistent trapping model of driven electron plasma waves and limits on stimulated Raman scatter. *Physics of Plasmas*, 8(11):4784–4799, 2001.

[36] L. Divol, E. A. Williams, B. I. Cohen, A. B. Langdon, and B. F. Lasinski. A reduced model of kinetic effects related to the saturation of stimulated Brillouin scattering. Technical Report UCRL-JC-155169, Lawrence Livermore National Laboratory, 2003.

[37] H. X. Vu, D. F. DuBois, and B. Bezzerides. Inflation threshold: a nonlinear trapping0induced threshold for the rapid onset of stimulated Raman scattering from a single laser speckle. *Physics of Plasmas*, 14(1):012702/1–32, 2007.

[38] V. I. Arnold. *Mathematical Methods of Classical Mechanics*, page 100. Springer-Verlag, New York, NY, second edition, 1997.

[39] J. R. Cary and R. T.. Skodje. Reaction probability for sequential separatrix crossing. *Physical Review Letters*, 61(16):1795–1798, 1988.

[40] J. R. Cary and R. T. Skodje. Phase change between separatrix crossings. *Physica D*, 36:287–316, 1989.

[41] Y. Elskens and D. F. Escande. Slowly pulsating sweep homoclinic tangles where islands must be small: an extension of adiabatic theory. *Nonlinearity*, 4(3):615–667, 1991.

[42] D. Bénisti and L. Gremillet. Nonlinear plasma response to a slowly varying electrostatic wave, and application to stimulated Raman scattering. *Physics of Plasmas*, 14(4):042304/1–4, 2007.

[43] C. G. Wells and S. T. C. Siklos. The adiabatic invariance of the action variable in classical dynamics. *European Journal of Physics*, 28:105–112, 2006.

[44] R. B. W. Best. On the motion of charged particles in a slightly damped sinusoidal potential wave. *Physica D*, 40:182–196, 1968.

[45] A. V. Timofeev. On the constancy of the adiabatic invariant on variation of the nature of motion. *Soviet Physics JETP*, 48:656, 1978.

[46] A. I. Neishtadt. Change in adiabatic invariant at a separatrix. *Soviet Journal of Plasma Physics*, 12(8):568–573, 1986.

[47] J. R. Cary, D. F. Escande, and J. L. Tennyson. Adiabatic-invariant change due to separatrix crossing. *Physical Review A*, 34(5):4256–4275, 1986.

[48] J. H. Hannay. Accuracy loss in action invariance in adiabatic change of one-freedom Hamiltonian. *Journal of Physics A: Mathematical and General*, 19:L1067–L1072, 1986.

[49] J. D. Dawson. One-dimensional plasma model. *Physics of Fluids*, 5(4):445–459, 1962.

[50] C. J. McKinstrie and M. Yu. The role of ion momentum in stimulated Raman scattering. *Physics of Fluids B*, 3(11):3041–3045, 1991.

[51] G. Shvets, N. J. Fisch, and A. Pukhov. Acceleration and compression of charged particle bunches using counterpropagating laser beams. *IEEE Transactions on Plasma Science*, 28(4):1194–1201, 2000.

[52] A. J. Lichtenberg and M. A. Lieberman. *Regular and Stochastic Motion*. Springer-Verlag, New York, NY, 1983.

[53] I. S. Gradshteyn and I. M. Ryzhik, editors. *Table of Integrals, Series, and Products*. Academic Press, New York, NY, 1980.

[54] A. Vlasov. On the kinetic theory of an assembly of particles with collective interaction. *Journal of Physics (USSR)*, 9:25–40, 1945.

[55] M. Buchanan and J. Dorning. Nonlinear electrostatic waves in collisionless plasma. *Physical Review E*, 52(3):3015–3033, 1995.

[56] D. C. Barnes. The bounce-kinetic model or driven nonlinear Langmuir waves. *Physics of Plasmas*, 11(3):903–917, 2004.

[57] W. B. Colson and S. K. Ride. The nonlinear wave equation for free electron lasers driven by single particle equations. *Physics Letters A*, 76A(5-6):379–382, 1980.

[58] G. Shvets, J. S. Wurtele, and B. A. Shadwick. Analysis and simulation of Raman backscatter in underdense plasmas. *Physics of Plasmas*, 4(5):1872–1880, 1997.

[59] B. I. Cohen and A. N. Kaufman. Beat heating of a plasma. *Physical Review Letters.*, 29(9):581–584, 1972.

[60] H. Kim. Frequency shifts of large-amplitude plasma waves. *Physics of Fluids*, 19(9):13621364, 1976.

[61] H. X. Vu, D. F. DuBois, and B. Bezzerides. Kinetic inflation of stimulated Raman backscatter in regimes of high linear Landau damping. *Physics of Plasmas*, 9(5):1745–1763, 2002.

[62] L. Yin, W. Daughton, B. J. Albright, K. J. Bowers, D. .S. Montgomery, and J. L. Kline. Nonlinear backward stimulated Raman scattering from electron beam acoustic modes in the kinetic regime. *Physics of Plasmas*, 13:072701/1–13, 2006.

[63] D. S. Montgomery, J. .A. Cobble, J. C. Fernandez, R. J.. Focia, R. P. Johnson, N. Renard-LeGalloudec, H. A. Rose, and D. A. Russell. Recent trident single hot spot experiments: Evidence for kinetic effects, and observation of Langmuir decay instability cascade. *Physics of Plasmas*, 9(5):2311–2320, 2002.

[64] M. N. Rosenbluth, R. B. White, and C. S. Liu. Temporal evolution of a three-wave parametric instability. *Physical Review Letters*, 31(19):1190–1193, 1973.

[65] G. L. Lamb. Analytical descriptions of ultrashort pulse propagation in a resonant medium. *Reviews of Modern Physics*, 43(2):99–124, 1971.

[66] C. E. Capjack, C. R. James, and J. N. McMullin. Plasma KrF laser pulse compressor. *Journal of Applied Physics*, 53(6):4046–4053, 1982.

[67] C. K. Birdsall and A. B.Langdon. *Plasma Physics via Computer Simulation*. Institute of Physics Publishing, Philadelphia, PA, 1991.

[68] H. X. Vu, B. Bezzerides, and D. F. DuBois. A fully kinetic, reduced-description particle-in-cell model for simulating parametric instabilities. *Journal of computational physics*, 156(1):12–42, 1999.

[69] M. S. Hur, G. Penn, J. S. Wurtele, and R. Lindberg. Slowly varying envelope kinetic, simulations of pulse amplification by Raman backscattering. *Physics of Plasmas*, 11(11):5204–5211, 2004.

[70] S. Brunner and E. J. Valeo. Trapped-particle instability leading to bursting in stimulated Raman scattering simulations. *Physical Review Letters*, 93(14):1455003/1–4, 2004.

[71] D. J. Strozzi, E. A. Williams, A. B. Langdon, and A. Bers. Kinetic enhancement of Raman backscatter, and electron acoustic Thomson scatter. *Physics of Plasmas*, 14(1):013104/1–13, 2007.

[72] G. M. Fraiman, N. A. Yampolsky, V. M. Malkin, and N. J. Fisch. Robustness of laser fronts in backward Raman amplifiers. *Physics of Plasmas*, 9(8):3617–3624, 2002.

[73] R. L. Seliger and G. B. Whitham. Variational principles in continuum mechanics. *Proceedings of the Royal Society A*, 305(1480):1–25, 1968.

[74] X. L. Chen and R. N. Sudan. Two-dimensional self-focusing of short intense laser pulse in underdense plasma. *Physics of Fluids B*, 5(4):1336–1348, 1993.

[75] F. H. Shu. *Physics of Astronomy Vol. II: Gas Dynamics*. University of Science Books, Sausalito, CA, 1992.

[76] M. S. Hur, R. R. Lindberg, A. E. Charman, J. S. Wurtele, and H. Suk. Electron kinetic effects on Raman backscatter in plasmas. *Physical Review Letters*, 95(11):115003/1–4, 2005.

[77] B. D. Fried and S. D. Conte, editors. *The Plasma Dispersion Function: The Hilbert Transform of the Gaussian*. Academic Press, New York, NY, 1961.

[78] A. Bers. Linear waves and instabilities. In C. DeWitt and J. Peynaud, editors, *Physique des Plasmas - Les Houches 1972*. Gordon and Breach, 1975.

[79] K. Nishikawa and M. Wakatani. *Plasma Physics*, chapter 7. Springer-Verlag, New York, NY, third edition, 2000.

[80] P. Bertrand and M. R. Feix. Frequency shift of non-linear electron plasma oscillation. *Physics Letters A*, 29(9):489–490, 1969.

[81] C. J. McKinstrie and D. W. Forslund. The detuning of relativistic Langmuir wave in the beatwave accelerator. *Physics of Fluids*, 30(3):904–908, 1987.

[82] D. R. Nicholson. *Introduction to Plasma Theory*. John Wiley & Sons, Inc, New York, NY, 1983.

[83] R. Sugihara, K. Yamanaka, Y. Ohsawa, and T. Kamimura. Initial damping of large amplitude waves. *Physics of Fluids*, 24(3):434–441, 1981.

[84] V. E. Zakharov and V. I. Karpman. Nonlinear attenuation of plasma waves. *JETP*, 16:490–499, 1963.

[85] C. Z. Cheng and G. Knorr. Integration of the Vlasov equation in configuration space. *Journal of Computational Physics*, 22(3):330–351, 1976.

[86] I. H. Oei and D. G. Swanson. Self-consistent finite amplitude wave damping. *Physics of Fluids*, 13(12):2218–2221, 1965.

[87] J. Canosa and J. Gazdag. Threshold conditions for electron trapping by nonlinear waves. *Physics of Fluids*, 17(11):2030–2039, 1974.

[88] M. V. Medvedev, P. H. Diamond, M. N. Rosenbluth, and V. I. Shevchenko. Asymptotic theory of nonlinear Landau damping and particle trapping in waves of finite amplitude. *Physical Review Letters*, 81(26):5824–5827, 1998.

[89] C. Lancellotti and J. J. Dorning. Time-asymptotic propagation in collisionless plasmas. *Physical Review E*, 68(2):026406/1–31, 2003.

[90] M. Brunetti, F. Califano, and F. Pegoraro. Asymptotic evolution of nonlinear Landau damping. *Physical Review E*, 62(3):4109–4114, 2000.

[91] A. V. Ivanov and I. H. Cairns. Nontrapping arrest of Langmuir wave damping near the threshold amplitude. *Physical Review Letters*, 96(17):175001/1–4, 2006.

[92] F. Y. F. Chu and C. F. F. Karney. Solution of the three-wave resonant equations with one wave heavily damped. *Physics of Fluids*, 20(10):1728–1732, 1977.

[93] J. C. Fernandez, J. .A. Cobble, D. .S. Montgomery, M. D. Wilke, and B. B. Afeyan. Observed insensitivity of stimulated Raman scattering on electron density. *Physics of Plasmas*, 7(9):3743–3750, 2000.

[94] Y. Ping, W. Cheng, S. Suckewer, D. S. Clark, and N. J. Fisch. Amplification of ultrashort laser pulses by a resonant Raman scheme in a gas-jet plasma. *Physical Review Letters*, 92(17):175007/1–4, 2004.

[95] S. V. Manakov. Pulse distribution in long laser amplifiers. *JETP Letters*, 35:237–239, 1982.

[96] J. Coste and C. Montes. Asymptotic evolution of stimulated Brillouin scattering: Implication for optical fibers. *Physical Review A*, 34(5):3940–3949, 1986.

[97] D. Strickland and G. Mourou. Compression of amplified chirped optical pulses. *Optics Communications*, 56(3):219–221, 1985.

[98] V. M. Malkin, G. Shvets, and N. J. Fisch. Ultra-powerful compact amplifiers for of short laser pulses. *Physics of Plasmas*, 7(5):2232–2240, 2000.

[99] Yu. A. Tsidulko, V. M. Malkin, and N. J. Fisch. Suppression of superluminous precursors in high-power backward Raman amplifiers. *Physical Review Letters*, 88(23):235004–1–3, 2002.

[100] N. A. Yampolsky, V. M. Malkin, and N. J. Fisch. Finite-duration seeding effects in powerful backward Raman amplifiers. *Physical Review E*, 69(3):36401/1–6, 2004.

[101] P. J. Morrison. Hamiltonian description of the ideal fluid. *Reviews of Modern Physics*, 70(2):467–521, 1998.

[102] C. Eckart. Variation principles of hydrodynamics. *Physics of Fluids*, 3(3):421–427, 1960.

[103] C. S. Gardner. Korteweg-de Vries equation and generalizations IV. Korteweg-de Vries equations as a Hamiltonian system. *Journal of Mathematical Physics*, 12(8):1548–1551, 1971.

[104] P. J. Morrison and J.M. Greene. Noncanonical Hamiltonian density formulation of hydrodynamics and ideal magnetohydrnamics. *Physical Review Letters*, 45(10):790–794, 1980.

[105] P. J. Spencer and A. N. Kaufman. Hamiltonian description of the ideal fluid. *Physical Review A*, 25(4):2437–2439, 1982.

[106] J. Larsson. Practical use of Lie algebra structure in non-dissipative fluid and plasma models. *Journal of Plasma Physics*, 64(2):155–178, 2000.

[107] A. J. Brizard. A new Lagrangian formulation for laser-plasma interactions. *Physics of Plasmas*, 5(4):1110–1117, 1998.

[108] D. C. dePackh. The water-bag model of a sheet electron beam. *Journal of Electronics and Control*, 13(5):417–424, 1962.

[109] P. Bertrand and M. R. Feix. Nonlinear electron plasma oscillations: the "water-bag model". *Physics Letters A*, 28(1):68–69, 1968.

[110] W. A. Newcomb. Warm relativistic electron fluid. *Physics of Fluids*, 25(5):846–851, 1982.

[111] B. A. Shadwick, G. M. Tarkenton, and E. H. Esarey. Hamiltonian description of low-temperature relativistic plasmas. *Physical Review Letters*, 93(17):175002, 2004.

[112] A. I. Akhiezer and G. Ya. Lyubarskii. On the non-linear theory of electron plasma oscillations. *Doklady Akademii Nauk SSSR*, 87(2):193–195, 1951.

[113] A. I. Akhiezer and R. V. Polovin. Relativistic plasma oscillations. *Soviet Physics JETP*, 3:696–697, 1956.

[114] P. L. Chu and D. E. Karbowiak. Cold plasma oscillations: an exact solution of the nonlinear equations. *IEEE Transactions on Plasma Science*, PS3(2):90–94, 1975.

[115] D. A. Hartmann and C. F. Driscoll. Measurements of the trapped particle sideband instability compared to the macroparticle model. *Physics of Plasmas*, 8(7):3457–3466, 2001.

[116] S.-N. Chow and T. Young. A geometric proof of separatrix crossing results. *Nonlinear Analysis*, 56:1047–1070, 2004.

[117] J. R. Cary, D. F. Escande, and J. L. Tennyson. Change of the adiabatic invariant due to separatrix crossing. *Physical Review Letters*, 56(20):2117–2120, 1986.

[118] J. Henrard. The adiabatic invariant in celestial mechanics. *Dynamics Reported 2*, pages 117–230, 1993.